

# Advances in the development and application of deep eutectic solvents

**Edited by**

Maria Luisa Di Gioia, Manoj B. Gawande  
and Ana Rita Duarte

**Published in**

Frontiers in Chemistry



## FRONTIERS EBOOK COPYRIGHT STATEMENT

The copyright in the text of individual articles in this ebook is the property of their respective authors or their respective institutions or funders. The copyright in graphics and images within each article may be subject to copyright of other parties. In both cases this is subject to a license granted to Frontiers.

The compilation of articles constituting this ebook is the property of Frontiers.

Each article within this ebook, and the ebook itself, are published under the most recent version of the Creative Commons CC-BY licence. The version current at the date of publication of this ebook is CC-BY 4.0. If the CC-BY licence is updated, the licence granted by Frontiers is automatically updated to the new version.

When exercising any right under the CC-BY licence, Frontiers must be attributed as the original publisher of the article or ebook, as applicable.

Authors have the responsibility of ensuring that any graphics or other materials which are the property of others may be included in the CC-BY licence, but this should be checked before relying on the CC-BY licence to reproduce those materials. Any copyright notices relating to those materials must be complied with.

Copyright and source acknowledgement notices may not be removed and must be displayed in any copy, derivative work or partial copy which includes the elements in question.

All copyright, and all rights therein, are protected by national and international copyright laws. The above represents a summary only. For further information please read Frontiers' Conditions for Website Use and Copyright Statement, and the applicable CC-BY licence.

ISSN 1664-8714  
ISBN 978-2-8325-4455-6  
DOI 10.3389/978-2-8325-4455-6

## About Frontiers

Frontiers is more than just an open access publisher of scholarly articles: it is a pioneering approach to the world of academia, radically improving the way scholarly research is managed. The grand vision of Frontiers is a world where all people have an equal opportunity to seek, share and generate knowledge. Frontiers provides immediate and permanent online open access to all its publications, but this alone is not enough to realize our grand goals.

## Frontiers journal series

The Frontiers journal series is a multi-tier and interdisciplinary set of open-access, online journals, promising a paradigm shift from the current review, selection and dissemination processes in academic publishing. All Frontiers journals are driven by researchers for researchers; therefore, they constitute a service to the scholarly community. At the same time, the *Frontiers journal series* operates on a revolutionary invention, the tiered publishing system, initially addressing specific communities of scholars, and gradually climbing up to broader public understanding, thus serving the interests of the lay society, too.

## Dedication to quality

Each Frontiers article is a landmark of the highest quality, thanks to genuinely collaborative interactions between authors and review editors, who include some of the world's best academicians. Research must be certified by peers before entering a stream of knowledge that may eventually reach the public - and shape society; therefore, Frontiers only applies the most rigorous and unbiased reviews. Frontiers revolutionizes research publishing by freely delivering the most outstanding research, evaluated with no bias from both the academic and social point of view. By applying the most advanced information technologies, Frontiers is catapulting scholarly publishing into a new generation.

## What are Frontiers Research Topics?

Frontiers Research Topics are very popular trademarks of the *Frontiers journals series*: they are collections of at least ten articles, all centered on a particular subject. With their unique mix of varied contributions from Original Research to Review Articles, Frontiers Research Topics unify the most influential researchers, the latest key findings and historical advances in a hot research area.

Find out more on how to host your own Frontiers Research Topic or contribute to one as an author by contacting the Frontiers editorial office: [frontiersin.org/about/contact](https://frontiersin.org/about/contact)

# Advances in the development and application of deep eutectic solvents

## Topic editors

Maria Luisa Di Gioia — University of Calabria, Italy

Manoj B. Gawande — Palacky University Olomouc, Olomouc, Czechia

Ana Rita Duarte — New University of Lisboa, Caparica, Portugal

## Citation

Di Gioia, M. L., Gawande, M. B., Duarte, A. R., eds. (2024). *Advances in the development and application of deep eutectic solvents*. Lausanne: Frontiers Media SA. doi: 10.3389/978-2-8325-4455-6

## Table of contents

- 04 **Editorial: Advances in the development and application of deep eutectic solvents**  
Maria Luisa Di Gioia, Ana Rita C. Duarte and Manoj B. Gawande
- 06 **Carbon Dioxide Solubility in Nonionic Deep Eutectic Solvents Containing Phenolic Alcohols**  
Ahmad Alhadid, Javid Safarov, Liudmila Mokrushina, Karsten Müller and Mirjana Minceva
- 14 **Natural Deep Eutectic Solvents Enhanced Electro-Enzymatic Conversion of CO<sub>2</sub> to Methanol**  
Zhibo Zhang, Hui Wang, Yi Nie, Xiangping Zhang and Xiaoyan Ji
- 22 **Extraction of Biocompatible Collagen From Blue Shark Skins Through the Conventional Extraction Process Intensification Using Natural Deep Eutectic Solvents**  
Miguel P. Batista, Naiara Fernández, Frédéric B. Gaspar, Maria do Rosário Bronze and Ana Rita C. Duarte
- 32 **Anthocyanic Vacuolar Inclusions: From Biosynthesis to Storage and Possible Applications**  
Kees Buhrman, Javiera Aravena-Calvo, Clara Ross Zaulich, Kasper Hinz and Tomas Laursen
- 41 **Green Synthesis of Thiazolidine-2,4-dione Derivatives and Their Lipxygenase Inhibition Activity With QSAR and Molecular Docking Studies**  
Melita Lončarić, Ivica Strelec, Valentina Pavić, Vesna Rastija, Maja Karnaš and Maja Molnar
- 56 **Investigation of carbon dioxide solubility in various families of deep eutectic solvents by the PC-SAFT EoS**  
Khalil Parvaneh, Reza Haghbakhsh, Ana Rita C. Duarte and Sona Raeissi
- 72 **Selective extraction and stabilization of bioactive compounds from rosemary leaves using a biphasic NADES**  
Carolina Vieira, Sílvia Rebocho, Rita Craveiro, Alexandre Paiva and Ana Rita C. Duarte
- 88 **Application of deep eutectic solvents in protein extraction and purification**  
Hou Bowen, Rabia Durrani, André Delavault, Erwann Durand, Jiang Chenyu, Long Yiyang, Song Lili, Song Jian, Huan Weiwei and Gao Fei
- 98 **MD simulations explain the excess molar enthalpies in pseudo-binary mixtures of a choline chloride-based deep eutectic solvent with water or methanol**  
Leon de Villiers Engelbrecht, Xiaoyan Ji, Carlo Maria Carbonaro, Aatto Laaksonen and Francesca Mocci





## OPEN ACCESS

EDITED AND REVIEWED BY  
James Clark,  
University of York, United Kingdom

## \*CORRESPONDENCE

Maria Luisa Di Gioia,  
✉ maria\_luisa.digioia@unical.it  
Ana Rita C. Duarte,  
✉ aduarte@fct.unl.pt  
Manoj B. Gawande,  
✉ mb.gawande@marj.ictmumbai.edu.in

RECEIVED 14 July 2023

ACCEPTED 21 July 2023

PUBLISHED 27 July 2023

## CITATION

Di Gioia ML, Duarte ARC and  
Gawande MB (2023), Editorial: Advances  
in the development and application of  
deep eutectic solvents.  
*Front. Chem.* 11:1258718.  
doi: 10.3389/fchem.2023.1258718

## COPYRIGHT

© 2023 Di Gioia, Duarte and Gawande.  
This is an open-access article distributed  
under the terms of the [Creative  
Commons Attribution License \(CC BY\)](#).  
The use, distribution or reproduction in  
other forums is permitted, provided the  
original author(s) and the copyright  
owner(s) are credited and that the original  
publication in this journal is cited, in  
accordance with accepted academic  
practice. No use, distribution or  
reproduction is permitted which does not  
comply with these terms.

# Editorial: Advances in the development and application of deep eutectic solvents

Maria Luisa Di Gioia<sup>1\*</sup>, Ana Rita C. Duarte<sup>2\*</sup> and  
Manoj B. Gawande<sup>3\*</sup>

<sup>1</sup>Department of Pharmacy, Health and Nutritional Sciences, University of Calabria, Arcavacata di Rende, Italy, <sup>2</sup>Nova School of Science and Technology, Faculty of Science and Technology, New University of Lisboa, Caparica, Portugal, <sup>3</sup>Department of Industrial and Engineering Chemistry, Institute of Chemical Technology, Jalna, Maharashtra, India

## KEYWORDS

green chemistry, reactive deep eutectic solvents, deep eutectic solvent (DES), green solvents, therapeutic deep eutectic solvents

## Editorial on the Research Topic

**Advances in the development and application of deep eutectic solvents**

## 1 Introduction

The discovery of deep eutectic solvents (DES) was a major breakthrough in green and sustainable chemistry. Notably, DES distinctive properties have increased their applications in different research areas, attracting attention as a means of achieving sustainable chemistry. DES are excellent solvents and/or catalysts used in organic synthesis, in extracting bioactive compounds from natural matrices, and in solubilizing gases.

The Research Topic “*Advances in the development and application of Deep Eutectic Solvents*,” comprehends a Research Topic of nine articles (seven original research papers, and two reviews), highlighting the most recent and relevant applications of DESs.

Nowadays, environmental issues and the energy crisis are some of the most important challenges faced by researchers. DESs physically dissolve gases, and are employed for gas capture and gas separation in various industries (Paludetto Pelaquim et al., 2021). Three of the published papers in the Research Topic dealing with this striking aspect. The proper choice of the hydrogen-bond donor as the constituent of the DES, is a fundamental issue in solubility of gas as it affects the absorption capacity. Alhadid et al. evaluate the feasibility of exploiting nonionic phenolic alcohols based DESs as solvents for carbon dioxide (CO<sub>2</sub>) capture applications. The nonionic DESs show higher stability and ability in terms of CO<sub>2</sub> solubility respect to ionic Liquids (ILs) and ionic DESs already proposed in the literature.

In order to assess the capability of DESs for such tasks, the thermodynamic modelling of CO<sub>2</sub> solubility in DESs has been pursued by several researchers. Parvaneh et al. investigate the performance of the Perturbed Chain- Statistical Associating Fluid Theory (PC-SAFT). The authors developed the largest data bank, up to date, of CO<sub>2</sub> solubility in DESs, consisting of 109 different DESs over wide ranges of temperatures and pressures. The work shows the PC-SAFT model to be very valuable for screening and feasibility studies to select potential DESs among the innumerable options today available.

The challenge of reduction greenhouse gas emissions can also be addressed through the conversion of CO<sub>2</sub> into high value-added chemicals or fuels. This recycling technology is presented by [Zhang et al.](#) which design four new kinds of natural deep eutectic solvents (NADES) to be employed as the co-electrolyte in converting CO<sub>2</sub> into methanol via electro-enzymatic processes. The serine and glycerol DES shows high CO<sub>2</sub> solubility, high electro-catalytic activity as well as high methanol production, resulting in a promising approach in the CO<sub>2</sub> capture research field.

Recently, a plethora of extraction techniques using NADES has arisen as eco-friendly alternatives to conventional extraction procedures, especially for the recovery of bioactive compounds from waste. The Research Topic includes three original research papers and one review dealing with this application. [Vieira et al.](#) provide an important contribution, suggesting the possibility of performing a fractionated extraction of bioactive compounds from rosemary waste, using a biphasic system composed by two immiscible DESs. Each phase of this system selectively extract the compounds of interest, selecting them by polarity. Another paper from [Batista et al.](#) focuses on the sustainable extraction of proteins from renewable sources. In particular, they propose a straightforward extraction approach using a citric acid:xylitol:water NADES for the recovery of biocompatible collagen from skin waste, resulting from the blue shark fishing industry. The procedure avoids any pre-treatment of the raw materials, and significantly improves the extraction yields, when compared to the traditional procedures.

The use of DESs as medium for protein extraction and purification is also addressed in the review by [Bowen et al.](#) DESs maintain the biological and/or functional activity of the extracted proteins, and improve their stability. Nevertheless, selection of hydrogen-bonding donor (HDB), the presence of water during DES formation, and the structure–function relationship existing between the extracted proteins and DESs should be taken into account.

In some cases, protein solubilization processes can be hindered by the DES viscosity which is mainly related to hydrogen bonds. The addition of cosolvents to choline chloride (ChCl)-based DESs is more and more investigated for reducing their high viscosities. [Engelbrecht et al.](#) contribute to the Research Topic with a manuscript reporting a computational investigation aiming to explain experimental observations made on excess molar enthalpies in pseudo-binary mixtures of a ChCl/ethylene glycol DES with water or methanol. The molecular dynamics simulation reveals an intriguing difference in the interaction modes of the two cosolvents with the DES chloride anion. As a result, they draw the conclusion that various intermolecular interactions in the resultant DES/cosolvent may favor one application over another. DESs are investigated also in organic synthesis where they find application as solvents, and often also as reagents and/or catalysts. In this context, the manuscript by [Lončarić et al.](#) reports on the synthesis of a particular class of pharmacologically active heterocyclic compounds, such as thiazolidine-2,4-dione derivatives, using DES that act as both

solvents and catalysts. The ChCl: *N*-methylurea DES affords the pure products in good to high yields via a simple precipitation by adding water. Most importantly, the recyclability of the system confirms the greenness of the procedure.

The second review published in this article Research Topic by [Buhrman et al.](#) aims to provide evidence and stimulate researchers to a more in-depth knowledge of the occurrence of NADES as a third liquid phase in living organisms as proposed for the first time by [Choi et al., \(2011\)](#). Their hypothesis was that NADES may play an important role in solubilizing, storing, and transporting poorly water-soluble metabolites in living cells, adjusting the water content of plants, and protecting cells when in harsh conditions ([Choi et al., 2011](#)). [Buhrman et al.](#) provide a critical and organized overview of all the data that supports the assumption that there is a link between accumulation of anthocyanin flavonoids in highly concentrated inclusions and the presence of NADES as an inert solvent. These types of mixtures could represent an important aspect of the natural environment in cells.

## Author contributions

MD: Conceptualization, Writing–original draft, Writing–review and editing. AD: Conceptualization, Writing–original draft, Writing–review and editing. MG: Conceptualization, Writing–original draft, Writing–review and editing.

## Acknowledgments

As Guest Editors, we would like to appreciate all the authors for their valuable contributions and the referees for their excellent work in reviewing the submitted manuscripts.

## Conflict of interest

The authors declare that the research was conducted in the absence of any commercial or financial relationships that could be construed as a potential conflict of interest.

## Publisher's note

All claims expressed in this article are solely those of the authors and do not necessarily represent those of their affiliated organizations, or those of the publisher, the editors and the reviewers. Any product that may be evaluated in this article, or claim that may be made by its manufacturer, is not guaranteed or endorsed by the publisher.

## References

- Choi, Y. H., van Spronsen, J., Dai, Y., Verberne, M., Hollmann, F., Arends, I. W., et al. (2011). Are natural deep eutectic solvents the missing link in understanding cellular metabolism and physiology? *Plant Physiol.* 156, 1701–1705. doi:10.1104/pp.111.178426
- Paludetto Pelaquim, F., Barbosa Neto, A. M., Lucini Dalmolin, I. A., and da Costa, M. C. (2021). Gas solubility using deep eutectic solvents: Review and analysis. *Ind. Eng. Chem. Res.* 60 (24), 8607–8620. doi:10.1021/acs.iecr.1c00947



# Carbon Dioxide Solubility in Nonionic Deep Eutectic Solvents Containing Phenolic Alcohols

Ahmad Alhadid<sup>1\*†</sup>, Javid Safarov<sup>2\*†</sup>, Liudmila Mokrushina<sup>3</sup>, Karsten Müller<sup>2</sup> and Mirjana Minceva<sup>1</sup>

<sup>1</sup>Biothermodynamics, TUM School of Life Sciences, Technical University of Munich (TUM), Freising, Germany, <sup>2</sup>Institute of Technical Thermodynamics, University of Rostock, Rostock, Germany, <sup>3</sup>Institute of Separation Science and Technology, Friedrich-Alexander-Universität Erlangen-Nürnberg (FAU), Erlangen, Germany

## OPEN ACCESS

### Edited by:

Manoj B. Gawande,  
Palacky University Olomouc, Czechia

### Reviewed by:

Andrea Mezzetta,  
University of Pisa, Italy  
Alessandro Triolo,  
Italian National Research Council, Italy

### \*Correspondence:

Ahmad Alhadid  
ahmad.alhadid@tum.de  
Javid Safarov  
javid.safarov@uni-rostock.de

<sup>†</sup>These authors have contributed  
equally to this work and share first  
authorship

### Specialty section:

This article was submitted to  
Green and Sustainable Chemistry,  
a section of the journal  
Frontiers in Chemistry

**Received:** 28 January 2022

**Accepted:** 08 March 2022

**Published:** 22 March 2022

### Citation:

Alhadid A, Safarov J, Mokrushina L,  
Müller K and Minceva M (2022) Carbon  
Dioxide Solubility in Nonionic Deep  
Eutectic Solvents Containing  
Phenolic Alcohols.  
Front. Chem. 10:864663.  
doi: 10.3389/fchem.2022.864663

Deep eutectic solvents (DES) are a new class of green solvents that have shown unique properties in several process applications. This study evaluates nonionic DES containing phenolic alcohols as solvents for carbon dioxide (CO<sub>2</sub>) capture applications. Potential phenolic alcohols and the molar ratio between DES constituents were preselected for experimental investigations based on the conductor-like screening model for realistic solvation (COSMO-RS). CO<sub>2</sub> solubility was experimentally determined in two different DES, namely, L-menthol/thymol in 1:2 molar ratio and thymol/2,6-xyleneol in 1:1 molar ratio, at various temperatures and pressures. CO<sub>2</sub> solubility in the studied systems was higher than that reported in the literature for ionic DES and ionic liquids. This study demonstrates that nonionic DES containing phenolic alcohols can be excellent, inexpensive, and simple solvents for CO<sub>2</sub> capture.

**Keywords:** CO<sub>2</sub> capture, COSMO-RS, ionic liquids, hydrophobic deep eutectic solvents, green solvents

## INTRODUCTION

An increasing relevance has developed in removing carbon dioxide (CO<sub>2</sub>) from gas mixtures, such as flue gas or biogas. Absorption in liquid solvents, in addition to membrane and absorption-based processes, is a major technology in this field. For many years, aqueous solutions of amines have been used for CO<sub>2</sub> absorption. However, they suffer from some drawbacks, such as high vapor pressure, which causes evaporation during solvent regeneration. Recently, ionic liquids (IL) have drawn attention for CO<sub>2</sub> capture application because of their negligible vapor pressure (Albo et al., 2010; Shiflett et al., 2010). Furthermore, the properties of IL can be tailored to the requirements of the specific application by combining different cations and anions (Jork et al., 2005). Although the hygroscopicity of IL can be overcome by using polymerized IL to prepare membranes for CO<sub>2</sub> capture applications (Kammakakam et al., 2020; Galiano et al., 2021), the issues of IL cost, instability, and purity remain (Sowmiah et al., 2009).

Nevertheless, owing to the aforementioned problems of IL, researchers have focused on an alternative solvent class that has some similarities to IL, while avoiding some of their drawbacks. Deep eutectic solvents (DES) are eutectic mixtures with a large depression in the eutectic temperature obtained by mixing a hydrogen bond acceptor and donor. DES are a new class of designer solvents, which can also be prepared by simple mixing of natural and nontoxic components, usually referred to as Natural DES (NADES) (Smith et al., 2014; van Osch et al., 2020). Similar to IL, physicochemical properties of DES can be tuned by selecting their constituents and additionally molar ratios of those. Moreover, DES are easier and less expensive to prepare compared to IL. Therefore, more attention is directed to their use in several process

**TABLE 1** | Prepared eutectic mixtures, their molar ratio, and water content.

Eutectic mixture	Mole ratio	Water content/ppm
L-menthol/thymol	1:2	144.2 ± 2.1
Thymol/2,6-xyleneol	1:1	108.4 ± 6.7

applications, for example, in liquid–liquid chromatography (Roehrer et al., 2016; Bezold and Minceva, 2019; Cai and Qiu, 2019), extraction of bioactive compounds (Kalthor and Ghandi, 2019; Makoš et al., 2020; Perna et al., 2020; Rodríguez-Llorente et al., 2020; Fernández et al., 2022), and crystallization (Emami and Shayanfar, 2020; Hall et al., 2020; Hamilton et al., 2020; Potticary et al., 2020).

CO<sub>2</sub> capture is one application that can benefit from DES. Existing studies have demonstrated the potential of DES for CO<sub>2</sub> capture (Krishnan et al., 2020; Song et al., 2020; Wazeer et al., 2021a; Wazeer et al., 2021b). However, most studies investigating CO<sub>2</sub> capture in DES proposed using ionic DES, which has the same drawbacks as those related to IL, especially in terms of hygroscopicity. Recently, hydrophobic DES based on natural and inexpensive nonionic constituents has attracted much attention (van Osch et al., 2019). Hydrophobic DES containing L-menthol possess outstanding properties, such as low viscosity and eutectic temperatures, especially when L-menthol is mixed with phenolic alcohols, such as thymol or carvacrol (Alhadid et al., 2020a; Alhadid et al., 2020b; Alhadid et al., 2021a; Alhadid et al., 2021b). Phenolic IL are good solvents for CO<sub>2</sub> capture applications (Vafaezadeh et al., 2015). Therefore, hydrophobic DES containing phenolic alcohols are assumed to be promising candidates for CO<sub>2</sub> capture applications.

Nevertheless, the large pool of substances that can form DES can make selecting the DES constituents challenging. Furthermore, the ratio between the constituents can be tuned, which is an additional degree of freedom during the selection of DES constituents. Therefore, a predictive screening method could noticeably assist in preselecting DES constituents for CO<sub>2</sub> capture applications. The conductor-like screening model for realistic solvation (COSMO-RS) is a predictive thermodynamic model based on quantum mechanics and statistical thermodynamics (Klamt, 1995; Klamt et al., 1998; Eckert and Klamt, 2002). COSMO-RS successfully provides qualitative predictions for screening IL and ionic DES for gas capture applications (Völkl et al., 2012; Song et al., 2020; Liu et al., 2021; Qin et al., 2021).

This study investigates nonionic DES containing phenolic alcohols as potential solvents for CO<sub>2</sub> capture. COSMO-RS was used to screen a list of possible DES containing L-menthol and phenolic alcohols to preselect those with the highest CO<sub>2</sub> solubility. Further, CO<sub>2</sub> solubility was experimentally investigated for selected DES systems at various temperatures and pressures using an isochoric method.

## MATERIALS AND METHODS

### Eutectic Mixture Preparation

Pure components (L-menthol, purity ≥99%, Sigma Aldrich; thymol, purity ≥99%, Sigma Aldrich; 2,6-xyleneol, purity 99%,

Acros Organics), was mixed under continuous stirring and gentle heating until a clear homogenous liquid was formed. The water content of the prepared eutectic mixtures was measured in triplicate using Karl Fischer Coulometer (Hanna Instrument, United States), and the results are shown in **Table 1**.

### Carbon Dioxide Solubility Experiments

Before measurements, DES were degassed under vacuum for 48 h at a temperature of  $T = 413.15$  K. After degassing, no mass loss was observed for the DES, indicating that there was no change in the stoichiometry between constituents and their negligible volatility under the experimental conditions. CO<sub>2</sub> from Westfalen AG, Germany, with a purity of 99.995% (quality 4.5), was used without further purification. The experiments were performed using a pressure-drop isochoric method at various temperatures and pressures. The apparatus and operational procedures of solubility measurements are described in detail in previous studies (Safarov et al., 2013; Safarov et al., 2014). For the current measurements, the installation was used without modification. The temperature in the measuring cell was held constant (at  $T = 293.15$ – $323.15$  K) with an uncertainty of  $u(T) = 0.030$  K. A pressure transducer with an accuracy of 0.1% was used to measure the pressure of CO<sub>2</sub> filled in the gas reservoir. The temperature inside the gas reservoir was measured with an uncertainty of  $u(T) = 0.015$  K. The initial amount of CO<sub>2</sub> in the gas reservoir was determined from its pressure and temperature using the Span and Wagner equation of state (Span and Wagner, 1996).

To determine the concentration of CO<sub>2</sub> in the solution, liquid and gas densities under experimental temperature and pressure were required. The density of DES was measured using a density meter (Density meter Easy D40, Mettler-Toledo GmbH, Germany), and the results are indicated in **Table 2**. The mass of CO<sub>2</sub> in the gas phase was calculated using its density and volume. The gas volume in the cell was found by deducting the liquid volume from the total cell volume. The increase in the liquid volume because of dissolved CO<sub>2</sub> was neglected (Safarov et al., 2013).

### Correlation of the Gas Solubility

Henry's law for a binary system (liquid + CO<sub>2</sub>) for a non-ideal gas phase can be given as (Prausnitz and Shair, 1961)

$$y_{\text{CO}_2} \cdot \phi_{\text{CO}_2}(T, p) \cdot p = x_{\text{CO}_2} \cdot H_{\text{CO}_2} \quad (1)$$

**TABLE 2** | Density of eutectic mixtures measured in this work<sup>a</sup>.

$T/\text{K}$	$\rho/\text{kg m}^{-3}$	
	L-menthol/thymol (1:2)	Thymol/2,6-xyleneol (1:1)
293.15	947.6	992.2
303.15	940.0	983.9
313.15	932.5	975.6
323.15	924.8	967.2

<sup>a</sup>Standard uncertainty  $u(\rho) = 0.05 \text{ kg m}^{-3}$

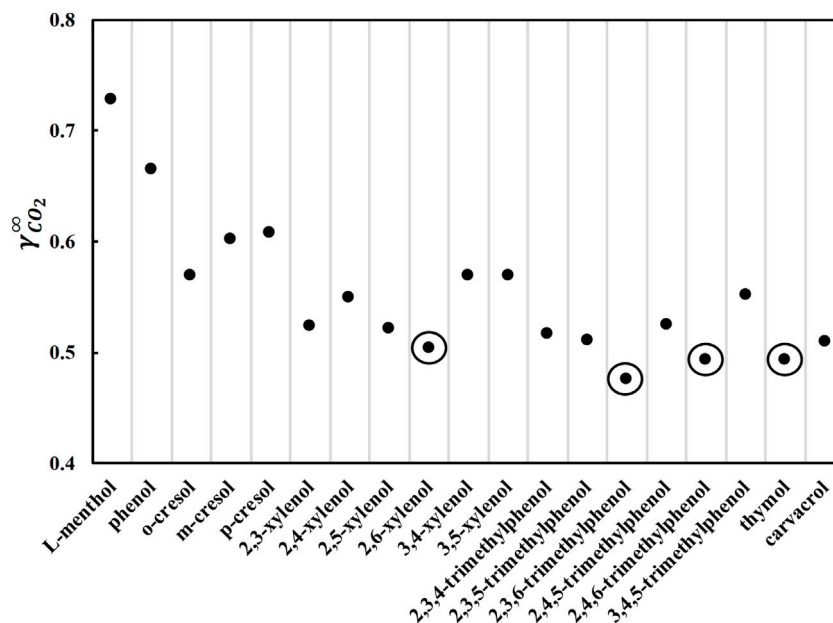


**FIGURE 1** | Activity coefficients at infinite dilution of carbon dioxide in pure L-menthol and various phenolic alcohols at 293.15 K calculated by COSMO-RS.

**TABLE 3** | Experimental carbon dioxide (CO<sub>2</sub>) solubility (both in weight percent  $w_{\text{CO}_2}$  and in mole fraction  $x_{\text{CO}_2}$ ) in the L-menthol/thymol (MTH) eutectic system and calculated CO<sub>2</sub> fugacity coefficient ( $\phi_{\text{CO}_2}$ ) at various temperatures T and pressures p.<sup>a</sup>

T/K	p/MPa	$w_{\text{CO}_2}$ , %	$x_{\text{CO}_2}$ /Mole fraction	$\phi_{\text{CO}_2}$ <sup>b</sup>
323.11	4.1939	11.410	0.3082	0.8453
313.12	4.1543	12.090	0.3224	0.8295
303.18	4.0967	13.409	0.3488	0.8121
293.15	4.0201	15.769	0.3931	0.7931
323.15	3.5059	9.290	0.2616	0.8701
313.16	3.4703	10.173	0.2815	0.8570
303.13	3.4247	11.780	0.3159	0.8426
293.13	3.3691	13.335	0.3474	0.8265
323.14	2.5790	7.090	0.2088	0.9039
313.18	2.5541	7.615	0.2219	0.8942
303.13	2.5229	8.347	0.2395	0.8835
293.14	2.4860	9.297	0.2617	0.8716
323.02	1.6819	4.644	0.1442	0.9369
313.18	1.6662	5.027	0.1547	0.9305
302.98	1.6478	5.436	0.1659	0.9235
293.15	1.6281	5.937	0.1792	0.9155

<sup>a</sup>Standard uncertainties  $u$  are:  $u(T) = 0.030$  K,  $u(p) = 0.1\%$ ,  $u(w) = 0.01$  wt%, and  $u(x) = 0.0001$  mol fraction.

<sup>b</sup>Calculated using the Span and Wagner equation of state (Span and Wagner, 1996) implemented in ThermoFluids (Springer, V. 1.0).

where  $y_{\text{CO}_2}$  and  $x_{\text{CO}_2}$  are the mole fraction of CO<sub>2</sub> in the gas and liquid phases, respectively;  $\phi_{\text{CO}_2}$  is the fugacity coefficient of CO<sub>2</sub> in the gas phase, and  $H_{\text{CO}_2}$  is Henry's constant. Due to the negligible vapor pressure of the studied eutectic mixtures at studied temperatures (Xin et al., 2021) (see also **Supplementary Table S1** in **Supplementary Material** for calculations), the gas phase can be assumed as pure CO<sub>2</sub>, i.e.,  $y_{\text{CO}_2} = 1$  (see also **Supplementary Table S1** in

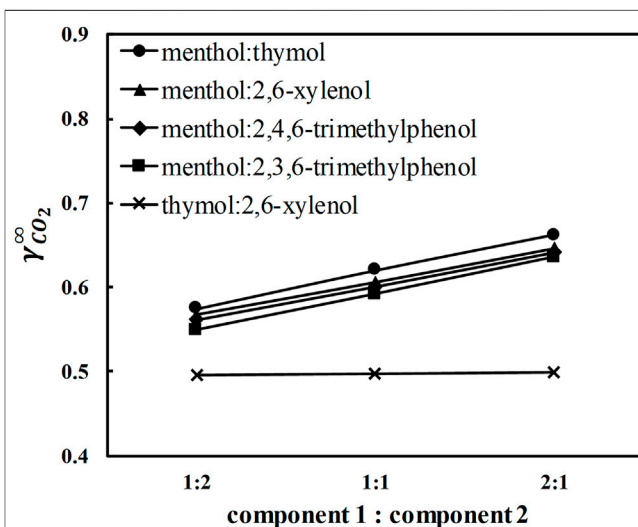


**FIGURE 2** | Activity coefficients at infinite dilution of carbon dioxide in selected eutectic mixtures at 293.15 K calculated by COSMO-RS.

**Supplementary Material** for calculations). Henry's constant can be defined using the following equation.

$$H_{\text{CO}_2} = \lim_{p \rightarrow 0} \left[ \frac{\phi_{\text{CO}_2}(T, p) \cdot p}{x_{\text{CO}_2}} \right] \quad (2)$$

## COSMO-RS Calculations

The solubility of CO<sub>2</sub> in eutectic mixtures was screened a priori by evaluating CO<sub>2</sub> activity coefficients at infinite dilution. The



**TABLE 4 |** Experimental carbon dioxide (CO<sub>2</sub>) solubility (both in weight percent  $w_{\text{CO}_2}$  and in mole fraction  $x_{\text{CO}_2}$ ) in the thymol/2,6-xyleneol (T26X) eutectic system and CO<sub>2</sub> calculated fugacity coefficient ( $\phi_{\text{CO}_2}$ ) at various temperatures T and pressures p.<sup>a</sup>

T/K	p/MPa	$w_{\text{CO}_2}$ , %	$x_{\text{CO}_2}$ /Mole fraction	$\phi_{\text{CO}_2}$ <sup>b</sup>
322.90	4.0853	11.549	0.2878	0.8492
313.13	4.0441	12.563	0.3078	0.8339
303.17	3.9840	14.856	0.3506	0.8172
293.22	3.9057	17.093	0.3895	0.7990
323.14	3.3380	9.512	0.2455	0.8762
313.15	3.3029	10.417	0.2646	0.8638
303.13	3.2563	11.456	0.2859	0.8502
293.14	3.1988	13.073	0.3176	0.8352
323.13	2.6988	7.477	0.2000	0.8995
313.15	2.6696	8.022	0.2125	0.8895
303.16	2.6344	9.205	0.2388	0.8784
293.15	2.5932	10.284	0.2619	0.8661
323.14	1.6670	4.462	0.1263	0.9375
313.15	1.6500	4.909	0.1377	0.9313
303.16	1.6300	5.398	0.1501	0.9243
293.15	1.6070	6.057	0.1663	0.9166

<sup>a</sup>Standard uncertainties  $u$  are:  $u(T) = 0.030$  K,  $u(p) = 0.1\%$ ,  $u(w) = 0.01$  wt%, and  $u(x) = 0.0001$  mol fraction.

<sup>b</sup>Calculated using the Span and Wagner equation of state (Span and Wagner, 1996) implemented in ThermoFluids (Springer, V. 1.0).

activity coefficients of CO<sub>2</sub> at infinite dilution in different pure constituents and eutectic mixtures were calculated using the COSMO-RS model (BIOVIA COSMOtherm X19, Dassault Systèmes) and BP\_TZVP\_19. ctd parameters. Molecular conformations of components were obtained using BIOVIA COSMOconf 17 (Dassault Systèmes). The geometry optimization and screening charge density were determined by density functional theory calculations using BP86 functional and def-TZVP basis set by Turbomole version 6.6 (TURBOMOLE GmbH).

## RESULTS AND DISCUSSION

### Screening With COSMO-RS

To enable the usage of a DES in CO<sub>2</sub> capture applications, the DES should 1) be liquid in the appropriate temperature range, i.e., approximately room temperature; and 2) be a good solvent for CO<sub>2</sub>. A number of nonionic DES containing phenolic alcohols can satisfy these two criteria. The phenolic alcohols considered in this study are phenol, methylphenols (cresols), dimethylphenols (xylenols), trimethylphenols, and two natural phenolic terpenes, thymol (2-isopropyl-5-methylphenol) and carvacrol (5-isopropyl-2-methylphenol). Phenolic alcohols with higher molecular weights or dihydroxy benzenes were not considered because they are not expected to form liquid DES at room temperature because of their high melting temperature and enthalpy (Alhadid et al., 2019). When phenolic alcohols are mixed with L-menthol, a significant negative deviation from the ideal behavior is expected (Alhadid et al., 2020b; Alhadid et al., 2021a). The negative deviation from the ideal behavior results in the formation of DES with a sufficiently low melting temperature. Thus, it is desirable to have L-menthol as a DES

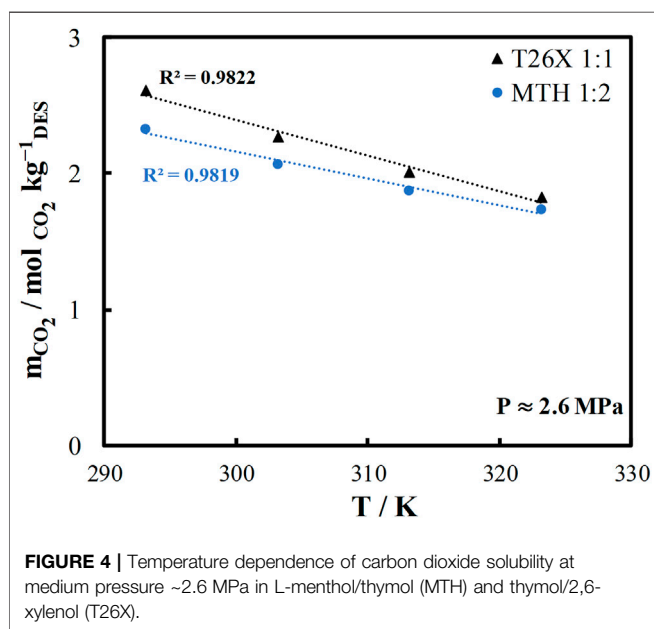
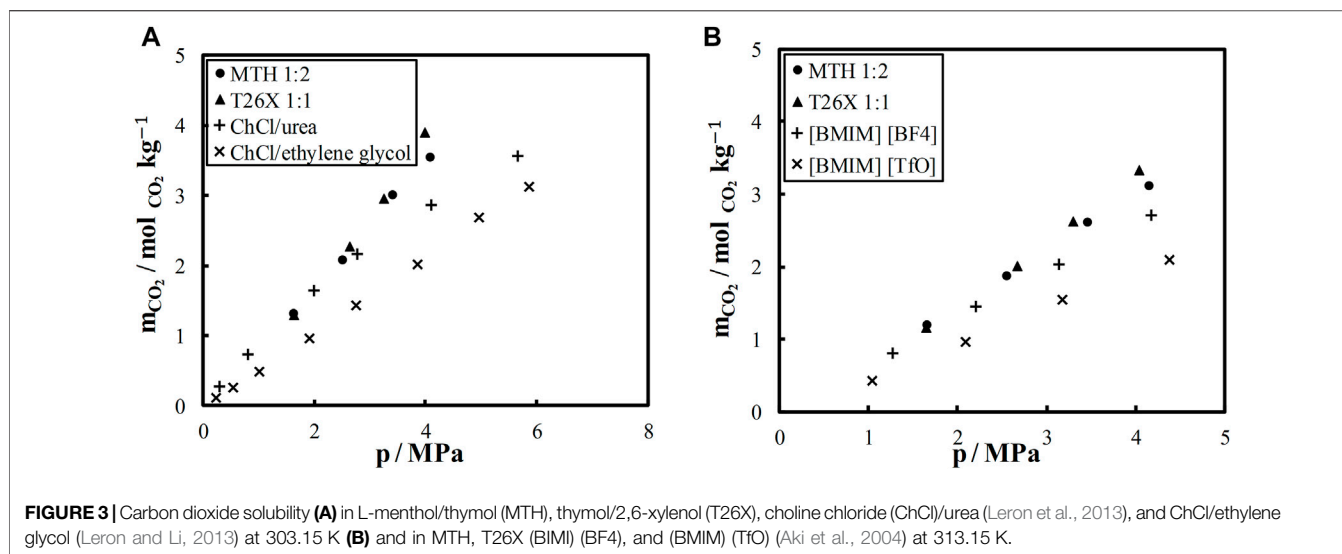
**TABLE 5 |** Calculated carbon dioxide Henry's constant ( $H_{\text{CO}_2}$ ) in the studied systems.

T/K	$H_{\text{CO}_2}$ /MPa	
	L-menthol/thymol (1:2)	Thymol/2,6-xyleneol (1:1)
293.15	8.52 ± 0.13	9.45 ± 0.32
303.15	8.98 ± 0.13	10.45 ± 0.23
313.15	9.61 ± 0.25	11.46 ± 0.15
323.15	10.51 ± 0.30	12.52 ± 0.17

constituent. First, the activity coefficients of CO<sub>2</sub> at infinite dilution were calculated using COSMO-RS in pure constituents at 293.15 K because the physicochemical properties of pure constituents influence the physicochemical properties of DES (Alhadid et al., 2021b), and the results are shown in **Figure 1**. As COSMO-RS is based on quantum mechanical calculations, the calculated activity coefficients implicitly include the atomistic rationalization and quantify the intermolecular interactions between CO<sub>2</sub> and the constituents in the liquid phase. The low CO<sub>2</sub> activity coefficient values indicate strong intermolecular interactions between CO<sub>2</sub> and the constituents and, accordingly, high CO<sub>2</sub> solubility. The calculated CO<sub>2</sub> activity coefficients in all phenolic alcohols are lower than in L-menthol (cyclohexyl alcohol) (**Figure 1**), proving that CO<sub>2</sub> solubility is relatively high in phenolic alcohols.

**Figure 1** shows that the limiting activity coefficients decrease with the addition of methyl groups to phenolic alcohols. The general order of the CO<sub>2</sub> activity coefficients in phenolic alcohols is phenol > methylphenol (cresol) > dimethylphenol (xyleneol) > trimethylphenols. Furthermore, compared to thymol and carvacrol, substituting a methyl group with an isopropyl group, i.e., 2,5-xyleneol, decreases CO<sub>2</sub> limiting activity coefficients. By comparing different isomers, the limiting activity coefficients are lower in isomers with methyl groups at position 2, i.e., close to the hydroxyl group. Furthermore, the lowest values of CO<sub>2</sub> activity coefficients are observed in dimethyl and trimethyl isomers with a methyl group on the two and six positions, respectively. The CO<sub>2</sub> activity coefficient in thymol is lower than that in carvacrol, as the isopropyl group is nearer to the hydroxyl group in thymol than to carvacrol. Therefore, the structure of the phenolic alcohol influences CO<sub>2</sub> solubility. The four marked phenolic alcohols with the lowest limiting activity coefficient values in CO<sub>2</sub> were considered potential DES constituents for further screening.

Further, potential DES containing L-menthol with 2,6-xyleneol, thymol, 2,3,6-trimethylphenol, and 2,4,6-trimethylphenol were screened using COSMO-RS. The calculated activity coefficients of CO<sub>2</sub> at infinite dilution in five different DES and ratios between the constituents at 293.15 K are shown in **Figure 2**. CO<sub>2</sub> activity coefficients in L-menthol-based DES at any molar ratio are in the order L-menthol:thymol (MTH) > L-menthol:2,6-xyleneol (M26X) > L-menthol:2,4,6-trimethylphenol (M246) > L-menthol:2,3,6-trimethylphenol (M236) (**Figure 2**), which is consistent with the order of CO<sub>2</sub> activity coefficients in the pure phenolic alcohols present in the DES (see **Figure 1**).



Moreover, increasing the molar ratio of the phenolic alcohol to L-menthol decreases CO<sub>2</sub> activity coefficients. Therefore, it is logical to select L-menthol-based DES containing trimethylphenols in a 1:2 ratio between the constituents as potential solvents for CO<sub>2</sub> capture. However, melting properties of pure constituents influence the melting temperature of the DES (Alhadid et al., 2019). M236 and M246 in 1:2 ratio are solid at room temperature, which is attributed to the high melting temperature of 2,3,6- and 2,4,6-trimethylphenols ( $T_m = 331.2$  and  $342.15 \text{ K}$ , respectively) (Verevkin, 1999). MTH and M26X in 1:2 ratio are liquid at room temperature (Alhadid et al., 2021a), which indicates that both can be considered for further experimental investigation. CO<sub>2</sub> activity coefficients in MTH and M26X at 1:2 ratio are of

similar values (Figure 2). However, MTH is considered a better option because of the low toxicity of thymol compared to 2,6-xyleneol. Therefore, MTH was chosen for measurements.

Next, eutectic mixtures containing two phenolic alcohols were considered. These eutectic mixtures are expected to show ideal solution behavior with no significant decrease in the melting temperature of the mixture relative to pure constituents (Alhadid et al., 2019). For such mixtures, the melting temperature of the DES at any ratio between constituents can be obtained from the solid-liquid phase diagram based on the pure constituent melting properties. A brief explanation of solid-liquid equilibrium calculations is given in the **Supplementary Material**. Based on the ideal solution model calculations, thymol: 2,6-xyleneol (T26X) eutectic system should form a liquid mixture at room temperature. The calculated eutectic composition and temperature for T26X are  $x_{e,\text{thymol}} = 0.46$ , and  $T_e = 292.8 \text{ K}$ , respectively (see **Supplementary Material** for details about the calculations). Altering the ratio between constituents in T26X does not influence CO<sub>2</sub> activity coefficients (Figure 2), in contrast to what is observed in L-menthol-based DES. Thus, the molar ratio close to the eutectic ratio of the T26X system ( $\sim 1:1$  ratio) was selected to ensure that the mixture is liquid at room temperature. Eventually, the two DES, MTH in 1:2 ratio, and T26X in 1:1 ratio were selected for the solubility measurements.

## Experimental Solubility

CO<sub>2</sub> solubility in the two DES was measured based on the pressure-drop isochoric method at four different pressures ( $\sim 4$ ,  $3$ ,  $2$ , and  $1 \text{ MPa}$ ) and four different temperatures ( $293.15$ ,  $303.15$ ,  $313.15$ , and  $323.15 \text{ K}$ ). The CO<sub>2</sub> solubility in weight percentage ( $w_{\text{CO}_2}$ ) and mole fraction ( $x_{\text{CO}_2}$ ), as well as its fugacity coefficient ( $\phi_{\text{CO}_2}$ ) calculated using Span and Wagner equation of state for the MTH and T26X system are shown in **Tables 3, 4**, respectively. The values of Henry's constant at different temperatures calculated using Eq. 2 are shown in **Table 5**. As one would expect, the solubility of CO<sub>2</sub> in the two studied systems decreases as temperature increases.

Further, the CO<sub>2</sub> solubility in the studied DES was compared with that in some ionic DES and IL reported in the literature. The comparison was made in terms of molality, i.e., moles of CO<sub>2</sub> absorbed per mass of solvent. The results are shown in **Figure 3**. CO<sub>2</sub> solubility at 303.15 K in two ionic DES, namely, choline chloride (ChCl)/urea and ChCl/ethylene glycol in 1:2 molar ratio, is compared with the two DES from this study in **Figure 3A**. As seen, CO<sub>2</sub> solubility is significantly higher in nonionic DES than in ionic DES, especially at high pressures (**Figure 3A**). The CO<sub>2</sub> solubility in MTH and T26X is also higher than in the two IL (BMIM) (BF<sub>4</sub>) and (BMIM) (TfO), as shown in **Figure 3B**. In addition to good CO<sub>2</sub> solubility, nonionic DES are more stable, less hygroscopic, and less expensive than IL and ionic DES.

The solvent capacity to absorb CO<sub>2</sub> is not the only selection criterion to consider when selecting a solvent for CO<sub>2</sub> capture applications. The temperature dependence of CO<sub>2</sub> solubility is critical as well because CO<sub>2</sub> should be absorbed with high solubility and desorbed from the solvent at a higher temperature for solvent regeneration. Thus, a strong temperature dependence is required for CO<sub>2</sub> solubility to reduce the energy demand for desorption. The temperature dependence of CO<sub>2</sub> solubility in the two DES being studied is shown in **Figure 4**. The T26X system shows a slightly higher CO<sub>2</sub> solubility than the MTH system. Furthermore, the T26X system has a stronger temperature dependence. Therefore, the T26X system can be identified as a very promising candidate for CO<sub>2</sub> capture applications.

## CONCLUSION

This study examines the use of nonionic DES for CO<sub>2</sub> capture applications. DES were designed to contain phenolic alcohols for improving CO<sub>2</sub> solubility and L-menthol to decrease the melting temperature of the DES. COSMO-RS was used to preselect the DES constituents from a pool of possible phenolic alcohols and to tune the molar ratio between the constituents. It was found that the structure of phenolic alcohols can influence CO<sub>2</sub> solubility. Furthermore, increasing the phenolic alcohol molar content in the DES can enhance the CO<sub>2</sub> solubility. However, the selection of the constituents and their molar ratio was restricted by the melting temperature of the DES. The COSMO-RS screening results identified two potential DES: MTH in 1:2 molar ratio and T26X in 1:1 molar ratio.

## REFERENCES

- Aki, S. N. V. K., Mellein, B. R., Saurer, E. M., and Brennecke, J. F. (2004). High-Pressure Phase Behavior of Carbon Dioxide with Imidazolium-Based Ionic Liquids. *J. Phys. Chem. B* 108 (52), 20355–20365. doi:10.1021/jp046895+
- Albo, J., Luis, P., and Iribien, A. (2010). Carbon Dioxide Capture from Flue Gases Using a Cross-Flow Membrane Contactor and the Ionic Liquid 1-Ethyl-3-Methylimidazolium Ethylsulfate. *Ind. Eng. Chem. Res.* 49 (21), 11045–11051. doi:10.1021/ie1014266
- Alhadid, A., Jandl, C., Mokrushina, L., and Minceva, M. (2021a). Experimental Investigation and Modeling of Cocrystal Formation in L-Menthol/Thymol Eutectic System. *Cryst. Growth Des.* 21 (11), 6083–6091. doi:10.1021/acs.cgd.1c00306

In the two preselected DES, the CO<sub>2</sub> solubility was studied experimentally using a pressure-drop isochoric method at various temperatures and pressures. The high experimentally determined CO<sub>2</sub> solubility in the two DES validated the COSMO-RS preselection, demonstrating the model's advantage as a screening tool. CO<sub>2</sub> solubility in the DES proposed in this study is significantly higher than in ionic DES and IL proposed in the literature. Furthermore, the temperature dependence of CO<sub>2</sub> solubility in DES proves their suitability for CO<sub>2</sub> capture applications. The high solubility of CO<sub>2</sub> at lower temperatures and its high decrease at higher temperatures make the two DES promising candidates for CO<sub>2</sub> capture. This study shows that simple and widely available organic substances can be used to form novel solvents with unique properties.

## DATA AVAILABILITY STATEMENT

The original contributions presented in the study are included in the article/**Supplementary Material**, further inquiries can be directed to the corresponding authors.

## AUTHOR CONTRIBUTIONS

Conceptualization: AA; Investigation: AA and JS; Formal Analysis: AA, JS, and LM; Writing–Original Draft: AA and JS; Writing–Review and Editing: LM, KM, and MM; Supervision: KM and MM.

## FUNDING

This work was supported by the German Research Foundation (DFG) and the Technical University of Munich (TUM) in the framework of the Open Access Publishing Program.

## SUPPLEMENTARY MATERIAL

The Supplementary Material for this article can be found online at: <https://www.frontiersin.org/articles/10.3389/fchem.2022.864663/full#supplementary-material>

- Alhadid, A., Mokrushina, L., and Minceva, M. (2020a). Design of Deep Eutectic Systems: A Simple Approach for Preselecting Eutectic Mixture Constituents. *Molecules* 25 (5), 1077. doi:10.3390/molecules25051077
- Alhadid, A., Mokrushina, L., and Minceva, M. (2020b). Formation of Glassy Phases and Polymorphism in Deep Eutectic Solvents. *J. Mol. Liquids* 314, 113667. doi:10.1016/j.molliq.2020.113667
- Alhadid, A., Mokrushina, L., and Minceva, M. (2021b). Influence of the Molecular Structure of Constituents and Liquid Phase Non-ideality on the Viscosity of Deep Eutectic Solvents. *Molecules* 26 (14), 4208. doi:10.3390/molecules26144208
- Alhadid, A., Mokrushina, L., and Minceva, M. (2019). Modeling of Solid-Liquid Equilibria in Deep Eutectic Solvents: A Parameter Study. *Molecules* 24 (12), 2334. doi:10.3390/molecules24122334



- Bezold, F., and Minceva, M. (2019). A Water-free Solvent System Containing an L-Menthol-Based Deep Eutectic Solvent for Centrifugal Partition Chromatography Applications. *J. Chromatogr. A* 1587, 166–171. doi:10.1016/j.chroma.2018.11.083
- Cai, T., and Qiu, H. (2019). Application of Deep Eutectic Solvents in Chromatography: A Review. *Trac Trends Anal. Chem.* 120, 115623. doi:10.1016/j.trac.2019.115623
- Eckert, F., and Klamt, A. (2002). Fast Solvent Screening via Quantum Chemistry: COSMO-RS Approach. *Aiche J.* 48 (2), 369–385. doi:10.1002/aic.690480220
- Emami, S., and Shayanfar, A. (2020). Deep Eutectic Solvents for Pharmaceutical Formulation and Drug Delivery Applications. *Pharm. Develop. Techn.* 25 (7), 779–796. doi:10.1080/10837450.2020.1735414
- Fernández, A., Longo, M. A., Deive, F. J., Álvarez, M. S., and Rodríguez, A. (2021). Effective Lipase Extraction: Designing a Natural Liquid Support for Immobilization. *Separat. Purif. Techn.* 278, 119601. doi:10.1016/j.seppur.2021.119601
- Galiano, F., Mancuso, R., Guazzelli, L., Mauri, M., Chiappe, C., Simonutti, R., et al. (2021). Phosphonium Ionic Liquid-Polyacrylate Copolymer Membranes for Improved CO<sub>2</sub> Separations. *J. Membr. Sci.* 635, 119479. doi:10.1016/j.memsci.2021.119479
- Hall, C. L., Potticary, J., Hamilton, V., Gaisford, S., Buanz, A., and Hall, S. R. (2020). Metastable Crystalline Phase Formation in Deep Eutectic Systems Revealed by Simultaneous Synchrotron XRD and DSC. *Chem. Commun.* 56 (73), 10726–10729. doi:10.1039/d0cc04696e
- Hamilton, V., Andrusenko, I., Potticary, J., Hall, C., Stenner, R., Mugnaioli, E., et al. (2020). Racemic Conglomerate Formation via Crystallization of Metaxalone from Volatile Deep Eutectic Solvents. *Cryst. Growth Des.* 20 (7), 4731–4739. doi:10.1021/acs.cgd.0c00497
- Jork, C., Kristen, C., Pieraccini, D., Stark, A., Chiappe, C., Beste, Y. A., et al. (2005). Tailor-made Ionic Liquids. *The J. Chem. Thermodynamics* 37 (6), 537–558. doi:10.1016/j.jct.2005.04.013
- Kalhor, P., and Ghandi, K. (2019). Deep Eutectic Solvents for Pretreatment, Extraction, and Catalysis of Biomass and Food Waste. *Molecules* 24 (22), 4012. doi:10.3390/molecules24224012
- Kammakakam, I., Bara, J. E., Jackson, E. M., Lertxundi, J., Mecerreyes, D., and Tomé, L. C. (2020). Tailored CO<sub>2</sub>-Philic Anionic Poly(ionic Liquid) Composite Membranes: Synthesis, Characterization, and Gas Transport Properties. *ACS Sustain. Chem. Eng.* 8 (15), 5954–5965. doi:10.1021/acsschemeng.0c00327
- Klamt, A. (1995). Conductor-like Screening Model for Real Solvents: A New Approach to the Quantitative Calculation of Solvation Phenomena. *J. Phys. Chem.* 99 (7), 2224–2235. doi:10.1021/j100007a062
- Klamt, A., Jonas, V., Bürger, T., and Lohrenz, J. C. W. (1998). Refinement and Parametrization of COSMO-RS. *J. Phys. Chem. A* 102 (26), 5074–5085. doi:10.1021/jp980017s
- Krishnan, A., Gopinath, K. P., Vo, D.-V. N., Malolan, R., Nagarajan, V. M., and Arun, J. (2020). Ionic Liquids, Deep Eutectic Solvents and Liquid Polymers as Green Solvents in Carbon Capture Technologies: A Review. *Environ. Chem. Lett.* 18 (6), 2031–2054. doi:10.1007/s10311-020-01057-y
- Leron, R. B., and Li, M. H. (2013). Solubility of carbon dioxide in a choline chloride-ethylene glycol based deep eutectic solvent. *Thermochimica Acta* 551, 14–19. doi:10.1016/j.tca.2012.09.041
- Leron, R. B., Caparanga, A., and Li, M. H. (2013). Carbon Dioxide Solubility in a Deep Eutectic Solvent Based on Choline Chloride and urea at T = 303.15–343.15 K and Moderate Pressures. *J. Taiwan Inst. Chem. Eng.* 44 (6), 879–885. doi:10.1016/j.tca.2012.09.041
- Liu, Y., Dai, Z., Zhang, Z., Zeng, S., Li, F., Zhang, X., et al. (2021). Ionic Liquids/deep Eutectic Solvents for CO<sub>2</sub> Capture: Reviewing and Evaluating. *Green. Energ. Environ.* 6 (3), 314–328. doi:10.1016/j.gee.2020.11.024
- Makoš, P., Slupek, E., and Gebicki, J. (2020). Hydrophobic Deep Eutectic Solvents in Microextraction Techniques-A Review. *Microchemical J.* 152, 104384. doi:10.1016/j.microc.2019.104384
- Perna, F. M., Vitale, P., and Capriati, V. (2020). Deep Eutectic Solvents and Their Applications as Green Solvents. *Curr. Opin. Green Sustain. Chem.* 21, 27–33. doi:10.1016/j.cogsc.2019.09.004
- Potticary, J., Hall, C., Hamilton, V., McCabe, J. F., and Hall, S. R. (2020). Crystallization from Volatile Deep Eutectic Solvents. *Cryst. Growth Des.* 20 (5), 2877–2884. doi:10.1021/acs.cgd.0c00399
- Prausnitz, J. M., and Shair, F. H. (1961). A Thermodynamic Correlation of Gas Solubilities. *Aiche J.* 7 (4), 682–687. doi:10.1002/aic.690070430
- Qin, H., Wang, Z., Zhou, T., and Song, Z. (2021). Comprehensive Evaluation of COSMO-RS for Predicting Ternary and Binary Ionic Liquid-Containing Vapor-Liquid Equilibria. *Ind. Eng. Chem. Res.* 60 (48), 17761–17777. doi:10.1021/acs.iecr.1c03940
- Rodríguez-Llorente, D., Cañada-Barcala, A., Álvarez-Torrellas, S., Águeda, V. I., García, J., and Larriba, M. (2020). A Review of the Use of Eutectic Solvents, Terpenes and Terpenoids in Liquid-Liquid Extraction Processes. *Processes* 8 (10), 1220. doi:10.3390/pr8101220
- Roehrer, S., Bezold, F., García, E. M., and Minceva, M. (2016). Deep Eutectic Solvents in Countercurrent and Centrifugal Partition Chromatography. *J. Chromatogr. A* 1434, 102–110. doi:10.1016/j.chroma.2016.01.024
- Safarov, J., Hamidova, R., Stephan, M., Kul, I., Shahverdiyev, A., and Hassel, E. (2014). Carbon Dioxide Solubility in 1-Hexyl-3-Methylimidazolium Bis(trifluoromethylsulfonyl)imide in a Wide Range of Temperatures and Pressures. *J. Phys. Chem. B* 118 (24), 6829–6838. doi:10.1021/jp5012044
- Safarov, J., Hamidova, R., Stephan, M., Schmotz, N., Kul, I., Shahverdiyev, A., et al. (2013). Carbon Dioxide Solubility in 1-Butyl-3-Methylimidazolium-Bis(trifluoromethylsulfonyl)imide over a Wide Range of Temperatures and Pressures. *J. Chem. Thermodynamics* 67, 181–189. doi:10.1016/j.jct.2013.08.008
- Shiflett, M. B., Drew, D. W., Cantini, R. A., and Yokozeki, A. (2010). Carbon Dioxide Capture Using Ionic Liquid 1-Butyl-3-Methylimidazolium Acetate. *Energy Fuels* 24 (10), 5781–5789. doi:10.1021/ef100868a
- Smith, E. L., Abbott, A. P., and Ryder, K. S. (2014). Deep Eutectic Solvents (DESs) and Their Applications. *Chem. Rev.* 114, 11060–11082. doi:10.1021/cr300162p
- Song, Z., Hu, X., Wu, H., Mei, M., Linke, S., Zhou, T., et al. (2020). Systematic Screening of Deep Eutectic Solvents as Sustainable Separation Media Exemplified by the CO<sub>2</sub> Capture Process. *ACS Sustain. Chem. Eng.* 8 (23), 8741–8751. doi:10.1021/acsschemeng.0c02490
- Sowmiah, S., Srinivasadesikan, V., Tseng, M.-C., and Chu, Y.-H. (2009). On the Chemical Stabilities of Ionic Liquids. *Molecules* 14, 3780–3813. doi:10.3390/molecules14093780
- Span, R., and Wagner, W. (1996). A New Equation of State for Carbon Dioxide Covering the Fluid Region from the Triple-Point Temperature to 1100 K at Pressures up to 800 MPa. *J. Phys. Chem. Reference Data* 25 (6), 1509–1596. doi:10.1063/1.555991
- Vafaezadeh, M., Aboudi, J., and Hashemi, M. M. (2015). A Novel Phenolic Ionic Liquid for 1.5 Molar CO<sub>2</sub> Capture: Combined Experimental and DFT Studies. *RSC Adv.* 5 (71), 58005–58009. doi:10.1039/C5RA09845A
- van Osch, D. J. G. P., Dietz, C. H. J. T., van Spronsen, J., Kroon, M. C., Gallucci, F., van Sint Annaland, M., et al. (2019). A Search for Natural Hydrophobic Deep Eutectic Solvents Based on Natural Components. *ACS Sustain. Chem. Eng.* 7 (3), 2933–2942. doi:10.1021/acsschemeng.8b03520
- van Osch, D. J. G. P., Dietz, C. H. J. T., Warrag, S. E. E., and Kroon, M. C. (2020). The Curious Case of Hydrophobic Deep Eutectic Solvents: A Story on the Discovery, Design, and Applications. *ACS Sustain. Chem. Eng.* 8 (29), 10591–10612. doi:10.1021/acsschemeng.0c00559
- Verevkin, S. P. (1999). Thermochemistry of Phenols: Butress Effects in Sterically Hindered Phenols. *J. Chem. Thermodynamics* 31 (11), 1397–1416. doi:10.1006/jcht.1999.0466
- Völkl, J., Müller, K., Mokrushina, L., and Arlt, W. (2012). A Priori Property Estimation of Physical and Reactive CO<sub>2</sub> Absorbents. *Chem. Eng. Technol.* 35 (3), 579–583. doi:10.1002/ceat.201100319
- Wazeer, I., AlNashef, I. M., Al-Zahrani, A. A., and Hadj-Kali, M. K. (2021a). The Subtle but Substantial Distinction between Ammonium- and Phosphonium-Based Deep Eutectic Solvents. *J. Mol. Liquids* 332, 115838. doi:10.1016/j.molliq.2021.115838
- Wazeer, I., Hadj-Kali, M. K., and Al-Nashef, I. M. (2021b). Utilization of Deep Eutectic Solvents to Reduce the Release of Hazardous Gases to the Atmosphere: A Critical Review. *Molecules* 26 (1), 75. doi:10.3390/molecules26010075

Xin, K., Roghair, I., Gallucci, F., and van Sint Annaland, M. (2021). Total Vapor Pressure of Hydrophobic Deep Eutectic Solvents: Experiments and Modelling. *J. Mol. Liquids* 325, 115227. doi:10.1016/j.molliq.2020.115227

**Conflict of Interest:** The authors declare that the research was conducted in the absence of any commercial or financial relationships that could be construed as a potential conflict of interest.

**Publisher's Note:** All claims expressed in this article are solely those of the authors and do not necessarily represent those of their affiliated organizations, or those of the publisher, the editors and the reviewers. Any product that may be evaluated in

this article, or claim that may be made by its manufacturer, is not guaranteed or endorsed by the publisher.

Copyright © 2022 Alhadid, Safarov, Mokrushina, Müller and Minceva. This is an open-access article distributed under the terms of the Creative Commons Attribution License (CC BY). The use, distribution or reproduction in other forums is permitted, provided the original author(s) and the copyright owner(s) are credited and that the original publication in this journal is cited, in accordance with accepted academic practice. No use, distribution or reproduction is permitted which does not comply with these terms.



# Natural Deep Eutectic Solvents Enhanced Electro-Enzymatic Conversion of CO<sub>2</sub> to Methanol

Zhibo Zhang<sup>1\*</sup>, Hui Wang<sup>2</sup>, Yi Nie<sup>3,4</sup>, Xiangping Zhang<sup>4</sup> and Xiaoyan Ji<sup>1\*</sup>

<sup>1</sup>Energy Engineering, Division of Energy Science, Luleå University of Technology, Luleå, Sweden, <sup>2</sup>State Key Laboratory of Materials-Oriented Chemical Engineering, Nanjing Tech University, Nanjing, China, <sup>3</sup>Zhengzhou Institute of Emerging Industrial Technology, Zhengzhou, China, <sup>4</sup>Beijing Key Laboratory of Ionic Liquids Clean Process, CAS Key Laboratory of Green Process and Engineering, State Key Laboratory of Multiphase Complex Systems, Institute of Process Engineering, Chinese Academy of Sciences, Beijing, China

## OPEN ACCESS

### Edited by:

Manoj B. Gawande,  
Palacky University Olomouc, Czechia

### Reviewed by:

Roberto Bernasconi,  
Politecnico di Milano, Italy  
Christoph Held,  
Technical University Dortmund,  
Germany

### \*Correspondence:

Zhibo Zhang  
zhibo.zhang@ltu.se  
Xiaoyan Ji  
xiaoyan.ji@ltu.se

### Specialty section:

This article was submitted to  
Green and Sustainable Chemistry,  
a section of the journal  
Frontiers in Chemistry

**Received:** 11 March 2022

**Accepted:** 07 April 2022

**Published:** 27 May 2022

### Citation:

Zhang Z, Wang H, Nie Y, Zhang X and  
Ji X (2022) Natural Deep Eutectic  
Solvents Enhanced Electro-Enzymatic  
Conversion of CO<sub>2</sub> to Methanol.  
Front. Chem. 10:894106.  
doi: 10.3389/fchem.2022.894106

Electro-enzymatic conversion of CO<sub>2</sub> offers a promising solution for CO<sub>2</sub> utilization, while the conversion rate and efficiency were disappointing. To address the challenge, four kinds of natural deep eutectic solvents (NADES) with desirable biocompatibility were developed for the first time and used as the co-electrolyte in the electro-enzymatic conversion of CO<sub>2</sub>. As a result, the SerGly-based solution presents high CO<sub>2</sub> solubility and high electrocatalytic activity, compared to the conventional buffer. By applying SerGly in the electro-enzymatic conversion of CO<sub>2</sub>, the yield of the product (methanol) is two times higher than that in the Tris-HCl buffer (0.22 mM) and 16 times higher than the control reaction.

**Keywords:** CO<sub>2</sub> conversion, enzyme, NADESs, electrocatalysis, methanol

## INTRODUCTION

To achieve energy sustainable development, the transformation of CO<sub>2</sub> to high-valued chemicals or fuels, e.g., methanol, is an ideal strategy to both alleviate climate issues (greenhouse effect) and promote resource recycling (Behrens et al., 2012). Up to now, extensive efforts have been made devoted to the methanol synthesis from CO<sub>2</sub> by using chemical, photochemical, electrochemical, and enzymatic conversion methods (Wang et al., 2011; Kondratenko et al., 2013; Zhang et al., 2021a). Due to the inherent thermodynamic stability and inertness of CO<sub>2</sub>, it is generally hard to convert CO<sub>2</sub>, typically along with high energy-demand, low efficiency, and low selectivity (Fu et al., 2020; Masood ul Hasan et al., 2021). Comparatively, enzymatic conversion of CO<sub>2</sub> can be promising solutions with high efficiency, high selectivity, and mild conditions with environmental friendliness (Shi et al., 2015).

Inspired by the biological metabolic pathway, sequential enzymatic conversion of CO<sub>2</sub> to methanol (CO<sub>2</sub> → formic acid → formaldehyde → methanol) can be realized by formate dehydrogenase (FDH), formaldehyde dehydrogenase (FaldDH), and alcohol dehydrogenase (ADH) (Wang et al., 2014). However, one of the biggest challenges in this multi-enzymatic reaction is cofactor NADH (reduced nicotinamide adenine dinucleotide) regeneration, since NADH as a sacrificial reagent provides enzyme with hydrogen and electrons at each step of reaction and then is oxidized to NAD<sup>+</sup> (oxidized nicotinamide adenine dinucleotide) (Wu et al., 2013). Besides, as this multi-enzymatic reaction is reversible, the byproduct NAD<sup>+</sup> has a negative effect on the equilibrium of reaction and exhibits an inhibitory effect on methanol production (Jaworek et al., 2021; Zhang et al., 2021d). Therefore, coupling the reduction of NAD<sup>+</sup> to NADH (NADH regeneration) with the enzymatic conversion is essential in which not only removes the byproduct and enhances CO<sub>2</sub> conversion but also cuts down the cost significantly to make the enzymatic reaction sustainable.

To date, enzymatic regeneration, photochemical regeneration, and electrochemical regeneration of NADH have been attempted in coupling with enzymatic conversion of CO<sub>2</sub> (Zhang et al., 2022). For example, Zhang et al. (2018) used glucose dehydrogenase for reducing NAD<sup>+</sup> to NADH integrating enzymatic conversion of CO<sub>2</sub> to methanol. Four enzymes, i.e., FDH, FaldDH, ADH, and glucose dehydrogenase, were co-immobilized in the regenerated cellulose membrane for enzymatic CO<sub>2</sub> conversion with cofactor regeneration. The results showed that the yield of methanol reached 73% in 30 min and then increased to 100% after coupling glucose dehydrogenase. The enzymatic regeneration was widely studied by other works (Voges et al., 2017a; Voges et al., 2017b). Rajesh et al. (Yadav et al., 2014) developed a porphyrin-based photosensitizer for photochemical regeneration of NADH. By combining enzymatic conversion of CO<sub>2</sub> to methanol, the methanol concentration with photochemical NADH regeneration was efficiently improved. Likewise, Chen et al. (2019) fabricated the Rh complex-based cathode for electrochemical reduction of NAD<sup>+</sup> to NADH. By integrating with the enzymatic conversion of CO<sub>2</sub> to formic acid, the formic acid was generated at a rate of 79 mM/h in a sustainable way, which is far higher than the currently reported works. Compared to the high cost of enzymatic regeneration and the unstable and complex system of photocatalytic regeneration, the electrochemical regeneration of NADH is much “cleaner” with lower cost and only electrons were consumed, being a better solution. However, the electro-enzymatic conversion of CO<sub>2</sub> also suffers from low conversion rate and efficiency, where the low CO<sub>2</sub> concentration and transfer rate as well as the electron transfer rate can be the reasons.

To address the above issue and improve reaction efficiency, developing a novel electrolyte, which can significantly dissolve CO<sub>2</sub> and improve electrocatalytic performance through enhancing CO<sub>2</sub> absorption and electron-transfer, can be a promising solution. Ionic liquids (ILs) are molten salts at room temperature with low vapour pressure, high conductivity, and wide electrochemical window, which have received much attention and been widely used in CO<sub>2</sub> capture, electrocatalysis, biocatalysis, and energy storage, etc. (Zhang et al., 2021b) DESs, with much easier preparation process while sharing similar properties to ILs, have also been widely used in capturing CO<sub>2</sub>, reducing overpotential in the electrocatalysis, and enhancing the activity of the enzyme in biocatalysis. For example, Zeng et al. (Yan et al., 2020) synthesized superbase DES that exhibited a superior high CO<sub>2</sub> absorption capacity up to 0.141 g-CO<sub>2</sub>/g-DES. Furthermore, Han et al. (Yang et al., 2019) fabricated copper selenide catalysts for the electroreduction of CO<sub>2</sub> to methanol. Under the support from ILs-based electrolyte, the current density reaches 41.5 mA/cm<sup>2</sup> with a Faradaic efficiency of 77.6%. Similarly, natural deep eutectic solvents (NADESs) were developed for biocatalysis, presenting high biocompatibility, and desirable performance. According to Yang et al. (2017), the yield of the reaction was significantly increased up to 181% by employing NADESs. All these publications demonstrated that using DESs-based electrolyte is promising to improve the CO<sub>2</sub> conversion in electro-enzymatic catalysis.

In this work, DESs were proposed to be used as the electrolyte in the reaction, which was expected to remarkably improve the efficiency of electro-enzymatic conversion of CO<sub>2</sub>. Four NADESs, i.e., glutamate glycerol (GluGly), serine glycerol (SerGly), arginine glycerol (ArgGly), histidine glycerol (HisGly), were synthesized for the first time. Characterization as well as determination of physiochemical properties and CO<sub>2</sub> capture capacity of NADESs were conducted. Besides, enzyme activity, enzymatic reaction, and electrocatalytic performance for NADH regeneration in the NADESs were investigated.

## EXPERIMENTAL SECTION

### Materials

Formate dehydrogenase from *Candida boidinii* (FDH, EC.1.2.1.2, homo-dimer, 76 kDa), formaldehyde dehydrogenase from *Pseudomonas* sp. (FaldDH, EC.1.2.1.46, homo-dimer, 150 kDa), yeast alcohol dehydrogenase (ADH, EC 1.1.1.1, 141 kDa), reduced and oxidized nicotinamide adenine dinucleotide (NADH/NAD<sup>+</sup>, 98 wt%), L-Histidine (99%), glycerol (99%), L-glutamic acid (99%), L-serine (99%), L-arginine (99%), dopamine hydrochloride (DA), poly (ethyleneimine) (PEI), 2,2'-bipyridyl-5,5'-dicarboxylic acid, and dichloro-(penta-methylcyclopentadienyl)rhodium (III) dimer ([Cp\*RhCl<sub>2</sub>]<sub>2</sub>) were purchased from Sigma-Aldrich (St Louis, MO, United States). CO<sub>2</sub> gas (>99.5%) in a cylinder was purchased from Linde Gas (Sweden).

### Synthesize of NADESs

NADESs were synthesized with the method referring to the literature (Ren et al., 2018). Taking SerGly as an example, SerGly was synthesized by mixing L-serine with glycerol at a molar ratio of 1:6, and the mixture was heated at 70°C until the liquid changed from colorless to colored. The unreacted amino acid was removed by centrifugation, and the obtained product was dried under vacuum at 60°C for 2 h. Similarly, other NADESs were synthesized following the same procedure, and the obtained NADESs were stored in a glassware dryer at ambient temperature. Finally, the yields of GluGly, SerGly, ArgGly, and HisGly were 92, 95, 100, and 89%, respectively.

### Activity Assay of FDH

The FDH activity was determined by monitoring the absorbance changes at 340 nm during the redox reactions catalyzed by the FDH at 25°C. The oxidation of formate was conducted in the conventional buffer and NADES-contained solution, respectively. The assay solution (2 ml) contains 20 µg of FDH, 100 mM sodium formate, and 1 mM NAD<sup>+</sup>. One unit of oxidation activity was defined as the amount of enzyme required to produce 1 µmol of NADH per minute under standard conditions.

### Electro-Enzymatic Reduction of NAD<sup>+</sup> to NADH and Characterization

Electrochemical regeneration of NADH was carried out using the CHI-760e electrochemical workstation in a conventional three-electrode H-cell. The Rh complex-grafted carbon felt fabricated

according to the previous work (Zhang et al., 2021c) served as the working electrode, and the platinum wire and Ag/AgCl/KCl (3 M) were used as the counter and reference electrodes, respectively. The anodic and cathodic chambers were filled with 10 ml Tris-HCl (50 mM) buffer and degassed using N<sub>2</sub> to prevent the oxidation of NADH. 1 mM NAD<sup>+</sup> was added to the solution and then reduced to NADH by using the Rh-grafted electrode. The progress of NAD<sup>+</sup> reduction was monitored with a spectrophotometer (Shimadzu) by measuring the absorbance at 340 nm. Cyclic voltammetry (CV) measurements were recorded at a scan rate of 50 mV·s<sup>-1</sup> and the potential range is from -1 to 0 V. The electrochemical impedance spectroscopic (EIS) was carried out at open circuit potential (OCP) within the frequency extent of 100–100,000 Hz and at an amplitude of 5 mV.

## CO<sub>2</sub> Solubility and Absorption Rate

CO<sub>2</sub> absorption was determined by weighting the samples (Yan et al., 2020). Typically, 5 g of NADES-based solution was added into an absorption glass tube with an inner diameter of 2.0 cm. Then, the absorption tube was partially immersed in a water bath at the desired temperature, and the standard uncertainty of temperature was ±0.1°C. After that, CO<sub>2</sub> was passed into the absorption tube at a flow rate of 100 ml/min. The weight of the captured CO<sub>2</sub> was obtained by the electronic balance with an accuracy of ±0.0001 g until CO<sub>2</sub> absorption in the DESs reached an equilibrium.

## Enzymatic Reaction

The conversion of CO<sub>2</sub> to methanol was performed in the setup of the H-cell with three-electrodes. A mixture (10 ml) of 1 mg FDH, 1 mg FaldDH, 1 mg ADH, and 1 mM NADH (7.09 mg) in the cathode was prepared and used in all enzymatic reactions. Before reaction, CO<sub>2</sub> gas was bubbled through 10 ml buffer solution (50 mM Tris-HCl buffer, pH 7.4) for 30 min to achieve CO<sub>2</sub> saturation in the solution. Applying for a reduction peak potential, the electro-enzymatic reaction was initiated, and the methanol concentration was determined by GC using the internal standard method.

## Analytic Methods

An Agilent 7890B gas chromatograph (GC) equipped with a flame ionization detector (250°C) and an HP-5 column (30 m × 0.25 mm, film thickness 0.25 μm) was used for analyzing the products in the liquid phase and determining the methanol concentration by using ethyl acetate as the internal standard. The NADH concentration was measured by the UV-vis spectrophotometer (UV-1280, Shimadzu). Thermogravimetric analyses (TGA) were performed using a thermal gravimetric analyzer (Netzsch, STA449 F5, Germany) and the samples were heated from 30 to 400°C at 20.0°C/min under the nitrogen atmosphere. The freezing point of each DES was determined by a differential scanning calorimeter (DSC) (Netzsch DSC 200F3, Germany), and the samples were heated from -78 to 50°C at 10.0°C/min. The density and viscosity were measured by the Anton Paar DMA 5000 density meter with an uncertainty of ±0.0005 g cm<sup>-3</sup> and Anton Paar AMVn with ±0.5% precision.

## RESULTS AND DISCUSSION

### Characterization and Physicochemical Properties of NADESs

In the synthesis of NADESs, it typically contains hydrogen bonding acceptor (HBA) and hydrogen bond donor (HBD), wherein the amino acid plays as hydrogen bonding acceptor (HBA), and glycerol serves as hydrogen bond donor (HBD). Taking glutamic acid as an example, the reaction between HBA and HBD was proposed in **Supplementary Figure S1**. To confirm the NADES formation, the synthesis process of NADESs was monitored by a UV-vis spectrometer in the wavelength ranging from 250 to 650 nm. In the beginning, the raw materials, amino acid and glycerol, do not have any absorption from 250 to 650 nm. As the reaction progressed, due to the formation of NADES, the absorption peak was observed for each NADES as shown in **Figure 1A**. Besides, the freezing point of NADESs was further detected by DSC. According to **Figure 1B**, the freezing points of GluGly (**Supplementary Figure S2**), SerGly, ArgGly, and HisGly were estimated to be -61, -72, -60, and -75°C, respectively, which are lower than those of amino acids (Glu: 199, Ser: 225, Arg: 260, and His: 277°C) and glycerol (17.8°C) (Do et al., 2020), also confirming the formation of NADESs successfully. The thermal stabilities of NADESs were analyzed by TG, as shown in **Figure 1C**. There is no obvious weight loss below 150°C for all the NADESs, indicating their high thermal stability. Also, these NADESs presented different thermal stabilities. Taking the mass loss of 50% as an example, the corresponding temperatures of GluGly, SerGly, ArgGly, and HisGly were respectively 178, 212, 214, and 228°C, and thus their thermal stabilities follow the order of ArgGly > SerGly > HisGly > GluGly. Furthermore, the obtained NADESs present super hydrophilic, which can be dissolved in water at any proportion.

The density and viscosity are key properties of the reaction media. The temperature-dependent densities and viscosities were measured as shown in **Figure 2** and listed in **Supplementary Table S1**. The results showed that the density decreases linearly with the increase of temperature for all NADESs, and follows the order of ArgGly > HisGly > SerGly > GluGly. The viscosity decreases non-linearly (sharply) with the increase of temperature for all NADESs, and follows the order of HisGly > SerGly > GluGly > ArgGly.

### Enzyme Activity in DESs

According to the kinetics of the multi-enzymatic reaction (Luo et al., 2015), the first two reactions (CO<sub>2</sub>→HCOOH→HCHO) were rate-limiting steps, and the second reaction (HCOOH→HCHO) was regulated by the product concentration of the first reaction. Therefore, the first reaction (CO<sub>2</sub>→HCOOH) plays a key role in the whole reaction, as confirmed by a previous study (Zhang et al., 2021c). Besides, biocatalyst FDH plays a key role in driving the first reaction, and thus the activity of FDH was evaluated in four NADESs (20% v/v) as well as a conventional buffer as a blank for comparison. As shown in **Figure 3**, the activity of FDH was enhanced by SerGly and GluGly, and SerGly presented the better enhancement with 384.6 U/mg, while the activities of FDH in ArgGly and HisGly were seriously decreased to 69.4 and 78.4 U/mg, respectively. To figure out



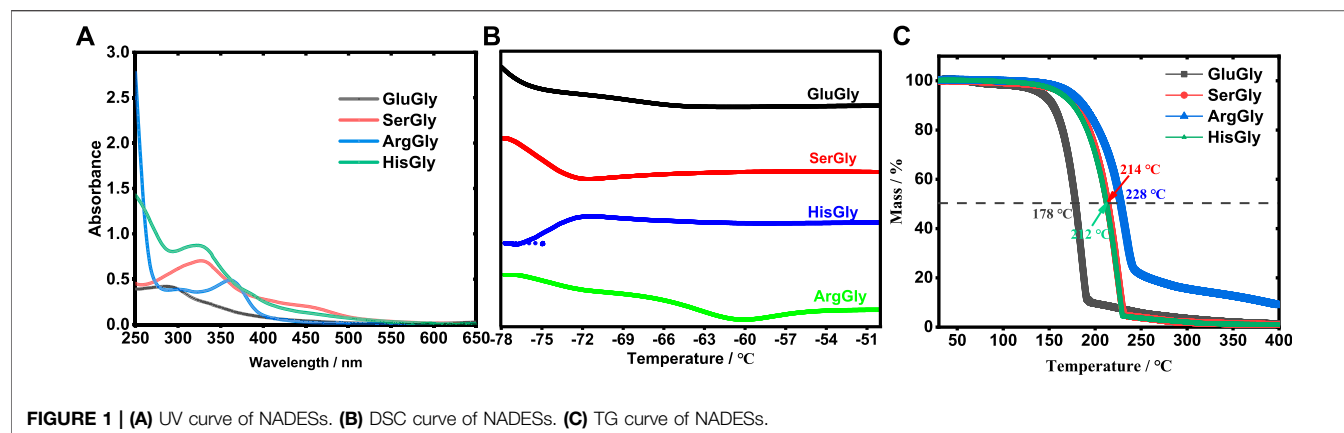


FIGURE 1 | (A) UV curve of NADESS. (B) DSC curve of NADESS. (C) TG curve of NADESS.

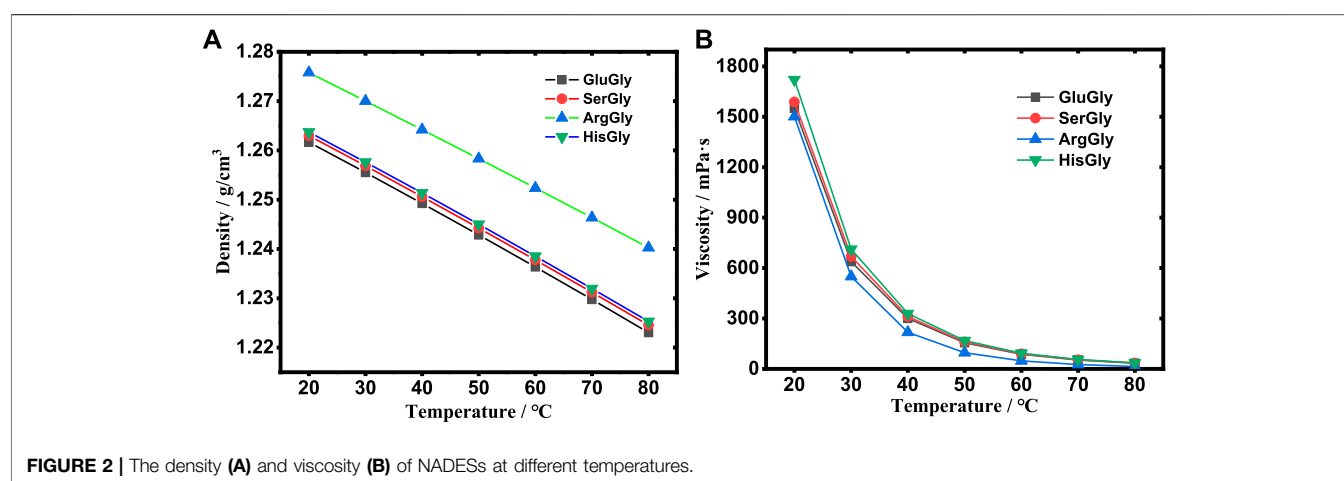


FIGURE 2 | The density (A) and viscosity (B) of NADESS at different temperatures.

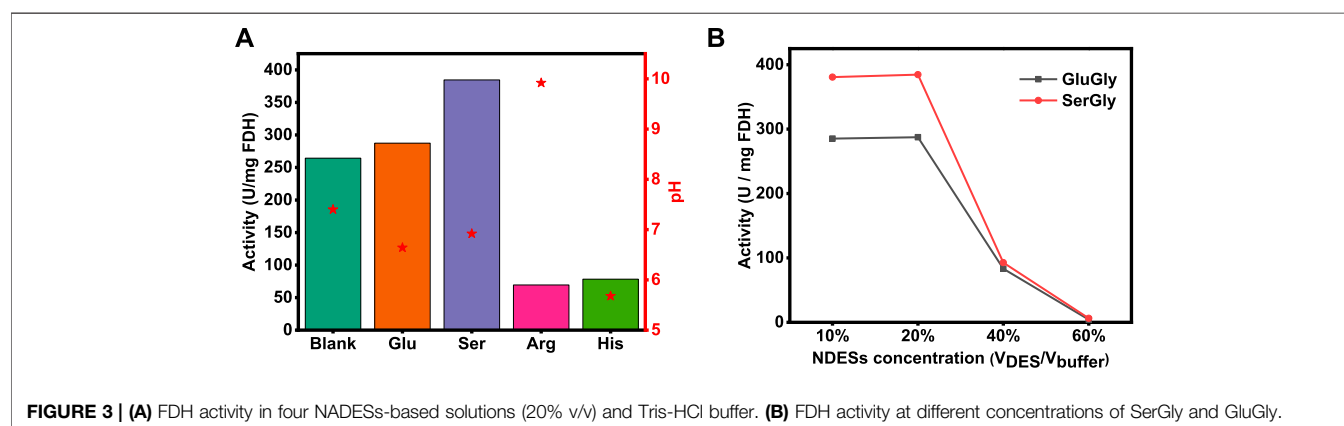
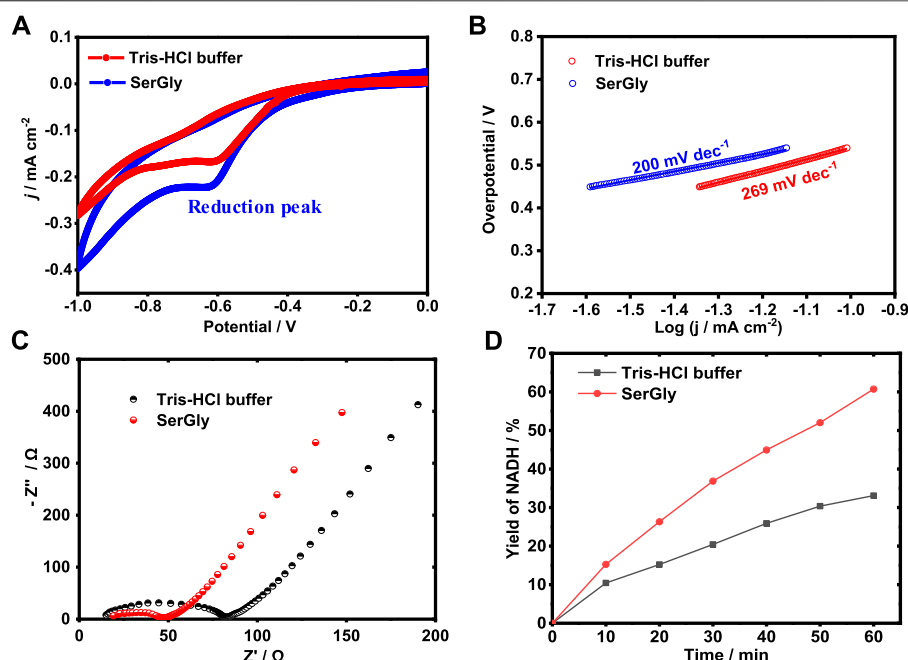


FIGURE 3 | (A) FDH activity in four NADESSs-based solutions (20% v/v) and Tris-HCl buffer. (B) FDH activity at different concentrations of SerGly and GluGly.

the reason, the pH values of different NADES-based solutions were examined, and those for SerGly and GluGly were close to the optimal pH of FDH (7.0), while the pHs of ArgGly-based and HisGly-based solution were 9.9 and 5.6, respectively. Therefore, the pH values that are far from the optimal value of FDH are probably the main reason for the activity decline. For the case that the pH values of NADESS are close to the optimal pH of FDH, the enhancement can be

explained as follows. Previous results revealed that the usage of ILs will increase the rigidity and stability of FDH, and also the substrate (CO<sub>2</sub>) residence time in the activity site of FDH (Zhang et al., 2018). The longer residence time will give more chances to adjust the substrate in the right position and thus make it more productive. If the enzyme is in an unfavorable media solution, the enzyme will not perform well with their unnormally folding conformation, leading to



**FIGURE 4 | (A)** Cyclic voltammogram (CV) curves of electrocatalyst in the SerGly-contained buffer and Tris-HCl buffer. **(B)** Tafel plot of electrocatalysts in the SerGly-contained buffer and Tris-HCl buffer. **(C)** Nyquist plots for electrocatalyst in the SerGly-contained buffer and Tris-HCl buffer. **(D)** Electro-reduction of NAD<sup>+</sup> to NADH in the SerGly-contained buffer and Tris-HCl buffer.

the decrease of the activity or even lose activity. Within the studied NADESs, SerGly with desirable pH exhibits the best enhancement on the enzyme activity.

To further identify the optimal NADESs concentration, the concentrations of SerGly and GluGly were set in the range from 10 to 60% ( $V_{\text{NADES}}/V_{\text{buffer}}$ ) and evaluated their impact. As shown in **Figure 3**, the enzyme activity was enhanced and kept well in the concentration of NADESs from 10 to 20%, because the rigidity and stability of FDH were increased with increasing concentration from 1 to 20%, as described above. Aqueous solutions (water-rich IL mixtures) have also been confirmed to be the best media for proteins, being consistent with experimental results in this study (Kohno and Ohno, 2012). With further increasing the NADESs concentration from 20%, the enzyme activity was sharply decreased, which was probably attributed to the break of electrostatic balance in proteins by the charge of DES when subjected to high salt (DES) concentrations (Weingartner et al., 2012). Once the electrostatic balance in proteins is broken, the hydrophobic interaction plays a main role, resulting in aggregation of enzyme and thus decreasing the active sites of enzyme exposure out. Therefore, a high concentration of NADES will decrease the enzyme activity. Above all, SerGly is the best among the developed NADESs and 20% is optimal concentration. Unless specific statement, 20% NADES-based aqueous solution was used in the following study.

## Electrochemical Regeneration of Cofactor

The high performance of reducing NAD<sup>+</sup> to NADH is crucial to achieving enzymatic conversion of CO<sub>2</sub> in a sustainable way. Electrochemical regeneration of NADH was used in this study. In

this part, the effect of buffers, i.e., DES-contained buffer (SerGly) and the conventional buffer (Tris-HCl), were investigated in the electrocatalysis and explore how the DES could boost the electrochemical reduction of NAD<sup>+</sup> to NADH. First, the electrocatalytic activities of electrocatalyst (Rh complex) in SerGly-contained solution and Tris-HCl solution were separately characterized by cyclic voltammetry (CV). As shown in **Figure 4A**, within the cathodic potential from -1 to 0 V, a reduction peak, was observed at -0.62 V, indicating the reduction of Rh<sup>III</sup> to Rh<sup>I</sup>, where the formed Rh<sup>I</sup> can efficiently reduce NAD<sup>+</sup> to NADH (Chen et al., 2019). At this reduction peak potential, the corresponding current density of SerGly-contained solution (-0.225 mA/cm<sup>2</sup>) is higher than that of conventional solution -0.166 mA/cm<sup>2</sup>, confirming a higher electron transfer and NAD<sup>+</sup> reduction efficiency in the SerGly-contained solution.

Next, the Tafel plot was separately examined in both solutions, as an indicator to quantify how easy/difficult to achieve a reaction, and the lower the overpotential, the easier the reaction (Kang et al., 2020). As presented in **Figure 4B**, the Tafel slope in SerGly-contained solution (200 dec<sup>-1</sup>) was lower than that in Tris-HCl buffer, indicating a lower overpotential under the given current density. This indicates a lower energy barrier in the SerGly-contained solution with a higher driving force. As reported by Faggion et al. report (Faggion et al., 2019), ILs could significantly reduce the overpotential in the electrochemical reduction of CO<sub>2</sub> and improve the electrochemical efficiency. This observation is consistent with our findings here.

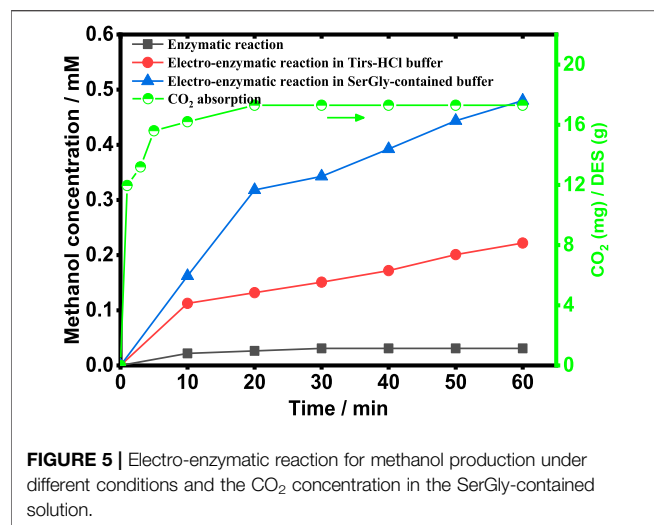


**FIGURE 5 |** Electro-enzymatic reaction for methanol production under different conditions and the CO<sub>2</sub> concentration in the SerGly-contained solution.

To reveal the difficulty of kinetic reaction, the interface between electrode and electrolyte was investigated by electrochemical impedance spectroscopy (EIS). **Figure 4C** exhibits typical results of impedance spectra (Nyquist plots), where  $Z'$  and  $Z''$  are the real variable and the negatively imaginary variable of impedance, respectively. A semi-circular part at high frequencies in **Figure 4C** corresponds to the electron-transfer limited process (the electrode/solution interface), and a linear part at low frequencies corresponds to the diffusion process. Charge transfer resistance ( $R_{ct}$ ) in the SerGly-contained solution was estimated to be 48  $\Omega$ , which is remarkably lower than that in the Tris-HCl buffer of 82  $\Omega$ . The results with lower  $R_{ct}$  in the SerGly-contained solution suggested the faster interfacial charge transfer rate between the electrolyte (SerGly) and the working electrode, which is superior to the Tris-HCl buffer in electrocatalysis principally.

To verify the enhancement of NAD<sup>+</sup> reduction by NADESs, the electrochemical reduction of NAD<sup>+</sup> to NADH was separately conducted in the SerGly-contained solution and Tris-HCl solution. As shown in **Figure 4D**, the yield of NADH in the SerGly-contained solution was 60% in 1 h, which was approximately two times higher than that in Tris-HCl buffer. The higher reduction rate of NAD<sup>+</sup> to NADH in SerGly-contained solution was attributed to higher electron transfer by SerGly, which has been demonstrated by the electrochemical characterization above. Therefore, besides serving as a co-solvent to enhance the enzyme activity, SerGly can also boost electrochemical conversion and is a desirable co-solvent for the enzymatic reaction.

## Multi-Enzymatic Reaction for Methanol Production

To establish a sustainable process to produce methanol and enhance the process by NADES, the enzymatic reaction coupled with NADH electro-regeneration in the SerGly-contained buffer and Tris-HCl buffer was implemented, and the control reaction (the enzymatic reaction without NADH

regeneration) was also studied for comparison. Therefore, three systems were designed and evaluated, as shown in **Figure 5**. The enzymatic reaction without NADH electro-regeneration quickly reached equilibrium with low methanol concentration (0.03 mM), since such multi-enzymatic reaction is reversible and CO<sub>2</sub> conversion was inhibited by the accumulation of byproduct NAD<sup>+</sup> over time (Luo et al., 2015). Applying with electro-reduction of NAD<sup>+</sup> to NADH, the methanol concentration was 0.22 mM, significantly increased up to 7 times higher than the control reaction. It indicated that the byproduct NAD<sup>+</sup> was efficiently reduced to cofactor NADH, achieving the removal of NAD<sup>+</sup> and the increased NADH concentration. To further boost the electro-enzymatic conversion of CO<sub>2</sub>, SerGly was used to enhance the whole process, i.e., remarkably increase the CO<sub>2</sub> conversion. As a result, the rate of methanol generation reached 0.48 mM/h, which is two times higher than that in the Tris-HCl buffer (0.22 mM/h) and 16 times higher than the control reaction. Being consistent with the above investigation, SerGly enhanced not only enzyme activity but also NADH electro-regeneration rate, which was probably the main reason to improve the CO<sub>2</sub> conversion. Besides, SerGly increased the CO<sub>2</sub> concentration in the solution. As shown in **Figure 5**, the CO<sub>2</sub> solubility in the SerGly-contained solution was 17.3 mg-CO<sub>2</sub>/g-DES at room temperature, which is 11 times higher than that in the Tris-HCl solution (1.5 mg-CO<sub>2</sub>/g-water). Zhang et al. (2021c) demonstrated that increasing the CO<sub>2</sub> concentration could significantly drive the reversible reaction forward and thus increase the CO<sub>2</sub> conversion in the enzymatic reaction. Therefore, SerGly plays a role in enhancing enzyme activity and cofactor electro-regeneration as well as in the enrichment of the substrate CO<sub>2</sub>, and finally enhances the process of the electro-enzymatic conversion of CO<sub>2</sub>.

## CONCLUSION

In this study, four NADESs, GluGly, SerGly, HisGly, and ArgGly, were developed and characterized for the first time. The performance of these NADESs was evaluated in the enzymatic reaction, in which SerGly presents the best results on the enzyme activity. The SerGly-based solution was further investigated in the electro-enzymatic conversion of CO<sub>2</sub>. It was found that 1) the CO<sub>2</sub> solubility in the SerGly-based solution is 11 times higher than that in the conventional buffer, contributing to the enhancement of the enzymatic CO<sub>2</sub> conversion; 2) NADH electro-regeneration rate was approximately 2 times higher than that in the conventional buffer, providing the fundamental condition to accelerate the CO<sub>2</sub> conversion, and 3) the methanol production from the multi-enzymatic conversion of CO<sub>2</sub> coupled with the NADH electro-regeneration is 2 times higher than that in the Tris-HCl buffer (0.22) and 16 times higher than the control reaction. This work developed a novel NADES with desirable biocompatibility, high electrocatalytic performance, and high CO<sub>2</sub> solubility, enhancing the whole process of electro-enzymatic conversion of CO<sub>2</sub> and being



promising for the enzymatic catalysis, electrocatalysis, and CO<sub>2</sub> capture research field.

## DATA AVAILABILITY STATEMENT

The original contributions presented in the study are included in the article/**Supplementary Material**, further inquiries can be directed to the corresponding authors.

## AUTHOR CONTRIBUTIONS

ZZ: Methodology, Formal analysis, Visualization, Writing—original draft, and Writing—review and editing. HW: Data Analysis. YN: Conceptualization, writing and editing. XZ:

Conceptualization, writing and editing. XJ: Conceptualization, Supervision, Writing—original draft, and Writing—review editing.

## FUNDING

The research work is financially supported by the Kempe foundation in Sweden. XJ thanks the financial support from the Swedish Energy Agency (P47500-1).

## SUPPLEMENTARY MATERIAL

The Supplementary Material for this article can be found online at: <https://www.frontiersin.org/articles/10.3389/fchem.2022.894106/full#supplementary-material>

## REFERENCES

- Behrens, M., Studt, F., Kasatkin, I., Kühl, S., Hävecker, M., Abild-Pedersen, F., et al. (2012). The Active Site of Methanol Synthesis over Cu/ZnO/Al<sub>2</sub>O<sub>3</sub> Industrial Catalysts. *Science* 336 (6083), 893–897. doi:10.1126/science.1219831
- Chen, Y., Li, P., Noh, H., Kung, C. W., Buru, C. T., Wang, X., et al. (2019). Stabilization of Formate Dehydrogenase in a Metal-Organic Framework for Bioelectrocatalytic Reduction of CO<sub>2</sub>. *Angew. Chem. Int. Ed.* 58 (23), 7682–7686. doi:10.1002/anie.201901981
- Do, H. T., Chua, Y. Z., Kumar, A., Pabsch, D., Hallermann, M., Zaitsau, D., et al. (2020). Melting Properties of Amino Acids and Their Solubility in Water. *RSC Adv.* 10 (72), 44205–44215. doi:10.1039/d0ra08947h
- Faggion, D., Gonçalves, W. D. G., and Dupont, J. (2019). CO<sub>2</sub> Electroreduction in Ionic Liquids. *Front. Chem.* 7, 102. doi:10.3389/fchem.2019.00102
- Fu, J., Jiang, K., Qiu, X., Yu, J., and Liu, M. (2020). Product Selectivity of Photocatalytic CO<sub>2</sub> Reduction Reactions. *Mater. Today* 32, 222–243. doi:10.1016/j.mattod.2019.06.009
- Jaworek, M. W., Gajardo-Parra, N. F., Sadowski, G., Winter, R., and Held, C. (2021). Boosting the Kinetic Efficiency of Formate Dehydrogenase by Combining the Effects of Temperature, High Pressure and Co-solvent Mixtures. *Colloids Surf. B-Biointerfaces* 208, 112127. doi:10.1016/j.colsurfb.2021.112127
- Kang, X., Wang, B., Hu, K., Lyu, K., Han, X., Spencer, B. F., et al. (2020). Quantitative Electro-Reduction of CO<sub>2</sub> to Liquid Fuel over Electro-Synthesized Metal-Organic Frameworks. *J. Am. Chem. Soc.* 142 (41), 17384–17392. doi:10.1021/jacs.0c05913
- Kohno, Y., and Ohno, H. (2012). Ionic Liquid/water Mixtures: from Hostility to Conciliation. *Chem. Commun.* 48 (57), 7119–7130. doi:10.1039/c2cc31638b
- Kondratenko, E. V., Mul, G., Baltrusaitis, J., Larrazábal, G. O., and Pérez-Ramírez, J. (2013). Status and Perspectives of CO<sub>2</sub> Conversion into Fuels and Chemicals by Catalytic, Photocatalytic and Electrocatalytic Processes. *Energy Environ. Sci.* 6 (11), 3112–3135. doi:10.1039/c3ee41272e
- Luo, J., Meyer, A. S., Mateiu, R. V., and Pinelo, M. (2015). Cascade Catalysis in Membranes with Enzyme Immobilization for Multi-Enzymatic Conversion of CO<sub>2</sub> to Methanol. *New Biotechnol.* 32 (3), 319–327. doi:10.1016/j.nbt.2015.02.006
- Masood ul Hasan, I., Peng, L., Mao, J., He, R., Wang, Y., Fu, J., et al. (2021). Carbon-based Metal-free Catalysts for Electrochemical CO<sub>2</sub> Reduction: Activity, Selectivity, and Stability. *Carbon Energy* 3 (1), 24–49. doi:10.1002/cey2.87
- Ren, H., Lian, S., Wang, X., Zhang, Y., and Duan, E. (2018). Exploiting the Hydrophilic Role of Natural Deep Eutectic Solvents for Greening CO<sub>2</sub> Capture. *J. Clean. Prod.* 193, 802–810. doi:10.1016/j.jclepro.2018.05.051
- Shi, J., Jiang, Y., Jiang, Z., Wang, X., Wang, X., Zhang, S., et al. (2015). Enzymatic Conversion of Carbon Dioxide. *Chem. Soc. Rev.* 44 (17), 5981–6000. doi:10.1039/c5cs00182j
- Voges, M., Fischer, C., Wolff, D., and Held, C. (2017a). Influence of Natural Solutes and Ionic Liquids on the Yield of Enzyme-Catalyzed Reactions: Measurements and Predictions. *Org. Process. Res. Dev.* 21 (7), 1059–1068. doi:10.1021/acs.oprd.7b00178
- Voges, M., Fischer, F., Neuhaus, M., Sadowski, G., and Held, C. (2017b). Measuring and Predicting Thermodynamic Limitation of an Alcohol Dehydrogenase Reaction. *Ind. Eng. Chem. Res.* 56 (19), 5535–5546. doi:10.1021/acs.iecr.7b01228
- Wang, W., Wang, S., Ma, X., and Gong, J. (2011). Recent Advances in Catalytic Hydrogenation of Carbon Dioxide. *Chem. Soc. Rev.* 40 (7), 3703–3727. doi:10.1039/c1cs15008a
- Wang, X., Li, Z., Shi, J., Wu, H., Jiang, Z., Zhang, W., et al. (2014). Bioinspired Approach to Multienzyme Cascade System Construction for Efficient Carbon Dioxide Reduction. *ACS Catal.* 4 (3), 962–972. doi:10.1021/cs401096c
- Weingärtner, H., Cabrele, C., and Herrmann, C. (2012). How Ionic Liquids Can Help to Stabilize Native Proteins. *Phys. Chem. Chem. Phys.* 14 (2), 415–426. doi:10.1039/c1cp21947b
- Wu, H., Tian, C., Song, X., Liu, C., Yang, D., and Jiang, Z. (2013). Methods for the Regeneration of Nicotinamide Coenzymes. *Green. Chem.* 15 (7), 1773–1789. doi:10.1039/c3gc37129h
- Yadav, R. K., Oh, G. H., Park, N.-J., Kumar, A., Kong, K.-j., and Baeg, J.-O. (2014). Highly Selective Solar-Driven Methanol from CO<sub>2</sub> by a Photocatalyst/Biocatalyst Integrated System. *J. Am. Chem. Soc.* 136 (48), 16728–16731. doi:10.1021/ja509650r
- Yan, H., Zhao, L., Bai, Y., Li, F., Dong, H., Wang, H., et al. (2020). Superbase Ionic Liquid-Based Deep Eutectic Solvents for Improving CO<sub>2</sub> Absorption. *ACS Sust. Chem. Eng.* 8 (6), 2523–2530. doi:10.1021/acssuschemeng.9b07128
- Yang, T.-X., Zhao, L.-Q., Wang, J., Song, G.-L., Liu, H.-M., Cheng, H., et al. (2017). Improving Whole-Cell Biocatalysis by Addition of Deep Eutectic Solvents and Natural Deep Eutectic Solvents. *ACS Sust. Chem. Eng.* 5 (7), 5713–5722. doi:10.1021/acssuschemeng.7b00285
- Yang, D., Zhu, Q., Chen, C., Liu, H., Liu, Z., Zhao, Z., et al. (2019). Selective Electroreduction of Carbon Dioxide to Methanol on Copper Selenide Nanocatalysts. *Nat. Commun.* 10, 677. doi:10.1038/s41467-019-08653-9
- Zhang, Z., Muschiol, J., Huang, Y., Sigurdardóttir, S. B., von Solms, N., Daugaard, A. E., et al. (2018). Efficient Ionic Liquid-Based Platform for Multi-Enzymatic Conversion of Carbon Dioxide to Methanol. *Green. Chem.* 20 (18), 4339–4348. doi:10.1039/c8gc02230e
- Zhang, F. L., Bai, Y., Nie, Y., Ji, X., and Zhang, X. (2021a). Application and Challenge of Ionic Liquids as Co-solvent for Electro-Enzymatic Conversion of CO<sub>2</sub> to Methanol. *Proc. Chin. Soc. Electr. Eng.* 41 (11), 3657–3665. doi:10.13334/j.0258-8013.pcsee.201956
- Zhang, Z. B., Li, F. F., Nie, Y., Zhang, X. P., Zhang, S. J., and Ji, X. Y. (2021b). Zinc-based Deep Eutectic Solvent - an Efficient Carbonic Anhydrase Mimic for CO<sub>2</sub> Hydration and Conversion. *Sep. Purif. Tech.* 276, 119446. doi:10.1016/j.seppur.2021.119446

- Zhang, Z., Li, J., Ji, M., Liu, Y., Wang, N., Zhang, X., et al. (2021c). Encapsulation of Multiple Enzymes in a Metal-Organic Framework with Enhanced Electro-Enzymatic Reduction of CO<sub>2</sub> to Methanol. *Green. Chem.* 23 (6), 2362–2371. doi:10.1039/d1gc00241d
- Zhang, Z. B., Vasiliu, T., Li, F. F., Laaksonen, A., Mocci, F., and Ji, X. Y. (2021d). Electrochemically Driven Efficient Enzymatic Conversion of CO<sub>2</sub> to Formic Acid with Artificial Cofactors. *J. Co2 Utilization* 52, 101679. doi:10.1016/j.jcou.2021.101679
- Zhang, Z., Zhang, X., and Ji, X. (2022). Developing and Regenerating Cofactors for Sustainable Enzymatic CO<sub>2</sub> Conversion. *Processes* 10 (2), 230. doi:10.3390/pr10020230

**Conflict of Interest:** The authors declare that the research was conducted in the absence of any commercial or financial relationships that could be construed as a potential conflict of interest.

The reviewer CH declared a past co-authorship with the author XJ to the handling editor.

**Publisher's Note:** All claims expressed in this article are solely those of the authors and do not necessarily represent those of their affiliated organizations, or those of the publisher, the editors and the reviewers. Any product that may be evaluated in this article, or claim that may be made by its manufacturer, is not guaranteed or endorsed by the publisher.

Copyright © 2022 Zhang, Wang, Nie, Zhang and Ji. This is an open-access article distributed under the terms of the Creative Commons Attribution License (CC BY). The use, distribution or reproduction in other forums is permitted, provided the original author(s) and the copyright owner(s) are credited and that the original publication in this journal is cited, in accordance with accepted academic practice. No use, distribution or reproduction is permitted which does not comply with these terms.



# Extraction of Biocompatible Collagen From Blue Shark Skins Through the Conventional Extraction Process Intensification Using Natural Deep Eutectic Solvents

Miguel P. Batista<sup>1,2</sup>, Naiara Fernández<sup>1</sup>, Frédéric B. Gaspar<sup>1,3</sup>, Maria do Rosário Bronze<sup>1,3,4</sup> and Ana Rita C. Duarte<sup>2\*</sup>

## OPEN ACCESS

### Edited by:

Tiancheng Mu,  
Renmin University of China, China

### Reviewed by:

Jikuan Qiu,  
Henan Normal University, China  
Lorenzo Guazzelli,  
University of Pisa, Italy

### \*Correspondence:

Ana Rita C. Duarte  
aduarte@fct.unl.pt

### Specialty section:

This article was submitted to  
Green and Sustainable Chemistry,  
a section of the journal  
Frontiers in Chemistry

**Received:** 05 May 2022

**Accepted:** 30 May 2022

**Published:** 16 June 2022

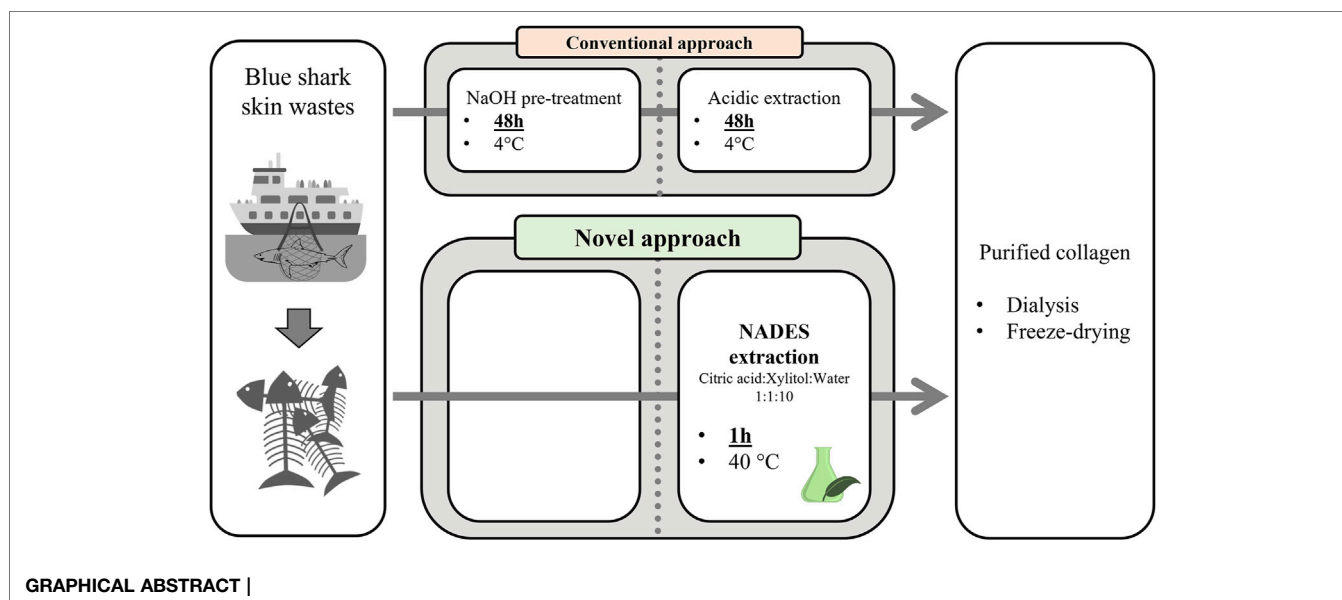
### Citation:

Batista MP, Fernández N, Gaspar FB,  
Bronze MdR and Duarte ARC (2022)  
Extraction of Biocompatible Collagen  
From Blue Shark Skins Through the  
Conventional Extraction Process  
Intensification Using Natural Deep  
Eutectic Solvents.  
Front. Chem. 10:937036.  
doi: 10.3389/fchem.2022.937036

<sup>1</sup>iBET, Instituto de Biologia Experimental e Tecnológica, Oeiras, Portugal, <sup>2</sup>LAQV-REQUIMTE, Departamento de Química, Faculdade de Ciências e Tecnologia, Universidade Nova de Lisboa, Caparica, Portugal, <sup>3</sup>Instituto de Tecnologia Química e Biológica António Xavier, Universidade Nova de Lisboa, Oeiras, Portugal, <sup>4</sup>FFULisboa, Faculty of Pharmacy, University of Lisbon, Lisbon, Portugal

The disposal of large amounts of skin waste resulting from the blue shark fishing industry presents several industrial and environmental waste management concerns. In addition, these marine subproducts are interesting sources of collagen, a fibrous protein that shows high social and economic interest in a broad range of biomedical, pharmaceutical, and cosmetic applications. However, blue shark wasted skins are a poorly explored matrix for this purpose, and conventional collagen recovery methodologies involve several pre-treatment steps, long extraction times and low temperatures. This work presents a new green and sustainable collagen extraction approach using a natural deep eutectic solvent composed of citric acid:xylitol:water at a 1:1:10 molar ratio, and the chemical characterization of the extracted collagen by discontinuous electrophoresis, thermogravimetric analysis, Fourier transformed infrared spectroscopy and circular dichroism. The extracted material was a pure type I collagen, and the novel approach presented an extraction yield 2.5 times higher than the conventional one, without pre-treatment of raw material and reducing the procedure time from 96 to 1 h. Furthermore, the *in vitro* cytotoxicity evaluation, performed with a mouse fibroblasts cell line, has proven the biocompatibility of the extracted material. Overall, the obtained results demonstrate a simple, quick, cheap and environmentally sustainable process to obtain marine collagen with promising properties for biomedical and cosmetic applications.

**Keywords:** extraction process intensification, marine waste valorization, natural deep eutectic solvent (NADES), blue sharkskin collagen, extract characterization



## 1 INTRODUCTION

Bioeconomic strategies in Europe involve turning organic waste and residues into valuable and safe bio-based products (European Commission, 2018). In EU-28, 88 Mt/year of food is wasted, with associated costs estimated at 143 B€ (Stenmarck et al., 2016). Among all wasted food, the fishing industries are responsible for discarding more than 50% of ocean fish tissues, including heads, skin, and viscera, representing a total of ca. 5.2 Mt/year in the EU (Caruso, 2015). The blue shark (*Prionace glauca*) is the most widely distributed and fished shark species globally. Its catch increased considerably in the late '90s for the consumption of shark meat, fillets, nutritional supplements, and fin soup (da Silva et al., 2021), leading to large amounts of shark skins being wasted. In the past, these residues were used for fertilizers or animal feed since they were considered of low value. However, several studies pointed out these marine by-products as excellent sources of high-added value biopolymers such as collagen (Jha and Kumar, 2019; Lionetto and Esposito Corcione, 2021; Mahmud et al., 2021). For instance, Vitorino & Filhos Lda (Peniche, Portugal), the raw material supplier for this study, is a good example, with a production of about 400 kg/day of blue shark skins as a result of industrial processing.

The fibrous collagen protein constitutes the primary structural element in the animal connective tissues (Shoulders and Raines, 2009). This protein consists of three parallel polypeptide  $\alpha$ -chains forming a triple helix structure, giving origin to more than 29 types of collagen (Shoulders and Raines, 2009; Ricard-Blum, 2011). Besides collagen type I being the main structural element of human tissues' extracellular matrix, collagen also has numerous intrinsic properties such as gelation capacity, biocompatibility, bioactivity, and biodegradability (Davison-Kotler et al., 2019; Lin et al., 2019; Coppola et al., 2020; Subhan et al., 2021). These aspects promote a high demand

for this protein to develop products for the pharmaceutical, biomedical, cosmetic, and food industries. According to Markets and Markets™, the global collagen market is expected to grow in the following years, estimated to be valued at USD 4.1 billion in 2021 and is projected to reach USD 5.3 billion by 2026. Bovine and porcine are the most common collagen sources. Nonetheless, marine sources, such as fish biomass and by-catch organisms, have been rising in the last years as alternatives for obtaining this protein (Coppola et al., 2020; Subhan et al., 2021). However, the blue shark skin wastes are a matrix barely explored for this purpose.

The extraction of collagen for topical biomedical applications is a widely studied topic, and several publications address collagen extraction from marine sources using conventional methodologies and alternative solvents, such as deep eutectic solvents (DES) (Addad et al., 2011; Liu et al., 2015; Sotelo et al., 2016; Bai et al., 2017; Carvalho et al., 2018; Elango et al., 2018; Slimane and Sadok, 2018; Govindharaj et al., 2019; Jafari et al., 2020; Liu et al., 2020; Priyanka et al., 2020; Seixas et al., 2020; Bisht et al., 2021; Blidi et al., 2021). Conventional extractions involve several pre-treatment steps, long extraction times, and low temperatures (Addad et al., 2011; Liu et al., 2015; Sotelo et al., 2016; Carvalho et al., 2018; Elango et al., 2018; Slimane and Sadok, 2018; Govindharaj et al., 2019; Jafari et al., 2020; Liu et al., 2020; Priyanka et al., 2020; Seixas et al., 2020; Blidi et al., 2021). Therefore, alternative methods are needed to implement feasible industrial processes. DES are defined as mixtures of two or more components that present a high melting point depression at a particular composition, becoming liquids at room temperature (Hansen et al., 2021). This type of solvents obtained by the interaction between a hydrogen-bond acceptor and a hydrogen-bond donor has gained much

relevance as a green and sustainable alternative to conventional industrial processes (Paiva et al., 2014; Hansen et al., 2021). These systems present several advantages, namely low price, a large number of different combinations, low toxicity, and biodegradability (Paiva et al., 2014; Hansen et al., 2021). More interest arises when the compounds that constitute the DES are primary metabolites, so-called natural DES or NADES. Representing all the green chemistry principles, the biocompatibility of NADES is of great interest when it comes to the pharmaceutical, medical, and food industries (Liu et al., 2018). Among the natural molecules, citric acid and xylitol have been widely used in forming NADES and have already been studied to extract phenolic and volatile aromatic compounds, metals, among others (Bajkacz and Adamek, 2017; Cunha and Fernandes, 2018; González et al., 2018; Aryati et al., 2020; Guinet et al., 2020; Oomen et al., 2020; Santana et al., 2020; Silva et al., 2020; Fanali et al., 2021; Osowska et al., 2021; Rodríguez-Juan et al., 2021). Although only a few published studies are related to their combined use, NADES composed of citric acid and xylitol, previously and extensively characterised by the works of Grønlien et al. and Guinet et al., present a promising potential for extracting biopolymers (Grønlien et al., 2020; Guinet et al., 2020). This is the case of the work by de Grønlien et al., who reported this NADES system as an adequate collagen solubilizing agent and as a potential excipient for collagen-based products (Grønlien et al., 2020).

This work aims to develop a new sustainable, faster, and more straightforward extraction of collagen with NADES composed of citric acid:xylitol:water to valorize currently undervalued blue shark skin wastes. The extract obtained by the proposed technology was compared to the one obtained using the conventional methodology in regard to protein purity and chemical characterization. Additionally, to evaluate the safety of the extracted material for potential topical applications, the *in vitro* cytotoxicity was evaluated on a mouse fibroblast cell line (NCTC clone 929 cells). This work is fully aligned with the circular economy concept by applying green and sustainable extraction techniques and promoting waste valorization through the isolation of a fibrous protein presenting a high social and economic interest with a low carbon footprint.

## 2 MATERIALS AND METHODS

### 2.1 Materials

Blue shark (*Prionace glauca*) skins were removed from cold-stored fish body parts in an industrial plant and kindly provided by Vitorino & Filhos, Lda (Peniche, Portugal). Skins were washed with ice-cold deionized water and stored frozen at a temperature of  $-20^{\circ}\text{C}$  until use. Acetic acid (99.7%) and citric acid were purchased from Panreac (Germany). Xylitol, commercial Type I collagen from calf skin and  $\beta$ -mercaptoethanol were supplied by Sigma-Aldrich (United States). The protein ladder Precision Plus Protein™ All Blue Prestained Protein Standard, Laemmli Sample

Buffer, Tris/Glycine/SDS Running Buffer, and Bio-Safe™ Coomassie Stain were purchased from Bio-Rad (United States). Minimum essential medium (MEM) with Earle's balanced salts and 2.0 mM L-glutamine, phosphate-buffered saline (PBS), pH = 7.4, and dimethyl sulfoxide (DMSO) were purchased from Sigma (United States). Non-essential amino acids (NEAA), fetal bovine serum (FBS) and 0.25% (w/v) Trypsin-EDTA were purchased from Gibco (Life Technologies, United States). CellTiter 96® Aqueous Non-Radioactive Cell Proliferation Assay (MTS) reagent assay was obtained from Promega (Madison, United States).

### 2.2 NADES Preparation

NADES composed of citric acid:xylitol:water (molar ratio 1:1:10) were prepared according to the method presented by Grønlien (Grønlien et al., 2020) with some modifications. The three-component mixture was weighed into a round bottom flask, and the mixture was stirred in an oil bath at  $50 \pm 5^{\circ}\text{C}$  until a homogenous and transparent liquid was obtained ( $\sim 2$  h).

### 2.3 NADES Viscosity Measurement

The shear viscosity of NADES was measured using a rheometer (MCR 102, Anton Parr, Kinexus Pro+, Malvern) mounted with a parallel plate geometry (PP 50, Anton Parr) with a gap of 1 mm and a constant shear rate of  $10\text{ s}^{-1}$ . A temperature scan was performed from 4 to  $55^{\circ}\text{C}$  at  $3^{\circ}\text{C}/\text{min}$ . Viscosity results are expressed as a mean of three measurements.

### 2.4 Extraction of Collagen From Blue Shark Skin

Two extraction techniques were performed. First, acid-soluble collagen was extracted following the conventional extraction described in the literature (Carvalho et al., 2018). Then, after preliminary optimization tests, the methodology was adapted for collagen extraction using NADES, with some modifications. Frozen skins were freeze-dried for 48 h and milled (Retsch Cross Beater Hammer Mill Sk1, Germany) to obtain a powder. Next, the skin powder was mixed with NADES in a sample: solvent ratio of 1:10 (w:w) for 1 h at  $40^{\circ}\text{C}$  with continuous stirring. The solution was then centrifuged (Fisher Scientific Marathon 22KBR, United States) at 4500 rpm for 20 min. The supernatant was then dialyzed for 72 h against distilled water, with the solutions being changed every 12 h. The resulting extract was freeze-dried for 24 h and stored at room temperature until further use.

### 2.5 Global Extraction Yield and Total Protein Content of the Extract

The extraction yield was calculated using Eq. 1.

$$\text{Yield (\%)} = \frac{\text{weight of dried extract}}{\text{weight of dried skins}} \times 100 \quad (1)$$

To determine the extract's protein content, the obtained freeze-dried samples were dissolved in 0.5 M acetic acid at appropriate concentration and the total protein content was



measured using the Lowry method, with bovine serum albumin as a standard (LOWRY et al., 1951).

## 2.6 Sodium Dodecyl Sulphate-Polyacrylamide Gel Electrophoresis (SDS-PAGE)

To evaluate the purity of the extracts and the molecular weight of the obtained protein fractions, a Bio-Rad Mini-PROTEAN® system (Bio-Rad, United States) was employed to separate proteins by SDS-PAGE. The lyophilized collagen samples were dissolved in 0.5 M acetic acid (2 mg/ml), mixed in a 1:1 (v/v) dilution with Laemmli sample buffer containing 5% (v/v)  $\beta$ -mercaptoethanol and heated for 10 min at 70°C to denature the proteins. The 7.5% Mini-PROTEAN® TGX™ Precast Protein Gel (12-well, 20  $\mu$ L) was loaded with 10  $\mu$ L protein ladder and 10  $\mu$ L from each collagen sample. The samples were run at 200 V for 30 min, and the gel was then stained using the Coomassie stain for 1 h with continuous stirring. Finally, the gel was detained in distilled water overnight and imaged using a 48-megapixel RGB camera.

## 2.7 Thermogravimetric Analysis (TGA)

To evaluate the thermal behavior profiles of the collagen extracts, TGA analysis was performed in a Thermal Analysis instrument (Labsys EVO, Setaram, Caluire, France), in an argon atmosphere, within a temperature range between 25 and 700°C and a 10°C/min heat ramp.

## 2.8 Fourier-Transform Infrared (FTIR) Spectroscopy

FTIR spectroscopy in attenuated total reflectance (ATR) mode was performed with a Thermo Scientific FTIR spectrometer (Class 1 Laser Product Nicolet 6100, San Jose, United States). The presence of collagen's characteristic chemical bonds/groups was evaluated by recording 32 scans between 4,000–650  $\text{cm}^{-1}$  with a resolution of 4  $\text{cm}^{-1}$ .

## 2.9 Protein Conformation

Circular dichroism (CD) spectra of extracts were recorded from 190 to 260 nm on a Chirascan™ qCD spectrometer/SX20 (Applied Photophysics, United Kingdom) using a 0.1  $\text{cm}^{-1}$  path length cuvette. Dry collagen was dissolved at 1 mg/ml in 0.5 M acetic acid. Samples were loaded at 4°C into precooled CD cuvettes.

## 2.10 Hg Quantification

The presence of mercury in the blue shark skin and collagen extracts was outsourced to Silliker Portugal, S.A. Mercury was quantified by atomic absorption spectrophotometry on a DMA-80 EVO equipment (Milestone, Sorisole, Italy), with previous thermal decomposition of the samples and mercury amalgamation. Mercury quantification results are expressed as a mean of three measurements.

## 2.11 Biocompatibility

### 2.11.1 Samples Preparation

The cytotoxicity of any leachables present in the collagen extracts that can migrate to the skin cells was evaluated following the methodology described in ISO 10993–5, a highly sensitive test used to determine medical devices' toxicity (LI et al., 2015). The leaching of the samples was conducted according to the principles of test sample extraction described in the ISO guidelines. Specimens of each collagen extract were placed in glass vials in contact with the cell culture medium, used as the leaching medium, in a 0.1 g/ml extraction ratio. Sample vials were kept in a shaking water bath at  $37 \pm 1^\circ\text{C}$  for 72 h. After extraction, the biocompatibility testing sample containing the extracted leachables were filter-sterilized using a 0.2  $\mu\text{m}$  syringe filter and used for the cytotoxicity test.

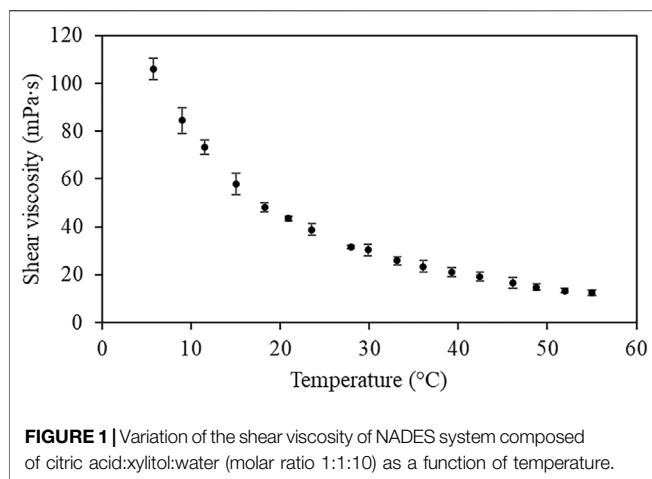
### 2.11.2 Cell Culture

Mouse fibroblasts NCTC clone 929 (ECACC 88102702) cells were purchased from the European Collection of Authenticated Cell Cultures (EACC, Public Health England, Salisbury, United Kingdom). Cells were routinely grown in a standard medium MEM supplemented with 1% (v/v) NEAA and 10% (v/v) heat-inactivated FBS. Stock cells were maintained as monolayers in 75  $\text{cm}^2$  culture flasks, subcultured every week (seeding 30,000 cells/ $\text{cm}^2$ ), and incubated at 37°C in a 5%  $\text{CO}_2$  humidified atmosphere. For cell passage, the cells were detached when confluence reached about 80% using 0.25% (v/v) trypsin/EDTA at 37°C. The cells were collected, and viability was determined using the standard trypan blue staining procedure. Cell counting was performed using a hemocytometer. All cellular assays described below were performed with cells between passages 10 and 25.

### 2.11.3 MTS Metabolic Activity Assay

Cell viability was quantified using the MTS cytotoxicity test, following the methodology described in the literature (Batista et al., 2020) with slight modifications. NCTC clone 929 cells were seeded into 96-well plates (100  $\mu\text{L}$  volume) with a density of  $1.0 \times 10^4$  cells/100  $\mu\text{L}$  and maintained in culture for 24 h (~1 doubling period) to form a semiconfluent monolayer. After 24 h, the culture media was replaced by 100  $\mu\text{L}$  of the prepared biocompatibility testing sample and cells were incubated for 24 h. Lastly, the biocompatibility testing sample was removed, cells were rinsed with PBS and incubated for 2 h with 100  $\mu\text{L}$  of MTS reagent assay, diluted according to the manufacturer's information. The absorbance was recorded at 490 nm using a microplate spectrophotometer (EPOCH, 219 Bio-Tek, United States). Experiments were performed in triplicate in three independent assays. The positive control of cytotoxicity was done with a treatment of 10% (v/v) DMSO solution diluted in MEM.

Results were expressed as a percentage of cellular viability (Viab.%) relative to the control (untreated cells). A cytotoxic effect was considered for viability percentages below 70%, according to ISO 10993–5.

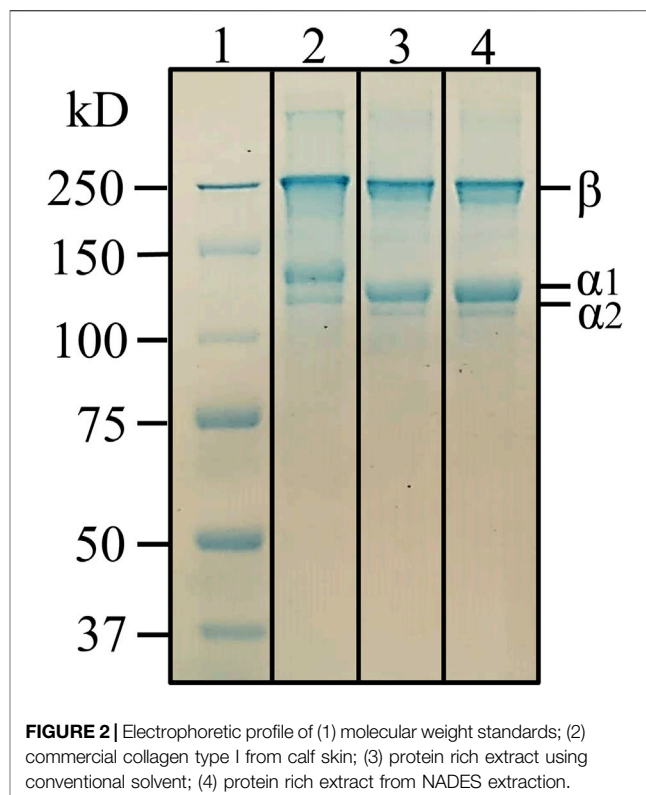


## 2.12 Statistical Analysis

Each experiment was performed at least in triplicate and all data are expressed as means  $\pm$  standard errors (SD). The statistical analysis of the data was performed using GraphPad Prism 6 (GraphPad Software, Inc., CA). All values were tested for normal distribution and equal variance. When homogeneous variances were confirmed, data were analyzed by One Way Analysis of Variance (ANOVA) coupled with Tukey's post hoc analysis to identify means with significant differences.

## 3 RESULTS AND DISCUSSION

Despite some published works describing collagen extraction from marine sources using solid-liquid extractions with conventional solvents and DES, blue shark skin wastes have been barely explored for this purpose (Addad et al., 2011; Liu et al., 2015; Sotelo et al., 2016; Bai et al., 2017; Carvalho et al., 2018; Elango et al., 2018; Slimane and Sadok, 2018; Govindharaj et al., 2019; Jafari et al., 2020; Liu et al., 2020; Priyanka et al., 2020; Seixas et al., 2020; Bisht et al., 2021; Blidi et al., 2021). Due to their ability to solubilize collagen and biocompatible properties, NADES are interesting candidates as extraction solvents and potential excipients in collagen-based products. Recently, two studies have been published on collagen extraction from cod skins using NADES systems composed of choline chloride-oxalic acid and urea-lactic acid (Bai et al., 2017; Bisht et al., 2021). Although these systems are classified as NADES, choline salts and their



esters (including choline chloride) and urea reaction products belong to the EU prohibited substances list in cosmetics (The European Parliament And The Council Of The European Union, 2009). This is a limitation for using these NADES as extraction solvents and product excipients of novel collagen-based products for potential applications in contact with the human skin. This work presents a new extraction methodology for recovering collagen from blue shark skins using bio-safe NADES. Based on the ability to dissolve collagen while maintaining its structural properties, the NADES system composed of citric acid:xylitol:water (molar ratio 1:1:10) was used to perform the extraction (Grønlien et al., 2020). Collagen was expected to be extracted through the protein diffusion to the liquid media due to the pH media decrease by the presence of citric acid. Xylitol was expected to act as a collagen thermostabilizing agent since polyols have been reported to stabilize the triple helix of collagen by binding to the protein surface and forming additional hydrogen bonds (Usha et al., 2006; Usha and Ramasami, 2008).

**TABLE 1** | Global extraction yield (%), extracts' protein content (%) and the protein extraction yield (%) of the extracts obtained from blue shark skins with conventional solvent and NADES.

Methodology	Operating conditions		Extraction yield (%)		Protein content (%)
	NaOH 2016Pre-treatment	Collagen extraction	Global	Protein	Extract
Conventional	48 h; 4°C	48 h; 4°C	7.57 $\pm$ 3.53	6.69 $\pm$ 3.12	88.3 $\pm$ 4.94
NADES	—	1 h; 40°C	18.6 $\pm$ 3.82	16.1 $\pm$ 3.30	86.5 $\pm$ 10.9

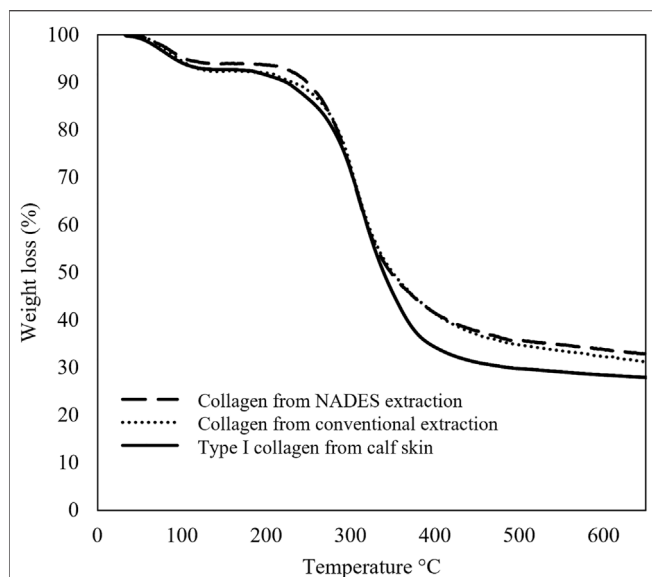


**FIGURE 3 |** TGA data of the collagen extracts obtained from blue shark skins with conventional solvent and NADES and collagen standard from calf skin.

### 3.1 NADES Viscosity

The inherent viscosity of most DES is an important factor in solid-liquid extractions as it regulates the mass transfer rate and influences the extraction yield. Although most DES exhibits relatively high viscosity, this property can be significantly controlled by temperature, mitigating the strength of intermolecular forces in DES, reducing their viscosity (Cunha and Fernandes, 2018; Liu et al., 2018). This physical characteristic is even more critical in this work since conventional collagen recovery methods are performed at low temperatures (about 4°C). **Figure 1** presents the viscosity values as a function of temperature for the NADES system adapted in our new collagen extraction methodology.

A decrease in NADES viscosity with increasing temperature is observed. As expected, this NADES presented high viscosity (106 mPa s) when employing the low temperatures used in the conventional extraction methodology of collagen (4°C). A temperature increase impacts the intermolecular forces of DES and consequently decreases the solvent viscosity (Liu et al., 2018). Therefore, the extraction temperature is an important factor in regulating mass transfer rate and influencing the extraction yield. To ensure a low viscosity of the NADES system without affecting the collagen structural properties, the temperature of 40°C was chosen to carry out the new NADES extraction method. Extractions at higher temperatures (60 and 80°C) resulted in the hydrolysis of the collagen (**Supplementary Figure S1.**).

### 3.2 Global and Protein Extraction Yield of the Extracts and Collagen Purity

For the novel collagen extraction approach, freeze-dried skin powder was mixed with NADES in a sample:solvent ratio of 1:10 (w:w) for 1 h at 40°C. Collagen was also extracted following the

conventional extraction methodology described in the literature (Carvalho et al., 2018). Both extracts were dialyzed, and the resulting acid-soluble collagen was freeze-dried. The global extraction yield, extracts' total protein content and the protein extraction yield are reported in **Table 1**.

The results showed a global extraction yield of 18.6% when collagen was recovered using NADES, 2.5 times higher than the yield obtained with conventional extraction (7.57%). Although blue shark skins are a barely explored matrix for collagen extraction, the results obtained with the conventional method agree with other works reported on the extraction of collagen from marine species skins (Jafari et al., 2020). In addition to the ability of citric acid:xylitol:water (molar ratio 1:1:10) NADES to dissolve collagen, this yield improvement may be related to the higher temperature (40°C) used in NADES extraction when compared to the conventional approach (4°C). As verified in **Figure 1**, the increasing temperature reduces the NADES viscosity, resulting in a higher mass transfer rate. The obtained results agree with the previous work of Bai et al., which showed that temperature has a positive influence on collagen extraction yield (Bai et al., 2017). Usually, collagen extraction involves extensive pre-treatment and extraction steps under low temperatures. However, the higher temperature combined with the chosen NADES system allowed to obtain a rich protein extract from shark skins, avoiding the raw material's pre-treatment step and a noticeable shorter extraction time (1 h). The conventional methods involve complex acidic/basic treatments and multiple stages for the isolation and precipitation of collagen, which contributes to the low extraction yield.

Total protein content in the extracts was quantified using the Lowry method. The results showed that both extracts are rich in protein, above 87% of total protein content. Therefore, a superior protein yield using NADES methodology was obtained. The molecular weight of the obtained protein fractions was assessed by SDS-PAGE. **Figure 2** shows SDS-PAGE band patterns of commercial calf skin collagen type I, used as standard, and the extracts obtained using NADES and the conventional methodologies.

Similar electrophoretic band patterns of the two obtained extracts with a commercial calf skin collagen standard were observed. This similarity of the bands' distribution and molecular weights suggests that both extracts contain highly pure type I collagen, with a structure of two distinct  $\alpha$ -chains of around 120 kDa and a beta component of about 200 kDa, a characteristic electrophoretic profile comparable with other fish species (Jafari et al., 2020). The slightly lower molecular weight of  $\alpha$ -chains from the extracted collagens, when compared to the standard, may be due to the differences in the collagen animal source. This result agrees with the literature, as collagen from marine sources has been associated with differences in the amino acid composition compared to mammalian collagen (Carvalho et al., 2018). This characteristic makes collagen from marine sources more susceptible to high-temperature degradation and more susceptible to hydrolysis (Sotelo et al., 2016). However, although NADES extraction is performed at 40°C, the absence of bands below 100 kDa suggests that the selected NADES system



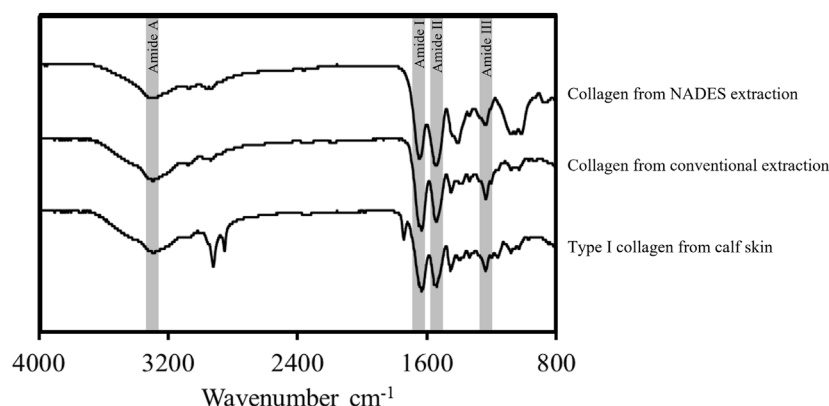


**FIGURE 4 |** FTIR spectra of the collagen extracts obtained from blue shark skins with conventional solvent and NADES and collagen standard from calf skin, exhibiting the main vibrations of collagen molecular organization, amide A, amide I, amide II, and amide III.

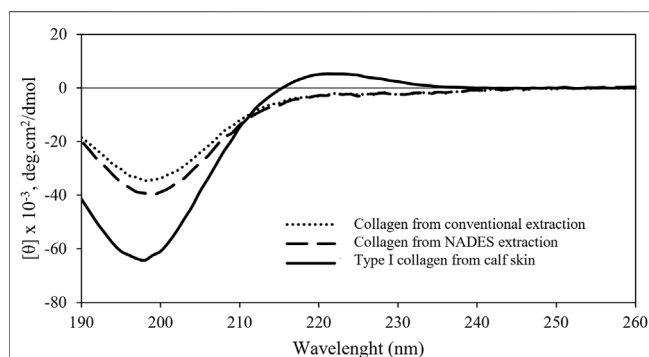


**FIGURE 5 |** CD spectra of the collagen extracts obtained from blue shark skins with conventional solvent and NADES and type I collagen standard from calf skin.

stabilized and prevented collagen degradation and that the extracted collagen has high purity.

To confirm the purity of the collagen extracts, TGA was performed. **Figure 3** compares the thermal behavior of the obtained samples with a commercial standard. TGA allows the analysis of different thermal decomposition profiles between samples, indicating the presence of potential contaminants.

The thermograms shown in **Figure 3** present similar profiles, with the final mass percentage tending to the same values (30%). TGA curves present weight loss in the range from room temperature to 150°C due to water evaporation and between 200 and 500°C associated with the decomposition of collagen. The slight differences may be due to marginally different moisture content between samples. Therefore, these results suggest that the collagen extracts obtained in this work have high purity.

### 3.3 FTIR

The FTIR spectra of both collagen extracts from blue shark skin and commercial type I collagen from calf skin are exhibited in **Figure 4**.

Despite the different extraction conditions and collagen sources, the overall spectra profiles presented in **Figure 4** are

**TABLE 2 |** Hg content of shark skins and collagen extract from NADES extraction.

Sample	Hg content (mg/kg dry weight)
Shark skins	1.64 (±0.48)
Collagen extract	< Detection limit (0.01 mg/kg)

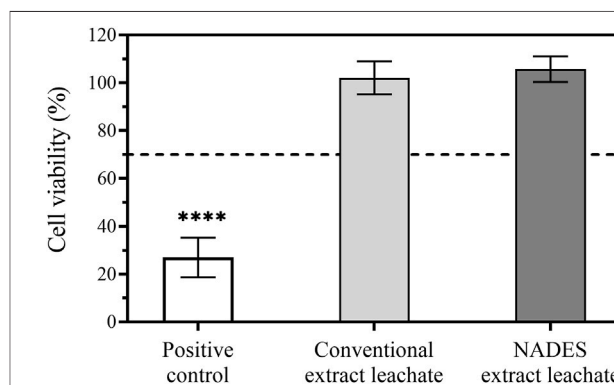


**FIGURE 6 |** Cytotoxicity assay using MTS reagent: leached extracts were incubated in NCTC clone 929 cell line for 24 h at 37°C and 5% CO<sub>2</sub> humidified atmosphere (mean ± SD, *n* = 3). Statistically significant differences comparing all conditions are indicated by \*\*\*\* (*p* < 0.0001).

similar, suggesting that all samples show comparable structures and chemical compositions. Typical bands of type I collagen's molecular chain, corresponding to amide A, amide I, amide II, and amide III, were observed (Silva et al., 2016; Elango et al., 2018; Jafari et al., 2020). The broad band of amide A, observed at 3000–3500 cm<sup>-1</sup>, is typical for the presence of N-H stretching coupled with hydrogen bonds. The peak for amide I, from the stretching vibrations of the carbonyl groups (C=O) in proteins, is observed at 1634 cm<sup>-1</sup>. The presence of amide II, attributed to N-H bending coupled with C-N stretching, is observed from the peak at 1550 cm<sup>-1</sup>. Finally, the peak of the amide III group from the N-H bending was identified at 1239 cm<sup>-1</sup>. The FTIR analysis

suggested that the extracts correspond to type I collagen as the commercial standard also analyzed. These results indicate that both extraction methods did not damage the functional groups present in the collagen triple helix.

### 3.4 Circular Dichroism

To assess whether the extracted collagen is in its native triple helical structure, the CD spectra of the different extracts were obtained and compared with the commercial type I collagen standard. This spectroscopy tool assesses if type I collagen has a well-defined CD transition with a positive peak around 222 nm, representing a triple helix conformation (Carvalho et al., 2018; Jafari et al., 2020). The results of the CD spectroscopy analysis are shown in **Figure 5**.

A negative peak of the extracted collagens is close to the negative peak of collagen standard in the 199 nm region. However, unlike the native collagen sample, none of the extracted collagens presented a positive peak in the 222 nm region, characteristic of the  $\alpha$  helix conformation. These results suggest that although the collagen extracts appear to have a rather complex secondary structure, at least partial protein denaturation occurred upon extraction. This could be due to the presence of dilute citric acid that could dissociate intermolecular interactions of collagen triple helix (Carvalho et al., 2018). These results suggest that the conventional and the proposed NADES methodologies do not ensure the total structural integrity of the biopolymer. However, the CD spectra similarity of both extracts suggests that the higher temperature of NADES extraction methodology is not responsible for the protein denaturation. Nevertheless, this has been a struggle found in different works of collagen extraction from other marine sources that reported similar spectra profiles, containing only a negative peak around 197–203 nm (Ikoma et al., 2003; Silva et al., 2016; Carvalho et al., 2018).

### 3.5 Hg Quantification

Several works have reported the bioaccumulation of Hg in blue shark tissues (Branco et al., 2004; Branco et al., 2007; Escobar-Sánchez et al., 2011). The presence of this contaminant can restrain the recovery of collagen from blue shark wastes for the development of novel biomedical products. Various international governing bodies such as the U.S. Pharmacopeia, European Commission or the U.S. Food and Drug Administration impose specific and strict regulations with limits for the elemental impurities content in products for biomedical, cosmetic, or food purposes (Barin et al., 2016; United States Pharmacopeia - USP, 2016; CBER, 2022). The content of Hg impurities in shark skins and collagen extract was determined by atomic absorption spectrophotometry.

**Table 2** presents the results of Hg quantification in the raw material and collagen extract obtained with NADES.

The blue shark wastes used for collagen recovery in this work presented a contamination of 1.64 ( $\pm 0.48$ ) mg Hg/kg skins dry weight. However, **Table 2** shows that the Hg content in the collagen extract obtained with the NADES extraction method was below the equipment detection and regulatory limits. These

results suggest that the new methodology for collagen recovery presented in this work prevents the concentration of Hg impurities from raw material in the final extract.

## 3.6 Biocompatibility

### 3.6.1 Cytotoxicity

To evaluate the potential of the extracted collagen for biomedical skin applications, the cytotoxicity on a mouse fibroblasts cell line was assessed (**Figure 6**). Due to the neutral pH of the cell culture medium, the extracted acid-soluble collagen does not solubilize, hindering the direct and homogeneous contact of the extract with the cells. So, the cytotoxicity of any leachables that can migrate from the extract to the skin cells was evaluated following the ISO 10993–5 methodology. This approach helps determine the biological reactivity of any substances that can be released from a medical device or material during clinical use and demonstrate the hazard potential of the product.

As shown in **Figure 6**, none of the leachates showed percentages of cytotoxicity below the standard threshold of 70%. The results show that possible leachable chemicals from the collagen extracts obtained with our novel methodology are noncytotoxic.

## 4 CONCLUSION

This work successfully extracted marine collagen from blue shark skins, a very abundant waste resulting from the fish industry. Collagen was obtained through a new sustainable, faster, and more straightforward extraction approach using NADES composed of citric acid:xylitol:water when compared with the conventionally used extraction. In fact, the procedure was effective without pre-treating raw materials, greatly reducing the extraction time from 96 to 1 h and, therefore, the associated processing costs. Additionally, the proposed methodology resulted in a 2.5 times improvement in extraction yield when compared to the traditional procedure, resulting in the isolation of more than 21% of the protein content of the blue shark skin studied in this work. The new operating conditions allowed to obtain collagen with similar properties in terms of purity, molecular weight, chemical composition, and cytotoxicity when compared to the collagen obtained by the conventional methodology. Overall, the obtained results provide essential data on the industry-favorable extraction process parameters, opening the possibility of a simple, quick, cost-effective, and environmentally sustainable process to obtain blue shark skin-derived collagen as a promising material for topical biomedical applications.

## DATA AVAILABILITY STATEMENT

The original contributions presented in the study are included in the article/**Supplementary Material**, further inquiries can be directed to the corresponding author.

## AUTHOR CONTRIBUTIONS

MB carried out the experiments and wrote the first draft of the manuscript. AD supervised the work. All authors contributed to the conception and design of the study, manuscript revision, read, and approved the submitted version.

## FUNDING

iNOVA4Health–UIDB/04462/2020 and UIDP/04462/2020, a program financially supported by Fundação para a Ciência e Tecnologia/Ministério da Ciência, Tecnologia e Ensino Superior, through national funds is acknowledged. This work has received also funding from the ERC-2016-CoG 725034 and was supported by the Associate Laboratory for Green Chemistry (LAQV), financed by national funds from FCT/MCTES (UIDB/50006/

2020). MB acknowledges FCT for the financial support through the 2020.05895.BD grant.

## ACKNOWLEDGMENTS

The authors acknowledge the financial support received from the Funding from INTERFACE Programme, through the Innovation, Technology and Circular Economy Fund (FITEC), is gratefully acknowledged.

## SUPPLEMENTARY MATERIAL

The Supplementary Material for this article can be found online at: <https://www.frontiersin.org/articles/10.3389/fchem.2022.937036/full#supplementary-material>

## REFERENCES

- Addad, S., Exposito, J.-Y., Faye, C., Ricard-Blum, S., and Lethias, C. (2011). Isolation, Characterization and Biological Evaluation of Jellyfish Collagen for Use in Biomedical Applications. *Mar. Drugs* 9 (6), 967–983. doi:10.3390/md9060967
- Aryati, W. D., Nadhira, A., Febianli, D., Fransisca, F., and Mun'im, A. (2020). Natural Deep Eutectic Solvents Ultrasound-Assisted Extraction (NADES-UAE) of Trans-cinnamaldehyde and Coumarin from Cinnamon Bark [*Cinnamomum Burmannii* (Nees T. Nees) Blume]. *JRP* 24 (3), 389–398. doi:10.35333/jrp.2020.161
- Bai, C., Wei, Q., and Ren, X. (2017). Selective Extraction of Collagen Peptides with High Purity from Cod Skins by Deep Eutectic Solvents. *ACS Sustain. Chem. Eng.* 5 (8), 7220–7227. doi:10.1021/acsschemeng.7b01439
- Bajkacz, S., and Adamek, J. (2017). Evaluation of New Natural Deep Eutectic Solvents for the Extraction of Isoflavones from Soy Products. *Talanta* 168, 329–335. doi:10.1016/j.talanta.2017.02.065
- Barin, J. S., Mello, P. A., Mesko, M. F., Duarte, F. A., and Flores, E. M. M. (2016). Determination of Elemental Impurities in Pharmaceutical Products and Related Matrices by ICP-Based Methods: a Review. *Anal. Bioanal. Chem.* 408 (17), 4547–4566. doi:10.1007/s00216-016-9471-6
- Batista, M. P., Gonçalves, V. S. S., Gaspar, F. B., Nogueira, I. D., Matias, A. A., and Gurikov, P. (2020). Novel Alginate-Chitosan Aerogel Fibres for Potential Wound Healing Applications. *Int. J. Biol. Macromol.* 156, 773–782. doi:10.1016/j.ijbiomac.2020.04.089
- Bisht, M., Martins, M., Dias, A. C. R. V., Ventura, S. P. M., and Coutinho, J. A. P. (2021). Uncovering the Potential of Aqueous Solutions of Deep Eutectic Solvents on the Extraction and Purification of Collagen Type I from Atlantic Codfish (*Gadus morhua*). *Green Chem.* 23 (22), 8940–8948. doi:10.1039/d1gc01432c
- Bliidi, O. El., Omari, N. El., Balahbib, A., Ghchime, R., Menyiy, N. El., Ibrahim, A., et al. (2021). Extraction Methods, Characterization and Biomedical Applications of Collagen: A Review. *Biointerface Res. Appl. Chem.* 11 (5), 13587–13613.
- Branco, V., Canário, J., Vale, C., Raimundo, J., and Reis, C. (2004). Total and Organic Mercury Concentrations in Muscle Tissue of the Blue Shark (*Prionace glauca* L.1758) from the Northeast Atlantic. *Mar. Pollut. Bull.* 49 (9–10), 871–874. doi:10.1016/j.marpolbul.2004.09.002
- Branco, V., Vale, C., Canário, J., and Santos, M. N. d. (2007). Mercury and Selenium in Blue Shark (*Prionace glauca*, L. 1758) and Swordfish (*Xiphias Gladius*, L. 1758) from Two Areas of the Atlantic Ocean. *Environ. Pollut.* 150 (3), 373–380. doi:10.1016/j.envpol.2007.01.040
- Caruso, G. (2015). Fishery Wastes and By-Products: A Resource to Be Valorised. *J. Fish. Sci.* 9 (4), 080–083.
- Carvalho, A. M., Marques, A. P., Silva, T. H., and Reis, R. L. (2018). Evaluation of the Potential of Collagen from Codfish Skin as a Biomaterial for Biomedical Applications. *Mar. Drugs* 16 (12), 1–14. doi:10.3390/md16120495
- Cber, F. D. A. (2022). Q3D (R1) Elemental Impurities Guidance for Industry. U S Dep Heal Hum Serv Food Drug Adm [Internet]. 2020;(March). Available from: <https://www.fda.gov/media/135956/download#:~:text=Class 1%3A The elements arsenic>.
- Coppola, D., Oliviero, M., Vitale, G. A., Lauritano, C., D'Ambra, I., Iannace, S., et al. (2020). Marine Collagen from Alternative and Sustainable Sources: Extraction, Processing and Applications. *Mar. Drugs* 18 (4), 214. doi:10.3390/md18040214
- Cunha, S. C., and Fernandes, J. O. (2018). Extraction Techniques with Deep Eutectic Solvents. *TrAC Trends Anal. Chem.* 105, 225–239. doi:10.1016/j.trac.2018.05.001
- da Silva, T. E. F., Lessa, R., and Santana, F. M. (2021). Current Knowledge on Biology, Fishing and Conservation of the Blue Shark (*Prionace glauca*). *Neotrop. Biol. Conserv.* 16 (1), 71–88. doi:10.3897/neotropical.16.58691
- Davison-Kotler, E., Marshall, W. S., and García-Gareta, E. (2019). Sources of Collagen for Biomaterials in Skin Wound Healing. *Bioengineering* 6 (3), 1–15. doi:10.3390/bioengineering6030056
- Elango, J., Lee, J. W., Wang, S., Henrotin, Y., De Val, J. E. M. S., M Regenstein, J., et al. (2018). Evaluation of Differentiated Bone Cells Proliferation by Blue Shark Skin Collagen via Biochemical for Bone Tissue Engineering. *Mar. Drugs* 16 (10), 350. doi:10.3390/md16100350
- Escobar-Sánchez, O., Galván-Magaña, F., and Rosiles-Martínez, R. (2011). Biomagnification of Mercury and Selenium in Blue Shark *Prionace glauca* from the Pacific Ocean off Mexico. *Biol. Trace Elem. Res.* 144 (1–3), 550–559. doi:10.1007/s12011-011-9040-y
- European Commission (2018). *A Sustainable Bioeconomy for Europe: Strengthening the Connection between Economy, society and the environment* [Internet]. Brussels, Belgium: Directorate-General for Research and Innovation. Available from: <https://data.europa.eu/doi/10.2777/478385>.
- Fanali, C., Gallo, V., Posta, S. Della., Dugo, L., Mazzeo, L., Cocchi, M., et al. (2021). Choline Chloride–Lactic Acid-Based NADES as an Extraction Medium in a Response Surface Methodology-Optimized Method for the Extraction of Phenolic Compounds from Hazelnut Skin. *Molecules* 26 (9), 2652. doi:10.3390/molecules26092652
- González, C. G., Mustafa, N. R., Wilson, E. G., Verpoorte, R., and Choi, Y. H. (2018). Application of Natural Deep Eutectic Solvents for the “Green” extraction of Vanillin from Vanilla Pods. *Flavour Fragr. J.* 33 (1), 91–96.
- Govindharaj, M., Roopavath, U. K., and Rath, S. N. (2019). Valorization of Discarded Marine Eel Fish Skin for Collagen Extraction as a 3D Printable Blue Biomaterial for Tissue Engineering. *J. Clean. Prod.* 230, 412–419. doi:10.1016/j.jclepro.2019.05.082
- Gronlien, K. G., Pedersen, M. E., and Tønnesen, H. H. (2020). A Natural Deep Eutectic Solvent (NADES) as Potential Excipient in Collagen-Based Products. *Int. J. Biol. Macromol.* 156, 394–402. doi:10.1016/j.ijbiomac.2020.04.026
- Guinet, Y., Paccou, L., and Hédoux, A. (2020). Analysis of Xylitol - Citric Acid System Forming Deep Eutectic Solvent: Application for Dissolving Poorly

- Water-Soluble Drugs. A Combination of Calorimetric and Raman Investigations. *J. Mol. Liq.* 318, 114317. doi:10.1016/j.molliq.2020.114317
- Hansen, B. B., Spittle, S., Chen, B., Poe, D., Zhang, Y., Klein, J. M., et al. (2021). Deep Eutectic Solvents: A Review of Fundamentals and Applications. *Chem. Rev.* 121 (3), 1232–1285. doi:10.1021/acs.chemrev.0c00385
- Ikoma, T., Kobayashi, H., Tanaka, J., Walsh, D., and Mann, S. (2003). Physical Properties of Type I Collagen Extracted from Fish Scales of *Pagrus major* and *Oreochromis niloticus*. *Int. J. Biol. Macromol.* 32 (3–5), 199–204. doi:10.1016/s0141-8130(03)00054-0
- Jafari, H., Lista, A., Siekapien, M. M., Ghaffari-Bohlouli, P., Nie, L., Alimoradi, H., et al. (2020). Fish Collagen: Extraction, Characterization, and Applications for Biomaterials Engineering. *Polym. (Basel)* 12 (10), 1–37. doi:10.3390/polym12102230
- Jha, A., and Kumar, A. (2019). Biobased Technologies for the Efficient Extraction of Biopolymers from Waste Biomass. *Bioprocess Biosyst. Eng.* 42 (12), 1893–1901. Available from. doi:10.1007/s00449-019-02199-2
- Li, W., Zhou, J., and Xu, Y. (2015). Study of the *In Vitro* Cytotoxicity Testing of Medical Devices. *Biomed. Rep.* 3 (5), 617–620. doi:10.3892/br.2015.481
- Lin, K., Zhang, D., Macedo, M. H., Cui, W., Sarmiento, B., and Shen, G. (2019). Advanced Collagen-Based Biomaterials for Regenerative Biomedicine. *Adv. Funct. Mater.* 29 (3), 1–16. doi:10.1002/adfm.201804943
- Lionetto, F., and Esposito Corcione, C. (2021). Recent Applications of Biopolymers Derived from Fish Industry Waste in Food Packaging. *Polym. (Basel)* 13 (14). doi:10.3390/polym13142337
- Liu, D., Wei, G., Li, T., Hu, J., Lu, N., Regenstein, J. M., et al. (2015). Effects of Alkaline Pretreatments and Acid Extraction Conditions on the Acid-Soluble Collagen from Grass Carp (*Ctenopharyngodon idella*) Skin. *Food Chem.* 172, 836–843. Available from. doi:10.1016/j.foodchem.2014.09.147
- Liu, J., Shibata, M., Ma, Q., Liu, F., Lu, Q., Shan, Q., et al. (2020). Characterization of Fish Collagen from Blue Shark Skin and its Application for Chitosan-Collagen Composite Coating to Preserve Red Porgy (*Pagrus major*) Meat. *J. Food Biochem.* 44 (8), e13265–14. doi:10.1111/jfbc.13265
- Liu, Y., Friesen, J. B., McAlpine, J. B., Lankin, D. C., Chen, S.-N., and Pauli, G. F. (2018). Natural Deep Eutectic Solvents: Properties, Applications, and Perspectives. *J. Nat. Prod.* 81 (3), 679–690. doi:10.1021/acs.jnatprod.7b00945
- Lowry, O., Rosebrough, N., Farr, A. L., and Randall, R. (1951). Protein Measurement with the Folin Phenol Reagent. *J. Biol. Chem.* 193 (1), 265–275. doi:10.1016/s0021-9258(19)52451-6
- Mahmud, N., Islam, J., and Tahergorabi, R. (2021). Marine Biopolymers: Applications in Food Packaging. *Processes* 9, 2245. doi:10.3390/pr9122245
- Oomen, W. W., Begines, P., Mustafa, N. R., Wilson, E. G., Verpoorte, R., and Choi, Y. H. (2020). Natural Deep Eutectic Solvent Extraction of Flavonoids of *Scutellaria baicalensis* as a Replacement for Conventional Organic Solvents. *Molecules* 25 (3), 1–11. doi:10.3390/molecules25030617
- Osowska, N., Paduszyński, K., Matczuk, M., and Ruzik, L. (2021). New Solvents for Metal Extraction - NADES. Prediction and Optimization of Efficient Extraction of Selected Metals by ICP-MS/MS. *J. Anal. At. Spectrom.* 36 (5), 946–953. doi:10.1039/d0ja00492h
- Paiva, A., Craveiro, R., Aroso, I., Martins, M., Reis, R. L., and Duarte, A. R. C. (2014). Natural Deep Eutectic Solvents - Solvents for the 21st Century. *ACS Sustain. Chem. Eng.* 2 (5), 1063–1071. doi:10.1021/sc500096j
- Priyanka, K., Adil, M., Begum, A. K. M., Revathi, K., and Kumar, A. (2020). Extraction of Acid Soluble Collagen from *Coryphaenahippurus* (Mahimahi) and its Application in Tissue Engineering. *Ann. Romanian Soc. Cell Biol.* 24 (1), 197–212.
- Ricard-Blum, S. (2011). The Collagen Family. *Cold Spring Harb. Perspect. Biol.* 3 (1), a004978–19. doi:10.1101/cshperspect.a004978
- Rodríguez-Juan, E., Rodríguez-Romero, C., Fernández-Bolaños, J., Florido, M. C., and García-Borrego, A. (2021). Phenolic Compounds from Virgin Olive Oil Obtained by Natural Deep Eutectic Solvent (NADES): Effect of the Extraction and Recovery Conditions. *J. Food Sci. Technol.* 58 (2), 552–561. doi:10.1007/s13197-020-04567-3
- Santana, A. P. R., Andrade, D. F., Guimarães, T. G. S., Amaral, C. D. B., Oliveira, A., and Gonzalez, M. H. (2020). Synthesis of Natural Deep Eutectic Solvents Using a Mixture Design for Extraction of Animal and Plant Samples Prior to ICP-MS Analysis. *Talanta* 216, 120956. doi:10.1016/j.talanta.2020.120956
- Seixas, M. J., Martins, E., Reis, R. L., and Silva, T. H. (2020). Extraction and Characterization of Collagen from Elasmobranch Byproducts for Potential Biomaterial Use. *Mar. Drugs* 18 (12), 1–18. doi:10.3390/md18120617
- Shoulders, M. D., and Raines, R. T. (2009). Collagen Structure and Stability. *Annu. Rev. Biochem.* 78, 929–958. doi:10.1146/annurev.biochem.77.032207.120833
- Silva, D. T. d., Pauletto, R., Cavalheiro, S. d. S., Bochi, V. C., Rodrigues, E., Weber, J., et al. (2020). Natural Deep Eutectic Solvents as a Biocompatible Tool for the Extraction of Blueberry Anthocyanins. *J. Food Compos. Analysis* 89, 103470. doi:10.1016/j.jfca.2020.103470
- Silva, J. C., Barros, A. A., Aroso, I. M., Fassini, D., Silva, T. H., Reis, R. L., et al. (2016). Extraction of Collagen/Gelatin from the Marine Demosponge *Chondrosia reniformis* (Nardo, 1847) Using Water Acidified with Carbon Dioxide - Process Optimization. *Ind. Eng. Chem. Res.* 55 (25), 6922–6930. doi:10.1021/acs.iecr.6b00523
- Slimane, E. B., and Sadok, S. (2018). Collagen from Cartilaginous Fish By-Products for a Potential Application in Bioactive Film Composite. *Mar. Drugs* 16 (6), 211. doi:10.3390/md16060211
- Sotelo, C. G., Comesaña, M. B., Ariza, P. R., and Pérez-Martín, R. I. (2016). Characterization of Collagen from Different Discarded Fish Species of the West Coast of the Iberian Peninsula. *J. Aquatic Food Prod. Technol.* 25 (3), 388–399. doi:10.1080/10498850.2013.865283
- Stenmarck, Å., Jensen, C., Quedsted, T., Moates, G., Cseh, B., Juul, S., et al. (2016). *Estimates of European Food Waste Levels*. [Internet]. Stockholm: IVL Swedish Environmental Research Institute - EU FUSIONS. Available from: <https://edepot.wur.nl/378674>.
- Subhan, F., Hussain, Z., Tauseef, I., Shehzad, A., and Wahid, F. (2021). A Review on Recent Advances and Applications of Fish Collagen. *Crit. Rev. Food Sci. Nutr.* 61 (6), 1027–1037. Available from. doi:10.1080/10408398.2020.1751585
- The European Parliament And The Council Of The European Union (2009). ER No. 1223/2009 of the European Parliament and of the Council of 30 November 2009 on Cosmetic Products. *Off. J. Eur. Union* 342/84–342/127.
- United States Pharmacopeia - USP (2016). Elemental Impurities- Limits. United States Pharmacopeia [Internet]. 2016;1–3. Available from: <https://www.usp.org/sites/default/files/usp/document/our-work/chemical-medicines/key-issues/c232-usp-39.pdf>.
- Usha, R., Raman, S. S., Subramanian, V., and Ramasami, T. (2006). Role of Polyols (Erythritol, Xylitol and Sorbitol) on the Structural Stabilization of Collagen. *Chem. Phys. Lett.* 430 (4–6), 391–396. doi:10.1016/j.cplett.2006.09.023
- Usha, R., and Ramasami, T. (2008). Stability of Collagen with Polyols against Guanidine Denaturation. *Colloids Surfaces B Biointerfaces* 61 (1), 39–42. doi:10.1016/j.colsurfb.2007.07.005

**Conflict of Interest:** The authors declare that the research was conducted in the absence of any commercial or financial relationships that could be construed as a potential conflict of interest.

**Publisher's Note:** All claims expressed in this article are solely those of the authors and do not necessarily represent those of their affiliated organizations, or those of the publisher, the editors and the reviewers. Any product that may be evaluated in this article, or claim that may be made by its manufacturer, is not guaranteed or endorsed by the publisher.

Copyright © 2022 Batista, Fernández, Gaspar, Bronze and Duarte. This is an open-access article distributed under the terms of the Creative Commons Attribution License (CC BY). The use, distribution or reproduction in other forums is permitted, provided the original author(s) and the copyright owner(s) are credited and that the original publication in this journal is cited, in accordance with accepted academic practice. No use, distribution or reproduction is permitted which does not comply with these terms.





# Anthocyanic Vacuolar Inclusions: From Biosynthesis to Storage and Possible Applications

Kees Buhrman<sup>1,2</sup>, Javiera Aravena-Calvo<sup>2</sup>, Clara Ross Zaulich<sup>2</sup>, Kasper Hinz<sup>2</sup> and Tomas Laursen<sup>2\*</sup>

<sup>1</sup>Faculty of Science, University of Amsterdam, Amsterdam, Netherlands, <sup>2</sup>Dynamic Metabolons Group, Section for Plant Biochemistry, Department for Plant and Environmental Sciences, University of Copenhagen, Copenhagen, Denmark

## OPEN ACCESS

### Edited by:

Manoj B. Gawande,  
Palacky University Olomouc, Czechia

### Reviewed by:

Evangelos Tatsis,  
Center for Excellence in Molecular  
Plant Sciences (CAS), China  
Zhang Zongying,  
Shandong Agricultural University,  
China

### \*Correspondence:

Tomas Laursen  
tola@plen.ku.dk

### Specialty section:

This article was submitted to  
Green and Sustainable Chemistry,  
a section of the journal  
Frontiers in Chemistry

Received: 05 April 2022

Accepted: 30 May 2022

Published: 28 June 2022

### Citation:

Buhrman K, Aravena-Calvo J,  
Ross Zaulich C, Hinz K and Laursen T  
(2022) Anthocyanic Vacuolar  
Inclusions: From Biosynthesis to  
Storage and Possible Applications.  
Front. Chem. 10:913324.  
doi: 10.3389/fchem.2022.913324

The ability of plants to accumulate specific metabolites in concentrations beyond their solubility in both aqueous and lipid environments remains a key question in plant biology. Natural Deep Eutectic Solvents (NADES) are mixtures of natural compounds in specific molar ratios, which interact through hydrogen bonding. This results in a viscous liquid that can solubilize high amounts of natural products while maintaining a negligible vapor pressure to prevent release of volatile compounds. While all the components are presents in plant cells, identifying experimental evidence for the occurrence of NADES phases remains a challenging quest. Accumulation of anthocyanin flavonoids in highly concentrated inclusions have been speculated to involve NADES as an inert solvent. The inherent pigment properties of anthocyanins provide an ideal system for studying the formation of NADES in a cellular environment. In this mini-review we discuss the biosynthesis of modified anthocyanins that facilitate their organization in condensates, their transport and storage as a specific type of phase separated inclusions in the vacuole, and the presence of NADES constituents as a natural solution for storing high amounts of flavonoids and other natural products. Finally, we highlight how the knowledge gathered from studying the discussed processes could be used for specific applications within synthetic biology to utilize NADES derived compartments for the production of valuable compounds where the production is challenged by poor solubility, toxic intermediates or unstable and volatile products.

**Keywords:** anthocyanic vacuolar inclusions, anthocyanins, natural deep eutectic solvents, anthocyanin transport, anthocyanin storage, heterologous production

## 1 INTRODUCTION

Flavonoids are aromatic specialized metabolites derived from the phenylpropanoid pathway present in plants. Anthocyanins are a subclass of flavonoids accumulating in the vacuole, giving rise to the color of most fruits, vegetables and flowers, ranging from red to purple and blue, in order to attract pollinators and seed dispersers to ensure plant reproduction (Winkel-Shirley, 2001). Additionally, anthocyanins accumulate in plant vegetative tissue, acting as photo-protection, absorbing UV light, and scavenging free radicals from PSII (Guo et al., 2008). Hence, anthocyanins and other flavonoids are of high interest as food supplements due to their antioxidant qualities promoting numerous health benefits (Konczak and Zhang, 2004; Davis et al., 2009). While their biosynthesis is well-characterized, the cellular circumstances enabling accumulation of high concentrations of

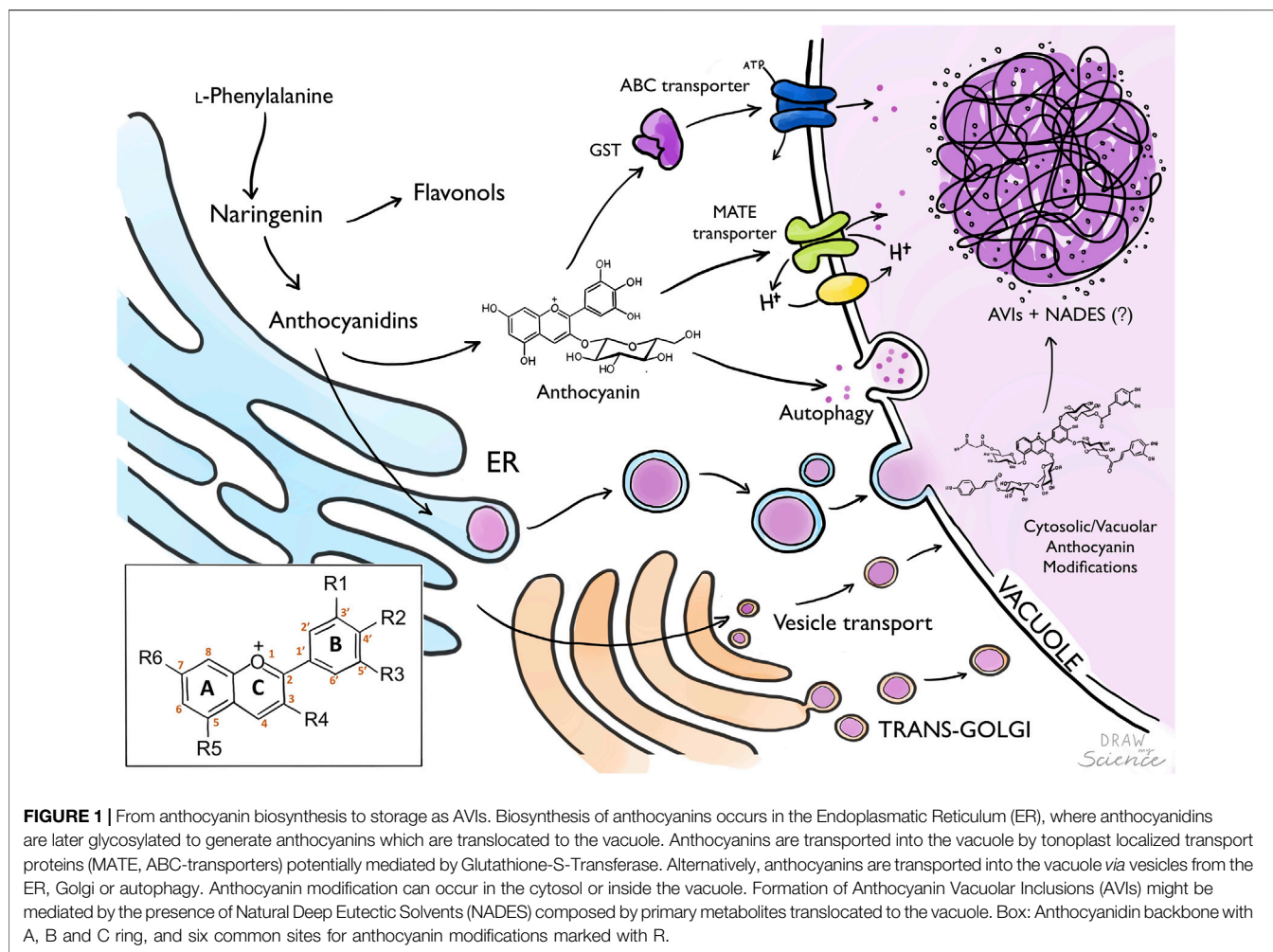
anthocyanins and specialized metabolites in general remain elusive. Examples of high accumulation of specialized metabolites in plants are dhurrin in *Sorghum bicolor* (30% of dry mass) (Kojima et al., 1979; Halkier and Möller, 1989), vanillin-glucoside in *Vanilla planifolia* (Brillouet et al., 2014; Gallage et al., 2018) and anthocyanins in *Lisianthus nigrescens* (up to 24% of dry mass) (Markham et al., 2004). In *Catharanthus roseus*, flowers with Anthocyanic Vacuolar Inclusions (AVIs) have an increased concentration of anthocyanin accumulation, and exhibit a darker flower color (Markham et al., 2000; Deguchi et al., 2020). The term AVI was coined by Markham et al. (Markham et al., 2000) investigating the storage of acylated anthocyanins as inclusions in *Lisianthus* (*Eustoma grandiflorum*) and cyanidin and delphinidin 3,5-*O*-diglucosides in carnation (*Dyanthus caryophyllus*). Following this study, presence and characteristics of AVIs were reported of in *Vitis vinifera* (Conn et al., 2003; Mizuno et al., 2006; Conn et al., 2010), rose (Gonnet, 2003), maize (Irani and Grotewold, 2005), apple (Bae et al., 2006), morning glory (Morita et al., 2005), eggplant (Umeda et al., 2006), lisianthus (Zhang et al., 2006; Chanoca et al., 2015; Kallam et al., 2017), carnation (Okamura et al., 2013), *Rhabdanthus solandri* (Zhang H. et al., 2014), *Catharanthus roseus* (Deguchi et al., 2020), sweet potato (Zhu et al., 2018), petunia (van der Krol et al., 1993; Qi et al., 2013) and black rice (Mackon et al., 2021). Despite of the unifying AVI term, their morphology differs dramatically per plant species. The unified nature of AVIs is further challenged by the variety of experimental setups using different types of microscopy, presence of membranes around AVIs in some species, and the specific types of anthocyanin-modifications accumulating in AVIs being investigated. Moreover, few of these studies propose an extensive mechanism for the aggregation process resulting in AVIs. In this review, we summarize previously identified factors involved in AVI formation and address how the vacuolar environment and solvent characteristics have remained underexposed in studies of AVIs. Additionally, we propose a link between the formation of certain types of AVIs and the existence of a NADES phase as third intracellular phase facilitating accumulation of natural products in concentrations beyond their solubility in water and oil. The existence of such a NADES phase provides a plausible explanation for the condensation of natural products. Finally, we explore how findings on AVI formation and NADES mixtures could provide an entire new engineering avenue for improved heterologous production of flavonoids.

## 1.1 Biosynthesis of Decorated Anthocyanins Involved in Formation of Anthocyanic Vacuolar Inclusions

The sequential steps leading to the biosynthesis of anthocyanins have been well described in the last 3 decades, and several studies indicate that this pathway is well conserved among plant species (Holton and Cornish, 1995; Winkel-Shirley, 2001; Liu et al., 2018; Yonekura-Sakakibara et al., 2019). Anthocyanins are part of the flavonoid branch derived from the core phenylpropanoid pathway where the amino acid phenylalanine is the only

precursor. A key branching point toward the flavonoid pathway occurs in the conversion of coumaroyl-CoA into chalcone and naringenin, mediated by chalcone synthase (CHS) and chalcone isomerase (CHI). Alternatively to anthocyanins, naringenin can be converted into flavonols by flavonol synthase (FLS) resulting in compounds such as quercetin and kaempferol, which can function as co-pigments of anthocyanins, or as floral UV-absorbing molecules attracting nocturnal pollinators (Sheehan et al., 2016). Branching out towards the anthocyanin biosynthetic pathway, flavanone-3-hydroxylase (F3H) converts naringenin to dihydrokaempferol, which is further hydroxylated in the B-ring by the action of cytochrome P450s flavonoid 3'-hydroxylase (F3'H) and flavonoid 3',5'-hydroxylase (F3'5'H) to yield dihydroquercetin and dihydromyricetin. These three dihydroflavonols constitute the precursors that enter the final steps for anthocyanin biosynthesis. They are converted into anthocyanidins by consequently dihydroflavonol 4-reductase (DFR) and anthocyanidin synthase (ANS) yielding pelargonidin, cyanidin and delphinidin, depending on the hydroxylation of the B-ring, which affects the color significantly (Figure 1). All naturally synthesized anthocyanidins are glycosylated on the 3-position by a cytosolic glycosyltransferase to increase stability, solubility and facilitate transport to the vacuole (Zhang Y. et al., 2014; Alseekh et al., 2020). Consequently, the compounds can be subjected to various modifications on the hydroxyl groups of the backbone structure (Figure 1), such as methylation, glycosylation, and acylation. The complexity of anthocyanin decorations differs widely among plant species from simple monoglucosides to multiple substitutions of different sugars and acylations (Provenzano et al., 2014). Additionally, the color of anthocyanins is also influenced by post-biosynthetic factors. These include the pH of the vacuole (Quattrocchio et al., 2006), molecular stacking through self-association or of other co-pigments (rev. in (Zhang Y. et al., 2014; Houghton et al., 2021)), and interactions with metal ions and flavonoids or other metabolites to form metal complexes, resulting in a blue color (Yoshida et al., 2009; Schreiber et al., 2010; Schreiber et al., 2011; Ito et al., 2019). There are no studies indicating that metal-anthocyanin complexing is involved in the formation of AVIs.

Several studies have suggested a few decorations to be critical for the condensation of anthocyanins in the vacuole. A pivotal study proposed a model for molecular stacking of anthocyanins by the folding of aromatic acyl groups over the C-ring of the anthocyanin, favoring color stability and AVI formation (Kallam et al., 2017; Houghton et al., 2021). This highlighted the role of aromatic acylation in AVI formation. Constitutive expression of two transcription factors from snapdragon in tobacco for production of cyanidin 3-*O*-rutinoside, while consequent expression of a *p*-coumaroyl coenzyme A (CoA) acyltransferase from *Arabidopsis* (At3AT) resulted in AVI formation. *In-vitro*, the extracted acylated anthocyanins condensed into aggregated structures with solubility decreasing under an increasing pH. The role of aromatic acylation was supported by accumulation of AVIs in *Delphinium Morning Skies*, containing anthocyanins with four benzoyl groups, compared to the less-acylated anthocyanins in *Delphinium*



*King Arthur* which displayed a uniform vacuolar anthocyanin distribution (Kallam et al., 2017). The importance of acylation is further supported in grape, where enrichment of acylated anthocyanins correlates with presence of AVIs (Conn et al., 2003; Mizuno et al., 2006), and *p*-coumaroylated anthocyanins in vesicle-like AVIs in *Arabidopsis*. However, AVIs do not only accumulate when anthocyanins are aromatically acylated, as in Carnation AVIs accumulate in mutants unable to malonylate (Okamura et al., 2013), and in *Rhabdanthamnus solandri* AVIs contain simpler anthocyanin-3-*O*-glucoside species (Zhang H. et al., 2014). Additionally, a *5gt* mutant unable to glycosylate at the 5-position exhibited an increased accumulation of AVIs (Pourcel et al., 2010). An NMR study showed that purified anthocyanin-3-*O*-glucosides and coumaroylated 3-*O*-glucoside anthocyanins self-associate *in-vitro* (Fernandes et al., 2015) which could be an indication why in different plant species AVIs are enriched in these type of anthocyanins. Based on thermodynamic analysis both methylation and hydroxylation of the anthocyanin B-ring was suggested to favor condensation (Leydet et al., 2012). However, overexpression of a F3'5'H from petunia in the tobacco cells accumulating cyanidin 3-*O*-rutinoside resulted in production of delphinidin 3-*O*-

rutinoside but no AVI formation (Kallam et al., 2017). In contrast, hydroxylation of the anthocyanin B-ring in *Petunia* by constitutive expression of F3'5'H from *Phalaenopsis* (orchid) resulted in accumulation of delphinidin and formation of visible AVIs (Qi et al., 2013). There is clear indication of aromatic acylation playing an important role in AVI formation. However, not in all AVIs, which allows for speculation on other factors involved in AVI formation.

## 1.2 Molecular Environment Facilitating Anthocyanic Vacuolar Inclusions Formation

When comparing the morphology of AVIs from different species (Figure 2), it is remarkable to see that they tend to group into a limited subset of structural determinants. Most AVIs are described as vesicle-like structures, where others have a round but more granular morphology. In *Arabidopsis* and *Lisianthus*, vesicle-shaped AVIs were enveloped by a membrane (Figure 2 (Chanoca et al., 2015)), making it likely similarly shaped AVIs have a membrane as well. The absence of a membrane around granular AVIs in *Lisianthus* and Tobacco indicates it may be common for similarly shaped AVIs to be membrane-less



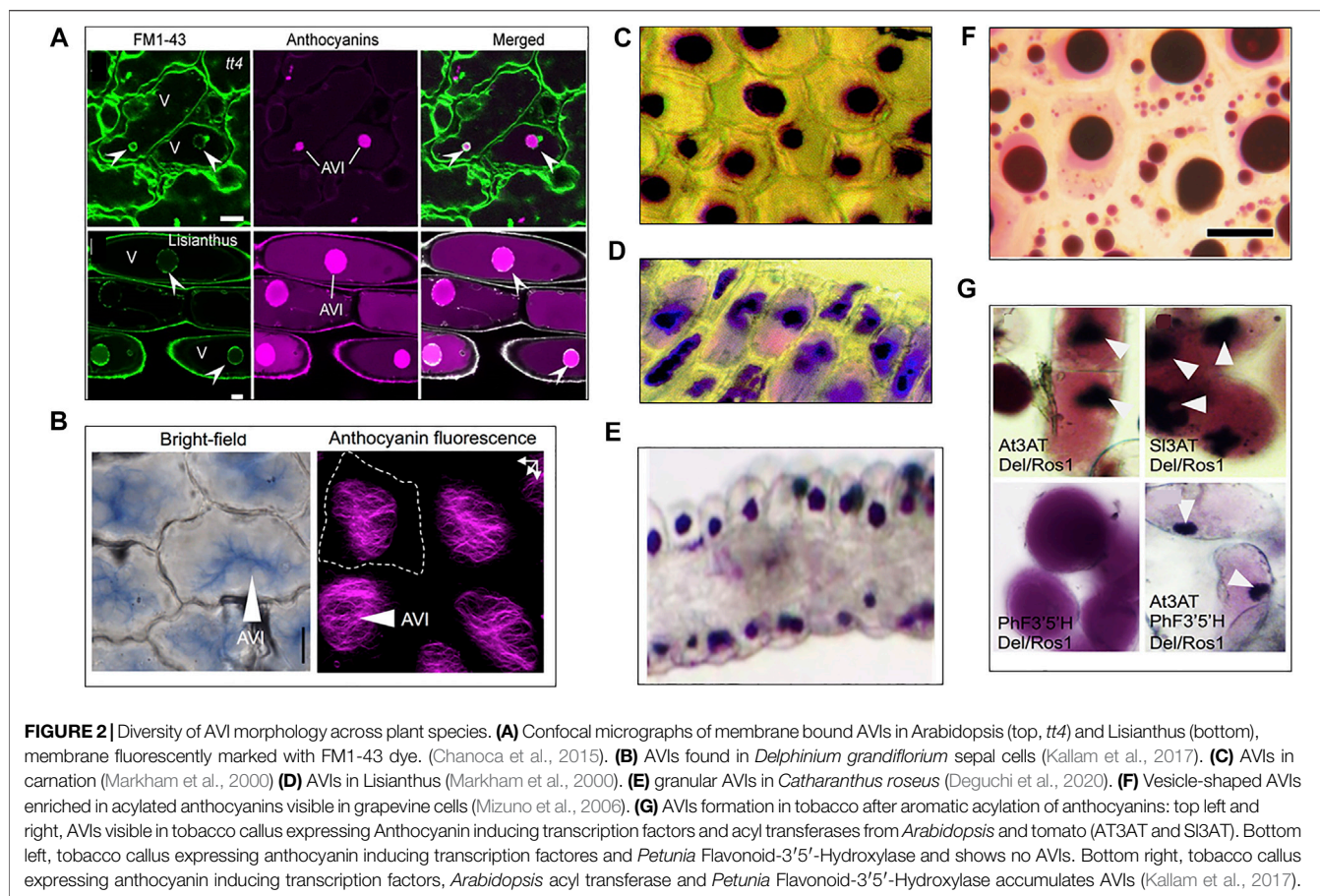


**FIGURE 2 |** Diversity of AVI morphology across plant species. **(A)** Confocal micrographs of membrane bound AVIs in Arabidopsis (top, *tt4*) and Lisianthus (bottom), membrane fluorescently marked with FM1-43 dye. (Chanoca et al., 2015). **(B)** AVIs found in *Delphinium grandiflorum* sepal cells (Kallam et al., 2017). **(C)** AVIs in carnation (Markham et al., 2000). **(D)** AVIs in Lisianthus (Markham et al., 2000). **(E)** granular AVIs in *Catharanthus roseus* (Deguchi et al., 2020). **(F)** Vesicle-shaped AVIs enriched in acylated anthocyanins visible in grapevine cells (Mizuno et al., 2006). **(G)** AVIs formation in tobacco after aromatic acylation of anthocyanins: top left and right, AVIs visible in tobacco callus expressing Anthocyanin inducing transcription factors and acyl transferases from *Arabidopsis* and tomato (AT3AT and SI3AT). Bottom left, tobacco callus expressing anthocyanin inducing transcription factors and *Petunia* Flavonoid-3'-5'-Hydroxylase and shows no AVIs. Bottom right, tobacco callus expressing anthocyanin inducing transcription factors, *Arabidopsis* acyl transferase and *Petunia* Flavonoid-3'-5'-Hydroxylase accumulates AVIs (Kallam et al., 2017).

(Markham et al., 2000; Kallam et al., 2017). Interestingly, the morphology of AVIs in *Delphinium grandiflorum* is radically different (Figure 2 (Kallam et al., 2017)), as they form a type of filamentous crystalline shape. Moreover, confocal micrographs of the AVIs and FM1-43 stained tissue seem to indicate an additional membrane-less separation of the region containing the AVI from the rest of the vacuole (Kallam et al., 2017). Besides the actual flavonoid composition inside the vacuole, the molecular environment facilitating anthocyanin condensation remains unexplored.

### 1.2.1 Proteinaceous Membraneless Compartments

Protein guided liquid-liquid phase separation is known from a variety of molecular processes providing membraneless sub-compartments preventing bulk equilibria (Banani et al., 2017; Zheng et al., 2021). The presence of disordered regions or entirely unstructured peptides facilitate such phase separation processes and may be a key driver for AVI formation. The presence of proteins in or around AVIs has been reported in Lisianthus (Markham et al., 2000) and sweet potato (Nozue et al., 1995; Nozue et al., 1997; Xu et al., 2001; Nozue et al., 2003). Markham et al. describe finding “proteinaceous” material in Lisianthus inclusions, however, there have not been any follow-up publications on the exact type of protein present in AVIs in these flowers (Markham et al., 2000). In sweet potato, expression

of a vacuolar protein (VP24) correlated with the accumulation of anthocyanins in vacuoles, and immunocytochemical detection showed the protein co-localized with AVIs (Nozue et al., 1995). A proteomics study underlined accumulation of VP24 in purple sweet potato, and proposed the protein could be involved in the degradation of anthocyanin-glutathione, although anthocyanin-glutathione conjugates have never been observed. The authors also propose that VCaB42 and VP24 together mediate microautophagy resulting in anthocyanin transport and membrane-bound AVI formation (Wang S. et al., 2016).

### 1.2.2 Natural Deep Eutectics Solvents and the Vacuolar Environment of Anthocyanic Vacuolar Inclusions

Beyond oil and water, Natural Deep Eutectic Solvents (NADES) may provide a third intracellular phase composed of stoichiometric mixtures of common general metabolites, such as amino acids, organic acids, sugars, and choline (Choi et al., 2011). Inspired by nature, the high solubility of specialized metabolites in NADES is being promoted as a “green” alternative to commonly used organic solvents for extraction of a broad diversity of specialized metabolites including the flavonols quercetin and kaempferol, and anthocyanins (Dai et al., 2013a; Dai et al., 2013b; Vanda et al., 2018). Moreover, enzymes of the biosynthetic pathway of dhurrin were able to



retain activity after incubation at various temperatures when incubated in a NADES mixture of glucose and tartrate, as opposed to glycerol or water (Knudsen et al., 2020). Additionally, enzymes in NADES mixtures have shown increased activity (Milano et al., 2017; Elgharabawy et al., 2018; Elgharabawy et al., 2020; Panić et al., 2021; Thomas and Kayser, 2022). The increased stability and activity of enzymes, high solubility of specialized metabolites, and omnipresence of the constituents of NADES mixtures in all types of organisms are indications that these types of mixtures could constitute an important aspect of the natural environment in cells. However, *in-vivo* proof of NADES mediated liquid-liquid phase-separation is still lacking. Although experimental proof is missing, the tonoplast membrane surrounding the vacuole contains a plethora of general metabolite transporters involved in the homeostasis of the cytosol (rev. in (Martinoia et al., 2012)), allowing vacuolar accumulation of general metabolites (Davies et al., 2006). Therefore, common NADES constituents such as organic acids and sugars can accumulate in high concentrations in the vacuole (Schulze et al., 2002; Lecourieux et al., 2014). The pioneering work proposing a biological function of a NADES phase in plant cells was based on analyses of general metabolites and the interaction between sucrose and malic acid into liquid crystals using NMR (Kim et al., 2010; Choi et al., 2011). Similar NMR methods could be applied on species accumulating high concentrations of specialized metabolites to identify NADES mixtures involved in their solubilization. The development of mass spectrometry imaging with subcellular resolution (Cornett et al., 2007; Bjarnholt et al., 2014) can provide a key approach to experimentally validate the existence of NADES sub-compartments. Such compartments could easily be co-localized with anthocyanins based on the inherent pigment properties. Additionally, micro-syringe or laser dissection to harvest sub-compartments facilitated by NADES mixtures could be an option to isolate and identify the metabolites involved in the solubilization, as has been proposed in a previous review on NADES and natural products (Møller and Laursen, 2021).

### 1.3 The Anthocyanin Traffic Routes From Biosynthesis to Anthocyanic Vacuolar Inclusions

Although biosynthesis occurs at the ER, the last decorations of anthocyanins and other specialized metabolites such as glycosylation and acylation may actually occur in the vacuole, using different types of acyl-sugars as donors (Matsuba et al., 2010; Sasaki et al., 2014; Orme et al., 2019; Yonekura-Sakakibara et al., 2019). This indicates that specific “mature” anthocyanins are selectively transported from the ER to the vacuole where the final decorations may result in their condensation into AVIs. Furthermore, this would provide a means to prevent aggregation in the cytosol. Multiple studies have been published on anthocyanin transport, yet still there is no consensus on the exact mode of transport (Braidot et al., 2008; Grotewold and Davies, 2008; Petrussa et al., 2013; Biała and Jasiński, 2018; Pečenkova et al., 2018; Kaur et al., 2021). Most likely,

anthocyanin transport may involve multiple routes depending on the plant, tissue and developmental stage, and perhaps the type of structural anthocyanin modification. One model proposes anthocyanins to be transported in vesicles from the ER to the vacuole, whereas the other model proposes a combined effort of cytoplasmic and tonoplast localized transporter proteins (Figure 1) (Zhao and Dixon, 2010). These models are not mutually exclusive.

#### 1.3.1 Selective Vacuolar Loading of Anthocyanins Governed by Transport Mechanism

Two key transporters are involved in active transport of mature anthocyanins across the tonoplast membrane. MATE-transporter proteins belong to the multidrug/oligosaccharidyl-lipid/polysaccharide (MOP) superfamily. These transporters have been shown to transport acylated anthocyanins in grape (Gomez et al., 2011), and malonylated anthocyanins in legume (Zhao et al., 2011). MATE-transporters use the electrochemical gradient of protons formed by tonoplast localized V-ATPases and a H<sup>+</sup>-pyrophosphatase for secondary active transport (Gaxiola et al., 2007; Gomez et al., 2009). ABC-transporters are involved in the transportation of glycosylated anthocyanins to the vacuole (Goodman et al., 2004; Francisco et al., 2013; Behrens et al., 2019). These transporters are dependent on reduced glutathione (GSH) provided by a glutathione-S-transferase (GST). Genes encoding GSTs have been frequently linked to anthocyanin transport and have been identified in many different plants such as *Petunia* (AN9), *Arabidopsis* (TT19), and grape (VvGST1 and VvGST4) (Alfenito et al., 1998; Mueller et al., 2000; Kitamura et al., 2004; Conn et al., 2010). Usually, GSTs form conjugates with their substrate, to facilitate transport across the tonoplast; however, anthocyanin-GSH conjugates have never been found (Mueller et al., 2000). The GST is therefore hypothesized to simply bind the anthocyanin and “escort” it to the transporter localized in the tonoplast with GSH. However, in *Arabidopsis* grown under conditions to induce anthocyanin accumulation (Poustka et al., 2007; Pourcel et al., 2010; Chanoca et al., 2015), the prevalence of AVIs increased when ABC-transporters were inhibited, as well as under glutathione depletion (Poustka et al., 2007). Additionally, *tt19* knock-out plants exhibited cytoplasmic anthocyanin aggregates, as well as AVIs, but little soluble vacuolar anthocyanins (Chanoca et al., 2015).

Alternative to active transport mediated by tonoplast localized transporters, anthocyanins may enter the vacuole via vesicle mediated transport (Zhang et al., 2006; Sun et al., 2012). In this route, flavonoids synthesized on the cytosolic site of the ER are transported to the lumen of the ER where they accumulate into vesicle-like structures (Figure 1). These structures have been observed to be associated with the formation of AVIs in the vacuole (Zhang et al., 2006; Conn et al., 2010). While these vesicles are visible by microscopy techniques, the evidence of canonical vesicle transport proteins such as cargo, GTPases, VSRs and SNAREs are still lacking (Conn et al., 2010; Zhao and Dixon, 2010). Therefore, it is hypothesized the anthocyanin vesicles are engulfed by autophagosomes and delivered to the vacuole by autophagy (macro and microautophagy) and stored as membrane surrounded AVIs (Figure 2) (Pourcel et al., 2010; Chanoca et al.,

2015). An extensive study on AVI formation and trafficking showed that AVIs formed after microautophagy, and that anthocyanins in the ER did not aggregate (Chanoca et al., 2015). This may imply the importance of vacuole-localised modifications of anthocyanins and their transport to the vacuole for the formation of anthocyanin biocondensates, which could be of value for successful heterologous synthesis of flavonoids.

## 2 DISCUSSION

Like many biological systems, the formation of AVIs is highly complex and may involve multiple processes ultimately leading to a variety of morphological distinct anthocyanin condensates in the vacuole. Here we highlight that hydroxylation of the B-ring, 3-O-glycosylation and aromatic acylation may be key for molecular stacking and condensation. The condensation process appears to happen in the vacuole potentially driven by further modifications catalyzed by vacuolar transferases. Some AVIs are membrane-less and typically appear grainy in structure whereas a membrane surrounds others, which display liquid droplet-like behavior such as fusion and homogeneous distribution of the anthocyanins (Figure 2). This morphology may be linked to the type of transport (Figure 1). In previous studies on AVI formation, the nature of the vacuolar environment of AVIs, and its role in AVI formation has remained underexposed. Experimental investigation of the vacuolar environment of AVIs is required to characterize the molecular environment governing formation of AVIs. Based on the *in vitro* effect of NADES mixture on enzyme stability and productivity, and the extraordinary solvent properties, we propose that NADES could provide the molecular environment in (plant) cells allowing high catalytic efficiency of enzymes, and high accumulation of specialized metabolites.

### 2.1 Synthetic Vacuolar Inclusions for Heterologous Production of Complex Flavonoids

Several flavonoids are in clinical trials as a potential treatment against life-style and aging induced chronic inflammation (Ginwala et al., 2019) and they are of interest as natural food colorants to replace synthetic dyes (Oplatowska-Stachowiak and Elliott, 2017). The bioactivity of these molecules depends on highly specific decorations and they are typically present in minute amounts in the natural plant sources. Synthesizing flavonoids in a sustainable and cost-efficient way fits in an agenda promoting a switch to sustainable circular synthesis of natural products (Sørensen et al., 2022), harnessing the ability of plants, as exhibited in apple calli (Wang N. et al., 2016) and tobacco cell culture (Appelhaugen et al., 2018), and scaling it to a larger scale. Plant cell culture (Appelhaugen et al., 2018) or microbial micro-factories both constitute promising sustainable ways of anthocyanin synthesis for commercial purposes. Plant cell culture benefits from the native presence of flavonoid and anthocyanin biosynthetic pathways in plants, where the overexpression of specific transcription factors would

lead to the activation of these pathways. (Appelhaugen et al., 2018). However, biosynthesis of more specific and modified anthocyanins would require many more steps to be introduced, which minimizes the initial benefit of a system activated by transcription factors. On the other hand, while heterologous synthesis of anthocyanins in microbes would require the introduction of entire pathways, they are cheaper to use, and have been heavily optimized for heterologous production of highly complex plant natural products (Luo et al., 2019; Srinivasan and Smolke, 2020) and therefore offer a system, that is, easier to scale-up. Within the last decades, studies have reported heterologous production of anthocyanins in both *Escherichia coli* and *Saccharomyces cerevisiae* [rev. in (Sunil and Shetty, 2022)]. A recurring problem during heterologous expression of biosynthetic pathways in microbial cells is secretion into the growth-media before the finalized product is synthesized, resulting in a mixture of intermediates and products. The knowledge gathered on biosynthesis, transport and storage of anthocyanins in plants could prove essential for the quest to engineer the next generation of micro factories for heterologous production of flavonoids in the vacuole of, e.g., yeast cells. Condensation into Synthetic Vacuolar Inclusions (SVIs) by targeted modifications in combination with directed transport within the yeast cells would prevent auto-toxicity and enable accumulation of molar concentrations of metabolites, as demonstrated in plant cells for storage of vanillin (Brillouet et al., 2014; Gallage et al., 2018), dhuririn (Kojima et al., 1979; Halkier and Møller, 1989), and anthocyanins (Markham et al., 2004). Like organisms from other kingdoms, yeast accumulates general metabolites required for formation of a NADES phase (Choi et al., 2011). Therefore, the *in-vivo* application of NADES derived SVIs in yeast cells might simply be achieved by introducing a transport system designed by plants for selective transport of anthocyanins with proper decorations required for condensation. Overall, this could present an entirely new approach to avoid auto-toxicity, leakage of non-decorated compounds and prevent cross-talk with native pathways. In summary, the importance of NADES in AVI formation remains a topic in need of further research which may become an essential stepping stone for future production of flavonoids in heterologous systems.

## AUTHOR CONTRIBUTIONS

KB edited and finalized the manuscript. KB, JA-C, and TL organized the manuscript. KB, JA-C, CR, and KH did the literature research, and wrote parts of the manuscript. JA-C designed Figure 1 and KB and JA-C made Figure 2. KB, JA-C, and TL provided comments and helped writing the final version.

## FUNDING

This work was supported by a Sapere Aude Starting Grant from the Independent Research Fund Denmark (7026-00041B) and a

Novo Nordisk Foundation Emerging Investigator Grant (NNF19OC0055356) to TL The Amsterdam University Fund and the Erasmus + programme co-funded KB's exchange in Copenhagen.

## REFERENCES

- Alfenito, M. R., Souer, E., Goodman, C. D., Buell, R., Mol, J., Koes, R., et al. (1998). Functional Complementation of Anthocyanin Sequestration in the Vacuole by Widely Divergent Glutathione S-Transferases. *Plant Cell* 10 (7), 1135–1149. doi:10.2307/3870717
- Alseikh, S., Perez de Souza, L., Benina, M., and Fernie, A. R. (2020). The Style and Substance of Plant Flavonoid Decoration; towards Defining Both Structure and Function. *Phytochemistry* 174, 112347. doi:10.1016/j.phytochem.2020.112347
- Appelhaeghe, I., Wulff-Vester, A. K., Wendell, M., Hvostlef-Eide, A.-K., Russell, J., Oertel, A., et al. (2018). Colour Bio-Factories: Towards Scale-Up Production of Anthocyanins in Plant Cell Cultures. *Metab. Eng.* 48, 218–232. doi:10.1016/j.ymben.2018.06.004
- Bae, R.-N., Kim, K.-W., Kim, T.-C., and Lee, S.-K. (2006). Anatomical Observations of Anthocyanin Rich Cells in Apple Skins. *HortSci* 41 (3), 733–736. doi:10.21273/HORTSCI.41.3.733
- Banani, S. F., Lee, H. O., Hyman, A. A., and Rosen, M. K. (2017). Biomolecular Condensates: Organizers of Cellular Biochemistry. *Nat. Rev. Mol. Cell Biol.* 18 (5), 285–298. doi:10.1038/nrm.2017.7
- Behrens, C. E., Smith, K. E., Iancu, C. V., Choe, J. Y., and Dean, J. V. (2019). Transport of Anthocyanins and Other Flavonoids by the Arabidopsis ATP-Binding Cassette Transporter AtABCC2. *Sci. Rep.* 9 (1), 437–515. doi:10.1038/s41598-018-37504-8
- Biala, W., and Jasiński, M. (2018). The Phenylpropanoid Case-It is Transport that Matters. *Front. Plant Sci.* 9, 1610. doi:10.3389/fpls.2018.01610
- Bjarnholt, N., Li, B., D'Alvise, J., and Janfelt, C. (2014). Mass Spectrometry Imaging of Plant Metabolites - Principles and Possibilities. *Nat. Prod. Rep.* 31 (6), 818–837. doi:10.1039/C3NP70100J
- Braidot, E., Zancani, M., Petrusa, E., Peresson, C., Bertolini, A., Patui, S., et al. (2008). Transport and Accumulation of Flavonoids in Grapevine (*Vitis vinifera* L.). *Plant Signal. Behav.* 3 (9), 626–632. doi:10.4161/psb.3.9.6686
- Brillouet, J.-M., Verdeil, J.-L., Odoux, E., Lartaud, M., Grisoni, M., and Conéjéro, G. (2014). Phenol Homeostasis Is Ensured in Vanilla Fruit by Storage under Solid Form in a New Chloroplast-Derived Organelle, the Phenyloplast. *J. Exp. Bot.* 65 (9), 2427–2435. doi:10.1093/jxb/eru126
- Chanoca, A., Kovinich, N., Burkel, B., Stecha, S., Bohorquez-Restrepo, A., Ueda, T., et al. (2015). Anthocyanin Vacuolar Inclusions Form by a Microautophagy Mechanism. *Plant Cell* 27 (9), 2545–2559. doi:10.1105/tpc.15.00589
- Choi, Y. H., van Spronsen, J., Dai, Y., Verberne, M., Hollmann, F., Arends, I. W. C. E., et al. (2011). Are Natural Deep Eutectic Solvents the Missing Link in Understanding Cellular Metabolism and Physiology? *Plant Physiol.* 156 (4), 1701–1705. doi:10.1104/pp.111.178426
- Conn, S., Zhang, W., and Franco, C. (2003). Anthocyanin Vacuolar Inclusions (AVIs) Selectively Bind Acylated Anthocyanins in *Vitis vinifera* L. (Grapevine) Suspension Culture. *Biotechnol. Lett.* 25 (11), 835–839. doi:10.1023/a:1024028603089
- Conn, S., Franco, C., and Zhang, W. (2010). Characterization of Anthocyanin Vacuolar Inclusions in *Vitis vinifera* L. Cell Suspension Cultures. *Planta* 231 (6), 1343–1360. doi:10.1007/s00425-010-1139-4
- Cornett, D. S., Reyzer, M. L., Chaurand, P., and Caprioli, R. M. (2007). MALDI Imaging Mass Spectrometry: Molecular Snapshots of Biochemical Systems. *Nat. Methods* 4 (10), 828–833. doi:10.1038/nmeth1094
- Dai, Y., van Spronsen, J., Witkamp, G.-J., Verpoorte, R., and Choi, Y. H. (2013a). Ionic Liquids and Deep Eutectic Solvents in Natural Products Research: Mixtures of Solids as Extraction Solvents. *J. Nat. Prod.* 76 (11), 2162–2173. doi:10.1021/np400051w
- Dai, Y., van Spronsen, J., Witkamp, G.-J., Verpoorte, R., and Choi, Y. H. (2013b). Natural Deep Eutectic Solvents as New Potential Media for Green Technology. *Anal. Chim. Acta* 766, 61–68. doi:10.1016/j.aca.2012.12.019

## ACKNOWLEDGMENTS

The authors would like to thank Draw my Science (www.drawmyscience.com) for assisting with figure design.

- Davies, C., Shin, R., Liu, W., Thomas, M. R., and Schachtman, D. P. (2006). Transporters Expressed during Grape Berry (*Vitis vinifera* L.) Development Are Associated with an Increase in Berry Size and Berry Potassium Accumulation. *J. Exp. Bot.* 57 (12), 3209–3216. doi:10.1093/jxb/erl091
- Davis, J. M., Murphy, E. A., and Carmichael, M. D. (2009). Effects of the Dietary Flavonoid Quercetin upon Performance and Health. *Curr. Sports Med. Rep.* 8 (4), 206–213. doi:10.1249/jsr.0b013e3181ae8959
- Deguchi, A., Tatsuzawa, F., and Miyoshi, K. (2020). A Blackish-Flowered Cultivar of *Catharanthus roseus* Accumulates High Concentrations of a Novel Anthocyanin with a Unique Feature of Aggregation in Weak Acid Solutions. *Dyes Pigments* 173, 108001. doi:10.1016/j.dyepig.2019.108001
- Elgharabawy, A. A., Hayyan, A., Hayyan, M., Rashid, S. N., Nor, M. R. M., Zulkifli, M. Y., et al. (2018). Shedding Light on Lipase Stability in Natural Deep Eutectic Solvents. *Chem. Biochem. Eng. Q.* 32 (3), 359–370. doi:10.15255/cabeq.2018.1335
- Elgharabawy, A. A. M., Hayyan, M., Hayyan, A., Basirun, W. J., Salleh, H. M., and Mirghani, M. E. S. (2020). A Grand Avenue to Integrate Deep Eutectic Solvents into Biomass Processing. *Biomass Bioenergy* 137, 105550. doi:10.1016/j.biombioe.2020.105550
- Fernandes, A., Brás, N. F., Mateus, N., and Freitas, V. d. (2015). A Study of Anthocyanin Self-Association by NMR Spectroscopy. *New J. Chem.* 39 (4), 2602–2611. doi:10.1039/C4NJ02339K
- Francisco, R. M., Regalado, A., Ageorges, A., Burla, B. J., Bassin, B., Eisenach, C., et al. (2013). ABCC1, an ATP Binding Cassette Protein from Grape Berry, Transports Anthocyanidin 3-O-Glucosides. *Plant Cell* 25 (5), 1840–1854. doi:10.1105/tpc.112.102152
- Gallage, N. J., Järgensen, K., Janfelt, C., Nielsen, A. J. Z., Naake, T., Duński, E., et al. (2018). The Intracellular Localization of the Vanillin Biosynthetic Machinery in Pods of *Vanilla planifolia*. *Plant Cell Physiol.* 59 (2), 304–318. doi:10.1093/pcp/pcx185
- Gaxiola, R. A., Palmgren, M. G., and Schumacher, K. (2007). Plant Proton Pumps. *FEBS Lett.* 581 (12), 2204–2214. doi:10.1016/j.febslet.2007.03.050
- Ginwala, R., Bhavsar, R., Chigbu, D. I., Jain, P., and Khan, Z. K. (2019). Potential Role of Flavonoids in Treating Chronic Inflammatory Diseases with a Special Focus on the Anti-inflammatory Activity of Apigenin. *Antioxidants* 8 (2), 35. doi:10.3390/antiox8020035
- Gomez, C., Terrier, N., Torregrosa, L., Vialat, S., Fournier-Level, A., Verriès, C., et al. (2009). Grapevine MATE-type Proteins Act as Vacuolar H<sup>+</sup>-Dependent Acylated Anthocyanin Transporters. *Plant Physiol.* 150 (1), 402–415. doi:10.1104/pp.109.135624
- Gomez, C., Conejero, G., Torregrosa, L., Cheynier, V., Terrier, N., and Ageorges, A. (2011). In Vivo grapevine Anthocyanin Transport Involves Vesicle-Mediated Trafficking and the Contribution of anthoMATE Transporters and GST. *Plant J.* 67 (6), 960–970. doi:10.1111/j.1365-3113.2011.04648.x
- Gonnet, J.-F. (2003). Origin of the Color of Cv. Rhapsody in Blue Rose and Some Other So-Called "Blue" Roses. *J. Agric. Food Chem.* 51 (17), 4990–4994. doi:10.1021/jf0343276
- Goodman, C. D., Casati, P., and Walbot, V. (2004). A Multidrug Resistance-Associated Protein Involved in Anthocyanin Transport in *Zea mays*. *Plant Cell* 16 (7), 1812–1826. doi:10.1105/tpc.022574
- Grotewold, E., and Davies, K. (2008). Trafficking and Sequestration of Anthocyanins. *Nat. Product. Commun.* 3 (8), 1934578X0800300. doi:10.1177/1934578X0800300806
- Guo, J., Han, W., and Wang, M. (2008). Ultraviolet and Environmental Stresses Involved in the Induction and Regulation of Anthocyanin Biosynthesis: a Review. *Afr. J. Biotechnol.* 7 (25), 4966–4972. doi:10.4314/AJB.V7I25.59709
- Halkier, B. A., and Möller, B. L. (1989). Biosynthesis of the Cyanogenic Glucoside Dhurrin in Seedlings of *Sorghum bicolor* (L.) Moench and Partial Purification of the Enzyme System Involved. *Plant Physiol.* 90 (4), 1552–1559. doi:10.1104/pp.90.4.1552

- Holton, T. A., and Cornish, E. C. (1995). Genetics and Biochemistry of Anthocyanin Biosynthesis. *Plant Cell* 7 (7), 1071–1083. doi:10.1105/tpc.7.7.1071
- Houghton, A., Appelhaugen, I., and Martin, C. (2021). Natural Blues: Structure Meets Function in Anthocyanins. *Plants* 10 (4), 726. doi:10.3390/plants10040726
- Irani, N. G., and Grotewold, E. (2005). Light-induced Morphological Alteration in Anthocyanin-Accumulating Vacuoles of Maize Cells. *BMC Plant Biol.* 5, 7. doi:10.1186/1471-2229-5-7
- Ito, T., Aoki, D., Fukushima, K., and Yoshida, K. (2019). Direct Mapping of Hydrangea Blue-Complex in Sepal Tissues of Hydrangea Macrophylla. *Sci. Rep.* 9 (1), 5450. doi:10.1038/s41598-019-41968-7
- Kallam, K., Appelhaugen, I., Luo, J., Albert, N., Zhang, H., Derolles, S., et al. (2017). Aromatic Decoration Determines the Formation of Anthocyanic Vacuolar Inclusions. *Curr. Biol.* 27 (7), 945–957. doi:10.1016/j.cub.2017.02.027
- Kaur, S., Sharma, N., Kapoor, P., Chunduri, V., Pandey, A. K., and Garg, M. (2021). Spotlight on the Overlapping Routes and Partners for Anthocyanin Transport in Plants. *Physiol. Plant.* 171 (4), 868–881. doi:10.1111/ppl.13378
- Kim, H. K., Choi, Y. H., and Verpoorte, R. (2010). NMR-based Metabolomic Analysis of Plants. *Nat. Protoc.* 5 (3), 536–549. doi:10.1038/nprot.2009.237
- Kitamura, S., Shikazono, N., and Tanaka, A. (2004). TRANSPARENT TESTA 19 Is Involved in the Accumulation of Both Anthocyanins and Proanthocyanidins in Arabidopsis. *Plant J.* 37 (1), 104–114. doi:10.1046/j.1365-3113x.2003.01943.x
- Knudsen, C., Bavishi, K., Viborg, K. M., Drew, D. P., Simonsen, H. T., Motawia, M. S., et al. (2020). Stabilization of Dhurrin Biosynthetic Enzymes from Sorghum Bicolor Using a Natural Deep Eutectic Solvent. *Phytochemistry* 170, 112214. doi:10.1016/j.phytochem.2019.112214
- Kojima, M., Poulton, J. E., Thayer, S. S., and Conn, E. E. (1979). Tissue Distributions of Dhurrin and of Enzymes Involved in its Metabolism in Leaves of Sorghum Bicolor. *Plant Physiol.* 63 (6), 1022–1028. doi:10.1104/pp.63.6.1022
- Konczak, I., and Zhang, W. (2004). Anthocyanins-More Than Nature's Colours. *J. Biomed. Biotechnol.* 2004 (5), 239–240. doi:10.1155/s1110724304047013
- Lecourieux, F., Kappel, C., Lecourieux, D., Serrano, A., Torres, E., Arce-Johnson, P., et al. (2014). An Update on Sugar Transport and Signalling in Grapevine. *J. Exp. Bot.* 65 (3), 821–832. doi:10.1093/jxb/ert394
- Leydet, Y., Gavarra, R., Petrov, V., Diniz, A. M., Jorge Parola, A., Lima, J. C., et al. (2012). The Effect of Self-Aggregation on the Determination of the Kinetic and Thermodynamic Constants of the Network of Chemical Reactions in 3-glucoside Anthocyanins. *Phytochemistry* 83, 125–135. doi:10.1016/j.phytochem.2012.06.022
- Liu, Y., Tikunov, Y., Schouten, R. E., Marcelis, L. F. M., Visser, R. G. F., and Bovy, A. (2018). Anthocyanin Biosynthesis and Degradation Mechanisms in Solanaceous Vegetables: A Review. *Front. Chem.* 6, 52. doi:10.3389/fchem.2018.00052
- Luo, X., Reiter, M. A., d'Espaux, L., Wong, J., Denby, C. M., Lechner, A., et al. (2019). Complete Biosynthesis of Cannabinoids and Their Unnatural Analogues in Yeast. *Nature* 567 (7746), 123–126. doi:10.1038/s41586-019-0978-9
- Mackon, E., Ma, Y., Jeazet Dongho Epse Mackon, G. C., Li, Q., Zhou, Q., and Liu, P. (2021). Subcellular Localization and Vesicular Structures of Anthocyanin Pigmentation by Fluorescence Imaging of Black Rice (*Oryza Sativa* L.) Stigma Protoplast. *Plants* 10 (4), 685. doi:10.3390/plants10040685
- Markham, K. R., Gould, K. S., Winefield, C. S., Mitchell, K. A., Bloor, S. J., and Boase, M. R. (2000). Anthocyanic Vacuolar Inclusions - Their Nature and Significance in Flower Colouration. *Phytochemistry* 55 (4), 327–336. doi:10.1016/s0031-9422(00)00246-6
- Markham, K. R., Bloor, S. J., Nicholson, R., Rivera, R., Shemluck, M., Kevan, P. G., et al. (2004). Black Flower Coloration in Wild *Lisianthus Nigrescens*: Its Chemistry and Ecological Consequences. *Z Naturforsch C J. Biosci.* 59 (9–10), 625–630. doi:10.1515/znc-2004-9-1003
- Martinoia, E., Meyer, S., De Angeli, A., and Nagy, R. (2012). Vacuolar Transporters in Their Physiological Context. *Annu. Rev. Plant Biol.* 63 (1), 183–213. doi:10.1146/annurev-arplant-042811-105608
- Matsuba, Y., Sasaki, N., Tera, M., Okamura, M., Abe, Y., Okamoto, E., et al. (2010). A Novel Glucosylation Reaction on Anthocyanins Catalyzed by Acyl-glucose-dependent Glucosyltransferase in the Petals of Carnation and Delphinium. *Plant Cell* 22 (10), 3374–3389. doi:10.1105/tpc.110.077487
- Milano, F., Giotta, L., Guascito, M. R., Agostiano, A., Sblendorio, S., Valli, L., et al. (2017). Functional Enzymes in Nonaqueous Environment: The Case of Photosynthetic Reaction Centers in Deep Eutectic Solvents. *ACS Sustain. Chem. Eng.* 5 (9), 7768–7776. doi:10.1021/acsschemeng.7b01270
- Mizuno, H., Hirano, K., and Okamoto, G. (2006). Effect of Anthocyanin Composition in Grape Skin on Anthocyanic Vacuolar Inclusion Development and Skin Coloration. *Vitis* 45 (4), 173–177. doi:10.5073/vitis.2006.45.173-177
- Møller, B. L., and Laursen, T. (2021). "Metabolons and Bio-Condensates: The Essence of Plant Plasticity and the Key Elements in Development of Green Production Systems," in *Advances in Botanical Research* (Amsterdam, Netherlands: Elsevier Publishing), 185–223.
- Morita, Y., Hoshino, A., Kikuchi, Y., Okuhara, H., Ono, E., Tanaka, Y., et al. (2005). Japanese Morning Glory Dusky Mutants Displaying Reddish-Brown or Purplish-Gray Flowers Are Deficient in a Novel Glycosylation Enzyme for Anthocyanin Biosynthesis, UDP-Glucose: Anthocyanidin 3-O-Glucoside-2''-O-Glucosyltransferase, Due to 4-bp Insertions in: A Novel Glucosyltransferase Gene and its Mutants. *Plant J.* 42 (3), 353–363. doi:10.1111/j.1365-3113x.2005.02383.x
- Mueller, L. A., Goodman, C. D., Silady, R. A., and Walbot, V. (2000). AN9, a Petunia Glutathione S-Transferase Required for Anthocyanin Sequestration, Is a Flavonoid-Binding Protein. *Plant Physiol.* 123 (4), 1561–1570. doi:10.1104/pp.123.4.1561
- Nozue, M., Kubo, H., Nishimura, M., and Yasuda, H. (1995). Detection and Characterization of a Vacuolar Protein (VP24) in Anthocyanin-Producing Cells of Sweet Potato in Suspension Culture. *Plant Cell Physiol.* 36 (5), 883–889. doi:10.1093/oxfordjournals.pcp.a078834
- Nozue, M., Yamada, K., Nakamura, T., Kubo, H., Kondo, M., and Nishimura, M. (1997). Expression of a Vacuolar Protein (VP24) in Anthocyanin-Producing Cells of Sweet Potato in Suspension Culture. *Plant Physiol.* 115 (3), 1065–1072. doi:10.1104/pp.115.3.1065
- Nozue, M., Baba, S., Kitamura, Y., Xu, W., Kubo, H., Nogawa, M., et al. (2003). VP24 Found in Anthocyanic Vacuolar Inclusions (AVIs) of Sweet Potato Cells is a Member of a Metalloprotease Family. *Biochem. Eng. J.* 14 (3), 199–205. doi:10.1016/S1369-703X(02)00223-1
- Okamura, M., Nakayama, M., Umemoto, N., Cano, E. A., Hase, Y., Nishizaki, Y., et al. (2013). Crossbreeding of a Metallic Color Carnation and Diversification of the Peculiar Coloration by Ion-Beam Irradiation. *Euphytica* 191 (1), 45–56. doi:10.1007/s10681-012-0859-x
- Oplowska-Stachowiak, M., and Elliott, C. T. (2017). Food Colors: Existing and Emerging Food Safety Concerns. *Crit. Rev. Food Sci. Nutr.* 57 (3), 524–548. doi:10.1080/10408398.2014.889652
- Orme, A., Louveau, T., Stephenson, M. J., Appelhaugen, I., Melton, R., Cheema, J., et al. (2019). A Noncanonical Vacuolar Sugar Transferase Required for Biosynthesis of Antimicrobial Defense Compounds in Oat. *Proc. Natl. Acad. Sci. U.S.A.* 116 (52), 27105–27114. doi:10.1073/pnas.1914652116
- Panić, M., Cvjetko Bubalo, M., and Radojčić Redovniković, I. (2021). Designing a Biocatalytic Process Involving Deep Eutectic Solvents. *J. Chem. Technol. Biotechnol.* 96 (1), 14–30. doi:10.1002/jctb.6545
- Pečenková, T., Marković, V., Sabol, P., Kulich, I., and Žárský, V. (2018). Exocyst and Autophagy-Related Membrane Trafficking in Plants. *J. Exp. Bot.* 69 (1), 47–57. doi:10.1093/jxb/erx363
- Petrussa, E., Braidot, E., Zancani, M., Peresson, C., Bertolini, A., Patui, S., et al. (2013). Plant Flavonoids-Biosynthesis, Transport and Involvement in Stress Responses. *Int. J. Mol. Sci.* 14 (7), 14950–14973. doi:10.3390/ijms140714950
- Pourcel, L., Irani, N. G., Lu, Y., Riedl, K., Schwartz, S., and Grotewold, E. (2010). The Formation of Anthocyanic Vacuolar Inclusions in *Arabidopsis thaliana* and Implications for the Sequestration of Anthocyanin Pigments. *Mol. Plant* 3 (1), 78–90. doi:10.1093/mp/ssp071
- Poustka, F., Irani, N. G., Feller, A., Lu, Y., Pourcel, L., Frame, K., et al. (2007). A Trafficking Pathway for Anthocyanins Overlaps with the Endoplasmic Reticulum-To-Vacuole Protein-Sorting Route in Arabidopsis and Contributes to the Formation of Vacuolar Inclusions. *Plant Physiol.* 145 (4), 1323–1335. doi:10.1104/pp.107.105064
- Provenzano, S., Spelt, C., Hosokawa, S., Nakamura, N., Brugliera, F., Demelis, L., et al. (2014). Genetic Control and Evolution of Anthocyanin Methylation. *Plant Physiol.* 165 (3), 962–977. doi:10.1104/pp.113.234526
- Qi, Y., Lou, Q., Quan, Y., Liu, Y., and Wang, Y. (2013). Flower-specific Expression of the Phalaenopsis Flavonoid 3', 5'-hydroxylase Modifies Flower Color



- Pigmentation in Petunia and Lilium. *Plant Cell Tiss. Organ Cult.* 115 (2), 263–273. doi:10.1007/s11240-013-0359-2
- Quattrocchio, F., Verweij, W., Kroon, A., Spelt, C., Mol, J., and Koes, R. (2006). PH4 of Petunia is an R2R3 MYB Protein that Activates Vacuolar Acidification through Interactions with Basic-Helix-Loop-Helix Transcription Factors of the Anthocyanin Pathway. *Plant Cell* 18 (5), 1274–1291. doi:10.1105/tpc.105.034041
- Sasaki, N., Nishizaki, Y., Ozeki, Y., and Miyahara, T. (2014). The Role of Acyl-Glucose in Anthocyanin Modifications. *Molecules* 19 (11), 18747–18766. doi:10.3390/molecules191118747
- Schreiber, H. D., Swink, A. M., and Godsey, T. D. (2010). The Chemical Mechanism for Al<sup>3+</sup> Complexing with Delphinidin: A Model for the Bluing of Hydrangea Sepals. *J. Inorg. Biochem.* 104 (7), 732–739. doi:10.1016/j.jinorgbio.2010.03.006
- Schreiber, H. D., Jones, A. H., Lariviere, C. M., Mayhew, K. M., and Cain, J. B. (2011). Role of Aluminum in Red-To-Blue Color Changes in Hydrangea Macrophylla Sepals. *Biomaterials* 24 (6), 1005–1015. doi:10.1007/s10534-011-9458-x
- Schulze, J., Tesfaye, M., Litjens, R. H. M. G., Bucciarrelli, B., Trepp, G., Miller, S., et al. (2002). Malate Plays a Central Role in Plant Nutrition. *Plant Soil* 247 (1), 133–139. doi:10.1007/978-94-017-2789-1\_10
- Sheehan, H., Moser, M., Klahre, U., Esfeld, K., Dell’Olive, A., Mandel, T., et al. (2016). MYB-FL Controls Gain and Loss of Floral UV Absorbance, a Key Trait Affecting Pollinator Preference and Reproductive Isolation. *Nat. Genet.* 48 (2), 159–166. doi:10.1038/ng.3462
- Sørensen, M., Andersen-Ranberg, J., Hankamer, B., and Møller, B. L. (2022). Circular Biomaterials through Harvesting Solar Energy and CO<sub>2</sub>. *Trends Plant Sci.* 27, 655. doi:10.1016/j.tplants.2022.03.001
- Srinivasan, P., and Smolke, C. D. (2020). Biosynthesis of Medicinal Tropane Alkaloids in Yeast. *Nature* 585 (7826), 614–619. doi:10.1038/s41586-020-2650-9
- Sun, Y., Li, H., and Huang, J. R. (2012). Arabidopsis TT19 Functions as a Carrier to Transport Anthocyanin from the Cytosol to Tonoplasts. *Mol. Plant* 5 (2), 387–400. doi:10.1093/mp/ssr110
- Sunil, L., and Shetty, N. P. (2022). Biosynthesis and Regulation of Anthocyanin Pathway Genes. *Appl. Microbiol. Biotechnol.* 106, 1–16. doi:10.1007/s00253-022-11835-z
- Thomas, F., and Kayser, O. (2022). Natural Deep Eutectic Solvents Enhance Cannabinoid Biotransformation. *Biochem. Eng. J.* 180, 108380. doi:10.1016/j.bej.2022.108380
- Umeda, T., Miyazaki, H., Yamamoto, A., Yatomi, M., Yamaguchi, M., and Matsuzoe, N. (2006). Relation of Anthocyanin in Skin of Eggplant Fruits to Light Environment. *J. Sci. High. Tech. Agric.* 18 (3), 193–199. doi:10.2525/shita.18.193
- van der Krol, A. R., Brunelle, A., Tsuchimoto, S., and Chua, N. H. (1993). Functional Analysis of Petunia Floral Homeotic MADS Box Gene pMADS1. *Genes Dev.* 7 (7a), 1214–1228. doi:10.1101/gad.7.7a.1214
- Vanda, H., Dai, Y., Wilson, E. G., Verpoorte, R., and Choi, Y. H. (2018). Green Solvents from Ionic Liquids and Deep Eutectic Solvents to Natural Deep Eutectic Solvents. *Comptes Rendus Chim.* 21 (6), 628–638. doi:10.1016/j.crci.2018.04.002
- Wang, N., Zhang, Z., Jiang, S., Xu, H., Wang, Y., Feng, S., et al. (2016a). Synergistic Effects of Light and Temperature on Anthocyanin Biosynthesis in Callus Cultures of Red-Fleshed Apple (*Malus Sieversii* F. Niedzwetzkyana). *Plant Cell Tiss. Organ Cult.* 127 (1), 217–227. doi:10.1007/s11240-016-1044-z
- Wang, S., Pan, D., Lv, X., Song, X., Qiu, Z., Huang, C., et al. (2016b). Proteomic Approach Reveals that Starch Degradation Contributes to Anthocyanin Accumulation in Tuberous Root of Purple Sweet Potato. *J. Proteomics* 143, 298–305. doi:10.1016/j.jpro.2016.03.010
- Winkel-Shirley, B. (2001). Flavonoid Biosynthesis. A Colorful Model for Genetics, Biochemistry, Cell Biology, and Biotechnology. *Plant Physiol.* 126 (2), 485–493. doi:10.1104/pp.126.2.485
- Xu, W., Shioiri, H., Kojima, M., and Nozue, M. (2001). Primary Structure and Expression of a 24-kD Vacuolar Protein (VP24) Precursor in Anthocyanin-Producing Cells of Sweet Potato in Suspension Culture. *Plant Physiol.* 125 (1), 447–455. doi:10.1104/pp.125.1.447
- Yonekura-Sakakibara, K., Higashi, Y., and Nakabayashi, R. (2019). The Origin and Evolution of Plant Flavonoid Metabolism. *Front. Plant Sci.* 10, 943. doi:10.3389/fpls.2019.00943
- Yoshida, K., Mori, M., and Kondo, T. (2009). Blue Flower Color Development by Anthocyanins: from Chemical Structure to Cell Physiology. *Nat. Prod. Rep.* 26 (7), 884–915. doi:10.1039/b800165k
- Zhang, H., Wang, L., Derolles, S., Bennett, R., and Davies, K. (2006). New Insight into the Structures and Formation of Anthocyanic Vacuolar Inclusions in Flower Petals. *BMC Plant Biol.* 6 (1), 29. doi:10.1186/1471-2229-6-29
- Zhang, H., Jordheim, M., Lewis, D. H., Arathoon, S., Andersen, Ø. M., and Davies, K. M. (2014a). Anthocyanins and Their Differential Accumulation in the Floral and Vegetative Tissues of a Shrub Species (*Rhabdanthamnus Solandri* A. Cunn.). *Sci. Hortic.* 165, 29–35. doi:10.1016/j.scienta.2013.10.032
- Zhang, Y., Butelli, E., and Martin, C. (2014b). Engineering Anthocyanin Biosynthesis in Plants. *Curr. Opin. Plant Biol.* 19, 81–90. doi:10.1016/j.pbi.2014.05.011
- Zhao, J., and Dixon, R. A. (2010). The ‘ins’ and ‘outs’ of Flavonoid Transport. *Trends Plant Sci.* 15 (2), 72–80. doi:10.1016/j.tplants.2009.11.006
- Zhao, J., Huhman, D., Shadle, G., He, X.-Z., Sumner, L. W., Tang, Y., et al. (2011). MATE2 Mediates Vacuolar Sequestration of Flavonoid Glycosides and Glycoside Malonates in *Medicago truncatula*. *Plant Cell* 23 (4), 1536–1555. doi:10.1105/tpc.110.080804
- Zheng, C., Xu, X., Zhang, L., and Lu, D. (2021). Liquid-Liquid Phase Separation Phenomenon on Protein Sorting within Chloroplasts. *Front. Physiol.* 12, 2416. doi:10.3389/fphys.2021.801212
- Zhu, H. M., Li, R., Su, X. D., and Zhu, M. J. (2018). Morphology of Anthocyanin Vacuolar Inclusions (AVIs) in Purple Sweet Potato. *Eur. J. Hortic. Sci.* 83, 364–373. doi:10.17660/eJHS.2018/83.6.4

**Conflict of Interest:** The authors declare that the research was conducted in the absence of any commercial or financial relationships that could be construed as a potential conflict of interest.

**Publisher’s Note:** All claims expressed in this article are solely those of the authors and do not necessarily represent those of their affiliated organizations, or those of the publisher, the editors and the reviewers. Any product that may be evaluated in this article, or claim that may be made by its manufacturer, is not guaranteed or endorsed by the publisher.

Copyright © 2022 Buhrman, Aravena-Calvo, Ross Zaulich, Hinz and Laursen. This is an open-access article distributed under the terms of the Creative Commons Attribution License (CC BY). The use, distribution or reproduction in other forums is permitted, provided the original author(s) and the copyright owner(s) are credited and that the original publication in this journal is cited, in accordance with accepted academic practice. No use, distribution or reproduction is permitted which does not comply with these terms.





# Green Synthesis of Thiazolidine-2,4-dione Derivatives and Their Lipoxygenase Inhibition Activity With QSAR and Molecular Docking Studies

Melita Lončarić<sup>1</sup>, Ivica Strelec<sup>1</sup>, Valentina Pavić<sup>2</sup>, Vesna Rastija<sup>3</sup>, Maja Karnaš<sup>3</sup> and Maja Molnar<sup>1\*</sup>

<sup>1</sup>Department of Applied Chemistry and Ecology, Faculty of Food Technology Osijek, Josip Juraj Strossmayer University of Osijek, Osijek, Croatia, <sup>2</sup>Department of Biology, Josip Juraj Strossmayer University of Osijek, Osijek, Croatia, <sup>3</sup>Department of Agroecology and Environmental Protection, Faculty of Agrobiotechnical Sciences Osijek, Josip Juraj Strossmayer University of Osijek, Osijek, Croatia

## OPEN ACCESS

### Edited by:

Manoj B. Gawande,  
Palacky University Olomouc, Czechia

### Reviewed by:

José Menezes,  
Esteem Industries Pvt Ltd., India  
Srinath Pashikanti,  
Idaho State University, United States

### \*Correspondence:

Maja Molnar  
mmolnar@ptfos.hr

### Specialty section:

This article was submitted to  
Green and Sustainable Chemistry,  
a section of the journal  
Frontiers in Chemistry

**Received:** 04 April 2022

**Accepted:** 23 May 2022

**Published:** 05 July 2022

### Citation:

Lončarić M, Strelec I, Pavić V,  
Rastija V, Karnaš M and Molnar M  
(2022) Green Synthesis of Thiazolidine-  
2,4-dione Derivatives and Their  
Lipoxygenase Inhibition Activity With  
QSAR and Molecular Docking Studies.  
Front. Chem. 10:912822.  
doi: 10.3389/fchem.2022.912822

Thiazolidinediones are five-membered, heterocyclic compounds that possess a number of pharmacological activities such as antihyperglycemic, antitumor, antiarthritic, anti-inflammatory, and antimicrobial. Conventional methods for their synthesis are often environmentally unacceptable due to the utilization of various catalysts and organic solvents. In this study, deep eutectic solvents were used in the synthesis of thiazolidinedione derivatives that acted as both solvents and catalysts. Initially, a screening of 20 choline chloride-based deep eutectic solvents for thiazolidinedione synthesis, *via* Knoevenagel condensation, was performed in order to find the most suitable solvent. Deep eutectic solvent, choline chloride, *N*-methylurea, was proven to be the best for further synthesis of 19 thiazolidinedione derivatives. Synthesized thiazolidinediones are obtained in yields from 21.49% to 90.90%. The synthesized compounds were tested for the inhibition of lipid peroxidation as well as for the inhibition of soy lipoxygenase enzyme activity. The antioxidant activity of the compounds was also determined by the ABTS and DPPH methods. Compounds showed lipoxygenase inhibition in the range from 7.7% to 76.3%. Quantitative structure–activity relationship model ( $R^2 = 0.88$ ;  $Q_{\text{loo}}^2 = 0.77$ ;  $F = 33.69$ ) for the inhibition of soybean lipoxygenase was obtained with descriptors *Mor29m*, *G2u*, and *MAXDP*. The molecular docking confirms experimentally obtained results, finding the binding affinity and interactions with the active sites of soybean LOX-3.

**Keywords:** 2,4-thiazolidinedione, synthesis, deep eutectic solvents, green chemistry, lipoxygenase, QSAR, molecular docking

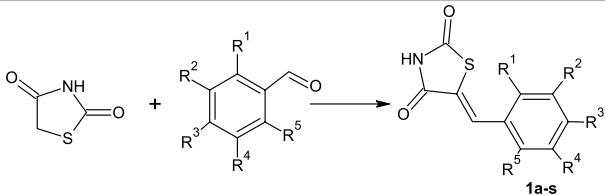
## 1 INTRODUCTION

Thiazolidine-2,4-dione is a five-membered, heterocyclic compound. Chemically, thiazole ring contains the carbonyl moiety at positions 2 and 4, the -NH group, and the methylene group (-CH<sub>2</sub>), which allows for various modifications of the molecule. Thiazolidine-2,4-dione derivatives are important heterocyclic compounds that possess a number of pharmacological activities such as antihyperglycemic, antitumor (Chadha et al., 2015), antiarthritic (da Rocha Junior et al., 2013), anti-inflammatory (Youssef et al., 2010), and antimicrobial (Albrecht et al., 2005). It is used in the production of drugs for diabetes mellitus (type 2) treatment. It belongs to the so-called glitazone drugs such as rosiglitazone, pioglitazone, lobeglitazone, and troglitazone (Chadha et al., 2015). Thiazolidinedione is used to inhibit metal corrosion in acidic solutions and as a reagent sensitive to heavy metals in analytical chemistry (Jain et al., 2013). Thiazolidinedione derivatives can inhibit certain enzymes such as aldose reductase, phosphoinositide-3-kinase, Pim kinase, cyclooxygenase, D-glutamate ligase, and histone deacetylase (Beharry et al., 2009; Jain et al., 2013; Kim et al., 2013). Some thiazolidinedione derivatives also showed good potential for lipoxygenase inhibition (Bozdag-Dündar et al., 2009; Avupati et al., 2018).

Lipoxygenases are enzymes that belong to dioxygenases containing iron and catalyze the oxidation of polyunsaturated fatty acids (Ivanov et al., 2010; Kavetsou et al., 2017). These enzymes are present in plants, mammals, and microorganisms (Sadeghian and Jabbari, 2016). Four seed isoforms of lipoxygenases (LOX-1, LOX-2, LOX-3a, LOX-3b) have been identified in soybean (*Glycine max*) (Axelrod et al., 1981). Due to the lack of other sufficient purified isoforms, soybean LOX-3 has been the most investigated isoform (Jothi et al., 2018). In lipoxygenase pathway, undesirable compounds may be formed causing side effects in plants and vegetables by changing color, creating unwanted odors, and changing the antioxidant properties (Chatterjee and Sharma, 2018). Some natural compounds, such as polyphenols (-)-epigallocatechin gallate (Skrzypczak-Jankun et al., 2003a), curcumin (Skrzypczak-Jankun et al., 2003b), quercetin (Sadik et al., 2003), and coumarins (Torres et al., 2013) can effectively inhibit this enzyme. Previous studies have shown that various synthesized organic compounds can inhibit lipoxygenase: thiazolyl derivatives (Tsolaki et al., 2018) and coumarin derivatives (Lončarić et al., 2020). The X-ray structures of soybean LOX-3 complexes with inhibitors such as 4-nitrocatechol (PDB ID: 1NO3) (Skrzypczak-Jankun et al., 2004) and protocatechuic acid (PDB ID: 1N8Q) (Borbulevych et al., 2004) were revealed providing a deeper insight into the mode of inhibition.

Organic compounds are still often synthesized by conventional synthetic procedures, including the usage of volatile organic solvents and harmful catalysts, showing adverse environmental and health effects. Following the new trends and concepts in green chemistry, the utilization of such harmful chemicals is to be avoided or at least minimized. A pursuit of environmentally acceptable solvents has led us to the

**TABLE 1 |** Reaction times and product yields obtained in different deep eutectic solvents.



HBA	HBD	Ratio ChCl:HBD	Time (h)	Y (%)
ChCl	Urea	1:2	2.5	22.8
	<i>N</i> -Methylurea	1:3	2	79.9
	Thiourea	1:2	6	6.4
	Glucose	1:1	9	17.9
	Fructose	1:1	8	14.1
	Xylitol	1:1	10	<sup>a</sup>
	Sorbitol	1:1	10	<sup>a</sup>
	Butan-1,4-diol	1:2	10	<sup>a</sup>
	Ethan-1,2-diol	1:2	10	<sup>a</sup>
	Glycerol	1:2	6	25.2
	Acetamide	1:2	10	<sup>a</sup>
	Malic acid	1:1	10	<sup>a</sup>
	Citric acid	1:2	10	<sup>a</sup>
	Tartaric acid	1:1	10	<sup>a</sup>
	Malonic acid	1:1	10	<sup>a</sup>
	Oxalic acid	1:1	10	<sup>a</sup>
	1,3-Dimethylurea	1:2	8	3.8
	Lactic acid	1:2	10	<sup>a</sup>
	Levulinic acid	1:2	10	<sup>a</sup>
	<i>trans</i> -Cinnamic acid	1:1	10	<sup>a</sup>

<sup>a</sup>No product obtained.

utilization of deep eutectic solvents (DESs). These solvents are characterized by low vapor pressure, non-flammability, and easy handling, in addition to being biodegradable, do not require any purification before use, and can be recycled and reused (Zhang et al., 2012).

The thiazolidinediones used in this research are synthesized in deep eutectic solvents without the usage of any organic solvents and catalysts. In this research, the inhibition of lipid peroxidation and lipoxygenase activity of thiazolidinedione derivatives were tested. In addition, the antioxidant activity of the examined thiazolidinediones was determined by DPPH and ABTS methods. The quantitative structure–activity relationship (QSAR) study was performed to reveal significant structural characteristics important for lipoxygenase inhibition. Molecular docking of the analyzed compounds to the soybean lipoxygenase (LOX)-3 was evaluated in order to compare the binding affinities with experimentally determined inhibitions and determined the interactions with the binding site of the enzyme.

## 2 MATERIALS AND METHODS

All chemicals used within this study were purchased from commercial suppliers. For thin-layer chromatography (TLC), fluorescent silica gel plates F254 (Merck, Darmstadt, Germany) were used, and TLC was performed in benzene:

acetone:acetic acid (8:1:1) as an eluent. Determination of melting points of compounds was conducted on the electrothermal melting point apparatus (Electrothermal Engineering Ltd., Rochford, United Kingdom). Mass spectra were recorded on an LC/MS/MS API 2000 sp (CA, United States). NMR spectra were recorded on a Bruker Avance 600 MHz NMR Spectrometer (Bruker Biospin GmbH, Rheinstetten, Germany) at 293 K in dimethylsulfoxide-*d*<sub>6</sub> (DMSO-*d*<sub>6</sub>). Spectrophotometric analysis were performed on ThermoSpectronic, Helios Gamma spectrophotometer (Thermo Fisher Scientific, Waltham, MA, United States).

## 2.1 General Procedure for the Synthesis of Deep Eutectic Solvents

Deep eutectic solvents (DESs) were obtained by mixing hydrogen bond acceptor (HBA) (choline chloride) and various hydrogen bond donors (HBDs) in molar ratios, as listed in **Table 1**. Choline chloride was mixed with appropriate HBDs, and the mixture was heated until a clear liquid was obtained.

## 2.2 General Procedure for the Synthesis of Thiazolidinedione Derivatives (1a–s)

Thiazolidinedione derivatives were synthesized by the Knoevenagel condensation. An equimolar amount of thiazolidine-2,4-dione and substituted benzaldehyde was added to the DES and stirred until completion of the reaction monitored by TLC. Upon the consumption of the reactants, water was added, and the precipitated product was filtered. Detailed procedure for each synthesized compound, as well as compound characterization, is given in **Section 2.4**.

### 2.2.1 General Procedure for the Recyclability of the DES

Recyclability experiments were performed on the model reaction in choline chloride: *N*-methylurea DES. After the reaction was finished, the addition of water precipitated the crude product, which was filtered off. Then, the water was evaporated from the mixture and the same reaction was conducted again, under the same conditions. This was repeated five times.

## 2.3 Inhibitory Activities

Inhibitory activities are measured in the presence of thiazolidinedione derivatives dissolved in DMSO at a concentration of 100  $\mu$ M. The soybean lipoxygenase inhibition assay, the inhibition of linoleic acid lipid peroxidation, and the reducing activity of the stable radical 1,1-diphenyl-picrylhydrazyl (DPPH) were determined, as described previously (Lončarić et al., 2020).

The ABTS<sup>•+</sup> method was performed according to the previously published procedures with several modifications (Osman et al., 2012). Solutions of the ABTS radical (7.4 mM) and potassium persulfate (2.6 mM) in water were mixed in a molar ratio of 1:1. The prepared mixture was left in the dark place at room temperature for 16 h. Thereafter, the prepared solution was diluted with DMSO to achieve a solution absorbance of  $1.0 \pm 0.02$  at 734 nm. All synthesized compounds were dissolved in DMSO and prepared

at a concentration of 1 mM. One hundred microliters of a compound solution in DMSO and 900  $\mu$ l of ABTS<sup>•+</sup> were mixed and allowed to stand for 90 min in a dark place to allow the reaction to proceed. The absorbance of the mixture was measured at 734 nm. The study was conducted in three parallels.

## 2.4 Compound Characterization (1a–s)

### 2.4.1 5-(2-Hydroxybenzylidene)

#### thiazolidine-2,4-dione (1a)

Using thiazolidinedione (0.234 g, 2 mmol) and salicylaldehyde (215  $\mu$ l, 2 mmol), in accordance with the general procedure, the title compound **1a** was obtained (0.159 g, 35.9% yield) as a yellow solid (m.p. 269–272°C). <sup>1</sup>H (600 MHz)  $\delta$  12.48 (s, 1H, NH), 10.48 (s, 1H, OH), 8.00 (s, 1H, CH), 7.30 (q, *J* = 7.92; 9.84; 7.26 Hz, 2H, arom.), 6.93 (q, *J* = 8.40; 9.48; 7.50 Hz, 2H, arom.). <sup>13</sup>C (150 MHz)  $\delta$  168.15; 167.50; 157.24; 132.20; 128.20; 126.27; 121.87; 119.64; 116.08. LC/MS (C<sub>10</sub>H<sub>7</sub>NO<sub>3</sub>S): *m/z*: 220.01 (M<sup>−</sup>) 221.23.

### 2.4.2 5-(4-Hydroxy-3-methoxybenzylidene)

#### thiazolidine-2,4-dione (1b)

Using thiazolidinedione (0.234 g, 2 mmol) and 4-hydroxy-3-methoxybenzaldehyde (0.304 g, 2 mmol), in accordance with the general procedure, the title compound **1b** was obtained (0.343 g, 68.3% yield) as a brown solid (m.p. 199–201°C). <sup>1</sup>H (300 MHz)  $\delta$  11.98 (s, 1H, NH), 9.94 (s, 1H, OH), 7.71 (s, 1H, CH), 7.17 (d, *J* = 1.89 Hz, 1H, arom.), 7.07 (dd, *J* = 8.34; 1.89 Hz, 1H, arom.), 6.93 (d, *J* = 8.25 Hz, 1H, arom.), 3.82 (s, 3H, OCH<sub>3</sub>). <sup>13</sup>C (150 MHz)  $\delta$  172.47; 168.52; 167.94; 149.89; 148.43; 130.06; 124.85; 124.59; 119.68; 116.71; 114.60. LC/MS (C<sub>11</sub>H<sub>9</sub>NO<sub>4</sub>S): *m/z*: 250.06 (M<sup>−</sup>) 251.26.

### 2.4.3 5-(2,5-Dihydroxybenzylidene)

#### thiazolidine-2,4-dione (1c)

Using thiazolidinedione (0.234 g, 2 mmol) and 2,5-dihydroxybenzaldehyde (0.276 g, 2 mmol), in accordance with the general procedure, the title compound **1c** was obtained (0.102 g, 21.5% yield) as a brown solid (m.p. 194–198°C). <sup>1</sup>H (600 MHz)  $\delta$  9.70 (s, 1H, OH), 7.61 (s, 1H, CH), 7.23 (d, *J* = 8.76 Hz, 1H, arom.), 6.98 (s, 1H, arom.), 6.92 (dd, *J* = 8.22; 1.68; 2.40 Hz, 1H, arom.). <sup>13</sup>C (150 MHz)  $\delta$  153.98; 144.08; 132.23; 128.61; 120.04; 117.85; 116.75; 110.91. LC/MS (C<sub>10</sub>H<sub>7</sub>NO<sub>4</sub>S): *m/z*: 258.82 (M<sup>−</sup>+Na) 237.23.

### 2.4.4 5-(3-Methoxybenzylidene)

#### thiazolidine-2,4-dione (1d)

Using thiazolidinedione (0.234 g, 2 mmol) and 3-methoxybenzaldehyde (245  $\mu$ l, 2 mmol), in accordance with the general procedure, the title compound **1d** was obtained (0.178 g, 37.8% yield) as a white solid (m.p. 194–197°C). <sup>1</sup>H (300 MHz)  $\delta$  12.62 (s, 1H, NH), 7.76 (s, 1H, CH), 7.45 (t, *J* = 8.16 Hz, 1H, arom.), 7.15 (d, *J* = 6.45 Hz, 2H, arom.), 7.06 (dd, *J* = 8.34; 1.89; 0.30 Hz, 1H, arom.), 3.80 (s, 3H, OCH<sub>3</sub>). <sup>13</sup>C (150 MHz)  $\delta$  168.28; 167.70; 160.08; 134.85; 132.21; 130.86; 122.36; 116.74; 115.76; 55.73. LC/MS (C<sub>11</sub>H<sub>9</sub>NO<sub>3</sub>S): *m/z*: 233.99 (M<sup>−</sup>) 235.26.

### 2.4.5 5-(3-Hydroxy-4-methoxybenzylidene)

#### thiazolidine-2,4-dione (1e)

Using thiazolidinedione (0.234 g, 2 mmol) and 3-hydroxy-4-methoxybenzaldehyde (0.304 g, 2 mmol), in accordance with

the general procedure, the title compound **1e** was obtained (0.271 g, 53.9% yield) as a yellow solid (m.p. 254–257°C). <sup>1</sup>H (600 MHz) δ 12.46 (s, 1H, NH), 9.47 (s, 1H, OH), 7.62 (s, 1H, CH), 7.06 (d, *J* = 2.16 Hz, 2H, arom.), 7.00 (d, *J* = 1.56 Hz, 1H, arom.), 3.81 (s, 3H, OCH<sub>3</sub>). <sup>13</sup>C (150 MHz) δ 168.03; 167.40; 149.99; 146.89; 132.24; 125.63; 123.45; 119.96; 115.84; 112.37; 55.63. LC/MS (C<sub>11</sub>H<sub>9</sub>NO<sub>4</sub>S): *m/z*: 250.00 (M<sup>-</sup>) 251.26.

#### 2.4.6 5-(3,4-Dihydroxybenzylidene)thiazolidine-2,4-dione (**1f**)

Using thiazolidinedione (0.234 g, 2 mmol) and 3,4-dihydroxybenzaldehyde (0.276 g, 2 mmol), in accordance with the general procedure, the title compound **1f** was obtained (0.139 g, 29.3% yield) as a brown solid (m.p. 270–271°C). <sup>1</sup>H (600 MHz) δ 12.42 (s, 1H, NH), 9.82 (s, 1H, OH), 9.44 (s, 1H, OH), 7.60 (s, 1H, CH), 6.99 (d, *J* = 1.98 Hz, 1H, arom.), 6.96 (q, *J* = 8.28; 1.95 Hz, 1H, arom.), 6.87 (d, *J* = 8.22 Hz, 1H, arom.). <sup>13</sup>C (150 MHz) δ 168.15; 166.53; 148.57; 145.82; 132.63; 124.28; 123.89; 118.72; 116.37; 116.22. LC/MS (C<sub>10</sub>H<sub>7</sub>NO<sub>4</sub>S): *m/z*: 236.01 (M<sup>-</sup>) 237.23.

#### 2.4.7 5-(3,4,5-Trimethoxybenzylidene)thiazolidine-2,4-dione (**1g**)

Using thiazolidinedione (0.234 g, 2 mmol) and 3,4,5-trimethoxybenzaldehyde (0.392 g, 2 mmol), in accordance with the general procedure, the title compound **1g** was obtained (0.341 g, 57.8% yield) as a yellow solid (m.p. 172–174°C). <sup>1</sup>H (600 MHz) δ 12.59 (s, 1H, NH), 7.72 (s, 1H, CH), 6.88 (s, 2H, arom.), 3.80 (s, 6H, OCH<sub>3</sub>), 3.70 (s, 3H, OCH<sub>3</sub>). <sup>13</sup>C (150 MHz) δ 167.81; 167.20; 155.15; 139.35; 132.05; 128.49; 122.41; 107.48; 60.16; 55.96. LC/MS (C<sub>13</sub>H<sub>13</sub>NO<sub>5</sub>S): *m/z*: 294.11 (M<sup>-</sup>) 295.31.

#### 2.4.8 5-(2,5-Dimethoxybenzylidene)thiazolidine-2,4-dione (**1h**)

Using thiazolidinedione (0.234 g, 2 mmol) and 2,5-dimethoxybenzaldehyde (0.332 g, 2 mmol), in accordance with the general procedure, the title compound **1h** was obtained (0.432 g, 81.3% yield) as a yellow solid (m.p. 220–223°C). <sup>1</sup>H (600 MHz) δ 12.56 (s, 1H, NH), 7.90 (s, 1H, CH), 7.07 (t, *J* = 2.64 Hz, 2H, arom.), 6.89 (d, *J* = 2.40 Hz, 1H, arom.), 3.82 (s, 3H, OCH<sub>3</sub>), 3.74 (s, 3H, OCH<sub>3</sub>). <sup>13</sup>C (150 MHz) δ 167.91; 167.28; 153.01; 152.36; 126.35; 123.79; 121.90; 117.57; 113.22; 113.00; 56.06; 55.47. LC/MS (C<sub>12</sub>H<sub>11</sub>NO<sub>4</sub>S): *m/z*: 263.99 (M<sup>-</sup>) 265.29.

#### 2.4.9 5-(3-Bromobenzylidene)thiazolidine-2,4-dione (**1i**)

Using thiazolidinedione (0.234 g, 2 mmol) and 3-bromobenzaldehyde (235 μl, 2 mmol), in accordance with the general procedure, the title compound **1i** was obtained (0.397 g, 69.8% yield) as a white solid (m.p. 210–212°C). <sup>1</sup>H (300 MHz) δ 12.69 (s, 1H, NH), 7.82 (t, *J* = 1.56 Hz, 1H, arom.), 7.78 (s, 1H, CH), 7.68 (m, 1H, arom.), 7.59 (d, *J* = 7.86 Hz, 1H, arom.), 7.50 (t, *J* = 7.82 Hz, 1H, arom.). <sup>13</sup>C (150 MHz) δ 168.05; 167.68; 135.98; 133.31; 133.23; 131.79; 130.46; 128.55; 125.92; 122.90. LC/MS (C<sub>10</sub>H<sub>6</sub>BrNO<sub>3</sub>S): *m/z*: 284.03 (M<sup>-</sup>) 284.13.

#### 2.4.10 5-(2-Hydroxy-5-nitrobenzylidene)thiazolidine-2,4-dione (**1j**)

Using thiazolidinedione (0.234 g, 2 mmol) and 5-nitrosalicylaldehyde (0.334 g, 2 mmol), in accordance with the general procedure, the title compound **1j** was obtained (0.334 g, 62.8% yield) as a red solid (m.p. 226–228°C). <sup>1</sup>H (600 MHz) δ 8.40 (s, 1H, OH), 8.17 (d, *J* = 2.82 Hz, 1H, arom.), 8.04 (dd, *J* = 9.24; 2.82 Hz, 1H, arom.), 7.85 (s, 1H, CH), 6.80 (d, *J* = 9.18 Hz, 1H, arom.). <sup>13</sup>C (150 MHz) δ 169.06; 127.19; 125.27; 125.07; 121.01; 117.88. LC/MS (C<sub>10</sub>H<sub>6</sub>N<sub>2</sub>O<sub>5</sub>S): *m/z*: 265.04 (M<sup>-</sup>) 266.23.

#### 2.4.11 5-(2-Methoxybenzylidene)thiazolidine-2,4-dione (**1k**)

Using thiazolidinedione (0.234 g, 2 mmol) and 2-methoxybenzaldehyde (0.241 μl, 2 mmol), in accordance with the general procedure, the title compound **1k** was obtained (0.334 g, 71.0% yield) as a yellow solid (m.p. 240–241°C). <sup>1</sup>H (600 MHz) δ 12.54 (s, 1H, NH), 7.95 (s, 1H, CH), 7.45–7.48 (m, 1H, arom.), 7.39 (dd, *J* = 7.74; 1.38 Hz, 1H, arom.), 7.14 (d, *J* = 8.22 Hz, 1H, arom.), 7.08 (t, *J* = 7.53 Hz, 1H, arom.), 3.87 (s, 3H, OCH<sub>3</sub>). <sup>13</sup>C (150 MHz) δ 168.09; 167.41; 132.36; 128.52; 126.42; 123.43; 121.41; 120.90; 111.82; 55.73. LC/MS (C<sub>11</sub>H<sub>9</sub>NO<sub>3</sub>S): *m/z*: 233.84 (M<sup>-</sup>) 235.26.

#### 2.4.12 5-(3-Hydroxybenzylidene)thiazolidine-2,4-dione (**1l**)

Using thiazolidinedione (0.234 g, 2 mmol) and 3-hydroxybenzaldehyde (0.244 g, 2 mmol), in accordance with the general procedure, the title compound **1l** was obtained (0.132 g, 29.7% yield) as a brown solid (m.p. 262–264°C). <sup>1</sup>H (300 MHz) δ 12.58 (s, 1H, NH), 9.82 (s, 1H, OH), 7.67 (s, 1H, CH), 7.31 (t, *J* = 7.89 Hz, 1H, arom.), 7.01 (d, *J* = 7.89 Hz, 1H, arom.), 6.96 (s, 1H, arom.), 6.86 (dd, *J* = 8.07; 1.76 Hz, 1H, arom.). <sup>13</sup>C (150 MHz) δ 168.42; 167.80; 158.32; 134.65; 132.45; 130.83; 123.75; 121.78; 118.19; 116.37. LC/MS (C<sub>10</sub>H<sub>7</sub>NO<sub>3</sub>S): *m/z*: 220.50 (M<sup>-</sup>) 221.23.

#### 2.4.13 5-(4-Hydroxybenzylidene)thiazolidine-2,4-dione (**1m**)

Using thiazolidinedione (0.234 g, 2 mmol) and 4-hydroxybenzaldehyde (0.244 g, 2 mmol), in accordance with the general procedure, the title compound **1m** was obtained (0.269 g, 60.8% yield) as a yellow solid (m.p. 296–297°C). <sup>1</sup>H (600 MHz) δ 12.43 (s, 1H, NH), 10.30 (s, 1H, OH), 7.69 (s, 1H, CH), 7.45 (d, *J* = 8.58 Hz, 2H, arom.), 6.91 (d, *J* = 8.64 Hz, 2H, arom.). <sup>13</sup>C (150 MHz) δ 168.05; 167.52; 159.84; 132.35; 132.24; 123.90; 118.97; 116.28. LC/MS (C<sub>10</sub>H<sub>7</sub>NO<sub>3</sub>S): *m/z*: 220.11 (M<sup>-</sup>) 221.23.

#### 2.4.14 5-(4-(Dimethylamino)benzylidene)thiazolidine-2,4-dione (**1n**)

Using thiazolidinedione (0.234 g, 2 mmol) and 4-dimethylaminobenzaldehyde (0.298 g, 2 mmol), in accordance with the general procedure, the title compound **1n** was obtained (0.451 g, 90.9% yield) as an orange solid (m.p.



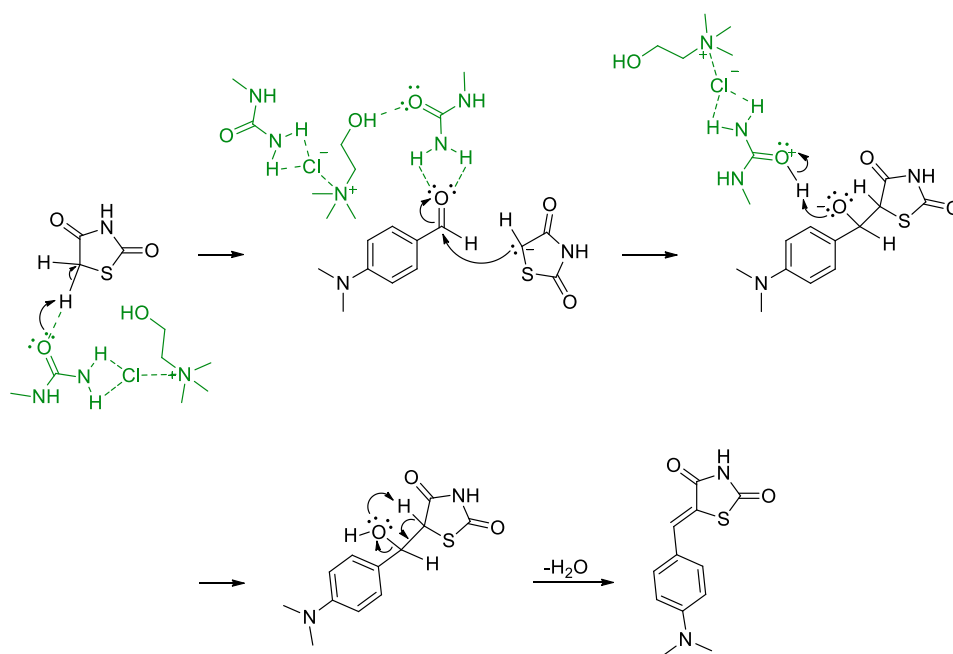


**FIGURE 1** | Proposed mechanism of Knoevenagel condensation for the synthesis of thiazolidinedione derivatives in DES..

286–289°C).  $^1\text{H}$  (600 MHz)  $\delta$  12.31 (s, 1H, NH), 7.66 (s, 1H, CH), 7.43 (d,  $J$  = 9.00 Hz, 2H, arom.), 6.82 (d,  $J$  = 9.00 Hz, 2H, arom.), 3.01 (s, 6H,  $\text{CH}_3$ ).  $^{13}\text{C}$  (150 MHz)  $\delta$  168.15; 167.57; 151.39; 132.84; 132.08; 127.75; 119.79; 115.69; 111.99. LC/MS ( $\text{C}_{12}\text{H}_{12}\text{N}_2\text{O}_2\text{S}$ ):  $m/z$ : 247.02 (M $^-$ ) 248.30.

#### 2.4.15 5-(4-(Benzyloxy)-2-hydroxybenzylidene)thiazolidine-2,4-dione (1o)

Using thiazolidinedione (0.117 g, 1 mmol) and 4-(benzyloxy) salicylaldehyde (0.228 g, 1 mmol), in accordance with the general procedure, the title compound **1o** was obtained (0.291 g, 88.9% yield) as a yellow solid (m.p. 184–188°C).  $^1\text{H}$  (600 MHz)  $\delta$  12.39 (s, 1H, NH), 10.54 (s, 1H, OH), 7.91 (s, 1H, CH), 7.44 (d,  $J$  = 8.46 Hz, 2H, arom), 7.40 (t,  $J$  = 7.47 Hz, 2H, arom.), 7.35 (m, 1H, arom.), 7.28 (d,  $J$  = 8.76 Hz, 1H, arom.), 6.65 (dd,  $J$  = 8.76; 2.46 Hz, 1H, arom.), 6.57 (d,  $J$  = 2.52 Hz, 1H, arom.), 5.11 (s, 2H,  $\text{CH}_2$ ).  $^{13}\text{C}$  (150 MHz)  $\delta$  161.08; 158.70; 136.57; 129.40; 128.44; 127.92; 127.69; 113.99; 106.85; 102.01; 69.28; 55.11; 53.13. LC/MS ( $\text{C}_{17}\text{H}_{11}\text{NO}_4\text{S}$ ):  $m/z$ : 326.20 (M $^+$ ) 325.34.

#### 2.4.16 5-(3-Fluorobenzylidene)thiazolidine-2,4-dione (1p)

Using thiazolidinedione (0.234 g, 2 mmol) and 3-fluorobenzaldehyde (212  $\mu\text{l}$ , 2 mmol), in accordance with the general procedure, the title compound **1p** was obtained (0.140 g, 31.4% yield) as a white solid (m.p. 169–171°C).  $^1\text{H}$  (600 MHz)  $\delta$  12.67 (s, 1H, NH), 7.78 (s, 1H, CH), 7.58 (q,  $J$  = 7.98; 6.18 Hz, 1H, arom.), 7.44 (dd,  $J$  = 9.96; 1.98 Hz, 1H, arom.), 7.42 (d,  $J$  = 7.92 Hz, 1H, arom.), 7.32 (ddd,  $J$  = 2.16; 8.46; 8.70 Hz, 1H, arom.).  $^{13}\text{C}$  (150 MHz)  $\delta$  167.54; 167.11; 163.03; 161.41; 135.35; 131.29; 130.31; 125.50; 119.97; 116.58. LC/MS ( $\text{C}_{10}\text{H}_6\text{FNO}_2\text{S}$ ):  $m/z$ : 222.31 (M $^-$ ) 223.22.

#### 2.4.17 5-(2,4-Dimethoxybenzylidene)thiazolidine-2,4-dione (1q)

Using thiazolidinedione (0.234 g, 2 mmol) and 2,4-dimethoxybenzaldehyde (0.332 g, 2 mmol), in accordance with the general procedure, the title compound **1q** was obtained (0.467 g, 87.9% yield) as a yellow solid (m.p. 251–253°C).  $^1\text{H}$  (300 MHz)  $\delta$  12.42 (s, 1H, NH), 7.90 (s, 1H, CH), 7.33 (d,  $J$  = 8.40 Hz, 1H, arom.), 6.69 (dd,  $J$  = 11.61; 2.40 Hz, 2H, arom.), 3.87 (s, 3H,  $\text{OCH}_3$ ), 3.82 (s, 3H,  $\text{OCH}_3$ ).  $^{13}\text{C}$  (150 MHz)  $\delta$  168.04; 163.52; 160.28; 130.52; 126.92; 120.34; 114.73; 106.74; 99.09; 56.38; 56.09. LC/MS ( $\text{C}_{12}\text{H}_{11}\text{NO}_4\text{S}$ ):  $m/z$ : 264.16 (M $^-$ ) 265.29.

#### 2.4.18 5-Benzylidenethiazolidine-2,4-dione (1r)

Using thiazolidinedione (0.234 g, 2 mmol) and benzaldehyde (205  $\mu\text{l}$ , 2 mmol), in accordance with the general procedure, the title compound **1r** was obtained (0.134 g, 32.7% yield) as a white solid (m.p. 251–254°C).  $^1\text{H}$  (600 MHz)  $\delta$  12.62 (s, 1H, NH), 7.80 (s, 1H, CH), 7.52 (m, 6H, arom.).  $^{13}\text{C}$  (150 MHz)  $\delta$  168.33; 167.77; 133.49; 132.24; 130.87; 130.46; 129.77; 124.01. LC/MS ( $\text{C}_{10}\text{H}_7\text{NO}_2\text{S}$ ):  $m/z$ : 204.22 (M $^-$ ) 205.23.

#### 2.4.19 5-((1H-Indol-3-yl)methylene)thiazolidine-2,4-dione (1s)

Using thiazolidinedione (0.234 g, 2 mmol) and indole-3-carboxaldehyde (0.290 g, 2 mmol), in accordance with the general procedure, the title compound **1s** was obtained (0.439 g, 89.8% yield) as a yellow solid (m.p. >300°C).  $^1\text{H}$  (600 MHz)  $\delta$  12.31 (s, 1H, NH), 12.12 (s, 1H, NH), 8.06 (s, 1H, CH), 7.88 (d,  $J$  = 7.86 Hz, 1H, arom.), 7.73 (d,  $J$  = 2.76 Hz, 1H, arom.), 7.51 (d,  $J$  = 8.04 Hz, 1H, arom.), 7.25 (t,  $J$  = 7.44 Hz, 1H, arom.), 7.19 (t,  $J$  = 7.38 Hz, 1H, arom.).  $^{13}\text{C}$  (150 MHz)  $\delta$  167.23;



**TABLE 2** | Comparison to other reported methods of thiazolidinedione synthesis.

Compound	Yield obtained in this research (%)	Method	Yield (%)	References
<b>1a</b>	35.9	Reflux in ethanol; piperidine	37	Ha et al. (2012)
		Ethanol; baker's yeast	40	Pratap et al. (2011)
		Tetrabutylammonium bromide; potassium carbonate	95	Durai Ananda Kumar et al. (2015)
		Water; KAl (SO <sub>4</sub> ) <sub>2</sub> · 12H <sub>2</sub> O; stirring	88	Shelke et al. (2010)
<b>1e</b>	53.9	Reflux in ethanol; piperidine	53	Ha et al. (2012)
<b>1f</b>	29.3	Water; KAl (SO <sub>4</sub> ) <sub>2</sub> · 12H <sub>2</sub> O; stirring	85	Shelke et al. (2010)
<b>1g</b>	57.8	Reflux in polyethylene glycol-300	78	Mahalle et al. (2008)
		Reflux in ethanol; piperidine	38	Ha et al. (2012)
<b>1h</b>	81.3	Tetrabutylammonium bromide; potassium carbonate	92	Durai Ananda Kumar et al. (2015)
<b>1i</b>	29.7	Tetrabutylammonium bromide; potassium carbonate	89	Durai Ananda Kumar et al. (2015)
<b>1m</b>	60.8	Mechanosynthesis; ammonium acetate	96	Metwally et al. (2011)
		Reflux in ethanol; piperidine	67	Ha et al. (2012)
		Ethanol: water (1:1); ionic liquid tetrabutylammonium hydroxide, stirring	92	Khazaei et al. (2014)
		Tetrabutylammonium bromide; potassium carbonate	91	Durai Ananda Kumar et al. (2015)
<b>1n</b>	90.9	Water; KAl (SO <sub>4</sub> ) <sub>2</sub> · 12H <sub>2</sub> O; stirring	92	Shelke et al. (2010)
		Ethanol: water (1:1); ionic liquid tetrabutylammonium hydroxide, stirring	90	Khazaei et al. (2014)
		Tetrabutylammonium bromide; potassium carbonate	92	Durai Ananda Kumar et al. (2015)
		Water; KAl (SO <sub>4</sub> ) <sub>2</sub> · 12H <sub>2</sub> O; stirring	87	Shelke et al. (2010)
<b>1q</b>	87.9	Reflux in ethanol; piperidine	96	Ha et al. (2012)
<b>1r</b>	32.7	Mechanosynthesis; ammonium acetate	96	Metwally et al. (2011)
		Ethanol: water (1:1); ionic liquid tetrabutylammonium hydroxide, stirring	90	Khazaei et al. (2014)
		Ethanol; baker's yeast	45	Pratap et al. (2011)
		Tetrabutylammonium bromide; potassium carbonate	93	Durai Ananda Kumar et al. (2015)
<b>1s</b>	89.8	Water; KAl (SO <sub>4</sub> ) <sub>2</sub> · 12H <sub>2</sub> O; stirring	95	Shelke et al. (2010)
		Reflux in toluene; L-proline	92	Riyaz et al. (2011)

**TABLE 3** | The impact of solvent recycling on product yield for model reaction.

Solvent	Yield (%)
Choline chloride: <i>N</i> -methylurea	70.43
1st recycle	75.53
2nd recycle	64.01
3rd recycle	62.25
4th recycle	63.35
5th recycle	61.88

136.16; 128.58; 126.75; 124.41; 123.02; 121.00; 118.29; 116.20; 112.36; 110.39. LC/MS (C<sub>12</sub>H<sub>8</sub>N<sub>2</sub>O<sub>2</sub>S): *m/z*: 243.05 (M<sup>-</sup>) 244.27.

## 2.5 Computational Methods

### 2.5.1 QSAR Study

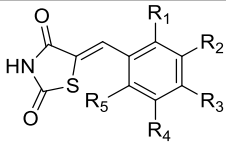
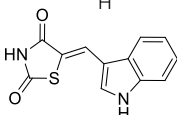
The activities of molecules expressed as the % inhibition of soybean lipoxygenase (LOX inh. %) were converted to the logarithmic values (log % LOX inh.). The 3D structures of 19 molecules were optimized by applying Spartan '08 (Wavefunction, Inc., Irvine, CA, United States) using the molecular mechanics force field (MM+) (Hocquet and Langg rd, 1998) and subsequently by the semiempirical PM3 method (Stewart, 1989). The molecular descriptors were generated using Parameter Client (Virtual Computational Chemistry Laboratory; <http://146.107.217.178/lab/pclient/>). The initial number of 1728 calculated descriptors was reduced on 568 exclusion of descriptors with zero and constant values, as descriptors that were too intercorrelated (>85%), using QSARINS-Chem 2.2.1 (University of Insubria, Varese, Italy). Generation of the QSAR model was performed

using QSARINS with a genetic algorithm, limiting the number of descriptors in the model (I) to three. Considering a reduced number of compounds, the set of molecules was not split on training and test, and the models were assessed by fitting criteria and internal cross-validation (Gramatica, 2013). In order to assess the reliability of the prediction of the modeled inhibition for the entire set of chemicals, the investigation of the applicability domain was performed. Williams plots were used to check the outliers and molecules outside of warning leverage (*h*<sup>\*</sup>), which is defined as  $3p'/n$ , where *n* is the number of training compounds and *p*' is the number of model-adjustable parameters (Gramatica, 2013).

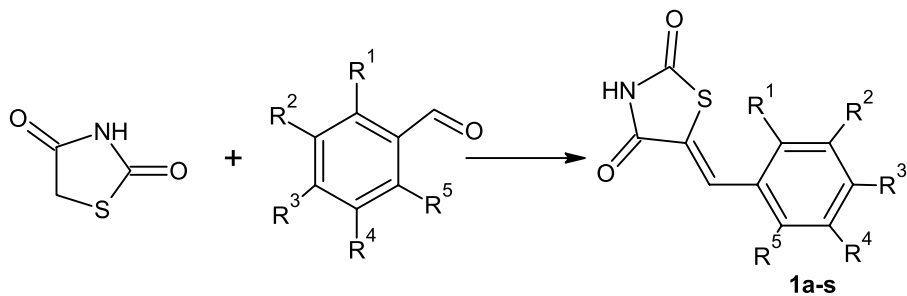
### 2.5.2 Molecular Docking

The crystal coordinates of the soybean LOX-3 (PDB ID: 1NO3) in the complex with ligand 4-nitrocatechol (PDB ID: 4NC) were downloaded from the Protein Data Bank (PDB; <https://www.rcsb.org/>). BIOVIA Discovery Studio 4.5 (Dassault Syst mes, France) was used for protein structure preparation and visualization, while iGEMDOCK (BioXGEM, Taiwan) was used for molecular docking. A set of the optimized structures of 19 thiazolidinediones were docked into the binding site of radius 8  , determined according to the ligand 4NC. Molecular docking was performed using the evolutionary method with parameters: the population size: 200, generations: 70, the number of poses: 3. iGEMDOCK generates protein–compound interaction profiles and rank compounds by pharmacological energy profiles mines the pharmacological interactions based on protein–compound interaction profiles. Pharmacological scoring function (*E*<sub>pharma</sub>/(kcal mol<sup>-1</sup>) is based on the pharmacological interactions (electrostatic (*E*), hydrogen-bonding (*H*), and van der Waals (*V*) (Hsu et al., 2011).

**TABLE 4 |** Structures of analyzed compounds, values of the experimentally determined inhibition of soybean lipoxygenase, the inhibition of lipid peroxidation induced by AAPH, DPPH, and radical scavenging ability (at 100  $\mu$ M concentrations of the compounds).

Compound						LP inh. (%) (100 $\mu$ M)	LOX inh. % (100 $\mu$ M)	LOX inh. IC <sub>50</sub> ( $\mu$ M)	DPPH (%) (100 $\mu$ M)	ABTS (%) (100 $\mu$ M)
	R <sub>1</sub>	R <sub>2</sub>	R <sub>3</sub>	R <sub>4</sub>	R <sub>5</sub>					
1a	OH	H	H	H	H	55.2	13.8	-	3.5	97.5
1b	H	OCH <sub>3</sub>	OH	H	H	36.5	8.5	-	27.9	99.7
1c	OH	H	H	OH	H	61.6	76.3	3.52	16.5	97.6
1d	H	OCH <sub>3</sub>	H	H	H	84.2	27.2	-	6.2	NA
1e	H	OH	OCH <sub>3</sub>	H	H	65.1	14.5	-	3.1	98.9
1f	H	OH	OH	H	H	50.4	13.4	-	57.6	100.0
1g	H	OCH <sub>3</sub>	OCH <sub>3</sub>	OCH <sub>3</sub>	H	46.3	7.3	-	3.3	NA
1h	OCH <sub>3</sub>	H	H	OCH <sub>3</sub>	H	62.4	17.6	-	4.2	NA
1i	H	Br	H	H	H	49.2	7.7	-	3.1	NA
1j	OH	H	H	NO <sub>2</sub>	H	76.9	18.3	-	9.6	49.3
1k	OCH <sub>3</sub>	H	H	H	H	55.9	30.31	-	3.8	NA
1l	H	OH	H	H	H	68.2	20.2	-	10.7	84.7
1m	H	H	OH	H	H	69.5	12.7	-	3.8	94.8
1n	H	H	NC <sub>2</sub> H <sub>6</sub>	H	H	23.0	12.5	-	7.6	74.7
1o	OH	H	OCH <sub>2</sub> PH	H	H	50.0	34.7	-	NA	100.0
1p	H	F	H	H	H	46.0	12.9	-	9.4	NA
1q	OCH <sub>3</sub>	H	OCH <sub>3</sub>	H	H	59.9	19.2	-	4.7	6.6
1r	H	H	H	H	H	56.7	18.8	-	3.6	NA
1s						82.9	71.1	7.46	2.7	84.2
						62.3	-	-	-	-
NDGA						-	80.8	-	-	-

NA, no activity; NDGA, nordihydroguaiaretic acid; DPPH-1, 1-diphenyl-picrylhydrazyl; ABTS, 2,2'-azino-bis(3-ethylbenzothiazoline-6-sulfonic acid); LP, lipid peroxidation; LOX, inh., soybean lipoxygenase inhibition.

**scheme 1 |** Synthesis of thiazolidinedione derivatives 1a-s.

### 3 RESULTS AND DISCUSSION

#### 3.1 Synthesis of Thiazolidinedione Derivatives

A series of thiazolidinedione derivatives were synthesized in various DESs *via* Knoevenagel condensation. Thiazolidinedione derivatives were synthesized in reactions between different substituted benzaldehydes and thiazolidinedione (**1a-s**) (**Scheme 1**). The structures of all obtained thiazolidinedione derivatives were

confirmed by different spectral methods (spectral data are shown in **Supplementary Material S1**).

In this research, a selected model reaction between 4-dimethylaminobenzaldehyde and thiazolidinedione was carried out in 20 different DESs listed in **Table 1**. Selected DESs were applied as both solvents and catalysts. Due to the high viscosity of some DESs or their melting points above room temperature, we chose a temperature of 80°C for all reactions. The product of model reaction (5-(4-(dimethylamino)benzylidene)thiazolidine-

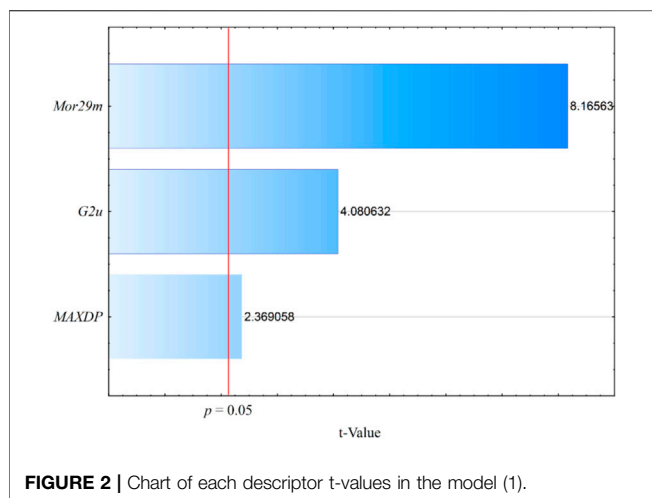


**FIGURE 2** | Chart of each descriptor t-values in the model (1).

2,4-dione) was obtained in seven DESs in which the hydrogen bond donors were amides (urea, *N*-methylurea, 1,3-dimethylurea, acetamide), thioamide (thiourea), alcohol (ethane-1,2-diol), and carboxylic acid (oxalic acid) (**Table 1**). The lowest reaction yield of 3.8% was obtained in ChCl: oxalic acid DES. The highest yield of 79.9% was obtained in ChCl: *N*-methylurea DES, while other yields were significantly lower and ranged from 3.8 to 25.2%. The reaction time ranged from 2 to 9 h. The longest duration of 9 h was shown by the reaction that took place in the reaction medium ChCl: 1,3-dimethylurea. ChCl: *N*-methylurea DES was selected as the most suitable solvent for further synthesis of thiazolidinedione derivatives, in which, with the highest product yield, the reaction took place in the shortest time of 2 h. If the product did not appear at the TLC plate after 10 h, the reaction was stopped. The duration of the chemical reaction as well as all the yields obtained in the mentioned DESs are shown in **Table 1**.

The proposed mechanism of the model reaction with DES ChCl: *N*-methylurea is shown in **Figure 1**. In the first step of the reaction, thiazolidinedione is deprotonated and protonated *N*-methylurea is formed. The deprotonated thiazolidinedione is added to the carbonyl carbon of the aldehyde, while oxygen takes the proton from the DES, dehydration occurs and thiazolidinediones are formed.

After solvent selection, various substituted aldehydes were reacted with thiazolidinedione to obtain the desired thiazolidinedione derivatives. All reactions were monitored by TLC and quenched with water after the disappearance of reactants on the TLC plate. The precipitated product was collected by filtration. The yields of thiazolidinedione series of compounds ranged from 21.5% to 90.9% (**Section 2.4**). The lowest yield was obtained for compound **1c**, while the highest yield was observed for compound **1n**. The isolated compounds' yield are highly dependent on the substituents on the aldehyde aromatic ring, which determine the aldehyde reactivity toward thiazolidinedione as well as the solubility of the synthesized compounds in water. Substituents on the aromatic ring can increase or decrease the positive character of carbonyl carbon in aldehydes, making them more or less susceptible to nucleophilic attack. Furthermore, they can also influence the

**TABLE 5** | Correlation matrix between descriptors included in model (1).

	log LOX inh. %	MAXDP	Mor29m	G2u
log LOX inh. %	1.00	−0.03	0.74	0.21
MAXDP	−0.03	1.00	0.33	−0.15
Mor29m	0.74	0.33	1.00	−0.31
G2u	0.21	−0.15	−0.31	1.00

**TABLE 6** | The statistical parameters of the QSAR models (1) and (2).

Parameter	Model (1)	Model (2)
$N_{\text{compounds}}$	19	18
$R^2$	0.82	0.88
$R^2_{\text{adj}}$	0.79	0.85
$s$	0.13	0.11
$F$	23.45	33.69
$K_{xx}$	0.27	0.29
$\Delta K$	0.05	0.10
$RMSE_{\text{tr}}$	0.11	0.10
$MAE_{\text{tr}}$	0.10	0.09
$CCC_{\text{tr}}$	0.90	0.94
$Q^2_{\text{LOO}}$	0.70	0.77
$Q^2_{\text{LMO}}$	0.66	0.75
$RMSE_{\text{cv}}$	0.15	0.14
$MAE_{\text{cv}}$	0.13	0.12
$PRESS_{\text{cv}}$	0.43	0.33
$CCC_{\text{cv}}$	0.83	0.88
$R^2_{\text{Yscr}}$	0.17	0.17
$Q^2_{\text{Yscr}}$	−0.38	−0.42
$RMSE_{\text{average Yscr}}$	0.25	0.25
$r^2_m$	0.67	0.70
Applicability domain		
$N_{\text{compounds outlier (st. res. > 2.0)}}$	1 ( <b>1a</b> )	−
$N_{\text{compounds out of app.dom}}$	−	−

LOO (the leave-one out); LMO (the leave-more out);  $R^2$  (coefficient of determination);  $R^2_{\text{adj}}$  (adjusted coefficient of determination);  $s$  (standard deviation of regression);  $F$  (Fisher ratio);  $K_{xx}$  (global correlation among descriptors);  $\Delta K$  (global correlation among descriptors);  $_{\text{tr}}$  = training set;  $_{\text{cv}}$  = cross-validation);  $_{\text{Yscr}}$  = Y-scramble; RMSE, root-mean-square error; MAE, mean absolute error; CCC, concordance correlation coefficient;  $Q^2$  = variance explained; PRESS, predictive error sum of squares;  $r^2_m$  = absolute difference between the  $R^2$  and  $R^2_0$  (determination coefficients with and without intercept);  $h^*$  (warning leverage for the applicability domain of the model).

compounds' water solubility. Since all reactions within this research were performed until the full consumption of reactants, the product solubility in water could have determined the isolated yield. The best yields are obtained for aldehydes with electron-donating groups, such as  $-\text{N}(\text{CH}_3)_2$  and  $-\text{OCH}_3$ , while the lowest yields were obtained in the compounds containing  $-\text{OH}$  groups. As already mentioned, this effect is probably a result of the higher solubility of these compounds in water. Since a simple precipitation of the product was accomplished by the addition of water in the reaction mixture, some compounds possessing higher water solubility could have been obtained in lower yields. For the sake of greenness and simplicity of the method, further extractions of such compounds were not performed. Some of the synthesized compounds have already been synthesized and published by various authors. The yields obtained by some conventional methods for some thiazolidinedione derivatives were

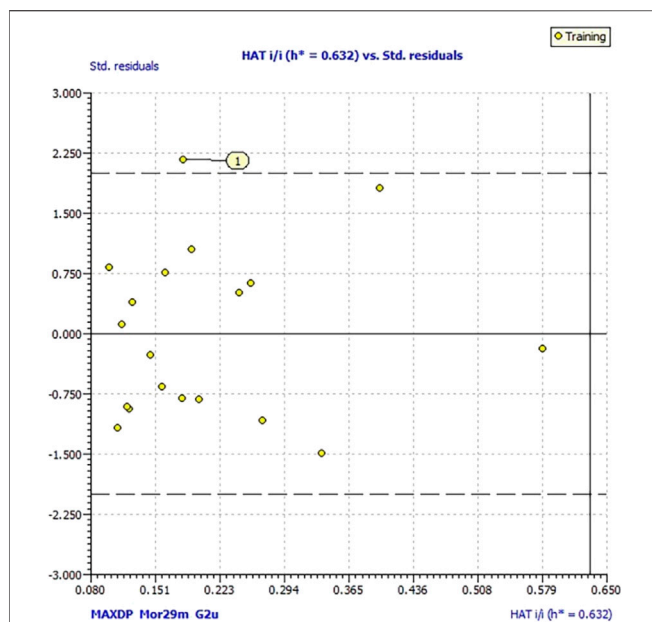


FIGURE 3 | Williams plot of applicability domain of the QSAR model (1).

compared to those obtained by our method (Table 2). As can be seen, the yields of some compounds obtained within this research are comparable to the reported data, while for some compounds, lower yields are obtained. It is important to accentuate that our method does not utilize any catalysts, while for most compounds, a purification step is also avoided. To emphasize the green character of this reaction, we also performed a recyclability experiment on the model reaction in choline chloride: *N*-methylurea DES. The results (Table 3) indicate that after five cycles, a yield slightly dropped from 70.43% to 61.88%.

### 3.2 Inhibitory Activity

The synthesized thiazolidinedione derivatives (1a–s) were tested for the inhibition of lipid peroxidation as well as the inhibitory activity against soybean lipoxygenase at a 100  $\mu$ M concentration in the reaction mixture. All the results are shown in Table 4. Thiazolidinedione derivatives inhibited the LOX activity in the range of 7.3%–76.3%. Of the 19 compounds tested, only two inhibited the LOX activity above 50%. The two compounds with the highest activity are 5-(2,5-dihydroxybenzylidene)thiazolidine-2,4-dione (1c) and 5-((1*H*-indol-3-yl)methylene)thiazolidine-2,4-dione (1s). The determined  $IC_{50}$  values for compounds 1c and 1s were 3.52 and 7.46  $\mu$ M, respectively. Compound 5-(3,4,5-trimethoxybenzylidene)thiazolidine-2,4-dione (1g), which has three methoxy groups substituted on the aromatic ring, had the lowest enzyme inhibition. Omar et al. (2020) carried out an evaluation of 31 thiazolidine-4-one-1,3,4-thiadiazole hybrids for their activity toward LOX. Results showed that increasing the length of the aliphatic substituent decreased the LOX inhibitory potency, while increasing the number of hydroxy groups decreased the inhibitory activity.

Similar trends were observed for derivatives with methoxy groups. Their results showed that a small hydrophobic group, at the 5th position of thiazolidinone, was required for good activity, while the 5th position of the thiazolidinone moiety should be unsubstituted. Marc et al. (2019) synthesized 12 new phenolic derivatives of thiazolidine-2,4-dione and found that in most cases, antioxidant activities were linked to the number of phenolic OH groups present in the molecules. Thiazolidinedione derivatives inhibited lipid peroxidation in the range of 23.0%–84.2%. The highest inhibition was achieved with the compound 5-(3-methoxybenzylidene)thiazolidine-2,4-dione (1d), while the lowest inhibition was achieved with the compound 5-(4-hydroxybenzylidene)thiazolidine-2,4-dione (1m). A high inhibition of lipid peroxidation of 82.9% was also shown by the compound 5-((1*H*-indol-3-yl)methylene)thiazolidine-2,4-dione (1s). Compounds with halogen substituents (1i) and (1p) showed similar lipid peroxidation inhibition values of 49.2% and 46.0%, respectively. All results were compared to appropriate standards. The results of the inhibition of the LOX activity were compared with the NDGA standard whose inhibition was 80.8%. The results of lipid peroxidation inhibition were compared with Trolox whose inhibition was 62.3%.

Thiazolidinedione derivatives inhibited ABTS radicals in the range of 6.6%–100.0% at a concentration of 100  $\mu$ M (Table 4). High inhibition values (>94%) of the ABTS radical were shown by the following compounds: 1a, 1b, 1c, 1e, 1f, 1m, and 1o, which had a substituted hydroxyl group on the phenyl ring. Compounds 1d, 1g, 1h, 1i, 1k, 1p, and 1r did not show activity at the tested concentration and had one or more methoxy groups or a halogen element substituted on the benzene ring. Inhibition values of DPPH radical were 2.7%–57.6%. The compound 5-(3,4-dihydroxybenzylidene)thiazolidine-2,4-dione (1f) had the highest inhibition, while the compound 5-((1*H*-indol-3-yl)methylene)thiazolidine-2,4-dione (1s) had the lowest activity. Compound 1o showed no activity. From the obtained results, it can be concluded that the compounds with a substituted hydroxyl group had high inhibition values of the ABTS radical, since the inhibition is achieved by donating a hydrogen atom. Inhibition values of the DPPH radical were much lower in comparison with the ABTS radical inhibition, perhaps because of a different reaction mechanism. It can be assumed that they react on the principle of the SET mechanism, and the tested compounds are not good electron donors (Shalaby and Shanab, 2013; Liang and Kitts, 2014; Li et al., 2018). It has already been shown that a catechol-like structure of a 3,4-dihydroxybenzylidene moiety greatly contributes to the antioxidant activity, both in ABTS (Kim et al., 2019; Ilyasov et al., 2020) and in DPPH scavenging activities (Molnar et al., 2012). Therefore, the presence of hydroxyl groups contributes to the increased antioxidant activity, while halogen, methoxy, phenoxy, and benzyloxy groups contribute to the increased inhibition of lipoxygenase activity and lipid peroxidation.

### 3.3 QSAR

Generation of QSAR models for the inhibition of soybean lipoxygenase was performed on the set of the 19 compounds.

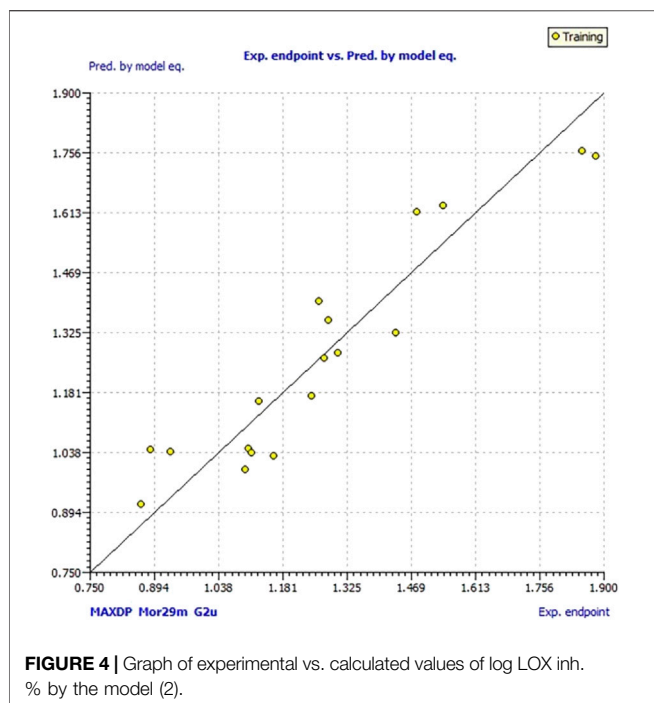


**FIGURE 4** | Graph of experimental vs. calculated values of log LOX inh. % by the model (2).

The data were not split into the training and test sets due to a limited number of compounds. The best QSAR model obtained is:

$$\log \text{LOX inh. \%} = 2.48 + 2.56\text{Mor29m} + 6.28\text{G2u} - 0.53\text{MAXDP}$$

$N = 19$

(1)

Descriptors in **Eq. 1** are listed in order of relative importance by their  $t$  values (coefficient divided by its standard error) shown in the chart (**Figure 2**). The molecular descriptor values have been tabulated in **Supplementary Material S2a**. Experimental and calculated log LOX inh. % by model (1) are shown in **Supplementary Material S2b**. Values of Pearson correlation coefficient ( $R < 0.70$ ) in the correlation matrix between the descriptors (**Table 5**) excluded their collinearity overfitting.

Also, the strong correlation between the descriptor *Mor29m* and LOX inhibitions could be observed ( $R = 0.74$ ). The parameters of fitting and internal validation for the QSAR model (1) are presented in **Table 6**. Low collinearity between the descriptors is confirmed by the low values of  $K_{xx}$  and  $\Delta K > 0.05$ . Model satisfied all fitting parameters:  $R^2 \geq 0.7$ ;  $R^2 - R^2_{\text{adj}} < 0.3$ ; and  $\text{RMSE}_{\text{tr}} < 0.3$ ;  $\text{CCC}_{\text{tr}} > 0.85$ . The model demonstrates a satisfactory stability in internal validation ( $Q^2_{\text{LOO}} \geq 0.5$ ;  $Q^2_{\text{LMO}} \geq 0.6$ ;  $\text{RMSE}_{\text{tr}} < \text{RMSE}_{\text{cv}}$ ;  $r^2_{\text{m}} \geq 0.6$ ) (Kiralj and Ferreira, 2009; Veerasamy et al., 2011). Parameters of Y-scrambling ( $R^2_{\text{Yscr}} < 0.2$ ;  $Q^2_{\text{Yscr}} < 0.2$ ) highlight that the model is robust and not obtained by chance correlation (Masand et al., 2019). The only failed parameter is the concordance correlation coefficient obtained by cross-validation ( $\text{CCC}_{\text{cv}}$ ) that is higher than 0.85. A lower value of this parameter indicates low reproducibility of cross-validation and thus lower accuracy of the proposed model (Lin, 1992). Inspection of the Williams plot of the applicability domain (**Figure 3**) revealed the one outlier, molecule **1a**, which has the greatest residual (0.25) between experimental and calculated values (**Supplementary Material S2b**). to measure the agreement. Molecules outside of the warning leverage ( $h^*$ ) were not identified. Exclusion of molecule **1a** from the data set, the following model was obtained using the same descriptors:

$$\log \text{LOX inh. \%} = 3.34 + 2.69\text{Mor29m} + 5.65\text{G2u} - 0.69\text{MAXDP}$$

$N = 18$

(2)

According to the statistical parameters presented in **Table 6**, a significantly improved model was obtained. It is especially improved  $\text{CCC}_{\text{cv}}$  on 0.88, which is greater than the threshold values (0.85), commonly used by the proposed validation criteria (Chirico and Gramatica, 2011). Graph of experimental vs. calculated values of log LOX inh. % by the model (2) is presented in **Figure 4**. The descriptor *Mor29m* belongs to the 3D molecular representations of the structure based on electron diffraction (3D-MoRSE) descriptors (Schuur et al., 1996). This descriptor codes pairs of atoms weighted by atomic mass at the scattering parameter 28 Å. (Devinyak et al., 2014). The relatively large scattering parameter of this descriptor conditions small discriminative power for interatomic differences between heavy atoms. The greater the number of atoms, higher the atomic

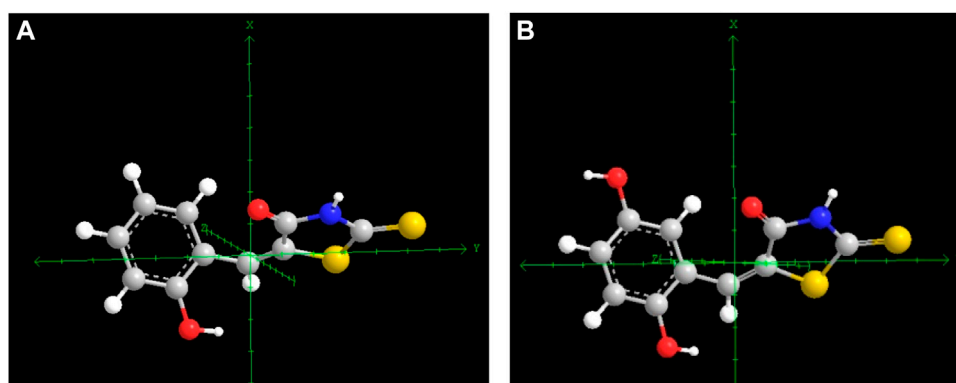


**FIGURE 5** | Difference in the symmetry of structures molecules **1a** (A) and **1c** (B) respect to axes y..



**TABLE 7** | Total energies of a predicted poses (fitness) and energies of interactions (hydrogen-bonding (*H*), van der Waals (*V*), and electrostatic (*E*)) between protein residue and ligand (kcal mol<sup>-1</sup>) in the binding site of soybean LOX-3 (1NO3).

Compound	Pose	Fitness	<i>H</i>	<i>V</i>	<i>E</i>
<b>1s</b>	2	-72.91	-18.42	-54.45	0.00
<b>1g</b>	2	-72.87	-1.60	-71.31	0.00
<b>1o</b>	0	-70.08	-9.48	-60.61	0.00
<b>1c</b>	2	-67.68	-11.74	-55.93	0.00
<b>1e</b>	2	-66.46	-2.73	-63.73	0.00
<b>4NC</b>	2	-64.74	-15.06	-51.49	1.81
<b>1b</b>	0	-64.62	-7.84	-56.78	0.00
<b>1j</b>	1	-63.72	-20.09	-44.82	1.19
<b>1a</b>	2	-63.65	-15.53	-48.12	0.00
<b>1q</b>	0	-62.70	-7.30	-55.40	0.00
<b>1n</b>	2	-62.47	-3.50	-58.97	0.00
<b>1h</b>	1	-61.41	-8.27	-53.13	0.00
<b>1f</b>	0	-60.81	-5.69	-55.12	0.00
<b>1d</b>	2	-60.66	-3.36	-57.30	0.00
<b>1k</b>	2	-60.13	0.00	-60.13	0.00
<b>1m</b>	2	-58.51	-9.36	-49.16	0.00
<b>1l</b>	2	-57.36	-2.50	-54.86	0.00
<b>1p</b>	1	-56.65	-3.17	-53.48	0.00
<b>1r</b>	2	-55.38	-10.50	-44.88	0.00
<b>1i</b>	1	-54.50	-7.00	-47.50	0.00

**TABLE 8** | Energy of the main interactions between LOX-3 residues and ligand **1s** (M = main chain; S = side chain).

H bond	Energy	van der Waals interaction	Energy
M-Gln514	-1.16	S-Gln514	-4.81
S-Gln514	-3.50	S-His518	-1.14
S-His518	-9.50	S-Trp519	-9.33
S-His523	-1.99	S-His523	-10.14
M-Ile857	-2.26	M-Asn558	-1.38
		S-Asn558	-0.47
		S-Leu565	-2.92
		S-Ile572	-1.77

mass at the short distance decreases the value of *Mor29m*, which influences lower inhibition. Thus, in the least active compound (**1g**) (log LOX inh. % = 0.86), the three methoxy groups are at the close positions, R<sub>2</sub>, R<sub>3</sub>, and R<sub>4</sub>, which lower *Mor29m* to a negative value (-0.9), while in **1h**, where the -OCH<sub>3</sub> are in distant positions, R<sub>1</sub> and R<sub>4</sub>, a value of *Mor29m* increased to 0.02 and inhibition effect is better (log LOX inh. % = 1.25). The most active compound, **1c**, has two hydroxyl groups in the distant positions (R<sub>1</sub> and R<sub>4</sub>), while the second most active, compound **1s**, instead of benzylidene group substituted with hydroxyl or methoxy groups possesses the unsubstituted indole group. Both compounds have positive values of *Mor29m* (0.04 and 0.16, respectively) (**Supplementary Material S2a**). The second variable in models (1) and (2) is *G2u*, unweighted three-dimensional molecular index (WHIM) descriptors. This descriptor evaluates molecular symmetry on the basis of the number of symmetric atoms along a second axis of the molecule (Todeschini and Gramatica, 1997). According to the positive coefficient of *G2u* in QSAR models (1–2), higher values of this descriptor imply molecules with enhanced LOX inhibition.

Therefore, molecule **1c** has one of the highest values of *G2u* (0.23) (**Supplementary Material S2a**). The two hydroxyl groups were symmetrically located at positions R<sub>1</sub> and R<sub>4</sub>, which probably affected the inhibitory activity. Molecule **1a**, which possesses only one hydroxyl group at the position R<sub>1</sub>, is asymmetrical; therefore, it has lower *G2u* (0.18) and a weaker inhibition effect (**Figure 5**). The third descriptor in QSAR models (1–2) is the topological descriptor, a maximal electrotopological positive variation (*MAXDP*). Molecular electrotopological variation is the sum over all atoms of the intrinsic state differences. *MAXDP* is a measure of the total charge transfer in the molecule and it is related to the electrophilicity of the molecule (Gramatica et al., 2000). The maximal value of descriptor *MAXDP* has molecule **1g** (4.65), which is also the least active (**Supplementary Material S2a**). This result is consistent with the QSAR study of lipid peroxidation-inhibition potential of phenolic compounds, which revealed that *MAXDP* also has negative contributions to the activity (Ray et al., 2008). A study by Roussaki et al. (2010), Roussaki et al. (2014) has shown that the presence of the prenyloxy group in coumarin derivatives enhances lipophilicity and thus their soybean lipoxygenase inhibitory activity. Our previous QSAR study of the coumarin derivatives for lipoxygenase inhibition revealed that molecules with more atoms and higher polarizabilities in a radius of 3.5 Å from the geometrical center increase lipoxygenase inhibition (Lončarić et al., 2020).

### 3.4 Molecular Docking With Soybean LOX-3

In order to predict the docked conformations, 19 synthesized thiazolidinediones, and extracted ligand **4NC**, as inhibitors of soybean LOX-3 (PDB ID: 1NO3), molecular docking was performed. The total energy of a predicted pose (fitness) and the energy of interactions between the protein residue and ligand are tabulated in **Table 7**. The results of molecular docking confirmed the experimentally obtained results. The highest binding energy has compound **1s**, which exhibited the second highest inhibition against LOX-3 (**Table 4**). The standard ligand, **4NC**, achieved only the sixth position in the score with a total energy of -64.74 kcal mol<sup>-1</sup>. The energies of the main interactions between compound **1s** and residues of the LOX-3 binding pocket are presented in **Table 8**. The docked position of the compound **1s** in the binding site of LOX-3 is presented in **Figure 6A**, while the 2D presentations of the main interactions with residues are shown in **Figure 6B**. Inhibitor **1s** is anchored in the hydrophobic channel lined by the side chains of Lue277, Ile857, Leu560, Ile557, and Ala561. Hydrogen bond generates nitrogen from thiazolidine with Gln514, while the carbon hydrogen bond is present between the oxygen atom and His518. Residue His523 generates a strong  $\pi$ -sigma interaction with the pyrrole ring. Indole group also generates interactions with Leu565, Lue277, Leu560, Ile557, and Ala561. X-ray structure of soybean LOX-3 complex with 4-nitrocatechol (**4NC**) revealed that the two hydroxyl groups interact with His523 (Skrzypczak-Jankun et al., 2004). The docking study of soybean LOX-3 with coumarin derivatives showed that those ligands formed H-bond interactions with His513, Gln514, His518, Trp519, and Asp766. The formation of H-bond between the oxygen atom from the benzoyl group (Lončarić et al., 2020) was important.

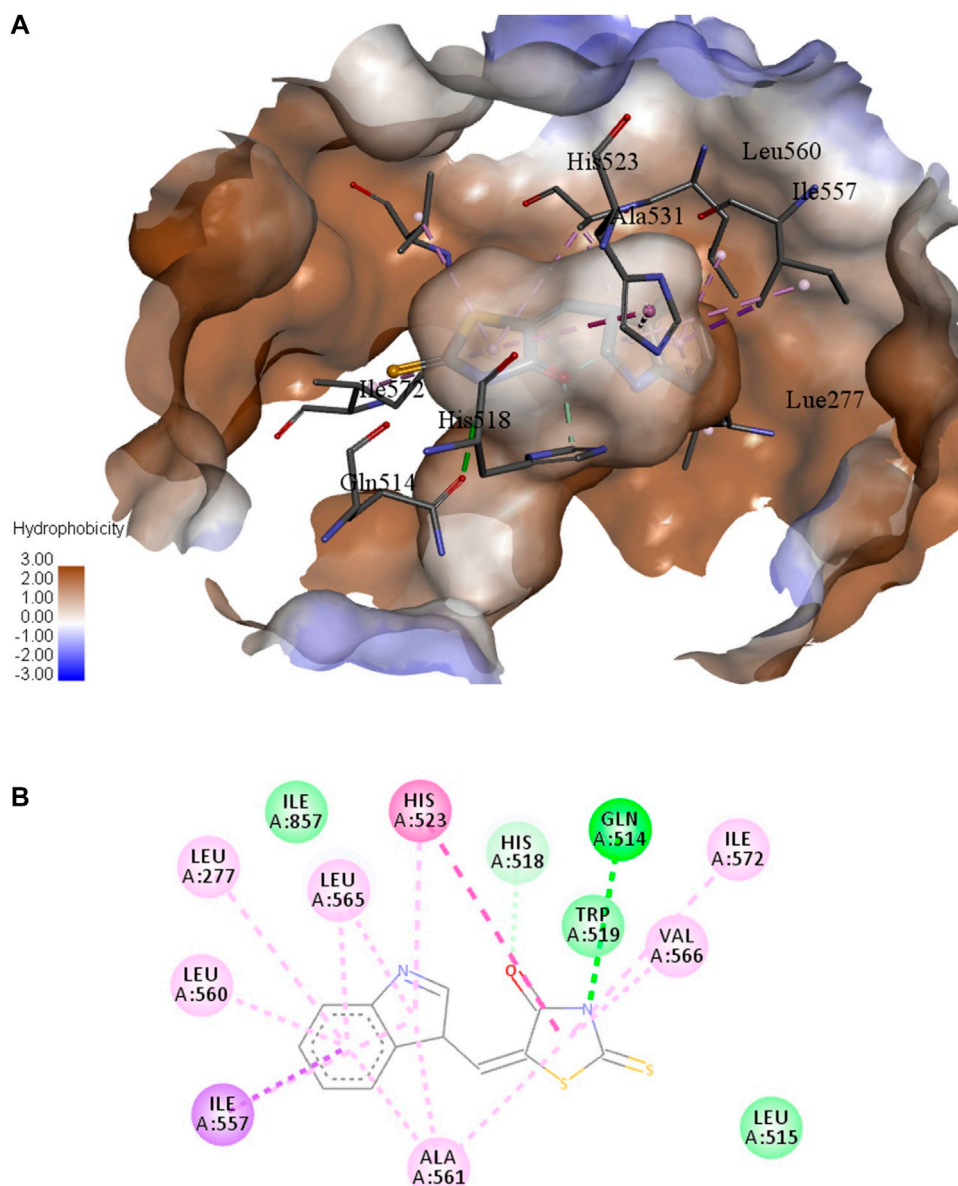


**FIGURE 6 | (A)** Hydrophobic surface representation of soybean LOX-3 binding site with docked compound **1s**. **(B)** 2D representation of the main interactions of compound **1s** with residues in binding site of LOX-3: green = conventional hydrogen bond; light green = van der Waals; very light green = carbon-hydrogen bond; dark purple =  $\pi$ -sigma; purple =  $\pi$ - $\pi$  T-shaped; light purple = alkyl and  $\pi$ -alkyl.

## 4 CONCLUSION

Thiazolidinedione derivatives were successfully synthesized in choline chloride-based deep eutectic solvents with yields ranging from 21.5% to 90.9%. After screening 20 different DESs, the most suitable solvent for the synthesis of mentioned compounds was proven to be ChCl: *N*-methylurea. The highest inhibition of the lipoxygenase activity of 76.3% was achieved with compound **1c** ( $IC_{50} = 3.52 \mu M$ ). Compound **1d** showed the highest inhibition of lipid peroxidation of 84.2%. Thiazolidinedione derivatives showed better inhibition of

the ABTS radical than the inhibition of the DPPH radical. The highest inhibition of the ABTS radical of 100% was achieved with compounds **1f** and **1o**. QSAR study revealed the essential structural features of thiazolidine-2,4-dione derivatives for the enhanced inhibition of the soybean LOX-3, such as larger distance between atoms, higher atomic mass, symmetrical distribution of the atomic group in the molecule, and lower electrophilicity of the molecule. Molecular docking confirmed the experimentally obtained results of LOX-3 inhibition and elucidated the mode of the interactions with residues in the hydrophobic binding pocket of LOX-3. Future

synthesis of thiazolidinediones as promising LOX-3 inhibitors should be limited to the lipophilic derivatives without hydroxyl and methoxy groups, or their symmetric distribution in order to prevent steric hindrance. Since thiazolidinediones are also known as insulin-sensitizing agents used in the treatment of type 2 diabetes as effective agents for attenuating insulin resistance, compounds can be tested for their anti-inflammatory and antidiabetic activities.

## DATA AVAILABILITY STATEMENT

The original contributions presented in the study are included in the article/**Supplementary Material**; further inquiries can be directed to the corresponding author.

## AUTHOR CONTRIBUTIONS

ML performed the synthesis and biological activity investigation; IS conceptualized the biological investigation

and was engaged in draft writing; VP was engaged in the biological investigation and result interpretation; VR performed QSAR and docking studies, as well as the result interpretation and article writing; MK was engaged in QSAR and docking studies; MM performed a structural investigation of the synthesized compounds, article writing, and obtained the funding for the research.

## FUNDING

This work was supported, in part, by the Croatian Science Foundation under the project “Green Technologies in Synthesis of Heterocyclic Compounds” (UIP-2017-05-6593).

## SUPPLEMENTARY MATERIAL

The Supplementary Material for this article can be found online at: <https://www.frontiersin.org/articles/10.3389/fchem.2022.912822/full#supplementary-material>

## REFERENCES

- Albrecht, U., Gördes, D., Schmidt, E., Thurow, K., Lalk, M., and Langer, P. (2005). Synthesis and Structure-Activity Relationships of 2-Alkylidenethiazolidine-4, 5-Diones as Antibiotic Agents. *Bioorg. Med. Chem.* 13 (14), 4402–4407. doi:10.1016/j.bmc.2005.04.046
- Avupati, V. R., Rani, Y., and Singh, A. (2018). Discovery of a Series of 5-Benzylidene-1, 3-Thiazolidine-2, 4-Dione-Linked Chalcone Hybrids as a Novel Class of 5-Lipoxygenase (5-LO) Inhibitors. *J. Young Pharma* 10 (2), 241–242. doi:10.5530/jyp.2018.10.53
- Axelrod, B., Cheesbrough, T. M., and Laakso, S. (1981). Lipoxygenase from Soybeans. *Methods Enzymol.* 71, 441–451. doi:10.1016/0076-6879(81)71055-3
- Beharry, Z., Zemskova, M., Mahajan, S., Zhang, F., Ma, J., Xia, Z., et al. (2009). Novel Benzylidene-Thiazolidine-2, 4-Diones Inhibit Pim Protein Kinase Activity and Induce Cell Cycle Arrest in Leukemia and Prostate Cancer Cells. *Mol. Cancer Ther.* 8 (6), 1473–1483. doi:10.1158/1535-7163.mct-08-1037
- Borbulevych, O. Y., Jankun, J., Selman, S. H., and Skrzypczak-Jankun, E. (2004). Lipoxygenase Interactions with Natural Flavonoid, Quercetin, Reveal a Complex with Protocatechuic Acid in its X-Ray Structure at 2.1 Å Resolution. *Proteins* 54, 13–19. doi:10.1002/prot.10579
- Bozdağ-Dündar, O., Çoban, T., Ceylan-Ünlüsoy, M., and Ertan, R. (2009). Radical Scavenging Capacities of Some Thiazolylthiazolidine-2, 4-Dione Derivatives. *Med. Chem. Res.* 18 (1), 1–7. doi:10.1007/s00044-007-9081-0
- Chadha, N., Bahia, M. S., Kaur, M., and Silakari, O. (2015). Thiazolidine-2, 4-Dione Derivatives: Programmed Chemical Weapons for Key Protein Targets of Various Pathological Conditions. *Bioorg. Med. Chem.* 23 (13), 2953–2974. doi:10.1016/j.bmc.2015.03.071
- Chatterjee, B., and Sharma, A. (2018). Fruit Enzymes and Their Application: A Review. *Int. J. Clin. Biomed. Res.* 4 (2), 84–88. doi:10.5455/ijcbr.2018.42.18
- Chirico, N., and Gramatica, P. (2011). Real External Predictivity of QSAR Models: How to Evaluate it? Comparison of Different Validation Criteria and Proposal of Using the Concordance Correlation Coefficient. *J. Chem. Inf. Model.* 51, 2320–2335. doi:10.1021/ci200211n
- da Rocha Junior, L. F., Rêgo, M. J., Cavalcanti, M. B., Pereira, M. C., Pitta, M. G., de Oliveira, P. S., et al. (2010). Synthesis of a Novel Thiazolidinedione and Evaluation of its Modulatory Effect on IFN- $\gamma$ , IL-6, IL-17A, and IL-22 Production in PBMCs from Rheumatoid Arthritis Patients. *BioMed Res. Int.* 2013, 926060. doi:10.1155/2013/926060
- Devinyak, O., Havrylyuk, D., and Lesyk, R. (2014). 3D-MoRSE Descriptors Explained. *J. Mol. Graph. Model.* 54, 194–203. doi:10.1016/j.jmgm.2014.10.006
- Durai Ananda Kumar, T., Swathi, N., Navatha, J., Subrahmanyam, C. V. S., and Satyanarayana, K. (2015). Tetrabutylammonium Bromide and K<sub>2</sub>CO<sub>3</sub>: An Eco-Benign Catalyst for the Synthesis of 5-Arylidene-1, 3-Thiazolidine-2, 4-Diones via Knoevenagel Condensation. *J. Sulfur Chem.* 36 (1), 105–115. doi:10.1080/17415993.2014.970555
- Gramatica, P., Corradi, M., and Consonni, V. (2000). Modelling and Prediction of Soil Sorption Coefficients of Non-Ionic Organic Pesticides by Molecular Descriptors. *Chemosphere* 41, 763–777. doi:10.1016/s0045-6535(99)00463-4
- Gramatica, P. (2013). “On the Development and Validation of QSAR Models,” in *Computational Toxicology. Methods in Molecular Biology (Methods and Protocols)*. Editors B. Reisfeld and A. Mayeno (Totowa, NJ, USA: Humana Press), 930, 499–526. doi:10.1007/978-1-62703-059-5\_21
- Ha, Y. M., Park, Y. J., Kim, J.-A., Park, D., Park, J. Y., Lee, H. J., et al. (2012). Design and Synthesis of 5-(Substituted Benzylidene) Thiazolidine-2, 4-Dione Derivatives as Novel Tyrosinase Inhibitors. *Eur. J. Chem. Med.* 49, 245–252. doi:10.1016/j.ejmech.2012.01.019
- Hocquet, A., and Langgärd, M. (1998). An Evaluation of the MM+ Force Field. *J. Mol. Model.* 4, 94–112. doi:10.1007/s008940050128
- Hsu, K.-C., Chen, Y.-F., Lin, S.-R., and Yang, J.-M. (2011). iGEMDOCK: A Graphical Environment of Enhancing GEMDOCK Using Pharmacological Interactions and Post-Screening Analysis. *BMC Bioinforma.* 12 (Suppl. S1), S33. doi:10.1186/1471-2105-12-S1-S33
- Ilyasov, I. R., Beloborodov, V. L., Selivanova, I. A., and Terekhov, R. P. (2020). ABTS/PP Decolorization Assay of Antioxidant Capacity Reaction Pathways. *Int. J. Mol. Sci.* 21, 1131. doi:10.3390/ijms21031131
- Ivanov, I., Heydeck, D., Hofheinz, K., Roffeis, J., O'Donnell, V. B., Kuhn, H., et al. (2010). Molecular Enzymology of Lipoxygenases. *Arch. Biochem. Biophys.* 503 (2), 161–174. doi:10.1016/j.jabb.2010.08.016
- Jain, V. S., Vora, D. K., and Ramaa, C. S. (2013). Thiazolidine-2, 4-Diones: Progress towards Multifarious Applications. *Bioorg. Med. Chem.* 21 (7), 1599–1620. doi:10.1016/j.bmc.2013.01.029
- Jothi, L., Saqib, A., Shivappa Karigar, C., and Sekhar, S. (2018). Molecular Docking of Seed Bioactives as Dual COX-2 and LOX-3 Inhibitors in

- Context to Osteoarthritis. *Pharmacogn. Commn.* 8 (3), 97–102. doi:10.5530/pc.2018.3.21
- Kavetsou, E., Gkionis, L., Galani, G., Gkolfinopoulou, C., Argyri, L., Pontiki, E., et al. (2017). Synthesis of Prenyloxy Coumarin Analogues and Evaluation of Their Antioxidant, Lipoxigenase (LOX) Inhibitory and Cytotoxic Activity. *Med. Chem. Res.* 26 (4), 856–866. doi:10.1007/s00044-017-1800-6
- Khazaei, A., Veisi, H., Safaei, M., and Ahmadian, H. (2014). Green Synthesis of 5-Arylidene-2, 4-Thiazolidinedione, 5-Benzylidene Rhodanine and Dihydrothiophene Derivatives Catalyzed by Hydrated Ionic Liquid Tetrabutylammonium Hydroxide in Aqueous Medium. *J. Sulfur Chem.* 35 (3), 270–278. doi:10.1080/17415993.2013.860142
- Kim, E., Kang, M., Liu, H., Cao, C., Liu, C., Bentley, W. E., et al. (2019). Pro- and Anti-Oxidant Properties of Redox-Active Catechol-Chitosan Films. *Front. Chem.* 7, 541. doi:10.3389/fchem.2019.00541
- Kim, S. H., Ha, Y. M., Moon, K. M., Choi, Y. J., Park, Y. J., Jeong, H. O., et al. (2013). Anti-Melanogenic Effect of (Z)-5-(2, 4-Dihydroxybenzylidene) Thiazolidine-2,4-Dione, a Novel Tyrosinase Inhibitor. *Arch. Pharm. Res.* 36 (10), 1189–1197. doi:10.1007/s12272-013-0184-5
- Kiralj, R., and Ferreira, M. M. C. (2009). Basic Validation Procedures for Regression Models in QSAR and QSPR Studies: Theory and Application. *J. Braz. Chem. Soc.* 20 (4), 770–787. doi:10.1590/s0103-50532009000400021
- Li, X., Chen, B., Xie, H., He, Y., Zhong, D., and Chen, D. (2018). Antioxidant Structure-Activity Relationship Analysis of Five Dihydrochalcones. *Molecules* 23 (5), 1162. doi:10.3390/molecules23051162
- Liang, N., and Kitts, D. (2014). Antioxidant Property of Coffee Components: Assessment of Methods that Define Mechanisms of Action. *Molecules* 19 (11), 19180–19208. doi:10.3390/molecules191119180
- Lin, L. I.-K. (1992). Assay Validation Using the Concordance Correlation Coefficient. *Biometrics* 48 (2), 599–604. doi:10.2307/2532314
- Lončarić, M., Strelec, I., Pavić, V., Šubarić, D., Rastija, V., and Molnar, M. (2020). Lipoxigenase Inhibition Activity of Coumarin Derivatives—QSAR and Molecular Docking Study. *Pharmaceuticals* 13 (7), 154. doi:10.3390/ph13070154
- Mahalle, S. R., Netankar, P. D., Bondge, S. P., and Mane, R. A. (2008). An Efficient Method for Knoevenagel Condensation: A Facile Synthesis of 5-Arylidene-2, 4-Thiazolidinedione. *Green Chem. Lett. Rev.* 1 (2), 103–106. doi:10.1080/17518250802139881
- Marc, G., Stana, A., Oniga, S. D., Pirnău, A., Vlase, L., and Oniga, O. (2019). New Phenolic Derivatives of Thiazolidine-2,4-Dione with Antioxidant and Antiradical Properties: Synthesis, Characterization, *In Vitro* Evaluation, and Quantum Studies. *Molecules* 24 (11), 2060. doi:10.3390/molecules24112060
- Masand, V. H., El-Sayed, N. N. E., Rastija, V., Rathore, M. M., and Karnaś, M. (2019). Identification of Prodigious and Under-Privileged Structural Features for RG7834 Analogs as Hepatitis B Virus Expression Inhibitor. *Med. Chem. Res.* 28, 2270–2278. doi:10.1007/s00044-019-02455-w
- Metwally, N. H., Rateb, N. M., and Zohdi, H. F. (2011). A Simple and Green Procedure for the Synthesis of 5-Arylidene-4-Thiazolidinones by Grinding. *Green Chem. Lett. Rev.* 4 (3), 225–228. doi:10.1080/17518253.2010.544330
- Molnar, M., Cacic, M., and Zec Zrinusic, S. (2012). Synthesis and Antioxidant Evaluation of Schiff Bases Derived from 2,6-Pyridinedicarboxylic Acid. *Lett. Org. Chem.* 9, 401–410. doi:10.2174/157017812801322480
- Omar, Y. M., Abdel-Moty, S. G., and Abdu-Allah, H. H. M. (2020). Further Insight into the Dual COX-2 and 15-LOX Anti-inflammatory Activity of 1,3,4-Thiadiazole-Thiazolidinone Hybrids: The Contribution of the Substituents at 5th Position Is Size Dependent. *Bioorg. Chem.* 97, 103657. doi:10.1016/j.bioorg.2020.103657
- Osman, H., Arshad, A., Lam, C. K., and Bagley, M. C. (2012). Microwave-Assisted Synthesis and Antioxidant Properties of Hydrazinyl Thiazolyl Coumarin Derivatives. *Chem. Cent. J.* 6 (1), 1–10. doi:10.1186/1752-153X-6-32
- Pratap, U. R., Jawale, D. V., Waghmare, R. A., Lingampalle, D. L., and Mane, R. A. (2011). Synthesis of 5-Arylidene-2, 4-Thiazolidinediones by Knoevenagel Condensation Catalyzed by Baker's Yeast. *New J. Chem.* 35 (1), 49–51. doi:10.1039/C0NJ00691B
- Ray, S., De, K., Sengupta, C., and Roy, K. (2008). QSAR Study of Lipid Peroxidation-Inhibition Potential of Some Phenolic Antioxidants. *Indian J. Biochem. Biophys.* 45, 198–205.
- Riyaz, S., Naidu, A., and Dubey, P. K. (2011). L-Proline-Catalyzed Synthesis of Novel 5-(1H-Indol-3-Yl-Methylene)-Thiazolidine-2, 4-Dione Derivatives as Potential Antihyperglycemic Agents. *Synth. Commun.* 41 (18), 2756–2762. doi:10.1080/00397911.2010.515352
- Roussaki, M., Kontogiorgis, C. A., Hadjipavlou-Litina, D., Hamilakis, S., and Detsi, A. (2010). A Novel Synthesis of 3-Aryl Coumarins and Evaluation of Their Antioxidant and Lipoxigenase Inhibitory Activity. *Bioorg. Med. Chem. Lett.* 20, 3889–3892. doi:10.1016/j.bmcl.2010.05.022
- Roussaki, M., Zelianais, K., Kavetsou, E., Hamilakis, S., Hadjipavlou-Litina, D., Kontogiorgis, C., et al. (2014). Structural Modifications of Coumarin Derivatives: Determination of Antioxidant and Lipoxigenase (LOX) Inhibitory Activity. *Bioorg. Med. Chem.* 22, 6586–6594. doi:10.1016/j.bmc.2014.10.008
- Sadeghian, H., and Jabbari, A. (2016). 15-Lipoxigenase Inhibitors: A Patent Review. *Expert Opin. Ther. Pat.* 26 (1), 65–88. doi:10.1517/13543776.2016.1113259
- Sadik, C. D., Sies, H., and Schewe, T. (2003). Inhibition of 15-Lipoxigenases by Flavonoids: Structure-Activity Relations and Mode of Action. *Biochem. Pharmacol.* 65, 773–781. doi:10.1016/S0006-2952(02)01621-0
- Schuur, J. H., Selzer, P., and Gasteiger, J. (1996). The Coding of the Three-Dimensional Structure of Molecules by Molecular Transforms and its Application to Structure-Spectra Correlations and Studies of Biological Activity. *J. Chem. Inf. Comput. Sci.* 36, 334–344. doi:10.1021/ci950164c
- Shalaby, A., and Shanab, S. M. (2013). Antioxidant Compounds, Assays of Determination and Mode of Action. *Afr. J. Pharm. Pharmacol.* 7 (10), 528–539. doi:10.5897/ajpp2013.3474
- Shelke, K. F., Sapkal, S. B., Kakade, G. K., Sadaphal, S. A., Shingate, B. B., and Shingate, M. S. (2010). Alum Catalyzed Simple and Efficient Synthesis of 5-Arylidene-2, 4-Thiazolidinedione in Aqueous Media. *Green Chem. Lett. Rev.* 3 (1), 17–21. doi:10.1080/17518250903478345
- Skrzypczak-Jankun, E., Borbulevych, O. Y., and Jankun, J. (2004). Soybean Lipoxigenase-3 in Complex with 4-Nitrocatechol. *Acta Crystallogr. D. Biol. Cryst.* 60, 613–615. doi:10.1107/S0907444904000861
- Skrzypczak-Jankun, E., Zhou, K., and Jankun, J. (2003a). Inhibition of Lipoxigenase by (-)-Epigallocatechin Gallate: X-Ray Analysis at 2.1 Å Reveals Degradation of EGCG and Shows Soybean LOX-3 Complex with EGC Instead. *Int. J. Mol. Med.* 12, 415–422. doi:10.3892/ijmm.12.4.415
- Skrzypczak-Jankun, E., Zhou, K., McCabe, N., Selman, S., and Jankun, J. (2003b). Structure of Curcumin in Complex with Lipoxigenase and its Significance in Cancer. *Int. J. Mol. Med.* 12, 17–24. doi:10.3892/ijmm.12.1.17
- Stewart, J. J. P. (1989). Optimization of Parameters for Semiempirical Methods I. Method. *J. Comput. Chem.* 10, 29–220. doi:10.1002/jcc.540100208
- Todeschini, R., and Gramatica, P. (1997). 3D-Modelling and Prediction by WHIM Descriptors. Part 6. Application of WHIM Descriptors in QSAR Studies. *Quant. Struct.-Act. Relat.* 16, 120–125. doi:10.1002/qsar.19970160204
- Torres, R., Mascayano, C., Núñez, C., Modak, B., and Faini, F. (2013). Coumarins of *Haplopappus Multifolius* and Derivative as Inhibitors of Lox: Evaluation *In-Vitro* and Docking Studies. *J. Chil. Chem. Soc.* 58 (4), 2027–2030. doi:10.4067/S0717-97072013000400027
- Tsolaki, E., Eleftheriou, P., Kartsev, V., Geronikaki, A., and Saxena, A. K. (2018). Application of Docking Analysis in the Prediction and Biological Evaluation of the Lipoxigenase Inhibitory Action of Thiazolyl Derivatives of Mycophenolic Acid. *Molecules* 23, 1621. doi:10.3390/molecules23071621
- Veerasamy, R., Rajak, H., Jain, A., Sivadasan, S., Varghese, C. P., and Kishore, R. (2011). Validation of QSAR Models - Strategies and Importance. *Int. J. Drug Discov.* 2 (3), 511–519.
- Youssef, A. M., Sydney White, M., Villanueva, E. B., El-Ashmawy, I. M., and Klegeris, A. (2010). Synthesis and Biological Evaluation of Novel Pyrazolyl-2, 4-Thiazolidinediones as Anti-Inflammatory and Neuroprotective Agents. *Bioorg. Med. Chem.* 18 (5), 2019–2028. doi:10.1016/j.bmc.2010.01.021



Zhang, Q., Vigier, K. D. O., Royer, S., and Jérôme, F. (2012). Deep Eutectic Solvents: Syntheses, Properties and Applications. *Chem. Soc. Rev.* 41 (21), 7108–7146. doi:10.1039/c2cs35178a

**Conflict of Interest:** The authors declare that the research was conducted in the absence of any commercial or financial relationships that could be construed as a potential conflict of interest.

**Publisher's Note:** All claims expressed in this article are solely those of the authors and do not necessarily represent those of their affiliated organizations, or those of

the publisher, the editors, and the reviewers. Any product that may be evaluated in this article, or claim that may be made by its manufacturer, is not guaranteed or endorsed by the publisher.

Copyright © 2022 Lončarić, Strelec, Pavić, Rastija, Karnaš and Molnar. This is an open-access article distributed under the terms of the Creative Commons Attribution License (CC BY). The use, distribution or reproduction in other forums is permitted, provided the original author(s) and the copyright owner(s) are credited and that the original publication in this journal is cited, in accordance with accepted academic practice. No use, distribution or reproduction is permitted which does not comply with these terms.





## OPEN ACCESS

## EDITED BY

Maria Luisa Di Gioia,  
University of Calabria, Italy

## REVIEWED BY

Guocai Tian,  
Kunming University of Science and  
Technology, China  
Hector Quinteros-Lama,  
University of Talca, Chile  
Ilya Polishuk,  
Ariel University, Israel

## \*CORRESPONDENCE

Sona Raeissi,  
raeissi@shirazu.ac.ir

## SPECIALTY SECTION

This article was submitted to Green and  
Sustainable Chemistry,  
a section of the journal  
Frontiers in Chemistry

RECEIVED 31 March 2022

ACCEPTED 04 July 2022

PUBLISHED 09 August 2022

## CITATION

Parvaneh K, Haghighbakhsh R, Duarte ARC  
and Raeissi S (2022), Investigation of  
carbon dioxide solubility in various  
families of deep eutectic solvents by the  
PC-SAFT EoS.  
*Front. Chem.* 10:909485.  
doi: 10.3389/fchem.2022.909485

## COPYRIGHT

© 2022 Parvaneh, Haghighbakhsh, Duarte  
and Raeissi. This is an open-access  
article distributed under the terms of the  
Creative Commons Attribution License  
(CC BY). The use, distribution or  
reproduction in other forums is  
permitted, provided the original  
author(s) and the copyright owner(s) are  
credited and that the original  
publication in this journal is cited, in  
accordance with accepted academic  
practice. No use, distribution or  
reproduction is permitted which does  
not comply with these terms.

# Investigation of carbon dioxide solubility in various families of deep eutectic solvents by the PC-SAFT EoS

Khalil Parvaneh<sup>1</sup>, Reza Haghighbakhsh<sup>2,3</sup>, Ana Rita C. Duarte<sup>3</sup> and Sona Raeissi<sup>4\*</sup>

<sup>1</sup>Department of Chemical Engineering, University of Gonabad, Gonabad, Iran, <sup>2</sup>Department of Chemical Engineering, Faculty of Engineering, University of Isfahan, Isfahan, Iran, <sup>3</sup>LAQV, REQUIMTE, Departamento de Química da Faculdade de Ciências e Tecnologia, Universidade Nova de Lisboa, Caparica, Portugal, <sup>4</sup>School of Chemical and Petroleum Engineering, Shiraz University, Shiraz, Iran

Having been introduced in 2003, Deep Eutectic Solvents (DESs) make up a most recent category of green solvents. Due to their unique characteristics, and also their tunable physical properties, DESs have shown high potentials for use in various applications. One of the investigated applications is CO<sub>2</sub> absorption. The thermodynamic modeling of CO<sub>2</sub> solubility in DESs has been pursued by a number of researchers to estimate the capacity and capability of DESs for such tasks. Among the advanced equations of state (EoSs), the Perturbed Chain-Statistical Associating Fluid Theory (PC-SAFT) is a well-known EoS. In this study, the performance of the PC-SAFT EoS for estimating CO<sub>2</sub> solubility in various DESs, within wide ranges of temperatures and pressures, was investigated. A large data bank, including 2542 CO<sub>2</sub> solubility data in 109 various-natured DESs was developed and used for this study. This is currently the most comprehensive study in the open literature on CO<sub>2</sub> solubility in DESs using an EoS. For modeling, the DES was considered as a pseudo-component with a 2B association scheme. CO<sub>2</sub> was considered as both an inert and a 2B-component and the results of each association scheme were compared. Considering the very challenging task of modeling a complex hydrogen bonding mixture with gases, the results of AARD% being lower than 10% for both of the investigated association schemes of CO<sub>2</sub>, showed that PC-SAFT is a suitable model for estimating CO<sub>2</sub> solubilities in various DESs. Also, by proposing generalized correlations to predict the PC-SAFT parameters, covering different families of DESs, the developed model provides a global technique to estimate CO<sub>2</sub> solubilities in new and upcoming DESs, avoiding the necessity of further experimental work. This can be most valuable for screening and feasibility studies to select potential DESs from the innumerable options available.

## KEYWORDS

association schemes, DES (deep eutectic solvents), CO<sub>2</sub>, vapor-liquid equilibria (VLE), phase behavior

## Introduction

Global warming is one of the most important issues of this century. Since 1980, an increase of about 0.6°C in the mean temperature of the globe (both the northern and southern hemispheres) has been reported (Florides and Christodoulides, 2009). The emissions of greenhouse gases, such as carbon dioxide, methane, and nitrous oxide into the atmosphere have their impact on this environmental crisis. Among the greenhouse gases, CO<sub>2</sub> plays a major role (Yamasaki, 2003; Florides and Christodoulides, 2009; Ali et al., 2014). Over the past decades, the concentration of carbon dioxide in the atmosphere has increased, partly because of industrial activities. Particularly, the burning of fossil fuels such as natural gas, petroleum, and coal in various industries causes CO<sub>2</sub> emissions (Yamasaki, 2003; Li et al., 2019). Therefore, the absorption of this gas is a serious concern (Mulia et al., 2017). One of the commonly used methods is absorption by conventional solvents. However, most conventional solvents are not sustainable and have, themselves, caused environmental damage in the recent decades. Finding sustainable and environmentally-friendly solvents, which have the desired properties for CO<sub>2</sub> absorption, is vital. In this respect, Deep Eutectic Solvents (DESs) are recently proposed green solvents which have also been investigated by researchers for CO<sub>2</sub> absorption (Abbott et al., 2003; Koel, 2005; Wells and Coombe, 2006; Hasib-ur-Rahman et al., 2010; Vega et al., 2010; Haghighbakhsh et al., 2019).

A DES is a mixture, consisting of at least two components that have the ability to establish new hydrogen bonds between the constituents. They are usually created by mixing a hydrogen bond acceptor (HBA), commonly a quaternary ammonium or phosphonium salt, and a hydrogen bond donor (HBD), such as metal salts or organic acids. DESs possess a number of desirable properties, such as having low vapor pressure, as well as being task-specific, easy to synthesize, cheap, non-flammable, sustainable, and biodegradable (Smith et al., 2014; Altamash et al., 2017; Ma et al., 2017; Haghighbakhsh et al., 2019; Haider et al., 2020; Khajeh et al., 2020).

These interesting properties have led to significant investigations on DESs in various fields. Researchers have studied DES applications covering, for example, nanotechnology (Smith et al., 2014), gas absorption (Mirza et al., 2017; Marcus, 2018; Li et al., 2019), catalytic reactions (Ilgen et al., 2009), purification of biodiesels (Abbott et al., 2007), biomass treatment (Xia et al., 2014) electrochemistry (Abbott et al., 2011), and drug solubilization (Morrison et al., 2009).

Regarding the field of gas absorption, up to now, researchers have focused on the absorption of CO<sub>2</sub> more than on other gases. Various DESs, having different chemical natures, have been considered for CO<sub>2</sub> absorption, and wide ranges of pressures and temperatures have been studied (Li et al., 2008; Zhang et al., 2012; Leron and Li, 2013a; Leron and Li, 2013b; Francisco et al., 2013; Leron et al., 2013; Chen et al., 2014; Li et al., 2014; Zubeir

et al., 2014; Lu et al., 2015; Mirza et al., 2015; Deng et al., 2016; Ji et al., 2016; Zubeir et al., 2016; Altamash et al., 2017; Ghaedi et al., 2017; Liu et al., 2017; Sarmad et al., 2017; Altamash et al., 2018; Haider et al., 2018; Li et al., 2018; Zubeir et al., 2018; Liu et al., 2019; Wang et al., 2019). These studies have accumulated a data bank for CO<sub>2</sub> absorption by DESs, providing vital information for pilot or industrial planning. Although many DESs have been investigated, their number is insignificant compared to the number of DESs remaining uninvestigated. There are countless DESs and they differ greatly in nature and variation. But the experimentation process is time-consuming and entails high expenses, and so, investigating CO<sub>2</sub> solubility for all is not possible. Therefore, developing global thermodynamic models for the estimation of CO<sub>2</sub> solubility in various DESs is a recommended procedure to overcome the mentioned limitations.

Besides, since DESs have been introduced only recently, few thermodynamic models have been investigated for their phase behavior with CO<sub>2</sub> (Florides and Christodoulides, 2009; Zubeir et al., 2014; Mirza et al., 2015; Zubeir et al., 2016; Animasahun et al., 2017; Dietz et al., 2017; Haghighbakhsh and Raeissi, 2017; Lloret et al., 2017). Simple cubic equations of state (EoSs), such as the Peng–Robinson (PR) and modified Peng–Robinson have been considered by some researchers (Florides and Christodoulides, 2009; Zubeir et al., 2014; Mirza et al., 2015). In these studies, a DES was considered as a pseudo-pure compound whose critical properties were calculated using a group-contribution procedure, namely, the modified Lydersen–Joback–Reid model (Joback and Reid, 1987). To achieve more reliable results, some researchers considered more complex models. Haghighbakhsh and Raeissi (2017) used the cubic plus association (CPA) equation of state to model the solubility of CO<sub>2</sub> in various DESs. They also investigated different association schemes of CO<sub>2</sub> and found that the inert scheme, with fewer fitting parameters, is the most accurate. Lloret et al. (2017) applied the Soft-SAFT (Soft-Statistical Associating Fluid Theory) EoS, to describe the density, surface tension, viscosity, and phase behavior of CO<sub>2</sub> with several tetraalkylammonium chloride-based DESs. They explored the two approaches of either describing the DESs as pseudo-compounds or treating them as combinations of their two independent constituents of HBA and HBD. Further, the effort was made to model CO<sub>2</sub> solubility in DES systems using the PC-SAFT (Perturbed Chain-Statistical Associating Fluid Theory) EoS, as a well-known version of the SAFT type family (Zubeir et al., 2016; Dietz et al., 2017; Animasahun et al., 2017; Aminian, 2021; Cea-Klapp et al., 2020). For the first time, Zubeir et al. (2016) used the PC-SAFT to peruse the phase behavior of a few DES + CO<sub>2</sub> mixtures at a temperature range between 298.15 and 318.15 K and pressures up to 2 MPa. They presented two strategies for calculating CO<sub>2</sub> + DES phase behavior, where the DES was either considered as a pseudo-pure component, in which the pure parameters were

calculated based on density data, or it was treated as two individual components (HBA and HBD). Dietz et al. (2017) applied the pseudo-pure approach for PC-SAFT modeling of CO<sub>2</sub> phase behavior for a few hydrophobic DESs, and reported reliable results with respect to the experimental data. Animasahun et al. (2017) also used the PC-SAFT, as well as two different cubic EoSs (Peng–Robinson and Soave-Redlich-Kwong) to estimate CO<sub>2</sub> solubilities in some DESs. They investigated 20 different CO<sub>2</sub> + DES systems, in which choline chloride was considered as the HBA in 16 of the systems. Only the association scheme of 2B was considered for carbon dioxide. Further, Aminian (Aminian, 2021) studied the phase behavior of systems containing ionic liquids (ILs) and DESs using the PC-SAFT EoS. Their investigated DESs were based on tetrabutylammonium chloride and tetrabutylammonium bromide (as the HBA), and levulinic acid and diethylene glycol (as the HBD) at two different molar ratios. Their phase equilibrium results by PC-SAFT were compared to the COSMO-RS model. Cea-Klapp et al. (2020) also applied the PC-SAFT EoS for calculating the phase equilibria of DES systems. By using temperature-dependent binary interaction parameters, they succeeded to present more reliable results, especially in the case of liquid-liquid equilibria in ternary systems.

Despite the advancements in DES modeling, there is still the need for further studies to improve the phase behavior modelling of such complex hydrogen-bonding components with CO<sub>2</sub>. In this study, the largest and most comprehensive data bank of CO<sub>2</sub> solubility in various families of DESs was developed, which is much more extended and generalized than any previous study. The experimental densities of DESs are used to optimize the pure PC-SAFT parameters of the DESs with different chemical natures. The phase behavior of carbon dioxide with various DESs is then modelled with the PC-SAFT EoS over wide ranges of pressures and temperatures. Two feasible association schemes of inert and 2B are considered for carbon dioxide, which has not yet been investigated for the PC-SAFT EoS. Furthermore, to make the model predictive, and so, suitable for feasibility and screening studies on DESs for carbon capture applications, generalized correlations are proposed for estimation of the PC-SAFT parameters.

## Theoretical background

### The perturbed-chain SAFT (PC-SAFT) equation of state

Gross and Sadowski (Gross and Sadowski, 2001; Gross and Sadowski, 2002) proposed the PC-SAFT equation of state based on the combination of different terms of the reduced Helmholtz energy. These terms are the reduced residual Helmholtz energy ( $\tilde{a}^{res}$ ), the reduced hard-chain Helmholtz energy ( $\tilde{a}^{hc}$ ), the

reduced dispersion Helmholtz energy ( $\tilde{a}^{disp}$ ), and the reduced associating contribution Helmholtz energy ( $\tilde{a}^{assoc}$ ), which is presented as follows.

$$\tilde{a}^{res} = \tilde{a}^{hc} + \tilde{a}^{disp} + \tilde{a}^{assoc} \quad (1)$$

The reduced hard-chain Helmholtz energy is expressed through (Eqs 2–(4)) (Gross and Sadowski, 2001; Gross and Sadowski, 2002; Parvaneh and Shariati, 2017; Haghbakhsh et al., 2018a; Haghbakhsh et al., 2018b).

$$\tilde{a}^{hc} = \bar{m}\tilde{a}^{hs} - \sum_i x_i (m_i - 1) \ln g_{ii}^{hs} \quad (2)$$

$$\tilde{a}^{hs} = \frac{1}{\zeta_0} \left[ \frac{3\zeta_1\zeta_2}{1-\zeta_3} + \frac{\zeta_2^3}{\zeta_3(1-\zeta_3)^2} + \left( \frac{\zeta_2^3}{\zeta_3^2} - \zeta_0 \right) \ln(1-\zeta_3) \right] \quad (3)$$

$$g_{ij}^{hs} = \frac{1}{1-\zeta_3} + \frac{d_i d_j}{d_i + d_j} \frac{3\zeta_2}{(1-\zeta_3)^2} + \left( \frac{d_i d_j}{d_i + d_j} \right)^2 \frac{2\zeta_2^2}{(1-\zeta_3)^3} \quad (4)$$

where  $\tilde{a}^{hs}$ ,  $m_i$ ,  $x_i$ , and  $g_{ij}^{hs}$  are the reduced Helmholtz energy of the hard sphere, the number of segments, chain mole fraction, and radial pair distribution function, respectively.  $d_i$  is the temperature-dependent hard segment diameter for component  $i$ , which is calculated using the following equations (Gross and Sadowski, 2001; Gross and Sadowski, 2002; Parvaneh and Shariati, 2017; Haghbakhsh et al., 2018a; Haghbakhsh et al., 2018b).

$$d_i = \sigma_i \left[ 1 - 0.12 \exp \left( - \frac{3\varepsilon_i}{k_B T} \right) \right] \quad (5)$$

$$\zeta_n = \frac{\pi}{6} \rho \sum_i x_i m_i d_i^n \quad n \in \{0, 1, 2, 3\} \quad (6)$$

where  $m_i$  (number of the segment),  $\sigma_i$  (segment diameter), and  $\varepsilon_i/k_B$  (segment energy) are the pure component parameters that should be optimized based on experimental data.

The functionality of the dispersion ( $\tilde{a}^{disp}$ ) and associating ( $\tilde{a}^{assoc}$ ) contributions are given through the following equations (Gross and Sadowski, 2001; Gross and Sadowski, 2002; Parvaneh and Shariati, 2017; Haghbakhsh et al., 2018a; Haghbakhsh et al., 2018b).

$$\tilde{a}^{disp} = -2\pi\rho I_1 \overline{m^2 \varepsilon \sigma^3} - \pi\rho \bar{m} C_1 I_2 \overline{m^2 \varepsilon^2 \sigma^3} \quad (7)$$

$$\tilde{a}^{assoc} = \sum_i x_i \sum_{A_i} \left( \ln X^{A_i} - \frac{X^{A_i}}{2} + \frac{M_i}{2} \right) \quad (8)$$

$$X^{A_i} = \left( 1 + \rho \sum_j x_j \sum_{B_j} X^{B_j} \Delta^{A_i B_j} \right)^{-1} \quad (9)$$

$$\Delta^{A_i B_j} = g_{ij}^{seg} \kappa^{A_i B_j} \sigma_{ij}^3 \left( \exp \left( \frac{\varepsilon^{A_i B_j}}{kT} \right) - 1 \right) \quad (10)$$

where  $X^{A_i}$ ,  $M_i$ , and  $\Delta^{A_i B_j}$  are the mole fraction of component  $i$  that is not bonded at site  $A$ , the number of association sites, and the association strength, respectively. In addition to  $m_i$ ,  $\sigma_i$ , and  $\varepsilon_i/k_B$ , the effective association volume ( $\kappa^{A_i B_i}$ ) and association energy

TABLE 1 The values of optimized PC-SAFT parameters for the investigated DESs in this study and carbon dioxide<sup>b</sup>.

Abbr.	$m_i$	$\sigma_i$ (Å)	$\varepsilon_i/k$ (K)	AARD %
DES1	3.6803	3.6018	420.74	0.26
DES2	9.4497	2.6755	309.65	0.28
DES3	8.9837	2.7142	327.52	0.23
DES4	7.0125	2.9335	340.12	0.23
DES5	10.3775	2.4586	343.99	0.44
DES6	9.3189	2.4892	336.29	0.4
DES7	8.7806	2.4332	339.50	0.53
DES8	9.7048	2.6265	318.15	0.09
DES9	3.2933	3.1822	381.91	0.15
DES10	3.4444	3.2491	355.21	0.17
DES11	3.4128	3.8870	335.16	0.05
DES12	3.4170	3.6864	358.76	0.02
DES13	3.3869	3.6223	354.27	0.03
DES14	3.5068	3.8034	332.58	0.06
DES15	3.4600	3.6919	332.86	0.13
DES16	3.5507	4.1042	327.82	0.05
DES17	3.5021	3.9730	327.72	0.02
DES18	3.4751	3.9429	332.31	0.03
DES19	7.5169	2.7308	359.28	0.69 <sup>a</sup>
DES20	6.9359	2.8935	349.74	0.67 <sup>a</sup>
DES21	7.1671	2.8281	342.91	0.59 <sup>a</sup>
DES22	6.6122	2.8056	380.24	0.57 <sup>a</sup>
DES23	5.7468	3.04907	407.43	0.63 <sup>a</sup>
DES24	3.1064	3.4753	387.70	0.15
DES25	3.4218	3.4959	395.86	0.12
DES26	3.3837	3.3711	348.92	0.05
DES27	4.3270	3.0785	350.00	0.11
DES28	4.3312	3.2648	391.45	0.17
DES29	3.6904	3.4178	390.63	0.17
DES30	4.6418	3.2047	393.62	0.10
DES31	5.3061	3.0173	332.52	0.10
DES32	6.6024	3.1179	348.71	0.70 <sup>a</sup>
DES33	7.8434	2.6487	356.71	0.66 <sup>a</sup>
DES34	6.3107	2.9103	345.30	0.30
DES35	4.6314	3.2144	361.14	0.22
DES36	3.7883	3.1277	320.39	0.30
DES37	6.2709	3.1457	368.99	0.69 <sup>a</sup>
DES38	8.4619	2.5881	345.22	0.14
DES39	7.5213	2.6746	347.78	0.08
DES40	6.7674	2.7601	354.09	0.07
DES41	5.3496	2.9241	310.00	0.42
DES42	9.1060	2.6631	351.98	0.21
DES43	7.0991	2.8825	352.35	0.08
DES44	5.5588	3.1125	341.30	0.08
DES45	6.1204	2.9585	396.20	0.60 <sup>a</sup>
DES46	5.1851	2.9327	284.13	0.62
DES47	5.4774	3.0834	323.72	0.10
DES48	3.7486	3.4475	291.86	0.08
DES49	3.0017	3.6851	280.52	0.09
DES50	6.3275	3.0243	377.26	0.66 <sup>a</sup>
DES51	7.1170	2.8502	347.81	0.62 <sup>a</sup>
DES52	7.1606	2.845	355.33	0.62 <sup>a</sup>
DES53	6.3374	2.8215	257.25	0.24

(Continued on following page)

TABLE 1 (Continued) The values of optimized PC-SAFT parameters for the investigated DESs in this study and carbon dioxide<sup>b</sup>.

Abbr.	$m_i$	$\sigma_i$ (Å)	$\epsilon_i/k$ (K)	AARD %
DES54	5.3589	2.9327	241.00	0.26
DES55	5.1909	2.9327	229.25	0.24
DES56	9.0710	2.8000	330.58	0.15
DES57	8.7878	2.8324	317.32	0.24
DES58	3.4365	3.2789	353.06	0.49 <sup>a</sup>
DES59	3.3586	3.1858	360.18	0.27
DES60	3.3674	3.1902	383.90	0.68 <sup>a</sup>
DES61	10.5724	2.5122	323.10	0.15
DES62	10.5806	2.5346	362.07	0.17
DES63	10.5485	2.5390	361.91	0.19
DES64	11.0243	3.3621	304.89	0.07
DES65	11.0359	3.3701	305.57	0.07
DES66	6.3126	3.0152	372.90	0.64 <sup>a</sup>
DES67	6.0238	2.9766	358.31	0.61 <sup>a</sup>
DES68	6.8842	2.9122	387.74	0.24
DES69	9.5777	2.6250	347.43	0.26
DES70	6.7541	3.2009	342.42	0.67 <sup>a</sup>
DES71	6.3977	3.1206	378.56	0.54 <sup>a</sup>
DES72	7.8481	3.5327	337.11	0.06
DES73	11.7300	2.6760	303.76	Zubeir et al. (2016)
DES74	10.5328	2.6760	338.00	Zubeir et al. (2016)
DES75	8.7261	2.9327	266.40	0.08
DES76	8.9204	2.8600	330.34	0.61 <sup>a</sup>
DES77	7.2637	3.0673	366.66	0.60 <sup>a</sup>
DES78	6.8383	2.9416	341.56	0.60 <sup>a</sup>
DES79	6.4777	2.9094	387.90	0.60 <sup>a</sup>
DES80	6.1411	3.0882	357.80	0.61 <sup>a</sup>
DES81	9.5816	2.9376	321.28	0.65 <sup>a</sup>
DES82	8.3764	2.9603	339.72	0.64 <sup>a</sup>
DES83	7.2833	3.0302	357.95	0.63 <sup>a</sup>
DES84	6.4463	2.7725	356.45	0.58 <sup>a</sup>
DES85	6.4289	2.7432	382.36	0.58 <sup>a</sup>
DES86	8.6644	2.9327	252.88	0.14
DES87	3.9823	3.7122	365.60	0.02
DES88	4.0299	3.7590	364.79	0.06
DES89	8.0400	2.5831	329.75	0.57 <sup>a</sup>
DES90	7.2645	2.5935	365.81	0.56 <sup>a</sup>
DES91	3.2607	3.7539	599.88	Zubeir et al. (2016)
DES92	5.5147	3.1379	280.15	0.10
DES93	8.8536	2.8989	344.45	0.60 <sup>a</sup>
DES94	5.2004	3.2659	350.74	0.05
DES95	4.9495	2.7400	379.67	0.48 <sup>a</sup>
DES96	2.9824	3.5678	506.01	Zubeir et al. (2016)
DES97	15.4820	3.1583	317.42	Dietz et al. (2017)
DES98	14.8000	3.2400	382.09	Dietz et al. (2017)
DES99	15.3220	3.1533	307.11	Dietz et al. (2017)
DES100	7.2315	2.5414	359.78	0.58 <sup>a</sup>
DES101	6.1747	2.7751	352.67	0.55 <sup>b</sup>
DES102	5.8932	2.6729	340.80	0.56 <sup>a</sup>
DES103	6.5848	2.7365	369.45	0.53 <sup>a</sup>
DES104	6.2763	2.7635	364.94	0.55 <sup>a</sup>
DES105	6.8388	2.7936	353.41	0.63 <sup>a</sup>

(Continued on following page)



TABLE 1 (Continued) The values of optimized PC-SAFT parameters for the investigated DESs in this study and carbon dioxide<sup>b</sup>.

Abbr.	$m_i$	$\sigma_i$ (Å)	$\epsilon_i/k$ (K)	AARD %
DES106	6.2883	2.9043	396.64	0.60 <sup>a</sup>
DES107	6.7412	2.9691	359.07	0.60 <sup>a</sup>
DES108	3.7112	3.3667	404.08	0.29
DES109	8.9137	2.6324	335.54	0.10
CO <sub>2</sub> (inert)	2.0729	2.7852	169.21	Gross and Sadowski, (2001)
CO <sub>2</sub> (2B) <sup>c</sup>	2.1051	2.7841	162.08	Baramaki et al. (2019)

<sup>a</sup>Density data was obtained according to Haghbakhsh et al.'s density model (Haghbakhsh et al., 2019).

<sup>b</sup>The values of the ( $\kappa^{AiBj}$ ) and ( $\epsilon^{AiBj}/k$ ) parameters were considered as 0.1 and 5,000, respectively, for all of the investigated DESs (Zubeir et al., 2016; Dietz et al., 2017).

<sup>c</sup>The values of the ( $\kappa^{AiBj}$ ) and ( $\epsilon^{AiBj}/k$ ) parameters of CO<sub>2</sub> for the association schemes of 2B are 0.03318 and 576.7, respectively (Baramaki et al., 2019).

( $\epsilon^{AiBj}/k$ ) are also pure compound constants that must be considered for associating compounds.

## Investigated compounds

In this research, the largest data bank, up to date, of CO<sub>2</sub> solubility in DESs, consisting of 109 various natured DESs, was collected from the open literature. This data bank consists of 2,542 data points, covering wide ranges of pressures and temperatures. **Supplementary Table S1** (Supplementary Material) presents the pressure, temperature, and CO<sub>2</sub> solubility ranges of the investigated DESs in this study. The corresponding literature reference of each DESs is also given in **Supplementary Table S1** (Li et al., 2008; Leron and Li, 2013a; Leron and Li, 2013b; Francisco et al., 2013; Leron et al., 2013; Chen et al., 2014; Li et al., 2014; Zubeir et al., 2014; Lu et al., 2015; Mirza et al., 2015; Deng et al., 2016; Ji et al., 2016; Zubeir et al., 2016; Altamash et al., 2017; Ghaedi et al., 2017; Liu et al., 2017; Sarmad et al., 2017; Altamash et al., 2018; Haider et al., 2018; Li et al., 2018; Zubeir et al., 2018; Liu et al., 2019; Wang et al., 2019). In the case of those limited DESs for which solubility data were presented by more than one research group, no discriminations were carried out and all of the data by all groups were considered in the development of the model.

## Results and discussion

The pseudo-component approach was used for modeling CO<sub>2</sub> + DES systems, which is a well-known model having been used for various DESs (Zubeir et al., 2016; Dietz et al., 2017; Lloret et al., 2017). The association scheme of 2B, as presented by Huang and Radosz (Huang and Radosz, 1990; Huang and Radosz, 1991), was considered for the pseudo-component DESs. The reason for considering the pseudo-component approach, and also choosing the 2B association scheme for DESs is by following the recommendations of many published

studies (Zubeir et al., 2016; Haghbakhsh and Raeissi, 2017; Lloret et al., 2017; Dietz et al., 2017; Animasahun et al., 2017; Aminian, 2021; Cea-Klapp et al., 2020). Almost all of the literature that have used the PC-SAFT EoS for modeling of DESs, have recommended the 2B association scheme for a pseudo-component DES. The schematic representation of the considered association schemes of the investigated systems are presented as Figure S1 of the Supplementary Material. For CO<sub>2</sub>, the inert and 2B association schemes are the most commonly used association schemes in the literature, as indicated by the studies of Haghbakhsh and Raeissi, and also Baramaki et al. (Haghbakhsh and Raeissi, 2017; Baramaki et al., 2019). Therefore, we chose to investigate and compare both of these schemes in this study.

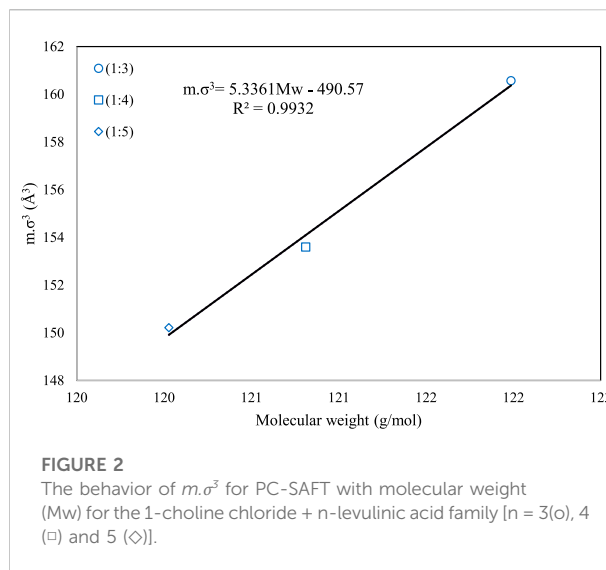
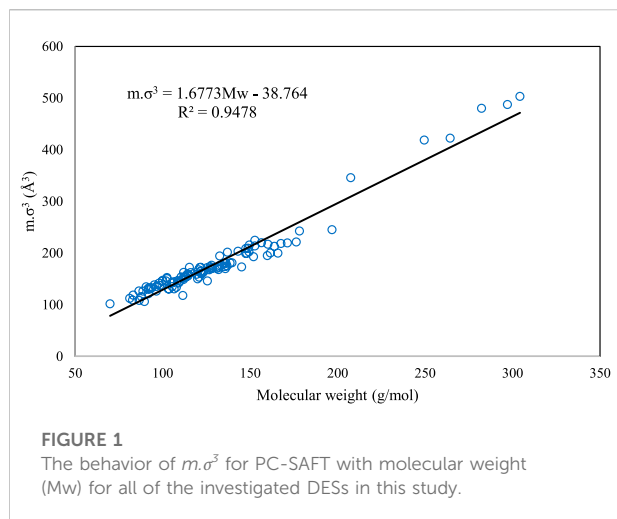
To model the phase behavior of CO<sub>2</sub> + DES systems, the first calculation step was to estimate the PC-SAFT pure parameters of  $m_i$  (segment number),  $\sigma_i$  (segment diameter),  $u_i/k$  (segment energy parameter),  $\kappa^{AiBj}$  (effective association volume), and  $\epsilon^{AiBj}/k$  (association energy). These five parameters are optimized to the liquid density data of the DESs based on Eq. (11) as the objective function.

$$OF = \sum_i^{Np} \left( \frac{\rho_i^{\text{exp}} - \rho_i^{\text{calc.}}}{\rho_i^{\text{exp}}} \right)^2 \quad (11)$$

in which,  $\rho_i^{\text{exp.}}$  and  $\rho_i^{\text{calc.}}$  are the experimental and calculated density, respectively, and  $Np$  is the number of the data points.

However, in order to reduce the number of adjustable parameters of the PC-SAFT EoS for DESs, the effective association volume ( $\kappa^{AiBj}$ ) and association energy ( $\epsilon^{AiBj}/k$ ) parameters were considered as 0.1 and 5,000, respectively (Zubeir et al., 2016; Dietz et al., 2017).

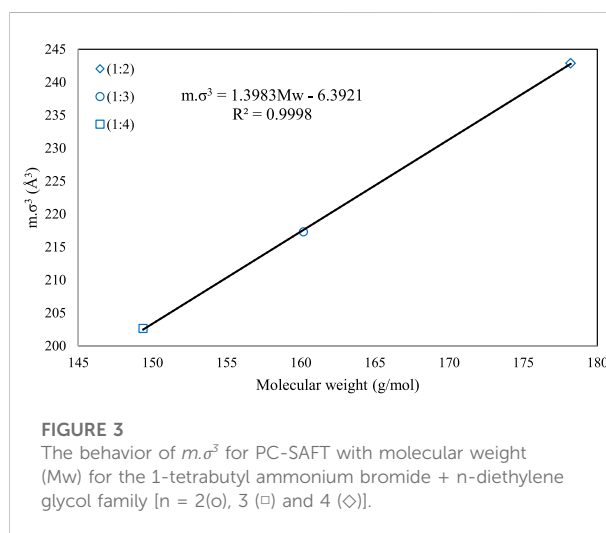
The number of literature density data for each DES, the range of liquid densities, and the corresponding reference are given in **Supplementary Table S2**. However, for some of the investigated DESs, no density data have been reported in the open literature. Thus, for those DESs, distinguished in **Supplementary Table S3**, the general density model of Haghbakhsh et al. (Haghbakhsh et al., 2019) was used to generate the density data. Haghbakhsh et al.'s density model (Haghbakhsh et al., 2019) is a function of



temperature, critical volume, critical temperature, and acentric factor of the DES pseudo-component. The modified Lydersen-Joback-Reid approach (Valderrama and Robles, 2007; Valderrama et al., 2008) and the Lee-Kesler mixing rules, which were presented by Knapp et al. (1982), were used to calculate the critical properties and acentric factors of the DESs that lacked density data. The results are presented in Supplementary Table S4 of the Supplementary material.

The three pure component parameters of PC-SAFT, optimized to the collected density data of the investigated DESs, are presented in Table 1. For some of the investigated DESs, the values of the PC-SAFT parameters were previously given in published studies, and in these cases, the literature values were considered, as reported in Table 1. For CO<sub>2</sub>, the values of the three pure component PC-SAFT parameters for both the association schemes of 2B and inert have been reported in the literature, and these values are also presented in Table 1. Furthermore, the effective association volume ( $\kappa^{AiBj}$ ) and association energy ( $\epsilon^{AiBj}/k$ ) parameters of CO<sub>2</sub> for the association schemes of 2B are 0.03318 and 576.7, respectively (Baramaki et al., 2019).

In order to check the consistency of the values of the calculated critical properties and the optimized PC-SAFT parameters for the investigated DESs, the thermodynamic evaluation of the global map of Polishuk et al. (2013) has been carried out. For this purpose, values for the reduced critical temperatures have been calculated according to Eq. (12). Since these values were calculated to be greater than 1 for all of the DESs, according to the thermodynamic analysis of Polishuk et al. (2013), no unrealistic values have been found for the calculated critical properties and optimized PC-SAFT parameters. The details of this evaluation are given in Supplementary Table S5 of the Supplementary Material.



$$T_c^* = \frac{T_c}{(\epsilon/k)} \quad (12)$$

Also, in order to have a more comprehensive investigation and provide predictive ability for the PC-SAFT model, a generalized correlation for the estimation of the PC-SAFT pure component parameters of the studied DESs was developed in this work, as presented by Eq. (13).

$$m\sigma^3 = 1.6773MW - 38.764 \quad (13)$$

where  $m$  is the segment number and  $\sigma$  is the segment diameter, which are related to the molecular weight, MW, of the DES. The graphical behavior of the developed generalized correlation for the studied DESs is depicted in Figure 1. In this figure, the relations of  $m\sigma^3$  of the PC-SAFT

TABLE 2 The values of optimized parameters and AARD% for the two predictive and correlative modes of PC-SAFT EoS by considering two association schemes for CO<sub>2</sub>.

	Inert (CO <sub>2</sub> )+ 2B (DES)				2B (CO <sub>2</sub> ) + 2B (DES)			
	Predictive	Correlative			Predictive	Correlative		
	$k_{ij} = 0$	$k_{ij}=a+b.T$			$k_{ij} = 0$	$k_{ij}=a+b.T$		
	AARD%	AARD%	a	b	AARD%	AARD%	a	b
DES1	91.22	44.48	0.00013	$1.53 \times 10^{-4}$	126.56	44.48	0.00015	$2.19 \times 10^{-4}$
DES2	64.98	1.61	-0.11915	$2.22 \times 10^{-4}$	55.74	1.57	-0.11216	$2.35 \times 10^{-4}$
DES3	74.24	1.87	-0.11839	$1.75 \times 10^{-4}$	67.35	1.85	-0.11027	$1.84 \times 10^{-4}$
DES4	47.11	1.62	-0.07758	$1.43 \times 10^{-4}$	30.64	1.57	-0.06605	$1.51 \times 10^{-4}$
DES5	96.54	7.35	-0.27373	$4.27 \times 10^{-4}$	95.75	7.37	-0.27141	$4.43 \times 10^{-4}$
DES6	94.78	4.50	-0.26806	$4.49 \times 10^{-4}$	93.38	4.56	-0.26533	$4.70 \times 10^{-4}$
DES7	97.22	8.75	-0.30329	$4.97 \times 10^{-4}$	96.40	8.85	-0.30089	$5.19 \times 10^{-4}$
DES8	84.25	3.03	-0.28205	$6.06 \times 10^{-4}$	80.35	3.07	-0.27692	$6.22 \times 10^{-4}$
DES9	50.18	15.13	0.18890	$-7.15 \times 10^{-4}$	23.12	15.10	0.21407	$-7.15 \times 10^{-4}$
DES10	35.17	16.54	0.22557	$-7.79 \times 10^{-4}$	27.00	17.02	0.25662	$-7.91 \times 10^{-4}$
DES11	15.97	12.60	0.01029	0	36.44	11.99	0.03583	0
DES12	14.13	9.89	-0.01059	0	18.28	9.17	0.01403	0
DES13	12.62	12.19	-0.00483	0	28.35	11.50	0.02027	0
DES14	23.36	8.22	0.00028	$6.12 \times 10^{-5}$	59.81	7.97	0.00017	$1.37 \times 10^{-4}$
DES15	10.69	4.84	0.02300	$-4.94 \times 10^{-5}$	46.84	4.78	0.04894	$-4.82 \times 10^{-5}$
DES16	29.48	10.83	0.03073	0	55.82	10.33	0.05537	0
DES17	40.11	8.17	0.03675	0	75.15	4.64	0.06205	0
DES18	58.86	11.08	0.04603	0	100.48	10.60	0.07128	0
DES19	89.24	9.00	-0.09664	0	85.68	8.62	-0.08488	0
DES20	47.49	46.35	0.01535	0	51.00	46.26	0.02943	0
DES21	75.08	5.62	-0.06410	0	66.55	5.43	-0.05068	0
DES22	92.91	21.23	-0.11819	0	90.35	20.76	-0.10513	0
DES23	90.59	17.11	-0.10412	0	87.14	16.58	-0.09010	0
DES24	27.27	13.94	0.22373	$-6.74 \times 10^{-4}$	69.48	13.93	0.25247	$-6.81 \times 10^{-4}$
DES25	14.51	10.08	0.23499	$-7.41 \times 10^{-4}$	31.66	10.15	0.27122	$-7.77 \times 10^{-4}$
DES26	242.5	6.73	0.00015	$2.53 \times 10^{-4}$	401.24	5.85	0.00017	$3.41 \times 10^{-4}$
DES27	41.47	3.69	-0.16969	$6.13 \times 10^{-4}$	105.49	3.63	-0.15445	$6.33 \times 10^{-4}$
DES28	46.44	2.35	-0.08064	$3.33 \times 10^{-4}$	105.76	2.38	-0.06356	$3.41 \times 10^{-4}$
DES29	175.43	3.72	0.00023	$2.00 \times 10^{-4}$	292.64	3.59	0.00466	$2.57 \times 10^{-4}$
DES30	10.77	2.37	0.01453	$-3.14 \times 10^{-5}$	54.45	2.35	0.03053	$-2.42 \times 10^{-5}$
DES31	7.95	2.54	-0.00028	$1.50 \times 10^{-5}$	50.52	2.51	0.00026	$7.44 \times 10^{-5}$
DES32	65.88	11.30	0.13579	$-6.05 \times 10^{-4}$	55.84	11.70	0.16771	$-6.54 \times 10^{-4}$
DES33	96.49	12.59	-0.14354	0	95.36	12.43	-0.13270	0
DES34	42.47	4.26	-0.16328	$4.35 \times 10^{-4}$	22.15	4.19	-0.15409	$4.55 \times 10^{-4}$
DES35	51.48	3.98	-0.10102	$4.04 \times 10^{-4}$	111.83	3.89	-0.08494	$4.16 \times 10^{-4}$
DES36	69.60	14.24	-0.20154	$7.22 \times 10^{-4}$	150.62	13.36	-0.17527	$7.21 \times 10^{-4}$
DES37	70.39	12.11	0.00014	$-1.99 \times 10^{-4}$	60.92	12.61	0.01277	$-1.88 \times 10^{-4}$
DES38	90.09	1.64	-0.19128	$2.78 \times 10^{-4}$	87.24	1.64	-0.18509	$2.92 \times 10^{-4}$
DES39	86.14	1.87	-0.17459	$2.60 \times 10^{-4}$	81.77	1.84	-0.16806	$2.77 \times 10^{-4}$
DES40	81.74	1.32	-0.13052	$1.52 \times 10^{-4}$	75.6	1.28	-0.12166	$1.67 \times 10^{-4}$
DES41	38.08	4.69	-0.25403	$6.93 \times 10^{-4}$	16.00	5.85	-0.21010	$6.25 \times 10^{-4}$
DES42	87.82	1.63	-0.20774	$3.74 \times 10^{-4}$	84.68	1.62	-0.20266	$3.88 \times 10^{-4}$

(Continued on following page)

TABLE 2 (Continued) The values of optimized parameters and AARD% for the two predictive and correlative modes of PC-SAFT EoS by considering two association schemes for CO<sub>2</sub>.

	Inert (CO <sub>2</sub> )+ 2B (DES)				2B (CO <sub>2</sub> ) + 2B (DES)			
	Predictive		Correlative		Predictive		Correlative	
	$k_{ij} = 0$		$k_{ij}=a+b.T$		$k_{ij} = 0$		$k_{ij}=a+b.T$	
	AARD%	AARD%	a	b	AARD%	AARD%	a	b
DES43	60.82	1.46	-0.12685	$2.59 \times 10^{-4}$	48.62	1.45	-0.11834	$2.75 \times 10^{-4}$
DES44	17.08	2.00	-0.06124	$2.28 \times 10^{-4}$	58.75	1.95	-0.04801	$2.43 \times 10^{-4}$
DES45	90.95	14.08	$1.07 \times 10^{-5}$	$-3.51 \times 10^{-4}$	87.80	14.17	0.03143	$-4.06 \times 10^{-4}$
DES46	92.22	1.95	-0.12822	$5.24 \times 10^{-4}$	173.20	2.12	-0.12631	$5.90 \times 10^{-4}$
DES47	8.23	2.17	-0.13986	$4.49 \times 10^{-4}$	41.11	2.13	-0.12790	$4.70 \times 10^{-4}$
DES48	183.48	2.90	-0.07176	$4.90 \times 10^{-4}$	291.85	2.91	-0.04673	$4.98 \times 10^{-4}$
DES49	268.21	1.56	-0.06274	$5.73 \times 10^{-4}$	408.56	1.51	-0.03684	$5.94 \times 10^{-4}$
DES50	80.55	16.73	-0.08185	$1.16 \times 10^{-6}$	74.09	17.04	-0.05477	$-3.92 \times 10^{-5}$
DES51	93.37	10.13	-0.13390	0	91.19	10.45	-0.12079	0
DES52	95.00	2.95	-0.14492	0	93.37	2.70	-0.13232	0
DES53	59.52	13.15	0.09203	$-1.99 \times 10^{-4}$	123.75	12.14	0.08996	$-1.24 \times 10^{-4}$
DES54	148.94	10.05	-0.03571	$3.35 \times 10^{-4}$	253.23	9.19	-0.01823	$3.59 \times 10^{-4}$
DES55	179.70	11.61	0.00036	$2.54 \times 10^{-4}$	298.03	10.60	0.00030	$3.45 \times 10^{-4}$
DES56	62.22	4.11	-0.18903	$4.56 \times 10^{-4}$	52.72	4.03	-0.18175	$4.68 \times 10^{-4}$
DES57	43.85	5.20	-0.15278	$3.96 \times 10^{-4}$	29.18	5.14	-0.14439	$4.08 \times 10^{-4}$
DES58	65.43	9.33	-0.06193	$3.09 \times 10^{-4}$	146.66	11.14	$1.35 \times 10^{-4}$	$2.06 \times 10^{-4}$
DES59	31.56	16.34	0.00023	$-6.22 \times 10^{-5}$	20.99	18.70	0.10159	$-2.87 \times 10^{-4}$
DES60	9.61	9.17	$5.31 \times 10^{-5}$	$-3.67 \times 10^{-6}$	45.95	10.70	$3.12 \times 10^{-4}$	$7.80 \times 10^{-5}$
DES61	91.19	1.83	-0.15568	$1.72 \times 10^{-4}$	89.07	1.86	-0.15005	$1.81 \times 10^{-4}$
DES62	97.44	1.42	-0.20506	$1.96 \times 10^{-4}$	96.89	1.38	-0.20029	$2.02 \times 10^{-4}$
DES63	97.47	1.05	-0.20657	$1.98 \times 10^{-4}$	96.92	1.06	-0.20309	$2.08 \times 10^{-4}$
DES64	39.39	0.98	-0.02250	$1.52 \times 10^{-4}$	59.71	0.98	-0.00839	$1.38 \times 10^{-4}$
DES65	38.21	1.47	0.00616	$5.60 \times 10^{-5}$	57.72	1.47	0.01427	$6.30 \times 10^{-5}$
DES66	44.22	30.06	-0.03073	0	34.47	29.77	-0.01633	0
DES67	77.22	28.16	-0.06353	0	68.69	27.76	-0.04826	0
DES68	73.02	9.81	-0.05605	0	64.25	9.98	-0.04362	0
DES69	78.22	39.33	-0.04963	0	72.55	39.23	-0.04048	0
DES70	125.55	45.05	0.07112	0	192.68	44.96	0.08641	0
DES71	67.71	4.10	-0.05765	0	57.26	3.72	-0.04374	0
DES72	41.75	1.00	-0.02222	$1.52 \times 10^{-4}$	68.61	1.17	-0.01099	$1.57 \times 10^{-4}$
DES73	74.86	2.56	-0.13172	$2.05 \times 10^{-4}$	69.74	2.32	-0.12671	$2.17 \times 10^{-4}$
DES74	89.89	2.33	-0.16478	$1.98 \times 10^{-4}$	87.67	2.08	-0.15906	$2.07 \times 10^{-4}$
DES75	15.98	2.77	-0.13366	$4.53 \times 10^{-4}$	44.26	2.78	-0.12424	$4.71 \times 10^{-4}$
DES76	69.09	10.47	-0.06013	0	60.87	10.34	-0.04888	0
DES77	40.12	4.27	-0.02607	0	23.16	4.17	-0.01340	0
DES78	45.95	4.68	-0.03197	0	26.96	4.61	-0.01747	0
DES79	81.79	1.70	-0.07782	0	75.60	1.58	-0.06490	0
DES80	67.29	9.38	-0.05996	0	56.25	9.26	-0.04474	0
DES81	40.80	12.19	-0.02841	0	27.18	12.11	-0.01752	0
DES82	61.42	9.00	-0.04933	0	51.33	8.89	-0.03764	0
DES83	71.14	3.85	-0.06241	0	62.79	3.78	-0.04975	0
DES84	95.41	14.63	-0.13818	0	93.64	14.61	-0.12323	0

(Continued on following page)

TABLE 2 (Continued) The values of optimized parameters and AARD% for the two predictive and correlative modes of PC-SAFT EoS by considering two association schemes for CO<sub>2</sub>.

	Inert (CO <sub>2</sub> )+ 2B (DES)				2B (CO <sub>2</sub> ) + 2B (DES)			
	Predictive		Correlative		Predictive		Correlative	
	$k_{ij} = 0$		$k_{ij}=a+b.T$		$k_{ij} = 0$		$k_{ij}=a+b.T$	
	AARD%	AARD%	a	b	AARD%	AARD%	a	b
DES85	98.21	13.43	-0.16905	0	97.53	13.69	-0.15537	0
DES86	45.79	1.75	-0.11529	$4.44 \times 10^{-4}$	82.85	1.77	-0.10450	$4.61 \times 10^{-4}$
DES87	17.84	7.31	$7.42 \times 10^{-5}$	$4.00 \times 10^{-5}$	52.84	7.08	0.00426	$9.32 \times 10^{-5}$
DES88	15.82	10.54	0.10802	$-3.10 \times 10^{-4}$	44.85	10.29	0.13815	$-3.39 \times 10^{-4}$
DES89	91.90	3.87	-0.10463	0	89.12	3.54	-0.09300	0
DES90	96.84	18.06	-0.13761	0	95.70	17.60	-0.12629	0
DES91	8.68	2.86	-0.04545	$1.58 \times 10^{-4}$	50.73	2.92	-0.03230	$1.70 \times 10^{-4}$
DES92	73.21	2.78	-0.09120	$4.09 \times 10^{-4}$	132.18	2.80	-0.07432	$4.23 \times 10^{-4}$
DES93	78.21	10.00	-0.07712	0	72.60	9.57	-0.06653	0
DES94	19.71	2.07	-0.10140	$3.56 \times 10^{-4}$	59.39	2.12	-0.08789	$3.71 \times 10^{-4}$
DES95	92.74	14.00	-0.11066	0	89.09	13.41	-0.09404	0
DES96	46.50	3.16	$3.20 \times 10^{-5}$	$6.47 \times 10^{-5}$	113.55	3.12	0.02309	$5.85 \times 10^{-5}$
DES97	27.87	0.59	-0.05763	$1.20 \times 10^{-4}$	21.06	0.62	-0.05198	$1.20 \times 10^{-4}$
DES98	72.06	1.83	-0.11720	$1.51 \times 10^{-4}$	69.84	2.03	-0.11460	$1.54 \times 10^{-4}$
DES99	17.67	0.70	-0.04276	$9.70 \times 10^{-5}$	9.53	0.58	-0.03989	$1.08 \times 10^{-4}$
DES100	98.39	4.34	-0.15918	0	97.79	4.26	-0.14756	0
DES101	89.66	7.78	-0.09991	0	85.44	7.94	-0.08463	0
DES102	97.06	20.36	-0.16026	0	95.72	21.77	-0.14326	0
DES103	92.33	10.77	-0.10894	0	89.43	10.33	-0.09581	0
DES104	90.17	13.43	-0.10066	0	86.31	13.51	-0.08664	0
DES105	55.88	23.02	-0.03057	0	40.09	22.88	-0.01694	0
DES106	83.20	5.12	-0.07731	0	77.19	5.11	-0.06412	0
DES107	64.43	3.60	-0.05155	0	52.60	3.75	-0.03774	0
DES108	21.75	5.60	0.01153	0	83.18	4.95	0.03643	0
DES109	87.83	2.98	-0.09378	0	84.13	2.20	-0.08230	0
Total	63.77	8.08			84.65	8.12		

EoS with respect to the molecular weight are shown for all 109 investigated DESs. As can be seen,  $m\sigma^3$  has an increasing behavior with increasing molecular weight. Despite the simplicity, this correlation succeeds to consider various DESs, having very different natures, with high accuracy.

Although the above correlation is global and can be used for all the DESs, we have also provided two family-specific correlations for higher accuracy. For the families of 1-choline chloride + n-levulinic acid ( $n = 3, 4, 5$ ) and 1-tetrabutyl ammonium bromide + n-diethylene glycol ( $n = 2, 3, 4$ ) specific correlations were developed and presented as Eqs (14), (15), respectively.

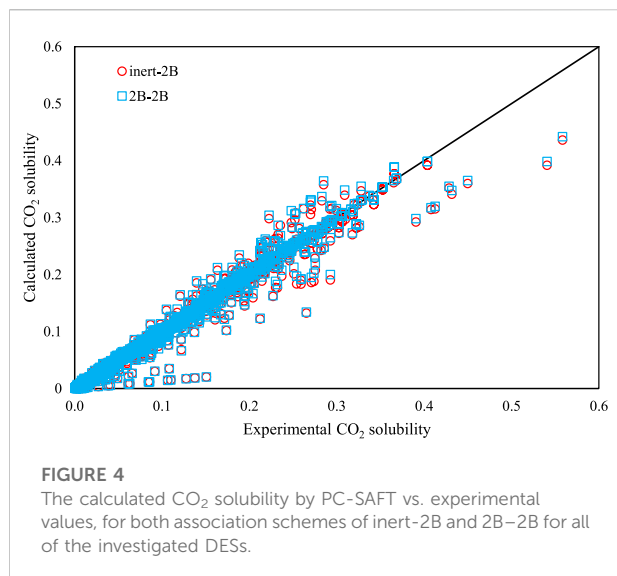
$$m\sigma^3 = 5.3361MW - 490.57 \quad (14)$$

$$m\sigma^3 = 1.3983MW - 6.3921 \quad (15)$$

Figures 2, 3 present the graphical behavior of these two specific family correlations with respect to molecular weight. As one would expect, one single generalized equation, correlated with only the molecular weight for all types of DESs with different natures and different molar ratios, is not as accurate (Figure 1) as the family-specific correlations, with constants that are fine-tuned to the particular structural family (Figures 2, 3).

Also, in order to investigate the predictive ability of the PC-SAFT model, CO<sub>2</sub> solubilities were calculated according to the two modes of prediction and correlation of PC-SAFT. In the prediction mode, the solubilities were achieved without considering any binary interaction parameters ( $k_{ij}$ ), while in





the correlation mode, binary interaction parameters were considered according to the following equation, with the purpose to correct the segment-segment interactions of dissimilar chains (Gross and Sadowski, 2001).

$$\varepsilon_{ij} = \sqrt{\varepsilon_i \varepsilon_j} (1 - k_{ij}) \quad (16)$$

To involve the effect of temperature on the binary interaction parameters, the temperature functionality of Eq. (17) was taken into account.

$$k_{ij} = a + b \times T \quad (17)$$

The two adjustable parameters ( $a$  and  $b$ ) were optimized based on the CO<sub>2</sub> solubility data in various DESs using the following objective function, and the values are reported in Table 2.

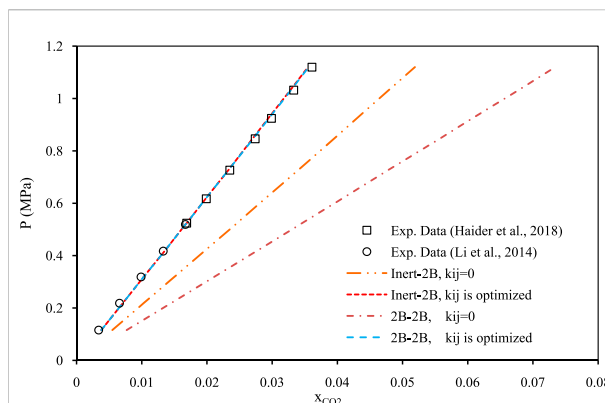
$$OF = \sum_i^{N_p} \left( \frac{x_i^{Exp.} - x_i^{Calc.}}{x_i^{Exp.}} \right)^2 \quad (18)$$

The results of PC-SAFT modeling for CO<sub>2</sub> solubilities in the investigated DESs were estimated and the errors were calculated by calculating AARD%, as given by Eq. (19).

$$AARD\% = \frac{100}{N_p} \sum_i^{N_p} \left| \frac{x_i^{Exp.} - x_i^{Calc.}}{x_i^{Exp.}} \right| \quad (19)$$

in which  $x_i^{Exp.}$  and  $x_i^{Calc.}$  are the experimental and calculated carbon dioxide solubilities, respectively, and  $N_p$  is the total number of data. Table 2 presents the calculated AARD% values for both the correlative and predictive modes, each also considering both the association schemes of 2B and inert for CO<sub>2</sub>.

Based on the results of Table 2 for CO<sub>2</sub> + DES, the predictive PC-SAFT EoS had a total AARD% of 63.77 and 84.65% for the inert-2B and 2B-2B modes, respectively. Therefore, on the average, the inert association scheme for CO<sub>2</sub> results in lower



AARD% than the 2B association scheme, most particularly, for DESs with choline chloride or tetrabutylphosphonium bromide as their HBA. However, for the majority of DESs whose pure PC-SAFT parameters were optimized based on the density data generated by Haghbakhsh et al.'s density model (Haghbakhsh et al., 2019), the results of the 2B association scheme had slightly lower AARD% values. But all in all, the results are not acceptable in these predictive modes of calculations. By considering adjusted binary interaction parameters, both of the association schemes improve significantly and produce acceptable errors. The inert-2B and 2B-2B cases resulted in total AARD% of 8.08% and 8.12%, respectively.

The trends between the calculated CO<sub>2</sub> solubility values by the PC-SAFT versus the corresponding experimental values are presented in Figure 4 for all of the investigated DESs, using both the association schemes of inert-2B and 2B-2B. A normal behavior is observed for the PC-SAFT by noticing that most of the results are located very close to the diagonal line. Also, this figure shows that the accuracy of PC-SAFT generally decreases in the region of high CO<sub>2</sub> absorption.

Figures 5–7 show pressure vs. CO<sub>2</sub> solubility for three random DESs at various temperatures. These three DESs are considered as representatives, applying the different methods of obtaining the pure PC-SAFT parameters. In Figure 5, the pure PC-SAFT parameters of choline chloride + diethylene glycol (1:4) were optimized based on its experimental density data, while in Figure 6, the pure PC-SAFT parameters of benzyltriethylammonium chloride (BTEAC) + acetic acid (1:2) were optimized based on the general density model of Haghbakhsh et al. (Haghbakhsh et al., 2019). Figure 7 represents the phase behavior of CO<sub>2</sub> with tetraethylammonium chloride (TEAC) + L-lactic acid (1:2), whose PC-SAFT parameters were taken from the literature. Figures 5–7 compare the trends of PC-SAFT-

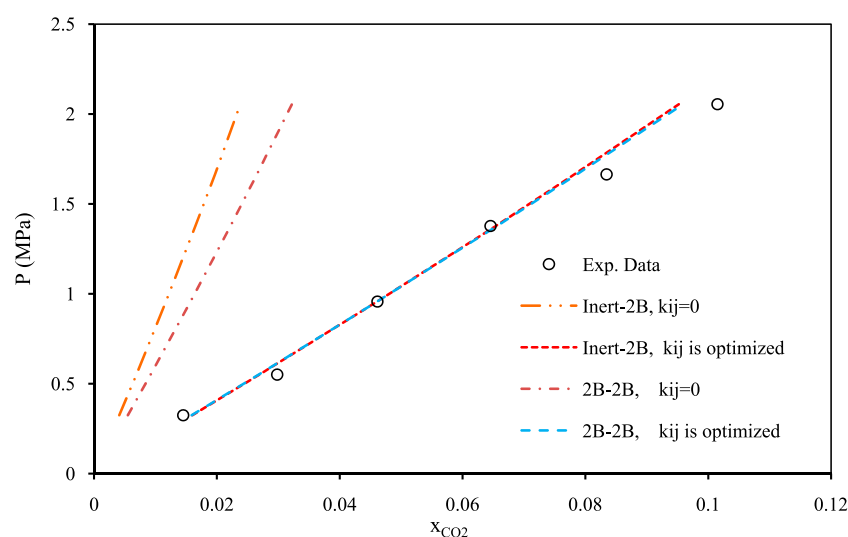


FIGURE 6

Comparison of two association schemes of PC-SAFT (inert-2B and 2B-2B) for solubility of CO<sub>2</sub> in benzyltriethylammonium chloride + acetic acid (1:2) (Sarmad et al., 2017) at the temperature of 298.15 K. The pure component PC-SAFT parameters of the DES were optimized using the density model of Haghbakhsh et al. (2019).

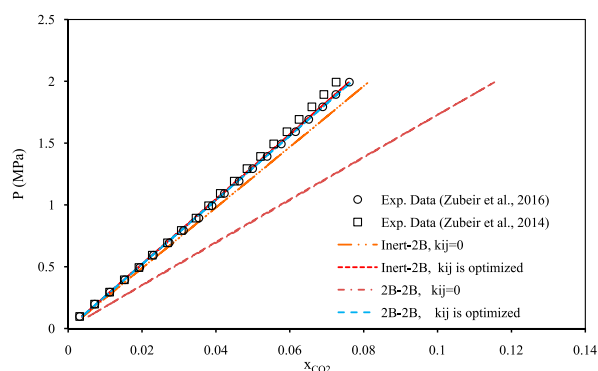


FIGURE 7

Comparison of two associations scheme of PC-SAFT (inert-2B and 2B-2B) for solubility of CO<sub>2</sub> in tetraethylammonium chloride + L-lactic acid (1:2) (Zubeir et al., 2016) and (Zubeir et al., 2014) at the temperature of 308 K. The pure PC-SAFT parameters of DES were taken from the literature (Zubeir et al., 2016).

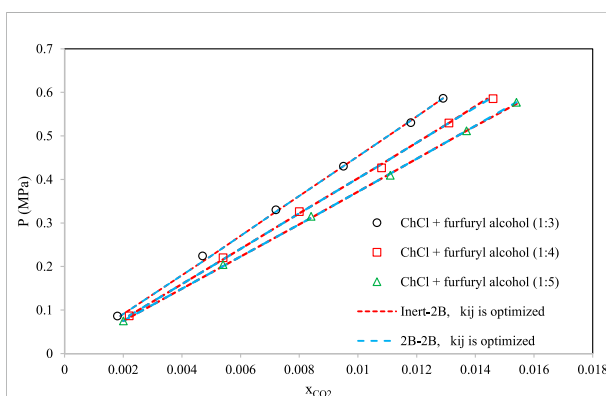
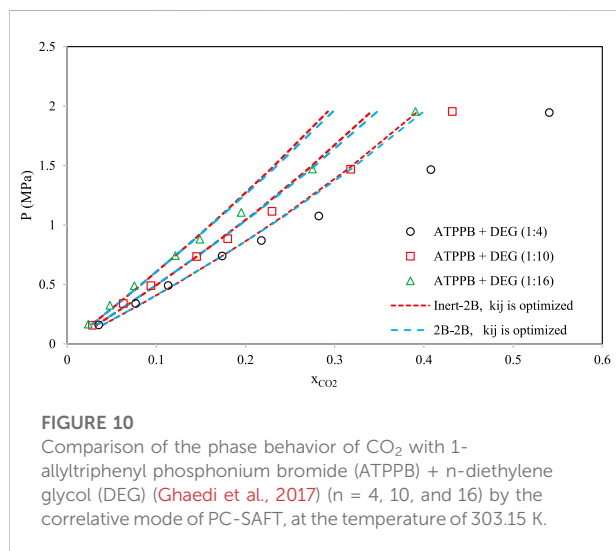
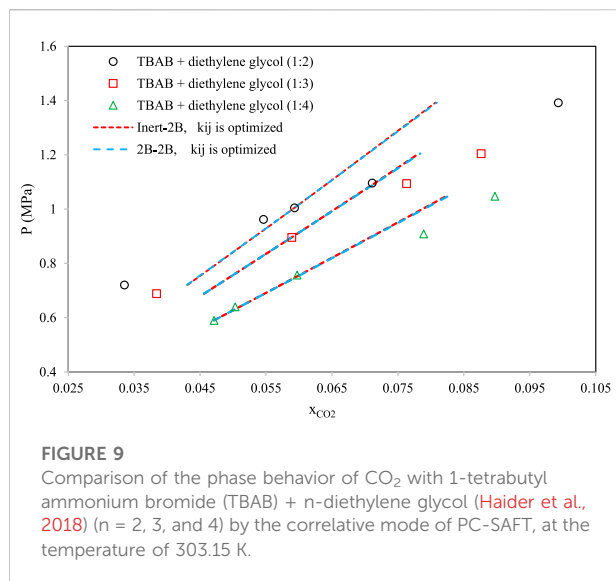


FIGURE 8

Comparison of the phase behaviors of CO<sub>2</sub> with choline chloride + n-furfuryl alcohol (Lu et al., 2015) ( $n = 3, 4$ , and  $5$ ) by the correlative mode of PC-SAFT, at the temperature of 333.15 K.

calculated phase behavior using both association schemes of inert and 2B to represent CO<sub>2</sub>. In all three figures, both the correlative and the predictive PC-SAFT results showed CO<sub>2</sub> solubility to have a linear function of pressure, consistent with the linear trend of the experimental data. This shows that PC-SAFT, even in its predictive mode, could successfully predict the solubility trends in the presented systems, however, it does need adjustment by including binary interaction parameters in order to produce

more reliable results with respect to the experimental values. The predictive PC-SAFT in Figure 6 shows overestimations of CO<sub>2</sub> solubility at fixed pressures, while it shows underestimations in Figures 5, 7. This shows a normal behavior for the predictive PC-SAFT, i.e., there is no systematic underestimation or overestimation by the model, as both cases are observed. Furthermore, these three figures show that the correlative PC-SAFT presents reliable agreement with the experimental values and trends for both the carbon dioxide association schemes of 2B and inert.



For further details, the solubility of CO<sub>2</sub> in different HBAs (choline chloride, allyltriphenyl phosphonium bromide, and tetrabutyl ammonium bromide) with different HBDs and various molar ratios are presented in the Supplementary section (Supplementary Figures S2–S4). It can be seen from these Supplementary figures that upon increasing the molar ratios of the glycols (ethylene glycol, diethylene glycol or triethylene glycol) as the HBD components of the investigated DESs, the CO<sub>2</sub> solubility decreases. The developed PC-SAFT models, in all cases, could follow these trends quite well.

Figures 8–10 aim to compare members of the same family of DESs (identical HBA and HBD but various molar ratios). By increasing the molar ratio (HBA with respect to HBD) in each family, the DESs show different capacities and trends for CO<sub>2</sub>

absorption. Figure 8 presents the correlative mode of the PC-SAFT model for choline chloride + n-furfuryl alcohol (n = 3, 4, and 5) at various molar ratios at a temperature of 333.15 K. As can be seen, the phase behavior of CO<sub>2</sub> with the chosen family of DES can be calculated precisely by both of the investigated schemes. In Figure 9, the phase behavior representations of CO<sub>2</sub> with 1-tetrabutyl ammonium bromide (TBAB) + n-diethylene glycol (n = 2, 3, and 4) are given at the temperature of 303.15 K. In this figure, by increasing the molar ratio of the HBD (diethylene glycol), CO<sub>2</sub> absorption increases. The experimental trends are very well followed by both of the investigated association schemes. Figure 10 exhibits the CO<sub>2</sub> solubility in 1-allyltriphenyl phosphonium bromide + n-diethylene glycol family (n = 4, 10, and 16) at the temperature of 303.15 K. Opposite to the DES family of Figure 9, in Figure 10, by increasing the molar ratio of diethylene glycol in this family, the solubility of CO<sub>2</sub> is decreasing, which is also followed by the correlative mode of PC-SAFT with good agreement.

Based on the achieved results, the inert scheme for CO<sub>2</sub>, in general, shows better results compared to the 2B scheme when the predictive mode is considered (when neglecting binary interaction parameters). Despite this, the predictive mode does not give acceptable results with either of the schemes. However, when considering binary interaction parameters, both association schemes of inert and 2B for CO<sub>2</sub> show trustworthy estimations with respect to the experimental trends.

## Conclusion

In contrast to previous studies focusing on a very limited number of DESs, in this study, the PC-SAFT EoS has been chosen as an associating EoS to estimate carbon dioxide solubilities in 109 deep eutectic solvents having different chemical natures over wide ranges of temperatures and pressures. This is indeed a thermodynamic challenge, considering that the DESs consist of various types of HBDs and HBAs, and at different molar ratios, resulting in complex interactions. High pressures further add to the challenge of thermodynamic modelling. Therefore, for the first time, this study gives an overview of the capabilities of this sophisticated model, as a tool for the general modelling of DES + CO<sub>2</sub> phase behavior. A large and most-recent data bank, consisting of 2,542 solubility data points, is used. To obtain the pure component parameters of PC-SAFT, which are not reported in the literature, a data bank of experimental densities was also collected, consisting of a total of 62 various DESs, with 656 density data points.

The pseudo-component approach was used in this study. The association scheme of 2B was considered for the DES pseudo-components, while the association schemes of inert and 2B were both investigated for carbon dioxide. For a more extensive investigation on the capability of the PC-SAFT EoS, predictive and correlative modes were both studied. In the predictive mode,

the CO<sub>2</sub> solubility was calculated without considering any binary interaction parameters ( $k_{ij}$ ), while in the correlative mode, a binary interaction parameter was considered as a function of temperature.

One of the greatest challenges in using associating equations of state, and thus limiting their use by researchers, is the determination of the pure component parameters. This is a cause of regret, because DESs are truly associating compounds, and only models that do consider these associations are theoretically sound models for such complex systems. To assist in the more widespread use of the PC-SAFT by researchers, a simple generalized correlation is proposed in this study to estimate the PC-SAFT pure component parameters of DESs. This generalized correlation is only a function of molecular weight, and so, easily applicable to any DES. In this way, the challenging step of parameter optimization by users is eliminated. The PC-SAFT, in the predictive mode, showed total AARD% of 63.77 and 84.65% for the inert-2B and 2B-2B modes, respectively. But in the correlative calculations, the inert-2B and 2B-2B modes, led to total AARD% of 8.08% and 8.12%, respectively. The calculated solubilities by the predictive mode showed that the inert scheme for CO<sub>2</sub> leads to less errors than the scheme of 2B, however, both schemes are inaccurate. By considering adjusted binary interaction parameters, the results improve significantly, with both the inert-2B and 2B-2B calculations showing reliable results with respect to the experimental trends. In its current state, DESs can still be considered as novel solvents with much unknowns. These limits also have their impact on the thermodynamic modelling of systems involving DESs. For accurate modelling, the number and strength of association bonds between carbon dioxide and the HBA or HBD molecules must be known. For example, performing NMR tests on these systems can provide valuable information. This is because systems of carbon dioxide with DESs are very complex, and in order to succeed in very accurate modeling, all the established associations in the mixture should be involved in the thermodynamic model. However, in this way, the model will become more complicated and time-consuming, but this is the cost of greater accuracy.

## Data availability statement

The original contributions presented in the study are included in the article/**Supplementary Material**, further inquiries can be directed to the corresponding author.

## References

Abbott, A. P., Barron, J. C., Frisch, G., Ryder, K. S., and Silva, A. F. (2011). The Effect of additives on zinc electro deposition from deep eutectic solvents. *Electrochim. Acta* 56, 5272–5279. doi:10.1016/j.electacta.2011.02.095

## Author contributions

Writing—original draft, conceptualization, formal analysis, data curation, software, KP; methodology, writing—review and editing, conceptualization, formal analysis, validation, RH; funding acquisition, supervision, writing—review and editing, AD; supervision, validation, writing - review and editing, SR.

## Funding

This project has received funding from the European Union's Horizon 2020—European Research Council (ERC)—under grant agreement No ERC-2016-CoG 725034.

## Acknowledgments

The authors are grateful to University of Isfahan, Universidade Nova de Lisboa, Shiraz University and University of Gonabad for providing facilities.

## Conflict of interest

The authors declare that the research was conducted in the absence of any commercial or financial relationships that could be construed as a potential conflict of interest.

## Publisher's note

All claims expressed in this article are solely those of the authors and do not necessarily represent those of their affiliated organizations, or those of the publisher, the editors and the reviewers. Any product that may be evaluated in this article, or claim that may be made by its manufacturer, is not guaranteed or endorsed by the publisher.

## Supplementary material

The Supplementary Material for this article can be found online at: <https://www.frontiersin.org/articles/10.3389/fchem.2022.909485/full#supplementary-material>

Abbott, A. P., Capper, G., Davies, D. L., Rasheed, R. K., and Tambyrajah, V. (2003). Novel solvent properties of choline chloride/urea mixtures. *Chem. Commun.* (1), 70–71. doi:10.1039/b210714g

- Abbott, A. P., Cullis, P. M., Gibson, M. J., Harris, R. C., and Raven, E. (2007). Extraction of glycerol from biodiesel into a eutectic based ionic liquid. *Green Chem.* 9 (8), 868. doi:10.1039/b702833d
- Ali, E., Hadj-Kali, M. K., Mulyono, S., Alnashif, I., Fakeeha, A., Mjalli, F., et al. (2014). Solubility of CO<sub>2</sub> in deep eutectic solvents: Experiments and modelling using the peng-robinson equation of state. *Chem. Eng. Res. Des.* 92 (10), 1898–1906. doi:10.1016/j.cherd.2014.02.004
- Altamash, T., Nasser, M. S., Elhamarnah, Y., Magzoub, M., Ullah, R., Anaya, B., et al. (2017). Gas solubility and rheological behavior of natural deep eutectic solvents (NADES) via combined experimental and molecular simulation techniques. *ChemistrySelect* 2 (24), 7278–7295. doi:10.1002/slct.201701223
- Altamash, T., Nasser, M. S., Elhamarnah, Y., Magzoub, M., Ullah, R., Qiblawey, H., et al. (2018). Gas solubility and rheological behavior study of betaine and alanine based natural deep eutectic solvents (NADES). *J. Mol. Liq.* 256, 286–295. doi:10.1016/j.molliq.2018.02.049
- Aminian, A. (2021). Modeling vapor-liquid equilibrium and liquid-liquid extraction of deep eutectic solvents and ionic liquids using perturbed-chain statistical associating fluid theory equation of state. Part II. *AIChE J.*
- Animasahun, O. H., Khan, M. N., and Peters, C. J. (2017). “Prediction of the CO<sub>2</sub> solubility in deep eutectic solvents: A comparative study between PC-SAFT and cubic equations of state,” in Abu Dhabi International Petroleum Exhibition and Conference. Society of Petroleum Engineers.
- Baramaki, Z., Arab Aboosadi, Z., and Esfandiari, N. (2019). Fluid phase equilibrium prediction of acid gas solubility in imidazolium-based ionic liquids with the Peng-Robinson and the PC-SAFT models. *Pet. Sci. Technol.* 37 (1), 110–117. doi:10.1080/10916466.2018.1511593
- Cea-Klapp, E., Polishuk, I., Canales, R. I., Quinteros-Lama, H., and Garrido, J. M. (2020). Estimation of thermodynamic properties and phase equilibria in systems of deep eutectic solvents by PC-SAFT EoS. *Ind. Eng. Chem. Res.* 59 (51), 22292–22300. doi:10.1021/acs.iecr.0c05109
- Chen, Y., Ai, N., Li, G., Shan, H., Cui, Y., Deng, D., et al. (2014). Solubilities of carbon dioxide in eutectic mixtures of choline chloride and dihydric alcohols. *J. Chem. Eng. Data* 59 (4), 1247–1253. doi:10.1021/je400884v
- Deng, D., Jiang, Y., Liu, X., Zhang, Z., and Ai, N. (2016). Investigation of solubilities of carbon dioxide in five levulinic acid-based deep eutectic solvents and their thermodynamic properties. *J. Chem. Thermodyn.* 103, 212–217. doi:10.1016/j.jct.2016.08.015
- Dietz, C. H., van Osch, D. J., Kroon, M. C., Sadowski, G., van Sint Annaland, M., Gallucci, F., et al. (2017). PC-SAFT modeling of CO<sub>2</sub> solubilities in hydrophobic deep eutectic solvents. *Fluid Phase Equilib.* 448, 94–98. doi:10.1016/j.fluid.2017.03.028
- Flórides, G. A., and Christodoulides, P. (2009). Global warming and carbon dioxide through sciences. *Environ. Int.* 35 (2), 390–401. doi:10.1016/j.envint.2008.07.007
- Francisco, M., van den Bruinhorst, A., Zubeir, L. F., Peters, C. J., and Kroon, M. C. (2013). A new low transition temperature mixture (LTTM) formed by choline chloride + lactic acid: Characterization as solvent for CO<sub>2</sub> capture. *Fluid Phase Equilib.* 340, 77–84. doi:10.1016/j.fluid.2012.12.001
- Ghaedi, H., Ayoub, M., Sufian, S., Shariff, A. M., Hailegiorgis, S. M., Khan, S. N., et al. (2017). CO<sub>2</sub> capture with the help of Phosphonium-based deep eutectic solvents. *J. Mol. Liq.* 243, 564–571. doi:10.1016/j.molliq.2017.08.046
- Gross, J., and Sadowski, G. (2002). Application of the perturbed-chain SAFT equation of state to associating systems. *Ind. Eng. Chem. Res.* 41, 5510–5515. doi:10.1021/ie010954d
- Gross, J., and Sadowski, G. (2001). Perturbed-Chain SAFT: An equation of state based on a perturbation theory for chain molecules. *Ind. Eng. Chem. Res.* 40, 1244–1260. doi:10.1021/ie0003887
- Haghighbakhsh, R., Bardool, R., Bakhtyari, A., Duarte, A. R. C., and Raeissi, S. (2019). Simple and global correlation for the densities of deep eutectic solvents. *J. Mol. Liq.* 296, 111830. doi:10.1016/j.molliq.2019.111830
- Haghighbakhsh, R., Parvaneh, K., Raeissi, S., and Shariati, A. (2018). A general viscosity model for deep eutectic solvents: The free volume theory coupled with association equations of state. *Fluid Phase Equilib.* 470, 193–202. doi:10.1016/j.fluid.2017.08.024
- Haghighbakhsh, R., and Raeissi, S. (2017). Modeling the phase behavior of carbon dioxide solubility in deep eutectic solvents with the cubic plus association equation of state. *J. Chem. Eng. Data* 63 (4), 897–906. doi:10.1021/acs.jced.7b00472
- Haghighbakhsh, R., Raeissi, S., Parvaneh, K., and Shariati, A. (2018). The friction theory for modeling the viscosities of deep eutectic solvents using the CPA and PC-SAFT equations of state. *J. Mol. Liq.* 249, 554–561. doi:10.1016/j.molliq.2017.11.054
- Haider, M. B., Jha, D., Kumar, R., and Sivagnanam, B. M. (2020). Ternary hydrophobic deep eutectic solvents for carbon dioxide absorption. *Int. J. Greenh. Gas Control* 92, 102839. doi:10.1016/j.ijggc.2019.102839
- Haider, M. B., Jha, D., Marriyappan Sivagnanam, B., and Kumar, R. (2018). Thermodynamic and kinetic studies of CO<sub>2</sub> capture by glycol and amine-based deep eutectic solvents. *J. Chem. Eng. Data* 63 (8), 2671–2680. doi:10.1021/acs.jced.8b00015
- Hasib-ur-Rahman, M., Sijaj, M., and Larachi, F. (2010). Ionic liquids for CO<sub>2</sub> capture-development and progress. *Chem. Eng. Process. Process Intensif.* 49 (4), 313–322. doi:10.1016/j.cep.2010.03.008
- Huang, S. H., and Radosz, M. (1990). Equation of state for small, large, polydisperse, and associating molecules. *Ind. Eng. Chem. Res.* 29, 2284–2294. doi:10.1021/ie00107a014
- Huang, S. H., and Radosz, M. (1991). Equation of state for small, large, polydisperse, and associating molecules: Extension to fluid mixtures. *Ind. Eng. Chem. Res.* 30, 1994–2005. doi:10.1021/ie00056a050
- Ilgel, F., Ott, D., Kralisch, D., Reil, C., Palmberger, A., König, B., et al. (2009). Conversion of carbohydrates into 5-hydroxymethylfurfural in highly concentrated low melting mixtures. *Green Chem.* 11 (12), 1948. doi:10.1039/b917548m
- Ji, Y., Hou, Y., Ren, S., Yao, C., and Wu, W. (2016). Phase equilibria of high pressure CO<sub>2</sub> and deep eutectic solvents formed by quaternary ammonium salts and phenol. *Fluid Phase Equilib.* 429, 14–20. doi:10.1016/j.fluid.2016.08.020
- Joback, K. G., and Reid, R. C. (1987). Estimation of pure-component properties from group contributions. *Chem. Eng. Commun.* 57, 233–243. doi:10.1080/00986448708960487
- Khajeh, A., Shakourian-Fard, M., and Parvaneh, K. (2020). Quantitative structure-property relationship for melting and freezing points of deep eutectic solvents. *J. Mol. Liq.* 114744.
- Knapp, H., Doring, R., Oellrich, L., Plocker, U., and Prausnitz, J. M. (1982). Vapor-liquid equilibria for mixtures of low boiling substances. *Chem. Data Ser. VI.*
- Koel, M. (2005). Ionic liquids in chemical analysis. *Crit. Rev. Anal. Chem.* 35 (3), 177–192. doi:10.1080/10408340500304016
- Leron, R. B., Caparanga, A., and Li, M. H. (2013). Carbon dioxide solubility in a deep eutectic solvent based on choline chloride and urea at T = 303.15–343.15 K and moderate pressures. *J. Taiwan Inst. Chem. Eng.* 44 (6), 879–885. doi:10.1016/j.jtice.2013.02.005
- Leron, R. B., and Li, M. H. (2013). Solubility of carbon dioxide in a choline chloride-ethylene glycol based deep eutectic solvent. *Thermochim. Acta* 551, 14–19. doi:10.1016/j.tca.2012.09.041
- Leron, R. B., and Li, M. H. (2013). Solubility of carbon dioxide in a eutectic mixture of choline chloride and glycerol at moderate pressures. *J. Chem. Thermodyn.* 57, 131–136. doi:10.1016/j.jct.2012.08.025
- Li, G., Deng, D., Chen, Y., Shan, H., and Ai, N. (2014). Solubilities and thermodynamic properties of CO<sub>2</sub> in choline-chloride based deep eutectic solvents. *J. Chem. Thermodyn.* 75, 58–62. doi:10.1016/j.jct.2014.04.012
- Li, X., Hou, M., Han, B., Wang, X., and Zou, L. (2008). Solubility of CO<sub>2</sub> in a choline chloride+ urea eutectic mixture. *J. Chem. Eng. Data* 53 (2), 548–550. doi:10.1021/jc700638u
- Li, X., Liu, X., and Deng, D. (2018). Solubilities and thermodynamic properties of CO<sub>2</sub> in four azole-based deep eutectic solvents. *J. Chem. Eng. Data* 63 (6), 2091–2096. doi:10.1021/acs.jced.8b00098
- Li, Z., Wang, L., Li, C., Cui, Y., Li, S., Yang, G., et al. (2019). Absorption of carbon dioxide using ethanalamine-based deep eutectic solvents. *ACS Sustain. Chem. Eng.* 7 (12), 10403–10414. doi:10.1021/acssuschemeng.9b00555
- Liu, F., Chen, W., Mi, J., Zhang, J. Y., Kan, X., Zhong, F. Y., et al. (2019). Thermodynamic and molecular insights into the absorption of H<sub>2</sub>S, CO<sub>2</sub>, and CH<sub>4</sub> in choline chloride plus urea mixtures. *AIChE J.* 65 (5), 16574. doi:10.1002/aic.16574
- Liu, X., Gao, B., Jiang, Y., Ai, N., and Deng, D. (2017). Solubilities and thermodynamic properties of carbon dioxide in guaiacol-based deep eutectic solvents. *J. Chem. Eng. Data* 62 (4), 1448–1455. doi:10.1021/acs.jced.6b01013
- Lloret, J. O., Vega, L. F., and Llovel, F. (2017). Accurate description of thermophysical properties of tetraalkylammonium chloride deep eutectic solvents with the soft-SAFT equation of state. *Fluid Phase Equilib.* 448, 81–93. doi:10.1016/j.fluid.2017.04.013
- Lu, M., Han, G., Jiang, Y., Zhang, X., Deng, D., Ai, N., et al. (2015). Solubilities of carbon dioxide in the eutectic mixture of levulinic acid (or furfuryl alcohol) and choline chloride. *J. Chem. Thermodyn.* 88, 72–77. doi:10.1016/j.jct.2015.04.021
- Ma, C., Sarmad, S., Mikkola, J. P., and Ji, X. (2017). Development of low-cost deep eutectic solvents for CO<sub>2</sub> capture. *Energy Procedia* 142, 3320–3325. doi:10.1016/j.egypro.2017.12.464
- Marcus, Y. (2018). Gas solubilities in deep eutectic solvents. *Monatsh. Chem.* 149 (2), 211–217. doi:10.1007/s00706-017-2031-8
- Mirza, N. R., Nicholas, N. J., Wu, Y., Mumford, K. A., Kentish, S. E., Stevens, G. W., et al. (2015). Experiments and thermodynamic modeling of the solubility of carbon dioxide in three different deep eutectic solvents (DESs). *J. Chem. Eng. Data* 60 (11), 3246–3252. doi:10.1021/acs.jced.5b00492



- Mirza, N. R., Nicholas, N. J., Wu, Y., Smith, K. H., Kentish, S. E., Stevens, G. W., et al. (2017). Viscosities and carbon dioxide solubilities of guanidine carbonate and malic acid-based eutectic solvents. *J. Chem. Eng. Data* 62 (1), 348–354. doi:10.1021/acs.jced.6b00680
- Morrison, H. G., Sun, C. C., and Neervannan, S. (2009). Characterization of thermal behavior of deep eutectic solvents and their potential as drug solubilization vehicles. *Int. J. Pharm.* X. 378, 136–139. doi:10.1016/j.ijpharm.2009.05.039
- Mulia, K., Putri, S., Krisanti, E., and Nasruddin, N. (2017). “Natural deep eutectic solvents (NADES) as green solvents for carbon dioxide capture,” in AIP Conference Proceedings (AIP Publishing LLC), 020022. doi:10.1063/1.497809518231
- Parvaneh, K., and Shariati, A. (2017). Quasi-chemical PC-SAFT: An extended perturbed chain-statistical associating fluid theory for lattice-fluid mixtures. *J. Phys. Chem. B* 121 (35), 8338–8347. doi:10.1021/acs.jpcc.7b05483
- Polishuk, I., Privat, R., and Jaubert, J. N. (2013). Novel methodology for analysis and evaluation of SAFT-type equations of state. *Ind. Eng. Chem. Res.* 52 (38), 13875–13885. doi:10.1021/ie4020155
- Sarmad, S., Xie, Y., Mikkola, J. P., and Ji, X. (2017). Screening of deep eutectic solvents (DESs) as green CO<sub>2</sub> sorbents: From solubility to viscosity. *New J. Chem.* 41 (1), 290–301. doi:10.1039/c6nj03140d
- Smith, E. L., Abbott, A. P., and Ryder, K. S. (2014). Deep eutectic solvents (DESs) and their applications. *Chem. Rev.* 114 (21), 11060–11082. doi:10.1021/cr300162p
- Valderrama, J. O., and Robles, P. A. (2007). Critical properties, normal boiling temperatures, and acentric factors of fifty ionic liquids. *Ind. Eng. Chem. Res.* 46, 1338–1344. doi:10.1021/ie0603058
- Valderrama, J. O., Sanga, W. W., and Lazzus, J. A. (2008). Critical properties, normal boiling temperature, and acentric factor of another 200 ionic liquids. *Ind. Eng. Chem. Res.* 47, 1318–1330. doi:10.1021/ie071055d
- Vega, L. F., Vilaseca, O., Llovel, F., and Andreu, J. S. (2010). Modeling ionic liquids and the solubility of gases in them: Recent advances and perspectives. *Fluid Phase Equilib.* 294 (1–2), 15–30. doi:10.1016/j.fluid.2010.02.006
- Wang, J., Cheng, H., Song, Z., Chen, L., Deng, L., Qi, Z., et al. (2019). Carbon dioxide solubility in phosphonium-based deep eutectic solvents: An experimental and molecular dynamics study. *Ind. Eng. Chem. Res.* 58 (37), 17514–17523. doi:10.1021/acs.iecr.9b03740
- Wells, A. S., and Coombe, V. T. (2006). On the freshwater ecotoxicity and biodegradation properties of some common ionic liquids. *Org. Process Res. Dev.* 10 (4), 794–798. doi:10.1021/op060048i
- Xia, S., Baker, G. A., Li, H., Ravula, S., and Zhao, H. (2014). Aqueous ionic liquids and deep eutectic solvents for cellulosic biomass pretreatment and saccharification. *RSC Adv.* 4, 10586. doi:10.1039/c3ra46149a
- Yamasaki, A. (2003). An overview of CO<sub>2</sub> mitigation options for global warming-emphasizing CO<sub>2</sub> sequestration options. *J. Chem. Eng. Jpn.* 36 (4), 361–375. doi:10.1252/jcej.36.361
- Zhang, Q., Vigier, K. D. O., Royer, S., and Jerome, F. (2012). Deep eutectic solvents: Syntheses, properties and applications. *Chem. Soc. Rev.* 41 (21), 7108. doi:10.1039/c2cs35178a
- Zubeir, L. F., Held, C., Sadowski, G., and Kroon, M. C. (2016). PC-SAFT modeling of CO<sub>2</sub> solubilities in deep eutectic solvents. *J. Phys. Chem. B* 120 (9), 2300–2310. doi:10.1021/acs.jpcc.5b07888
- Zubeir, L. F., Lacroix, M. H., and Kroon, M. C. (2014). Low transition temperature mixtures as innovative and sustainable CO<sub>2</sub> capture solvents. *J. Phys. Chem. B* 118 (49), 14429–14441. doi:10.1021/jp5089004
- Zubeir, L. F., Van Osch, D. J., Rocha, M. A., Banat, F., and Kroon, M. C. (2018). Carbon dioxide solubilities in decanoic acid-based hydrophobic deep eutectic solvents. *J. Chem. Eng. Data* 63 (4), 913–919. doi:10.1021/acs.jced.7b00534



## OPEN ACCESS

## EDITED BY

Miguel Angel Centeno,  
Institute of Materials Science of Seville  
(CSIC), Spain

## REVIEWED BY

Elena Ibañez,  
Institute of Food Science Research  
(CSIC), Spain  
Aditi Kundu,  
Division of Agricultural Chemicals  
(ICAR), India

## \*CORRESPONDENCE

Sílvia Rebocho,  
s.rebocho@campus.fct.unl.pt

## SPECIALTY SECTION

This article was submitted to Green and Sustainable Chemistry, a section of the journal Frontiers in Chemistry

RECEIVED 27 May 2022

ACCEPTED 07 July 2022

PUBLISHED 12 August 2022

## CITATION

Vieira C, Rebocho S, Craveiro R, Paiva A and Duarte ARC (2022), Selective extraction and stabilization of bioactive compounds from rosemary leaves using a biphasic NADES.  
*Front. Chem.* 10:954835.  
doi: 10.3389/fchem.2022.954835

## COPYRIGHT

© 2022 Vieira, Rebocho, Craveiro, Paiva and Duarte. This is an open-access article distributed under the terms of the Creative Commons Attribution License (CC BY). The use, distribution or reproduction in other forums is permitted, provided the original author(s) and the copyright owner(s) are credited and that the original publication in this journal is cited, in accordance with accepted academic practice. No use, distribution or reproduction is permitted which does not comply with these terms.

# Selective extraction and stabilization of bioactive compounds from rosemary leaves using a biphasic NADES

Carolina Vieira, Sílvia Rebocho\*, Rita Craveiro, Alexandre Paiva and Ana Rita C. Duarte

LAQV@REQUIMTE, Departamento de Química, NOVA School of Science and Technology, Universidade NOVA de Lisboa, Caparica, Portugal

Rosemary (*Rosmarinus officinalis*) is a natural source of bioactive compounds that have high antioxidant activity. It has been in use as a medicinal herb since ancient times, and it currently is in widespread use due to its inherent pharmacological and therapeutic potential, in the pharmaceutical, food, and cosmetic industries. Natural deep eutectic systems (NADESs) have recently been considered as suitable extraction solvents for bioactive compounds, with high solvent power, low toxicity, biodegradability, and low environmental impact. The present work concerns the extraction of compounds such as rosmarinic acid, carnosol, carnosic acid, and caffeic acid, from rosemary using NADESs. This extraction was carried out using heat and stirring (HS) and ultrasound-assisted extraction (UAE). A NADES composed of menthol and lauric acid at a molar ratio of 2:1 (Me:Lau) extracted carnosic acid and carnosol preferentially, showing that this NADES exhibits selectivity for nonpolar compounds. On the other hand, a system of lactic acid and glucose (LA:Glu (5:1)) extracted preferentially rosmarinic acid, which is a more polar compound. Taking advantage of the different polarities of these NADESs, a simultaneous extraction was carried out, where the two NADESs form a biphasic system. The system LA:Glu (5:1)/Men:Lau (2:1) presented the most promising results, reaching  $1.00 \pm 0.12$  mg of rosmarinic acid/g rosemary and  $0.26 \pm 0.04$  mg caffeic acid/g rosemary in the more polar phase and  $2.30 \pm 0.18$  mg of carnosol/g of rosemary and  $17.54 \pm 1.88$  mg carnosic acid/g rosemary in the nonpolar phase. This work reveals that it is possible to use two different systems at the same time and extract different compounds in a single-step process under the same conditions. NADESs are also reported to stabilize bioactive compounds, due to their interactions established with NADES components. To determine the stability of the extracts over time, the compounds of interest were quantified by HPLC at different time points. This allows the conclusion that bioactive compounds from rosemary were stable in NADESs for long periods of time; in particular, carnosic acid presented a decrease of only 25% in its antioxidant activity after 3 months, whereas the carnosic acid extracted and kept in the methanol was no longer detected after 15 days. The stabilizing ability of NADESs to extract phenolic/bioactive compounds shows a great promise for future industrial applications.

## KEYWORDS

natural deep eutectic systems, ultrasound-assisted extraction, *Rosmarinus officinalis*, antioxidants, rosmarinic acid

## 1 Introduction

Rosemary (*Rosmarinus officinalis*, Lamiaceae) is a green shrub plant that is originally from the Mediterranean region. It is a natural source of bioactive compounds, and its essential oil has powerful properties. It has been used since ancient times as a medicinal herb due to its healing properties for illnesses such as headache, dysmenorrhea, stomachache, epilepsy, rheumatic pain, spasms, nervous agitation, improvement of memory, hysteria, depression, and physical and mental fatigue (Borrás-Linares et al., 2014; Rahbardar and Hosseinzadeh, 2020). With its characteristic fragrance, rosemary can also be used as an aromatic plant in culinary or ornamental uses (Oliveira et al., 2019). Rosemary extract has been used for more than 20 years as a natural preservative in food due to its antioxidant activity (Birtic et al., 2015). In 2010, the European Commission classified some of the antioxidant constituents of rosemary as food additives (E392), namely carnosic acid and carnosol (Commission Directives 2010/67/EU and 2010/69/EU). However, the antioxidant activity of rosemary has been noted not only in the food industry, but also in the pharmaceutical area, due to its inherent pharmacological and therapeutic potential. These compounds are currently present in several cosmetic formulas, as well as in pharmaceutical products (Neves et al., 2018; Oliveira et al., 2019; González-Minero et al., 2020).

Among the phytochemicals present in this plant, carnosic acid, rosmarinic acid, carnosol, and caffeic acid have been highlighted. Interactions between these compounds can promote several pharmacological effects (Oliveira et al., 2019). Carnosic acid can promote anti-inflammatory (Wang et al., 2018), antiproliferative (Bourhia et al., 2019), and antitumor activity (Allegra et al., 2020), and it has inhibitory effect on digestive enzymes (lipase,  $\alpha$ -amylase, and  $\alpha$ -glucosidase) (Ercan and El, 2018), a suppressive effect on lipogenesis (Song et al., 2018), and a protective effect on photoreceptor cells (Albalawi et al., 2018). Rosmarinic acid has neuroprotective (Cui et al., 2018), antiproliferative (Ma et al., 2018), and antiviral activity (Tsukamoto et al., 2018), and it can be used for anxiety control (Makhathini et al., 2018) and as complementary agent to anticancer chemotherapy (Radziejewska et al., 2018). Carnosol shows anti-inflammatory (Oliviero et al., 2018), antifungal (Ramírez et al., 2018), antiproliferative (Aliebrahimi et al., 2018), and antidiabetic (Samarghandian et al., 2017) activities, and it is also has protective against renal injury (Zheng et al., 2018). Caffeic acid has many health benefits, including antioxidant properties and anti-inflammatory, anticancer, and antiviral capacities (Huang et al., 2018; Monteiro Espíndola et al., 2019).

Because of these beneficial effects, the demand for bioactive rosemary compounds in the pharmaceutical, food, and cosmetic industries has increased, as has the value of the plant, making it in high demand. Over the last two decades, an average of 120 scientific papers have been published on rosemary per year has, clearly showing interest in this plant (Andrade et al., 2018). Several aromatic plants are cultivated all over the world (including rosemary), and increased production of it has also generated more residues. From a sustainability point of view, the unused residues should be further valorized. They are a source of bioactive compounds, and their recovery makes them a source of added-value products.

The extraction of bioactive compounds from rosemary is usually carried out with traditional volatile organic solvents derived from petroleum. These solvents are toxic to humans and are harmful to the environment, as well as causing high energy consumption. Furthermore, organic solvents can leave traces in the extract, which may alter its bioactive properties.

Deep eutectic systems (DESs) are promising alternative extraction solvents (Chemat et al., 2015). DESs can be defined as mixtures of two or more components, solid or liquid, which establish strong intermolecular interactions at a given molar ratio, essentially hydrogen-bond interactions, causing a melting point depression of the DES in regard to the individual components, leading to a liquid system (in some cases, liquid at room temperature) (Hansen et al., 2021). Moreover, when its constituents are primary metabolites, namely, amino acids, organic acids, alcohols, or sugars, they are termed as natural DESs (NADESs), which are in some cases biocompatible, more biodegradable, and with lower toxicity. As solvents, NADESs have advantages over conventional solvents, due to their adjustable viscosity, polarity, solubilization power, and negligible volatility (Paiva et al., 2014). The presence in NADESs of the functional groups of carboxyl and hydroxyl, as well as of amino acids, is responsible for the intermolecular interactions and some of its characteristics, particularly their solubilizing behavior and physicochemical properties.

NADESs demonstrate excellent results from extraction compared to conventional solvents (Liu et al., 2018). NADESs have been proven to have a high extraction capacity for phenolic compounds due to the interactions established between phenolics and NADES constituent groups. They also show a higher extraction yield than conventional solvents, such as water or ethanol (Dai et al., 2013a; Paiva et al., 2014). In addition, depending on the use and safety of the NADES applied, the extracts do not require post-extraction purification. Furthermore, keeping the extracts in the NADES can increase their shelf-life and bioactivity, promoting their stability (Dai et al., 2014). It is noteworthy that from an economic and

environmental perspective, these systems present advantages concerning the simplicity of their preparation, their low cost, and their sustainability.

All of the studies of DESs as solvents in the extraction of polyphenols and flavonoids from rosemary are very recent. The most studied DESs are choline-chloride (ChCl)-based ones (Bajkacz and Adamek, 2018; Barbieri et al., 2020; Wojeicchowski et al., 2020, 2021; Calderón-Oliver and Ponce-Alquicira, 2021; Vladimir-Knežević et al., 2022). The use of ChCl combined with several compounds has been reported, for example, 1, 2-propanediol, reaching high levels of polyphenols (Barbieri et al., 2020; Wojeicchowski et al., 2021). Glyceline, or ChCl combined with glycerol (1:2), when used as a pretreatment in a proportion of 10% aqueous solution in the essential oil extraction from rosemary leaves, presents higher content of camphor, verbenone, and borneol and showed better antioxidant activity (Stanojević et al., 2021).

Extraction efficiency for the target compounds of rosemary has explored in more detail in hydrophilic DESs, particularly in ChCl-based DESs. The use of hydrophobic DES began later, with the aim of recovering fatty acids from aqueous media (Van Osch et al., 2015). Wang and his coworkers reported a study in which they compared DESs with different hydrophobicities, finding that hydrophobic DESs (e.g., menthol-based DESs) are more effective for the extraction hydrophobic compounds than hydrophilic DESs or traditional solvents (Wang et al., 2021). This indicates the infinite possibilities of DESs components and their combinations in promoting selectivity for the extraction and separation of certain bioactive compounds, as demonstrated with rosemary, as an example of a simultaneous extraction and fractionation of compounds with different polarities (Ali et al., 2019).

DES-based extraction has good extraction efficiency for bioactive compounds in plants (Ruesgas-Ramón et al., 2017; Tang and Row, 2020), although such extraction systems are ineffective for the simultaneous extraction of high-polarity and low-polarity compounds. Single-phase extractions with DESs are only able to extract compounds of similar polarity or analogues from plants (Cunha and Fernandes, 2018). In a work by Cao et al., a two-phase DES-based extraction is reported, in which a mixture of DESs of different polarities is used. This yielded a fractionated and selective extraction with a polar phase and a nonpolar phase, which extracted different compounds (Cao et al., 2018). Interestingly, it was also observed that two-phase systems could effectively enrich bioactive compounds with different polarities in the upper or lower phase, and the different phases could be easily separated after extraction process. These biphasic systems could act as a new paradigms in multicomponent extraction from plant residues, as well as from other different residues (Cao et al., 2018).

The purpose of this work is to extract compounds with added value from rosemary waste, using a more sustainable solvent such as a NADES. An initial screening established the optimal NADES

extraction conditions, such as temperature, solid-liquid ratio, time, and extraction methodology. We explored the different types of NADESs with different compositions, and we identified the stability of the extracts provided by these systems. Furthermore, a fractionated extraction using a biphasic system composed by NADESs with different polarities was performed, promoting an easier and more efficient separation process in a single step. This strategy allows the selectivity of the target bioactive compounds for each NADES to be explored, which is extremely advantageous for specific applications.

## 2 Materials and methods

### 2.1 Plant material

The rosemary leaves were provided by Aromáticas vivas Ltd., from the residues of this company's production. The plants were grown in Viana do Castelo (41°44'27.4"N 8°51'55.9"W), in the sub-region of Alto Minho in the northern region of Portugal, under optimal growth conditions defined by the company to meet high standards of food safety, quality, and sustainability. The initial water content of rosemary leaves was  $63.07 \pm 1.64\%$ .

The water content in the rosemary leaves was monitored with a hygrometer during drying process using mass difference (KERN DAB 100-3, Germany). Drying was carried out at room temperature, until the mass stabilized. This process was carried out over a period of 2 months. In the end, the percentage of water was  $8.79 \pm 0.16\%$ .

The plant material was ground (IKA tube-Mill control, Germany) to obtain fragments in the order of <0.5 mm in particle size (1 min at 1,200 rpm). The obtained rosemary powder was stored in plastic bags properly sealed and kept in a vacuum desiccator until further usage.

### 2.2 Chemicals

All chemical reagents were used as received after being purchased or kept in storage with no further treatment or purification. Lactic acid ( $\geq 85\%$  purity), D-glucose monohydrate ( $\geq 97.5\%$  purity), betaine ( $\geq 99\%$  purity), DL-menthol ( $\geq 95\%$  purity), myristic acid ( $\geq 98\%$  purity), lauric acid ( $\geq 98\%$  purity), D-sucrose (99.5% purity), D-sorbitol (98% purity), gallic acid ( $\geq 98\%$  purity), and Nile red and rosmarinic acid were all purchased from Sigma-Aldrich (St. Louis, Missouri, United States). Citric acid monohydrate (99.5% purity) and Folin-Ciocalteu phenol reagent were obtained from Panreac (Barcelona, Spain). Glycerol (99.5% purity) and DL-malic acid ( $\geq 99\%$  purity) were purchased from Scharlau (Barcelona, Spain). Ethylene glycol ( $\geq 99.5\%$  purity) and ethanol (99% purity) were obtained from Carlo Erba (Val-de-Reuil, France). L-proline (99% purity) and  $\beta$ -alanin (99% purity) were obtained from Alfa Aesar

TABLE 1 Composition, molar ratio, and physical appearance of the prepared NADESs.

NADES composition	Abbreviation	Molar ratio	Physical appearance
Betaine:ethylene glycol	B:EG	1:3	Transparent, colorless, slightly viscous liquid
Betaine:glycerol	B:Gly	1:2	Transparent, colorless viscous liquid
Citric acid:glycerol	Ca:Gly	1:1	Transparent, colorless viscous liquid
Citric acid:betaine	Ca:B	2:1	<sup>a</sup>
Lactic acid:glucose	La:Glu	5:1	Transparent, colorless liquid
Lactic acid:β alanin	La:Ba	1:1	Viscous white liquid
Lactic acid:betaine	La:B	2:1	Transparent, colorless liquid
Lactic acid:proline	P:La	3:1	Transparent, colorless liquid
Malic acid:sucrose	Ma:Su	1:1	<sup>a</sup>
Malic acid:glucose:glycerol	Ma:Glu:Gly	1:1:1	<sup>a</sup>
Malic acid:sorbitol	Ma:Sor	1:1	<sup>a</sup>
Menthol:lauric acid	Me:Lau	2:1	Transparent, colorless liquid
Menthol:myristic acid	Me:My	8:1	Transparent, colorless liquid
Menthol:lactic acid	Me:La	1:2	Transparent, colorless liquid
Trehalose:glycerol	T:Gly	1:30	Transparent, colorless slightly viscous liquid

<sup>a</sup>Systems that have not been successfully formed.

(Haverhill, Massachusetts, United States). Sodium carbonate (99.5–100% purity) was purchased from Merck (Darmstadt, Germany), and methanol was acquired from Honeywell (New Jersey, United States). Carnosol, carnosic acid, and caffeic acid were acquired from Biosynth (Newbury, England). Trehalose (99% purity) was kindly provided by Hayashibara Co., Ltd. (Okayama, Japan).

## 2.3 Preparation of NADES

All NADESs were prepared using the heating/stirring method previously reported by Dai and co-workers (Dai et al., 2013b), taking into account a specific molar ratio (Table 1). The components in their respective molar ratios were heated and stirred until a clear liquid was formed. To avoid the degradation of the components, the temperature was maintained below 50°C, except for system proline and lactic acid (P:La (1:3)), prepared at room temperature.

## 2.4 Characterization of NADES

### 2.4.1 Determination of the water content

The water content of each NADES was determined by Karl-Fischer titration using an 831 KF Coulometer with generator electrode (Metrohm). The water content of the plant material was determined using a moisture analyzer DAB (Kern). The obtained values were provided as an average of three measurements.

### 2.4.2 Determination of polarity by Nile red assay

The relative polarity of the prepared NADESs was obtained by determining the solvatochromic shift of the dye Nile red in ethanol, according to the procedure reported by Craveiro et al. (Craveiro et al., 2016), with slight modifications. The spectra were obtained using a UV-spectrophotometer (Thermo Scientific) measured at 400–800 nm at room temperature. Eq. 1 shows the polarity parameter calculated as molar transition energy ( $E_{NR}$ ) (Reichardt, 1994):

$$E_{NR} = \frac{28591}{\lambda_{\max}(nm)} \quad (1)$$

where  $E_{NR}$  is in kcal mol<sup>-1</sup> and  $\lambda_{\max}$  is the wavelength at the maximum absorbance in nm. All measurements were done in triplicate.

## 2.5 Extraction of bioactive compounds from rosemary leaves

NADES-based extraction was carried out the different conditions of heat and stirring extraction (HSE) and ultrasound-assisted extraction (UAE).

### 2.5.1 Heat and stirring extraction

For HSE extraction, crushed dried rosemary leaves were mixed with the NADESs at different solid/liquid (S:L) weight ratios (1:20, 1:30, and 1:40). The extractions were performed in cycles of 15 min in a hotplate stirrer (Stuart heat-stir CB162, United States; AGIMATIC ED-C. J.P. Selecta,



Spain) and stirred in a vortex for 1 min between cycles), according to procedures previously described by (Barbieri et al., 2020). There were two or four HSE cycles, lasting in 30 min and 1 h of extraction, respectively. The temperature was set to 40°C. The final extracts were centrifuged at 6,000 rpm for 20 min (Hermle), and the supernatant liquid was recovered and kept at 4°C. All of the extractions were done in triplicate.

### 2.5.2 Ultrasound-assisted extraction

As with previous extraction methods, crushed dried rosemary leaves were mixed with NADESs at different S:L ratios (1:20, 1:30, and 1:40). The UAE extractions were performed in cycles of 15 min in an ultrasound bath (100 W) and frequency of 50–60 Hz (Grant XUB5, United Kingdom), and stirred in a vortex for 1 min between cycles, according to the procedure described previously (Barbieri et al., 2020). There were two or four UAE cycles in this part as well, resulting in 30 min and 1 h extraction, respectively. The selected extraction temperatures were 40°C and 60°C, chosen to evaluate the effect on extraction yield. The final extracts were centrifuged at 6,000 rpm for 20 min (Hermle) and the supernatant liquid was recovered and kept at 4°C. All extractions were done in triplicate.

### 2.5.3 Soxhlet extraction

A mass of 2 g crushed dried rosemary leaves in a filter-paper bag was placed into the Soxhlet extraction chamber (250 ml) with 75 ml of methanol. The extraction was performed until the solvent was exhausted, and it was performed in triplicate. The residue was dried to remove the solvent at 40°C, and then it was weighed. The solvent in the solution was removed by evaporation, and the remaining solid (extract) was weighed and reserved.

### 2.5.4 Biphasic extraction

Biphasic/fractionated extraction was performed using two NADESs of opposed polarities, yielding a biphasic system. The crushed and dried rosemary leaves were mixed with the biphasic system, and extractions were carried out with varied S:L ratios (1:20, 1:30, and 1:40) and temperatures (40°C and 60°C). All extractions were performed in triplicate.

## 2.6 Determination of total phenolic content by the Folin-Ciocalteu method

The total phenolic content was performed according to the colorimetric Folin-Ciocalteu method (Yilmaz et al., 2015), and it was calculated from a standard curve obtained with different concentrations of gallic acid (25–1,000 mg/L). In this method, 20 µl each of the diluted

extracts was mixed with 1.58 ml distilled water and 100 µl Folin-Ciocalteu reagent. The mixture was vortexed and incubated at room temperature for 5–8 min. Following this, 300 µl of Na<sub>2</sub>CO<sub>3</sub> saturated solution was added, and each sample was incubated at 40°C for 30 min. The absorbance of the samples was measured at 750 nm using a UV spectrophotometer (Thermo Scientific). All assays were performed in triplicate, and the concentration of the samples was determined and expressed in mg/L of gallic acid equivalents (GAE).

## 2.7 Quantification and characterization of extracted components

A high-performance liquid chromatography (HPLC) apparatus used was an Agilent 1,100 series separation module HPLC system (Agilent, Santa Clara, California, United States) equipped with a pump, an autosampler, a column oven, and a multi-wavelength detector. The analytical column was a Phenomenex Luna C18 (Phenomenex, 4.6 mm × 250 mm, 5.0 µm, Torrance, California, EUA). The column temperature was maintained at 30°C. All of the injected samples were previously diluted in a 1:10 ratio in ethanol. The mobile phase was composed of A (1% acetic acid in water) and B (methanol) with a gradient elution as follows: 0–20 min, linear from 10% to 65% B; 20–40 min, linear from 65% to 100% B; 40–45 min, maintained at 100% B; 45–47 min, linear from 100% to 10% B; and then finally, holding for 3 min. The mobile phase was filtered through a 0.22 µm membrane filter (Filter-Lab, Barcelona, Spain) and degassed in a vacuum. The flow rate was set at 1.0 ml/min, and the injection volume was 20 µl. The rosmarinic acid, carnosol, carnosic acid, and caffeic acid were determined at 284 nm. The data acquisition and remote control of the HPLC system were performed using OpenLAB CDS Chemstation edition software (Agilent, Santa Clara, California, United States).

## 2.8 Study of extract stability

The extracts obtained from the biphasic extraction that showed most promising results were used to determine the stability of the bioactive compounds in the NADESs. Extracts obtained from the Soxhlet were also studied for the sake of comparison. The extracts were stored protected from light and at room temperature. The extracts were left for 90 days under the conditions noted above. During this time, samples were collected taken at 1, 3, 7, 15, 30, 60, and 90 days, and the evaluation of the concentration of each compound was monitored, using HPLC.

TABLE 2 Water content and viscosity of the selected and previously prepared NADESs.

NADES	Water content (wt%)	Viscosity at 40°C (mPa.s)
Me:My (8:1)	0.03 ± 0.003	13.96 ± 1.10
Me:Lau (2:1)	0.09 ± 0.01	58.84 ± 1.70
B:Gly (1:2)	0.67 ± 0.05	606.36 ± 8.70
B:EG (1:3)	0.83 ± 0.01	35.69 ± 2.20
T:Gly (1:30)	1.42 ± 0.05	439.00 ± 2.30
Me:La (1:2)	7.34 ± 0.16	58.84 ± 1.70
La:B (2:1)	9.17 ± 0.13	374.60 ± 0.00
P:La (3:1)	10.25 ± 0.19	179.52 ± 0.10
Ca:Gly (1:1)	10.65 ± 0.85	1654 ± 26.50
La:Glu (5:1)	10.78 ± 0.13	42.94 ± 1.70

## 2.9 Statistical analysis

All data was expressed as mean ± standard deviation of at least three independent experiments ( $n = 3$ ).  $p$ -values lower than 0.05 ( $p < 0.05$ ) were considered statistically significant (confidence interval of 95%). Statistical comparison of the means was made using the two-way ANOVA to investigate the statistical differences between the extractions and stability assays. Tukey's test was used to perform the post hoc comparisons of the means.

All calculations were performed using the software GraphPad Prism 8.0.1 (San Diego, CA, United States).

## 3 Results and discussion

### 3.1 Characterization of NADES

Several factors can influence extraction efficiency using NADESs as solvents, such as their water content, inherent polarity and viscosity, and the hydrogen bond ratio (HBD:HBA).

To assess and evaluate potential systems for the extraction of phenolic compounds from rosemary, 10 NADESs were prepared and characterized. Table 2 presents the water content of these NADESs, as well as the viscosity values at 40°C.

No water was added during the preparation of all of these NADESs. However, some NADES components contained water molecules in their composition, such as glucose and citric acid, which are both monohydrate, lactic acid, which has 15 wt% water content. Systems with menthol usually present a very low water content in their composition, being more hydrophobic and nonpolar.

Because the polarity of a solvent strongly impacts its solubilizing capacity (Dai et al., 2013b) and selectivity (Tang and Row, 2020), the polarity of the NADES was also measured (Figure 1).

As seen in Equation 1, lower  $E_{NR}$  values indicate higher polarity than the reference solvent (in this case ethanol). This implies that solvents with higher polarity change the dye's  $\lambda_{max}$  to higher wavelength values, resulting in smaller  $E_{NR}$  values. From Figure 1, it is observed that the more polar NADESs is Ca:Gly (1:1), followed by La:Glu (5:1), and the less polar ones are Me:Lau (2:1) and Me:My (8:1). The results are in agreement with

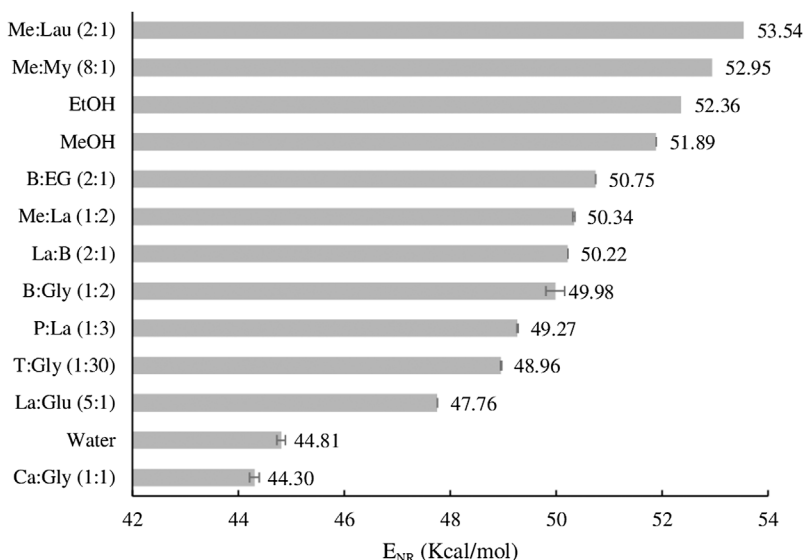


FIGURE 1

Relative polarity scale of the studied NADESs determined in ethanol, expressed as  $E_{NR}$  values.

TABLE 3 Results of the TPC in mg GAE/g rosemary and for the rosmarinic acid, carnosol, carnosic acid, and caffeic acid in mg/g rosemary for the extract obtained with methanol. Data are expressed as mean  $\pm$  SD.

TPC (mg GAE/g rosemary)	35.00 $\pm$ 7.35
Rosmarinic acid (mg/g rosemary)	1.36 $\pm$ 0.28
Carnosol (mg/rosemary)	7.28 $\pm$ 2.08
Carnosic acid (mg/g rosemary)	19.28 $\pm$ 3.00
Caffeic acid (mg/g rosemary)	0.28 $\pm$ 0.14

previous studies that have found that NADESs composed with organic acids tend to have a higher polarity (Dai et al., 2013b). In addition Dai et al. (2013b) reported that NADESs with amino acids and pure-sugar based, showed a polarity values closer to water (44.81 kcal mol<sup>-1</sup>), and finally, both sugar and polyalcohol based NADESs are less polar, with polarity values closer to the ones for methanol (51.89 kcal mol<sup>-1</sup>) and ethanol (52.36 kcal mol<sup>-1</sup>) (Dai et al., 2013b).

The polarities of NADESs are dependent on their composition and the character of its components, as well as on the amount of water present. Experimental studies previously reported by Craveiro et al. have explored the influence that the presence of water could have in shifting the polarity of the NADESs, showing that different water contents for the same NADESs result in small changes in the ENR value, such that the higher the water amount, the higher the polarity (Craveiro et al., 2016).

It was observed that viscosity is also dependent on the composition of the NADESs (Table 2). At 40°C, the NADESs that exhibit higher viscosity are those made with glycerol, being the highest value obtained for Ca:Gly (1:1). NADES viscosity decreases with increasing temperature and increasing water content (Liu et al., 2018), and the NADESs studied in this work show the same behavior. NADES viscosity influences the extraction efficiency, as it affects mass diffusion of the plant material and the NADES, so that NADESs presenting higher viscosities can yield lower extraction efficiencies.

## 3.2 Extract characterization

A Soxhlet extraction using a traditional organic solvent, methanol, was used to characterize the extract in terms of TPC and to quantify the four individual target compounds. The results obtained are presented in Table 3.

As can be observed (Table 3) the compounds rosmarinic acid, carnosol, carnosic acid, and caffeic acid amount to ~80% of the total amount of phenolic compounds in rosemary.

## 3.3 Extraction of bioactive compounds from rosemary leaves

### 3.3.1 NADES screening

Previously characterized NADESs were used to extract the same bioactive compounds to compare the results. The extraction conditions for NADESs were a S:L ratio of 1:20 at a temperature of 40°C for a period of 60 min. Furthermore, the extractions were performed using HSE and UAE. To evaluate the extraction efficiency of the four main compounds, rosmarinic acid, carnosol, carnosic acid, and caffeic acid, HPLC analysis was used to identify and quantify the target compounds. The HPLC results (Table 4) showed that the UAE method increases extraction efficiency of when compared with HSE. This is also in agreement with previously reported results that adopt this method for the extraction of phenolic compounds (Dai et al., 2013c; Radošević et al., 2016). The exception was system T:Gly (1:30), which revealed a higher quantity extracted of carnosol in HSE, the only compound detected in the extract, although it had a very low value compared to the other NADESs.

The NADES with the highest extraction efficiency was Me:La (1:2), as it extracted all compounds of interest with the highest yields. That is probably due to the composition of this NADES; menthol and lactic acid have different polarities, making the character of this system more amphiphilic. In fact, regarding the polarity results on Figure 1, Me:La (1:2) can be considered a NADES with low polarity. As noted, organic acid-based NADESs tend to have a higher polarity, and the alcohol-based ones are naturally less polar. In addition, this NADES has higher extraction yield than conventional extraction with Soxhlet.

NADES Ca:Gly (1:1) was discarded, as it exhibits low extraction yields. This system has a high viscosity, and as such, the mass transfer was compromised. Systems such as T:Gly (1:30) present lower viscosities but also did not show an extraction ability for the compounds of interest. All of these systems have glycerol in their composition, which can be responsible for their high viscosity (Table 2).

Taking into account all of the tested NADESs, the one that was able to extract all the target compounds was La:Glu (5:1) with either of the extraction techniques tested but rendering better results in UAE. Menthol-based NADESs could extract a higher concentration of the compounds, highlighting Me:La (1:2) with a strong input using UAE. Despite both, Me:Lau (2:1) and Me:My (8:1) reaching an excellent total extraction yield, these systems were not able to extract rosmarinic acid.

### 3.3.2 Optimization of single-phase NADES extraction

The previous results made it possible to verify that the system that presented the higher extraction yield in terms of concentration of all the compounds was Me:La (1:2). However, the fact that the other menthol-based NADESs do not extract rosmarinic acid was very important for choosing the

**TABLE 4** Extraction amount of rosmarinic acid, carnosol, carnosic acid, and caffeic acid (mg/g rosemary), extracted with different NADESs under the same extraction conditions, S:L ratio of 1:20, 40°C, and 60 min, using two different techniques HSE and UAE. Results are expressed as mean  $\pm$  SD. Statistically significant differences between the effect of the HSE and UAE using NADESs are represented by letters. Different letters indicate significant differences within each extraction technique.

Systems	HSE					UAE				
	Rosmarinic acid	Carnosol	Carnosic acid	Caffeic acid	Total	Rosmarinic acid	Carnosol	Carnosic acid	Caffeic acid	Total
La:Glu (5:1)	0.21 $\pm$ 0.07 <sup>a</sup>	0.32 $\pm$ 0.06 <sup>a</sup>	0.63 $\pm$ 0.07 <sup>a</sup>	0.14 $\pm$ 0.05 <sup>a</sup>	1.30 $\pm$ 0.22	0.28 $\pm$ 0.01 <sup>a</sup>	0.46 $\pm$ 0.08 <sup>a</sup>	1.36 $\pm$ 0.47 <sup>a</sup>	0.16 $\pm$ 0.04 <sup>a</sup>	2.26 $\pm$ 0.54
B:Gly (1:2)	n.d.	0.20 $\pm$ 0.09 <sup>a</sup>	n.d.	n.d.	0.20 $\pm$ 0.09	n.d.	0.33 $\pm$ 0.07 <sup>a</sup>	n.d.	n.d.	0.33 $\pm$ 0.07
T:Gly (1:30)	n.d.	0.31 $\pm$ 0.22 <sup>a</sup>	n.d.	n.d.	0.31 $\pm$ 0.22	n.d.	0.10 $\pm$ 0.01 <sup>a</sup>	n.d.	n.d.	0.10 $\pm$ 0.01
Me:My (8:1)	n.d.	0.59 $\pm$ 0.21 <sup>a</sup>	1.03 $\pm$ 0.57 <sup>a</sup>	n.d.	1.62 $\pm$ 1.31	n.d.	1.75 $\pm$ 0.27 <sup>ab</sup>	6.61 $\pm$ 1.33 <sup>b</sup>	n.d.	8.36 $\pm$ 3.44
Me:La (1:2)	0.77 $\pm$ 0.02 <sup>b</sup>	n.d.	0.63 $\pm$ 0.05 <sup>a</sup>	n.d.	1.40 $\pm$ 0.10	0.83 $\pm$ 0.06 <sup>ab</sup>	4.87 $\pm$ 2.25 <sup>bc</sup>	11.23 $\pm$ 0.74 <sup>c</sup>	0.46 $\pm$ 0.01 <sup>a</sup>	17.39 $\pm$ 5.00
Me:Lau (2:1)	n.d.	0.39 $\pm$ 0.03 <sup>a</sup>	6.72 $\pm$ 0.45 <sup>b</sup>	n.d.	7.11 $\pm$ 4.48	n.d.	1.57 $\pm$ 0.80 <sup>a</sup>	8.26 $\pm$ 0.21 <sup>b</sup>	n.d.	9.83 $\pm$ 4.73
La:P (3:1)	0.23 $\pm$ 0.01 <sup>a</sup>	n.d.	n.d.	n.d.	0.23 $\pm$ 0.01	0.22 $\pm$ 0.02 <sup>a</sup>	0.99 $\pm$ 0.22 <sup>a</sup>	2.27 $\pm$ 0.37 <sup>a</sup>	n.d.	3.48 $\pm$ 1.04
La:B (2:1)	0.16 $\pm$ 0.00 <sup>a</sup>	n.d.	n.d.	n.d.	0.16 $\pm$ 0.00	0.17 $\pm$ 0.00 <sup>ad</sup>	0.86 $\pm$ 0.10 <sup>ab</sup>	2.07 $\pm$ 0.19 <sup>a</sup>	n.d.	3.10 $\pm$ 0.96
B:EG (2:1)	0.19 $\pm$ 0.01 <sup>a</sup>	0.75 $\pm$ 0.11 <sup>a</sup>	n.d.	n.d.	0.94 $\pm$ 0.40	0.65 $\pm$ 0.44 <sup>ac</sup>	2.45 $\pm$ 0.17 <sup>abc</sup>	0.63 $\pm$ 0.38 <sup>a</sup>	0.11 $\pm$ 0.06 <sup>a</sup>	3.84 $\pm$ 1.02
Ca:Gly	n.d.	n.d.	n.d.	n.d.	n.d.	n.d.	n.d.	n.d.	n.d.	n.d.

n.d., not detected.

most promising NADES to optimize the process. Here, it is important to emphasize that our objective is not only the higher extraction yield but also to be able to combine it with the selectivity of the NADES regarding to our target compounds. From these results, we decided to choose two polar NADESs (La:Glu (5:1) and La:P (3:1)) and two nonpolar NADESs (Me:Lau (2:1) and Me:My (8:1)) for testing.

To study the influence of the S:L ratio in the extraction of these four compounds from rosemary, several extractions were performed, with S:L ratios of 1:20, 1:30, and 1:40. Extraction also varied, from 30 to 60 min of extraction, in mg of compound/g of rosemary.

Table 5 shows the concentration, in mg/g rosemary, of each compound of interest from rosemary, extracted using NADESs referred above, two polar systems (La:Glu (5:1) and P:La (1:3)), and two nonpolar systems (Me:Lau (2:1) and Me:My (8:1)), obtained from HPLC analysis.

Only La:Glu (5:1) and P:La (1:3) of the chosen NADESs were able to extract rosmarinic acid, which is in agreement with the previous data, related to their polarity. In Table 5, it is observed that in the extractions performed for 30 min, the yield of rosmarinic acid is lower. As Bajkacz et al. showed, longer extraction times tended to favor the extraction of polyphenols. Therefore, it is to be expected that at higher

temperatures, NADES viscosity will decrease, which promotes mass transfer, facilitating the migration of the species into the solvent. This yield is also dependent on the S:L ratio from 1:20 to 1:40, with a higher rosmarinic acid extraction yield for 1:40. Because the enhanced solubilization capacity in the extraction of the compounds of interest is influenced by the level of solvent penetration into the system matrix, the penetration tends to be more effective when the density of the solvent is lower. It is interesting to note that rosmarinic acid is not extracted by the menthol-based NADES due to its polarity.

The compound carnosol is extracted by all tested NADESs, and the higher extraction yields are obtained when using Me:Lau (2:1) and Me:My (8:1). This may be due to favorable interactions established between the NADES and carnosol and to more compatible polarities. Considering extraction time and S:L ratio, extraction yields are higher for 30 min and for a S:L of 1:20.

Carnosic acid extraction shows the same tendency as carnosol, as well as being extracted by all the NADESs under study, but the higher extraction yields are also obtained by menthol-based NADESs that have lower polarities. Due to their molecular similarity, carnosic acid and carnosol have close relative solubilities. According to Wojciechowski and his

**TABLE 5** Effects of UAE extraction time (30 and 60 min) and S:L ratio (1:20, 1:30, and 1:40) on the extracted content of each compound of interest from rosemary: rosmarinic acid, carnosol, carnosic acid, and caffeic acid (in mg of compound/g of rosemary) at 40°C. The results are expressed as mean  $\pm$  SD. Statistically significant differences between the ratios (1:20, 1:30, and 1:40) in each system are represented by letters. Different letters indicate significant differences within each system.

Systems/Time			40°C		
			1:20	1:30	1:40
La:Glu (5:1)	30 min	Rosmarinic acid	0.20 $\pm$ 0.08 <sup>a</sup>	0.17 $\pm$ 0.09 <sup>a</sup>	0.04 $\pm$ 0.01 <sup>a</sup>
		Carnosol	0.84 $\pm$ 0.01 <sup>a</sup>	0.58 $\pm$ 0.13 <sup>a</sup>	0.81 $\pm$ 0.03 <sup>a</sup>
		Carnosic acid	3.81 $\pm$ 1.92 <sup>a</sup>	2.99 $\pm$ 1.32 <sup>a</sup>	2.69 $\pm$ 0.26 <sup>a</sup>
		Caffeic acid	n.d.	n.d.	n.d.
	60 min	Rosmarinic acid	0.29 $\pm$ 0.08 <sup>a</sup>	0.37 $\pm$ 0.06 <sup>b</sup>	0.38 $\pm$ 0.21 <sup>b</sup>
		Carnosol	0.65 $\pm$ 0.12 <sup>a</sup>	0.78 $\pm$ 0.01 <sup>a</sup>	1.05 $\pm$ 0.15 <sup>a</sup>
		Carnosic acid	2.78 $\pm$ 0.70 <sup>a</sup>	4.41 $\pm$ 0.73 <sup>a</sup>	4.76 $\pm$ 0.403 <sup>a</sup>
		Caffeic acid	0.16 $\pm$ 0.04 <sup>a</sup>	0.08 $\pm$ 0.01 <sup>a</sup>	n.d.
La:P (3:1)	30 min	Rosmarinic acid	0.13 $\pm$ 0.08 <sup>a</sup>	0.07 $\pm$ 0.05 <sup>a</sup>	0.28 $\pm$ 0.15 <sup>b</sup>
		Carnosol	0.60 $\pm$ 0.02 <sup>a</sup>	n.d.	0.79 $\pm$ 0.20 <sup>a</sup>
		Carnosic acid	2.63 $\pm$ 0.39 <sup>a</sup>	1.67 $\pm$ 0.21 <sup>a</sup>	3.20 $\pm$ 0.18 <sup>a</sup>
		Caffeic acid	n.d.	n.d.	n.d.
	60 min	Rosmarinic acid	0.23 $\pm$ 0.02 <sup>a</sup>	0.24 $\pm$ 0.16 <sup>ab</sup>	0.38 $\pm$ 0.04 <sup>b</sup>
		Carnosol	0.99 $\pm$ 0.22 <sup>a</sup>	0.80 $\pm$ 0.41 <sup>a</sup>	1.51 $\pm$ 0.21 <sup>a</sup>
		Carnosic acid	2.27 $\pm$ 0.38 <sup>a</sup>	4.75 $\pm$ 2.39 <sup>a</sup>	4.51 $\pm$ 0.91 <sup>a</sup>
		Caffeic acid	n.d.	0.03 $\pm$ 0.01 <sup>b</sup>	n.d.
Me:Lau (2:1)	30 min	Rosmarinic acid	n.d.	n.d.	n.d.
		Carnosol	1.99 $\pm$ 0.10 <sup>b</sup>	1.42 $\pm$ 0.33 <sup>abc</sup>	2.17 $\pm$ 0.44 <sup>ab</sup>
		Carnosic acid	6.66 $\pm$ 1.90 <sup>ab</sup>	5.65 $\pm$ 2.24 <sup>ab</sup>	5.34 $\pm$ 1.52 <sup>a</sup>
		Caffeic acid	n.d.	n.d.	n.d.
	60 min	Rosmarinic acid	n.d.	n.d.	n.d.
		Carnosol	1.57 $\pm$ 0.80 <sup>ab</sup>	1.15 $\pm$ 0.26 <sup>ac</sup>	1.83 $\pm$ 0.34 <sup>ab</sup>
		Carnosic acid	6.72 $\pm$ 0.45 <sup>ab</sup>	4.44 $\pm$ 1.11 <sup>a</sup>	4.21 $\pm$ 0.91 <sup>a</sup>
		Caffeic acid	n.d.	n.d.	n.d.
Me:My (8:1)	30 min	Rosmarinic acid	n.d.	n.d.	n.d.
		Carnosol	1.21 $\pm$ 0.28 <sup>ab</sup>	1.09 $\pm$ 0.24 <sup>ac</sup>	1.22 $\pm$ 0.16 <sup>a</sup>
		Carnosic acid	6.26 $\pm$ 2.10 <sup>ab</sup>	7.52 $\pm$ 1.40 <sup>ab</sup>	6.57 $\pm$ 0.91 <sup>ab</sup>
		Caffeic acid	n.d.	n.d.	n.d.
	60 min	Rosmarinic acid	n.d.	n.d.	n.d.
		Carnosol	1.75 $\pm$ 0.27 <sup>b</sup>	1.05 $\pm$ 0.29 <sup>ac</sup>	0.92 $\pm$ 0.34 <sup>a</sup>
		Carnosic acid	6.61 $\pm$ 1.33 <sup>ab</sup>	4.87 $\pm$ 2.04 <sup>a</sup>	4.91 $\pm$ 1.67 <sup>a</sup>
		Caffeic acid	n.d.	n.d.	n.d.

n.d., not detected.

coworkers the relative solubilities of these biomolecules were lower after water addition, possibly due to their high level of hydrophobicity, which confirms these results (Wojciechowski et al., 2021).

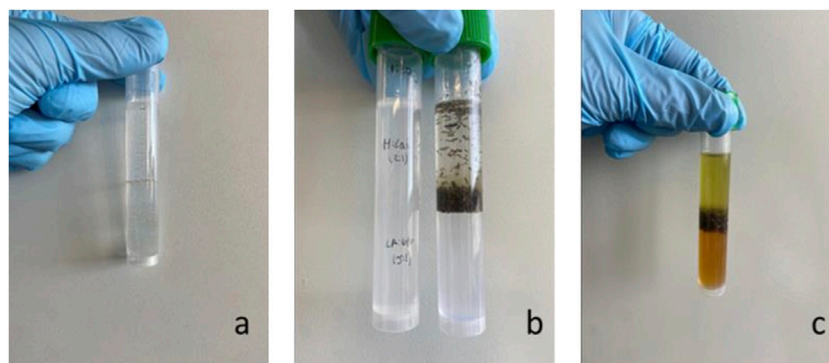
Caffeic acid is only extracted when with the use of lactic acid-based NADESs and for S:L values of 1:20 and 1:30.

Table 5 shows that it is possible for the tested NADES to present selectivity towards specific compounds, a very important feature when designing an extraction process.

### 3.3.3 Biphasic NADES extraction

The conclusions of this work demonstrate that NADESs exhibit extraction selectivity. Hence, a different extraction strategy was tested and explored. By designing a NADES biphasic extraction system, it is possible to promote extraction efficiency and the further separation of compounds with different polarities (Tang and Row, 2020). Identifying the best choice of NADESs for each phase is a goal of this approach, where the miscibility between the two NADES phases should not occur, as



**FIGURE 2**

Biphasic system with nonpolar and polar NADESs (A); biphasic system with nonpolar and polar NADESs before extraction (B) and after extraction (C). System represented: Me:Lau (2:1) on top and La:Glu (5:1) below.

seen in **Figure 2A**. This is made possible by combining NADESs with different polarities.

For this strategy, two polar systems (La:Glu (5:1) and P:La (1:3)) and two nonpolar systems (Me:Lau (2:1) and Me:My (8:1)) were chosen for the optimization of the biphasic UAE experiments. The extraction efficiencies of rosmarinic acid, carnosol, carnosic acid, and caffeic acid were tested under different S:L ratios at two temperatures (40°C and 60°C) over 60 min. The biphasic systems under study were combinations of the four NADESs, resulting in four combinations: 1) La:Glu (5:1)/Me:Lau (2:1), 2) La:Glu (5:1)/Me:My (8:1), 3) P:La (1:3)/Me:Lau (2:1) and 4) P:La (1:3)/Me:My (8:1).

Equal volumes of each NADES were used, and extractions were carried out. The two immiscible fractions were separated and analyzed individually. As can be observed in **Figure 2C**, a different color is observed in each phase of the extracts. This visual evidence shows that the different phases of the biphasic system are enriched in different compounds.

At 40°C, the most promising combination for extraction efficiency is system 1, with an S:L ratio of 1:30. This combination extracted 30% more of rosmarinic than the ratio 1:40 under the same conditions in the hydrophilic phase (La:Glu (5:1)).

Carnosic acid extracted in highest amount, with the highest values obtained in the nonpolar phase of the La:Glu systems (1 and 2),  $12.34 \pm 2.63$  and  $12.33 \pm 1.18$  mg/g rosemary, respectively. This compound exhibited similar behavior to carnosol concerning the S:L ratio, indicating higher concentrations at 1:30 and 1:40.

Carnosol was extracted at higher amounts in the following order of S:L ratio  $1:40 > 1:30 > 1:20$ , analyzing the nonpolar fraction at 40°C. Rosmarinic acid was not detected in any nonpolar phase of the four systems, independent of temperature or ratio. This confirms the extraction selectivity of biphasic NADESs.

Systems 3 and 4 showed the highest extraction yields of caffeic acid in the polar phase, when extracted with an S:L ratio of 1:20 (~0.12 mg/g rosemary), being the La:P (3:1), the most selective NADES towards this compound. When the P:La (1:3) was present in the combination of systems, caffeic acid showed a preferential tendency over the other solvents. In **Table 6** the influence that the S:L ratio has on the extractability of this compound can be seen, such that it is higher for higher S:L ratios. Systems 1 and 2 revealed a low selectivity for caffeic acid, as only trace amounts were detected in both phases. In systems 3 and 4, caffeic acid was not detected in the nonpolar phase.

At 60°C, La:Glu based systems (1 and 2) had the best results for the extraction of rosmarinic acid, ratio of 1:20.

Regarding carnosol, the systems that presented the highest yield were Me:My (8:1), with an S:L ratio of 1:30, from the nonpolar phase of the biphasic system 4 ( $2.59 \pm 0.25$  mg/g rosemary). However, compared with the results of Me:Lau (2:1) with an S:L ratio of 1:30 ( $2.38 \pm 0.25$  mg/g rosemary) and Me:My (8:1), with an S:L ratio of 1:40 ( $2.36 \pm 0.00$  mg/g rosemary), static analysis revealed no significant differences between these systems, being shown to be suitable for the extraction of carnosol.

At 60°C, the increased concentration of carnosic acid is evident, due to the nonpolar phase of all systems, in particular at the ratio 1:20.

Caffeic acid also showed an increased concentration with increased temperature. In general, the best results were observed for the ratio 1:20. Caffeic acid was not detected in the nonpolar phase of systems 3 and 4, similar to what occurred at 40°C.

The extraction efficiencies significantly changed with increased temperature, as can be seen in **Table 6**. An increase in the concentration of bioactive compounds was observed for all systems at increases in temperature from 40°C to 60°C. These results also suggest an S:L ratio of 1:20 tends to be the most suitable ratio in UAE biphasic extractions at 60°C.

**TABLE 6** Concentrations of rosmarinic acid, carnosol, carnosic acid, and caffeic acid (mg of compound/g rosemary) in the biphasic systems, varying the UAE S:L ratio (1:20, 1:30, and 1:40) and temperature (40°C and 60°C). Results are expressed as mean  $\pm$  SD. Statistically significant differences between the ratios (1:20, 1:30, and 1:40) in each system for each compound are represented by letters. Different letters indicate significant differences within each system.

Systems			40°C			60°C		
		Compounds	1:20	1:30	1:40	1:20	1:30	1:40
1	La:Glu (5:1)	Rosmarinic acid	0.21 $\pm$ 0.13 <sup>a</sup>	0.26 $\pm$ 0.10 <sup>a</sup>	0.08 $\pm$ 0.02 <sup>a</sup>	1.00 $\pm$ 0.12 <sup>a</sup>	0.58 $\pm$ 0.09 <sup>a</sup>	0.39 $\pm$ 0.06 <sup>a</sup>
		Carnosol	0.27 $\pm$ 0.12 <sup>a</sup>	n.d.	n.d.	0.32 $\pm$ 0.02 <sup>a</sup>	0.31 $\pm$ 0.06 <sup>a</sup>	0.26 $\pm$ 0.13 <sup>a</sup>
		Carnosic acid	0.33 $\pm$ 0.10 <sup>a</sup>	n.d.	0.63 $\pm$ 0.22 <sup>a</sup>	0.83 $\pm$ 0.11 <sup>a</sup>	0.52 $\pm$ 0.05 <sup>a</sup>	0.70 $\pm$ 0.15 <sup>a</sup>
		Caffeic acid	0.05 $\pm$ 0.00 <sup>a</sup>	0.06 $\pm$ 0.02 <sup>a</sup>	0.01 $\pm$ 0.00 <sup>a</sup>	0.26 $\pm$ 0.04 <sup>a</sup>	0.12 $\pm$ 0.02 <sup>a</sup>	0.07 $\pm$ 0.02 <sup>a</sup>
	Men:Lau (2:1)	Rosmarinic acid	n.d.	n.d.	n.d.	n.d.	n.d.	n.d.
		Carnosol	1.19 $\pm$ 0.34 <sup>b</sup>	1.70 $\pm$ 0.33 <sup>a</sup>	1.42 $\pm$ 0.37 <sup>a</sup>	2.30 $\pm$ 0.18 <sup>b</sup>	2.15 $\pm$ 0.04 <sup>b</sup>	2.24 $\pm$ 0.10 <sup>b</sup>
		Carnosic acid	7.71 $\pm$ 2.13 <sup>b</sup>	12.34 $\pm$ 2.63 <sup>b</sup>	9.60 $\pm$ 2.43 <sup>b</sup>	17.54 $\pm$ 1.88 <sup>b</sup>	14.49 $\pm$ 0.58 <sup>b</sup>	13.23 $\pm$ 0.42 <sup>b</sup>
		Caffeic acid	0.08 $\pm$ 0.00 <sup>b</sup>	0.01 $\pm$ 0.00 <sup>b</sup>	n.d.	0.09 $\pm$ 0.00 <sup>b</sup>	0.09 $\pm$ 0.00 <sup>a</sup>	n.d.
2	La:Glu (5:1)	Rosmarinic acid	0.18 $\pm$ 0.07 <sup>a</sup>	0.25 $\pm$ 0.03 <sup>a</sup>	0.17 $\pm$ 0.08 <sup>a</sup>	0.82 $\pm$ 0.12 <sup>a</sup>	0.51 $\pm$ 0.18 <sup>a</sup>	0.50 $\pm$ 0.14 <sup>b</sup>
		Carnosol	0.17 $\pm$ 0.04 <sup>a</sup>	n.d.	n.d.	0.34 $\pm$ 0.04 <sup>a</sup>	0.31 $\pm$ 0.04 <sup>a</sup>	0.35 $\pm$ 0.01 <sup>a</sup>
		Carnosic acid	0.40 $\pm$ 0.17 <sup>a</sup>	0.28 $\pm$ 0.00 <sup>a</sup>	0.99 $\pm$ 0.06 <sup>a</sup>	0.90 $\pm$ 0.10 <sup>a</sup>	0.91 $\pm$ 0.44 <sup>a</sup>	0.48 $\pm$ 0.18 <sup>a</sup>
		Caffeic acid	0.05 $\pm$ 0.00 <sup>ab</sup>	0.05 $\pm$ 0.00 <sup>a</sup>	0.01 $\pm$ 0.00 <sup>a</sup>	0.19 $\pm$ 0.04 <sup>c</sup>	0.11 $\pm$ 0.04 <sup>a</sup>	0.08 $\pm$ 0.01 <sup>a</sup>
	Me:My (8:1)	Rosmarinic acid	n.d.	n.d.	n.d.	n.d.	n.d.	n.d.
		Carnosol	1.04 $\pm$ 0.05 <sup>b</sup>	1.65 $\pm$ 0.12 <sup>a</sup>	1.73 $\pm$ 0.27 <sup>a</sup>	2.23 $\pm$ 0.02 <sup>b</sup>	2.03 $\pm$ 0.11 <sup>b</sup>	2.36 $\pm$ 0.08 <sup>b</sup>
		Carnosic acid	5.99 $\pm$ 0.59 <sup>b</sup>	12.33 $\pm$ 1.18 <sup>b</sup>	11.88 $\pm$ 2.24 <sup>b</sup>	16.68 $\pm$ 0.48 <sup>b</sup>	14.48 $\pm$ 0.33 <sup>b</sup>	12.47 $\pm$ 0.57 <sup>b</sup>
		Caffeic acid	0.07 $\pm$ 0.02 <sup>ab</sup>	0.06 $\pm$ 0.01 <sup>a</sup>	0.03 $\pm$ 0.01 <sup>a</sup>	0.20 $\pm$ 0.02 <sup>ac</sup>	0.09 $\pm$ 0.00 <sup>a</sup>	0.12 $\pm$ 0.0 <sup>a</sup>
3	La:P (3:1)	Rosmarinic acid	0.19 $\pm$ 0.12 <sup>a</sup>	0.08 $\pm$ 0.07 <sup>b</sup>	0.15 $\pm$ 0.09 <sup>a</sup>	0.41 $\pm$ 0.05 <sup>b</sup>	0.51 $\pm$ 0.16 <sup>a</sup>	0.17 $\pm$ 0.09 <sup>c</sup>
		Carnosol	0.60 $\pm$ 0.03 <sup>ab</sup>	0.53 $\pm$ 0.17 <sup>b</sup>	0.66 $\pm$ 0.36 <sup>b</sup>	1.26 $\pm$ 0.07 <sup>bc</sup>	1.05 $\pm$ 0.20 <sup>bc</sup>	1.29 $\pm$ 0.20 <sup>bc</sup>
		Carnosic acid	0.81 $\pm$ 0.00 <sup>a</sup>	0.95 $\pm$ 0.42 <sup>a</sup>	0.90 $\pm$ 0.11 <sup>a</sup>	2.34 $\pm$ 0.05 <sup>a</sup>	2.24 $\pm$ 0.29 <sup>abc</sup>	1.30 $\pm$ 0.39 <sup>a</sup>
		Caffeic acid	0.12 $\pm$ 0.02 <sup>bc</sup>	0.06 $\pm$ 0.02 <sup>a</sup>	0.03 $\pm$ 0.00 <sup>ab</sup>	0.33 $\pm$ 0.01 <sup>cd</sup>	0.20 $\pm$ 0.01 <sup>b</sup>	0.12 $\pm$ 0.06 <sup>a</sup>
	Men:Lau (2:1)	Rosmarinic acid	n.d.	n.d.	n.d.	n.d.	n.d.	n.d.
		Carnosol	0.95 $\pm$ 0.15 <sup>b</sup>	0.95 $\pm$ 0.30 <sup>b</sup>	1.13 $\pm$ 0.23 <sup>abc</sup>	2.32 $\pm$ 0.03 <sup>b</sup>	2.38 $\pm$ 0.25 <sup>bd</sup>	2.02 $\pm$ 0.05 <sup>b</sup>
		Carnosic acid	5.29 $\pm$ 1.16 <sup>b</sup>	6.02 $\pm$ 2.43 <sup>bc</sup>	7.21 $\pm$ 1.54 <sup>bc</sup>	15.18 $\pm$ 0.31 <sup>bc</sup>	15.84 $\pm$ 0.94 <sup>b</sup>	11.34 $\pm$ 0.21 <sup>bc</sup>
		Caffeic acid	n.d.	n.d.	n.d.	n.d.	n.d.	n.d.
4	La:P (3:1)	Rosmarinic acid	0.17 $\pm$ 0.07 <sup>a</sup>	0.10 $\pm$ 0.04 <sup>b</sup>	0.05 $\pm$ 0.02 <sup>a</sup>	0.35 $\pm$ 0.03 <sup>bc</sup>	0.38 $\pm$ 0.04 <sup>ab</sup>	0.13 $\pm$ 0.05 <sup>cd</sup>
		Carnosol	0.50 $\pm$ 0.04 <sup>ab</sup>	0.43 $\pm$ 0.02 <sup>bc</sup>	0.82 $\pm$ 0.25 <sup>b</sup>	1.09 $\pm$ 0.14 <sup>bc</sup>	1.13 $\pm$ 0.16 <sup>bc</sup>	1.21 $\pm$ 0.11 <sup>bc</sup>
		Carnosic acid	0.56 $\pm$ 0.06 <sup>a</sup>	0.92 $\pm$ 0.10 <sup>a</sup>	0.76 $\pm$ 0.12 <sup>a</sup>	1.99 $\pm$ 0.36 <sup>a</sup>	2.30 $\pm$ 0.08 <sup>abc</sup>	1.08 $\pm$ 0.14 <sup>ac</sup>
		Caffeic acid	0.11 $\pm$ 0.01 <sup>bc</sup>	0.06 $\pm$ 0.03 <sup>a</sup>	0.06 $\pm$ 0.01 <sup>b</sup>	0.18 $\pm$ 0.00 <sup>c</sup>	0.24 $\pm$ 0.05 <sup>bc</sup>	0.10 $\pm$ 0.01 <sup>a</sup>
	Me:My (8:1)	Rosmarinic acid	n.d.	n.d.	n.d.	n.d.	n.d.	n.d.
		Carnosol	0.85 $\pm$ 0.08 <sup>b</sup>	0.43 $\pm$ 0.02 <sup>b</sup>	0.82 $\pm$ 0.25 <sup>abc</sup>	2.16 $\pm$ 0.16 <sup>b</sup>	2.59 $\pm$ 0.25 <sup>bce</sup>	2.11 $\pm$ 0.21 <sup>b</sup>
		Carnosic acid	4.48 $\pm$ 0.72 <sup>bc</sup>	6.55 $\pm$ 0.24 <sup>bc</sup>	6.79 $\pm$ 0.51 <sup>bc</sup>	14.75 $\pm$ 1.30 <sup>bc</sup>	16.99 $\pm$ 1.05 <sup>bc</sup>	12.51 $\pm$ 0.51 <sup>b</sup>
		Caffeic acid	n.d.	n.d.	n.d.	n.d.	n.d.	n.d.

n.d., not detected.

In addition, all combinations showed selectivity, indicating that the bioactive compounds with variable polarity from rosemary were extracted selectively. Biphasic extractions of NADESs can not only extract with higher amounts of phenolic compounds but can also select compounds of different characters, based on their polarity. Compounds such as rosmarinic acid and caffeic acid were only extracted by nonpolar NADESs, while less polar compounds as carnosol and carnosic acid, were extracted in higher amounts by nonpolar NADESs.

### 3.4 Selectivity and partition coefficient

Partition separation processes are mainly used in the separation and purification of natural products. Both are based on same principle, which consists in the distribution of a solute immiscible compounds in two phases composed of a mixture of solvents. The selection of the ideal two-phase system is the key, which must ensure an adequate distribution of the solute between the two liquid phases. In this case, we investigate four combinations of two NADESs

TABLE 7 Partition coefficient ( $K$ ) of rosmarinic acid, carnosol, carnosic acid, and caffeic acid in each biphasic system under different ratio conditions (1:20, 1:30, and 1:40) and temperatures (40°C and 60°C).

Systems	Compounds	40°C			60°C		
		1:20	1:30	1:40	1:20	1:30	1:40
La:Glu (5:1)/Me:Lau (2:1)	Rosmarinic acid	0	0	0	0	0	0
	Carnosol	4.41	0	0	7.19	6.94	8.62
	Carnosic acid	23.36	0	2.25	21.13	27.87	18.90
	Caffeic acid	1.64	0.22	0.25	0.35	0.78	0
La:Glu (5:1)/Me:My (8:1)	Rosmarinic acid	0	0	0	0	0	0
	Carnosol	6.12	0	0	6.56	6.55	6.74
	Carnosic acid	14.98	44.04	12.00	18.53	15.91	25.98
	Caffeic acid	0.18	1.25	2.94	1.07	0.84	1.44
La:P (3:1)/Me:Lau (2:1)	Rosmarinic acid	0	0	0	0	0	0
	Carnosol	1.58	1.79	1.71	1.84	2.27	1.57
	Carnosic acid	6.53	6.34	8.01	6.49	7.07	8.72
	Caffeic acid	0	0	0	0	0	0
La:P (3:1)/Me:My (8:1)	Rosmarinic acid	0	0	0	0	0	0
	Carnosol	1.70	2.35	1.24	1.98	2.29	1.74
	Carnosic acid	8.00	7.12	8.93	7.41	7.39	11.58
	Caffeic acid	0	0	0	0	0	0

that are immiscible to study the selectivity of four compounds which present different polarities.

To study the selectivity of the compounds between the two phases, the partition coefficient ( $K$ ) was determined for each compound in the different systems (1–4), according to Eq. 2, for the different S:L ratios and temperatures.

$$K = \frac{[C]_{(nonpolar\ phase)}}{[C]_{(polar\ phase)}} \quad (2)$$

The results are presented in Table 7.

The higher the partition coefficient of a compound, the higher the concentration of that compound in the nonpolar NADES in regards to the polar. Carnosic acid is the compound that presents the highest partition coefficient, followed by carnosol. This was expected, according to the previous results of concentration obtained by HPLC and due to the hydrophobic character of both compounds. The most suitable system for efficient and recovery of carnosol and carnosic acid is the combination of La:Glu (5:1), with Me:Lau (2:1) or Me:My (8:1). Due to the polarity of rosmarinic acid, the partition coefficient is zero for all systems, revealing that all rosmarinic acid that was extracted using this approach remains in the hydrophilic phase. The same occurs with caffeic acid but only in the La:P (3:1)-based systems, although in La:Glu (5:1)-based systems, the partition coefficient of this compound present lower values, showing a more hydrophilic character. These results clearly show that biphasic systems based on La:P (3:1) are suitable for the

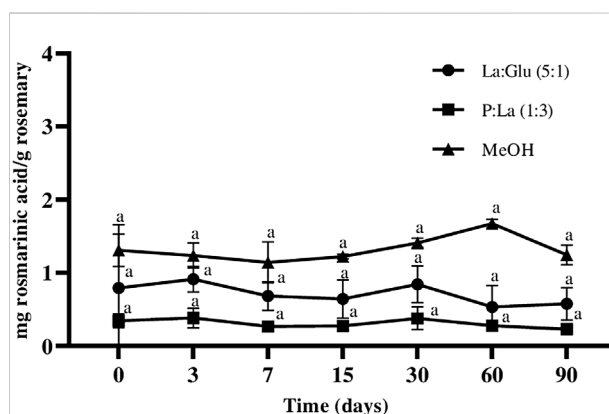


FIGURE 3

Influence of time on the content of rosmarinic acid extracted and kept in NADESs and MeOH. Values are the average of three independent extracts replicates  $\pm$ SD based on triplicate values. Statistically significant differences between the time points in each system are represented by letters. Different letters indicate significant differences within each system.

efficient and sustainable recovery of rosmarinic and caffeic acids and La:Glu (5:1)-based systems revealed the best results for carnosol and carnosic acid. This shows that the lower the polarity of the compound, the higher the partition coefficient. For temperature and S:L, the best results were achieved at higher temperatures (60°C) and lower S:L (1:30/1:40).

The use of NADES biphasic systems allows the design of an effective extraction strategy in which each phase is enriched

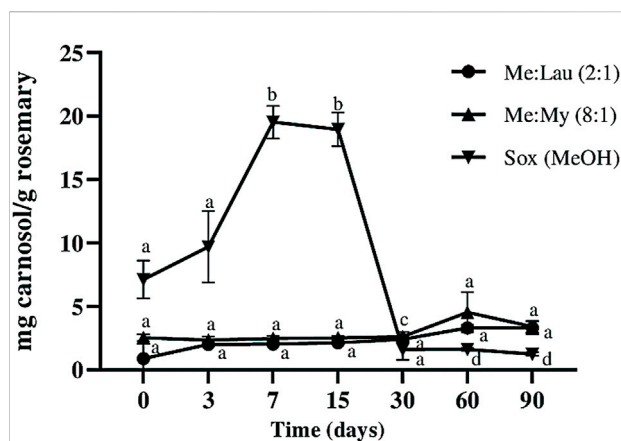


FIGURE 4

Influence of time on the extracted content of carnosol (C) in NADESs and methanol. Values are the average of three independent extracts replicates  $\pm$ SD based on triplicate values. Statistically significant differences between the time points in each system are represented by letters. Different letters indicate significant differences within each system.

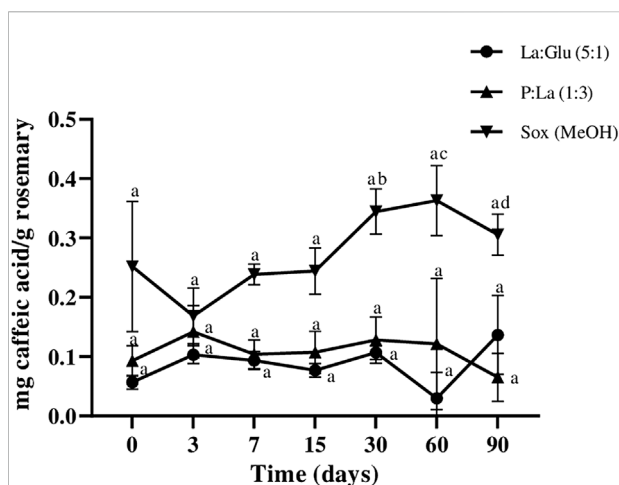


FIGURE 6

Influence of time on the extracted content of caffeic acid in NADESs and methanol. Values are the averages of three independent extract replicates  $\pm$ SD based on triplicate values. Statistically significant differences between the time points in each system are represented by letters. Different letters indicate significant differences within each system.

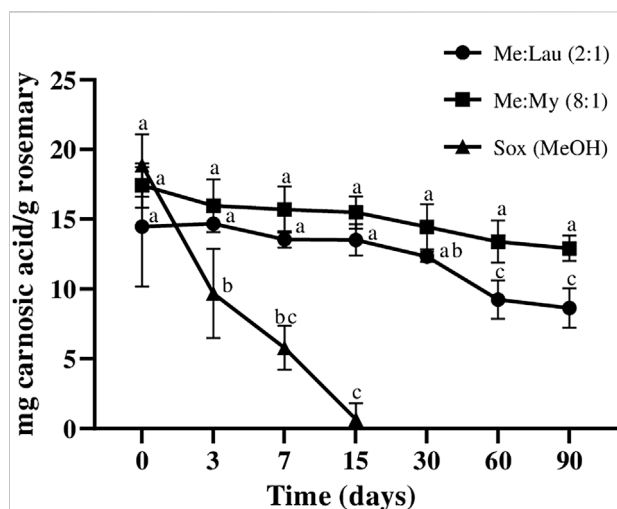


FIGURE 5

Influence of time on the extracted content of camosic acid (CA) in NADESs and methanol. Values are the average of three independent extracts replicates  $\pm$ SD based on triplicate values. Statistically significant differences between the time points in each system are represented by letters. Different letters indicate significant differences within each system.

in the bioactive compounds with different polarities. In a single step, it is possible to selectively extract the target compounds and to modify with the temperature and S:L ratio at the same time. This strategy allowed to demonstrate that it is possible to obtain a single phase with no traces of rosmarinic acid.

### 3.5 Stability tests

Recently, it has been hypothesized that NADESs can have a stabilizing role towards certain molecules such as phenolic compounds and increase their stability for longer periods of time without losing their antioxidant activity. To evaluate the effect of NADESs on the stability on the obtained rosemary extracts for long periods of time, HPLC analysis of each fraction of the biphasic system was carried out.

The biphasic systems used for this study, were system 1 and system 4, with an S:L ratio of 1:20 and 1:30, respectively, at 60°C and with extraction time of 60 min.

#### 3.5.1 Quantification of bioactive compounds—HPLC

Over time, the concentration of rosmarinic acid in the extracts of La:Glu (5:1), La:P (1:3), and MeOH showed small variations (Figure 3). However, statistical analysis demonstrates no significant differences between the values of each time point were verified. These results show that rosmarinic acid is stable in NADES La:Glu (5:1) and P:La (1:3), at least for 90 days. Additionally, extracts obtained with MeOH, were also stable during the 90 days. Rosmarinic acid was not detected on nonpolar phases, Me:Lau (2:1) and Me:My (8:1), respectively.

Carnosol is a derivative of carnosic acid when oxidized. This is a very common occurrence in plants under stress conditions. As a result, this may cause a strong decrease in carnosic acid and consequent accumulation of carnosol in the obtained extracts (Loussouarn et al., 2017). This can be correlated with the results obtained in this study. As we can observe in Figure 4 and Figure 5

there is a decrease in carnolic acid amount, and consequently an increase in carnosol. In the MeOH extracts this degradation was clearly more evident. At day 7, there was a loss of ~72% of the carnolic acid, which caused an increase of ~63% of carnosol (statistical difference  $p \leq 0.001$ ). Carnosol was not detected on La:Glu (5:1). The other NADESs showed a potential stabilizing ability for this compound, since its concentration remained constant during 90 days and no significant differences were verified by statistical analysis.

Carnolic acid content in the MeOH extract decreased over time, until it was not detected after 30 days (Figure 5), and after 15 days a decrease of almost 100% was already observed (statistical difference  $p \leq 0.0001$ ). The amount of carnolic acid remained stable in both Me:Lau (2:1) and Me:My (8:1) extracts after 15 days. In Me:My (8:1) remains stable until day 60 (no statistical differences were verified), on the other hand for Me:Lau (2:1), statistical analysis revealed a small difference after day 30 ( $p \leq 0.05$ ), maintained stable until day 90.

These NADESs showed to be appropriate for the stabilization of this bioactive compound. Carnolic acid was not detected on P:Lau (1:3) and in La:Glu (5:1) extracts, only a trace was detected, being nonsignificant when compared with the other systems.

Regarding caffeic acid content, Figure 6 shows that all extracts kept the compound stable for 90 days, except the one obtained with MeOH, which showed some fluctuations, as confirmed by statistical analysis. Thus suggests that the NADESs of P:Lau (1:3), La:Glu (5:1), and Me:Lau (2:1) provide good stability. However, the amounts of caffeic acid detected in these extracts were very low. Caffeic acid was not detected in Me:My (8:1).

Biphasic extracts of NADESs with different polarities had the ability to stabilize the bioactive compounds with the same character. In a general way, the four extracted bioactive compounds from rosemary under this study remained stable for at least 90 days with NADESs and presented a greater stability capacity than MeOH, in particular for carnolic acid.

The stabilization capacity of NADESs may have a direct association with viscosity. The viscosity of NADESs restricts the movement of molecules inside the extracts and allows more stable molecular interactions between the solvent and compounds, which prevents the degradation of the bioactive compounds extracted.

## 4 Conclusion

In this work, a methodology was proposed to use different NADESs as solvents to extract different compounds of interest from rosemary.

In the first approach, a screening of 10 NADESs at fixed extraction parameters was carried out. For comparison, conventional extractions using methanol were also performed. This study showed that NADESs composed of lactic acid (La:Glu (5:1) and P:Lau (1:3)) extracted higher amounts of bioactive phenolic compounds. In addition, Me:

La (1:2) was the best NADES for rosmarinic acid, carnosol, carnolic acid, and caffeic acid. extraction (S:L ratio of 1:20 at 40°C performed for 60 min). UAE showed an increase in extraction yield when compared to the extractions performed by heat and stirring.

In addition, the optimization of extraction parameters revealed that an extraction time of 60 min was more efficient in the extraction of phenolic compounds.

The studied NADESs showed selectivity, according to their polar or nonpolar character and affinity to the compounds to be extracted. For the extract of Me:Lau (2:1), carnolic acid and carnosol had the predominant affinities. Rosmarinic acid was not detected for this extract, which indicated the selectivity of this NADES for nonpolar compounds.

Therefore, taking advantage of NADES extraction selectivity, a new approach was tested—an extraction with two-phase systems, where two immiscible DESs are used for extraction, and each phase will selectively extract the compounds of interest. From the results, it was possible to conclude that the biphasic NADES system can effectively increase the extraction yield and select compounds based on their polarity. As bioactive compounds with different polarities were found in the extraction phases with opposite polarities; for example, rosmarinic acid was not extracted by nonpolar systems but was detected in polar ones. The four studied bioactive compounds present in rosemary and were identified in extracts from biphasic system composed by La:Glu (5:1)/Me:Lau (2:1), with an S:L ratio of 1:20 at 60°C. This shows that biphasic NADESs are efficient for the extraction of phenolic compounds from rosemary. The results also show that NADESs present selectivity towards specific compounds and that using a biphasic system composed of NADESs of different polarities allows the simultaneous selective extraction of different compounds, facilitating its additional separation.

Following the stability of the four compounds of interest over time, a higher stability is observed in the NADESs La:Glu (5:1), Me:Lau (2:1), La:P (1:3), and Me:My (8:1) relative to MeOH. These NADES extracts remained stable up to 3 months, which shows that the use of NADESs as extraction solvents may not require the separation of the solvent from the extract, as NADESs improve extract stability.

This extraction strategy presents advantages over the conventionally used extraction methods and can play a crucial role in industrial applications and when scaling-up the process is envisaged. The extracts obtained with NADESs present the advantages of being used directly without additional purification processes and without the addition of preservatives. This provides the extracts several benefits for further applications in the pharmaceutical, cosmetic, or food industry, according to the therapeutic properties of the compounds present in these extracts.



## Data availability statement

The raw data supporting the conclusions of this article will be made available by the authors, without undue reservation.

## Author contributions

CV, SR, and RC: conceptualization; CV and SR: methodology; SR: software (statistical analysis); CV and SR: writing—original draft preparation; SR, RC, and RD: writing—review and editing; SR, RC, AP, and RD: supervision. All authors have read and agree to the published version of the manuscript.

## Funding

This project has received funding from the European Research Council (ERC) under the European Union's Horizon 2020 research and innovation program, under grant agreement No ERC-2016-CoG 725034. This work was also supported by the Associate Laboratory for Green Chemistry-LAQV which is financed by national funds from FCT/MCTES (UID/QUI/50006/2019).

## References

- Albalawi, A., Alhasani, R. H. A., Biswas, L., Reilly, J., Akhtar, S., Shu, X., et al. (2018). Carnosic acid attenuates acrylamide-induced retinal toxicity in zebrafish embryos. *Exp. Eye Res.* 175, 103–114. doi:10.1016/j.exer.2018.06.018
- Ali, A., Chua, B. L., and Chow, Y. H. (2019). An insight into the extraction and fractionation technologies of the essential oils and bioactive compounds in *Rosmarinus officinalis* L.: Past, present and future. *TrAC Trends Anal. Chem.* 118, 338–351. doi:10.1016/j.trac.2019.05.040
- Aliebrahimi, S., Kouhsari, S. M., Arab, S. S., Shadboorestan, A., and Ostad, S. N. (2018). Phytochemicals, withaferin A and carnosol, overcome pancreatic cancer stem cells as c-Met inhibitors. *Biomed. Pharmacother.* 106, 1527–1536. doi:10.1016/j.biopha.2018.07.055
- Allegra, A., Tonacci, A., Pioggia, G., Musolino, C., and Gangemi, S. (2020). Anticancer activity of *rosmarinus officinalis* L.: Mechanisms of action and therapeutic potentials. *Nutrients* 12, 1739. doi:10.3390/nu12061739
- Andrade, J. M., Faustino, C., García, C., Ladeiras, D., Reis, C. P., Rijo, P., et al. (2018). *Rosmarinus officinalis* L.: An update review of its phytochemistry and biological activity. *Future Sci. OA* 4, FSO283. doi:10.4155/fsoa-2017-0124
- Bajkacz, S., and Adamek, J. (2018). Development of a method based on natural deep eutectic solvents for extraction of flavonoids from food samples. *Food Anal. Methods* 11, 1330–1344. doi:10.1007/s12161-017-1118-5
- Barbieri, J. B., Goltz, C., Batistão Cavalheiro, F., Theodoro Toci, A., Igarashi-Mafra, L., Mafra, M. R., et al. (2020). Deep eutectic solvents applied in the extraction and stabilization of rosemary (*Rosmarinus officinalis* L.) phenolic compounds. *Ind. Crops Prod.* 144, 112049. doi:10.1016/j.indcrop.2019.112049
- Birtic, S., Dussort, P., Pierre, F., Bily, A. C., and Roller, M. (2015). Carnosic acid. *Phytochemistry* 115, 9–19. doi:10.1016/j.phytochem.2014.12.026
- Borrás-Linares, I., Stojanović, Z., Quirantes-Piné, R., Arráez-Román, D., Švarc-Gajić, J., Fernández-Gutiérrez, A., et al. (2014). *Rosmarinus officinalis* leaves as a natural source of bioactive compounds. *Int. J. Mol. Sci.* 15, 20585–20606. doi:10.3390/ijms151120585
- Bourhia, M., Laasri, F. E., Aourik, H., Boukhris, A., Ullah, R., Bari, A., et al. (2019/2019). Antioxidant and antiproliferative activities of bioactive compounds

## Acknowledgments

Authors would like to thank to the company Aromáticas Vivas, Ltd. For kindly supply the plant material to this research and to Hayashibara Co., Ltd. for kindly providing trehalose samples used in eutectic mixtures. HPLC data obtained by the Analysis Laboratory LAQV REQUIMTE–Chemistry department, FCT NOVA–Portugal.

## Conflict of interest

The authors declare that the research was conducted in the absence of any commercial or financial relationships that could be construed as a potential conflict of interest.

## Publisher's note

All claims expressed in this article are solely those of the authors and do not necessarily represent those of their affiliated organizations, or those of the publisher, the editors, and the reviewers. Any product that may be evaluated in this article, or claim that may be made by its manufacturer, is not guaranteed or endorsed by the publisher.

contained in *rosmarinus officinalis* used in the mediterranean diet. *Evidence-Based Complementary Altern. Med.*, 2019: 1–7. doi:10.1155/2019/7623830

Calderón-Oliver, M., and Ponce-Alquicira, E. (2021). Environmentally friendly techniques and their comparison in the extraction of natural antioxidants from green tea, rosemary, clove, and oregano. *Molecules* 26, 1869. doi:10.3390/molecules26071869

Cao, J., Chen, L., Li, M., Cao, F., Zhao, L., Su, E., et al. (2018). Two-phase systems developed with hydrophilic and hydrophobic deep eutectic solvents for simultaneously extracting various bioactive compounds with different polarities. *Green Chem.* 20, 1879–1886. doi:10.1039/c7gc03820h

Chemat, F., Rombaut, N., Pierson, J. T., and Bily, A. (2015). “Green extraction: From concepts to research, education, and economical opportunities,” in *Green extraction of natural products: Theory and practice*. Editors F. Chemat and J. Strube (Weinheim, Germany: Wiley VCH), 1–36.

Craveiro, R., Aroso, I., Flammia, V., Carvalho, T., Viciosa, M. T., Dionísio, M., et al. (2016). Properties and thermal behavior of natural deep eutectic solvents. *J. Mol. Liq.* 215, 534–540. doi:10.1016/j.molliq.2016.01.038

Cui, H. Y., Zhang, X. J., Yang, Y., Zhang, C., Zhu, C. H., Miao, J. Y., et al. (2018). Rosmarinic acid elicits neuroprotection in ischemic stroke via Nrf2 and heme oxygenase 1 signaling. *Neural Regen. Res.* 13, 2119. doi:10.4103/1673-5374.241463

Cunha, S. C., and Fernandes, J. O. (2018). Extraction techniques with deep eutectic solvents. *TrAC Trends Anal. Chem.* 105, 225–239. doi:10.1016/j.trac.2018.05.001

Dai, Y., van Spronsen, J., Witkamp, G. J., Verpoorte, R., and Choi, Y. H. (2013b). Natural deep eutectic solvents as new potential media for green technology. *Anal. Chim. Acta* X. 766, 61–68. doi:10.1016/j.aca.2012.12.019

Dai, Y., Van Spronsen, J., and Witkamp, G. (2013a). Natural deep eutectic solvents as new potential media for green technology. *Anal. Chim. Acta* 766, 61–68. doi:10.1016/j.aca.2012.12.019

Dai, Y., Verpoorte, R., and Choi, Y. H. (2014). Natural deep eutectic solvents providing enhanced stability of natural colorants from safflower (*Carthamus tinctorius*). *Food Chem.* x. 159, 116–121. doi:10.1016/j.foodchem.2014.02.155

- Dai, Y., Witkamp, G. J., Verpoorte, R., and Choi, Y. H. (2013c). Natural deep eutectic solvents as a new extraction media for phenolic metabolites in carthamus tinctorius L. *Anal. Chem.* 85, 6272–6278. doi:10.1021/ac400432p
- Ercan, P., and El, S. N. (2018). Bioaccessibility and inhibitory effects on digestive enzymes of carnosic acid in sage and rosemary. *Int. J. Biol. Macromol.* 115, 933–939. doi:10.1016/j.jbiomac.2018.04.139
- González-Minero, F., Bravo-Días, L., and Ayala-Gómez, A. (2020). *Rosmarinus officinalis* L. (Rosemary): An ancient plant with uses in personal healthcare and cosmetics. *Cosmetics* 7, 77. doi:10.3390/cosmetics7040077
- Hansen, B. B., Spittle, S., Chen, B., Poe, D., Zhang, Y., Klein, J. M., et al. (2021). Deep eutectic solvents: A review of fundamentals and applications. *Chem. Rev.* 121, 1232–1285. doi:10.1021/acs.chemrev.0c00385
- Huang, X., Xi, Y., Pan, Q., Mao, Z., Zhang, R., Ma, X., et al. (2018). Caffeic acid protects against IL-1 $\beta$ -induced inflammatory responses and cartilage degradation in articular chondrocytes. *Biomed. Pharmacother.* 107, 433–439. doi:10.1016/j.biopha.2018.07.161
- Liu, Y., Friesen, J. B., McAlpine, J. B., Lankin, D. C., Chen, S. N., Pauli, G. F., et al. (2018). Natural deep eutectic solvents: Properties, applications, and perspectives. *J. Nat. Prod.* 81, 679–690. doi:10.1021/acs.jnatprod.7b00945
- Loussouarn, M., Krieger-Liszka, A., Svilar, L., Bily, A., Birtic, S., Havaux, M., et al. (2017). Carnosic acid and carnosol, two major antioxidants of rosemary, act through different mechanisms. *Plant Physiol.* 175, 1381–1394. doi:10.1104/pp.17.01183
- Ma, Z. J., Yan, H., Wang, Y. J., Yang, Y., Li, X. B., Shi, A. C., et al. (2018). Proteomics analysis demonstrating rosmarinic acid suppresses cell growth by blocking the glycolytic pathway in human HepG2 cells. *Biomed. Pharmacother.* 105, 334–349. doi:10.1016/j.biopha.2018.05.129
- Makhathini, K. B., Mabandla, M. V., and Daniels, W. M. U. (2018). Rosmarinic acid reverses the deleterious effects of repetitive stress and tat protein. *Behav. Brain Res.* 353, 203–209. doi:10.1016/j.bbr.2018.07.010
- Monteiro Espindola, K. M., Ferreira, R. G., Mosquera Narvaez, L. E., Rocha Silva Rosario, A. C., Machado Da Silva, A. H., Bispo Silva, A. G., et al. (2019). Chemical and pharmacological aspects of caffeic acid and its activity in hepatocarcinoma. *Front. Oncol.* 9, 541. doi:10.3389/fonc.2019.00541
- Neves, J. A., Neves, J. A., and Oliveira, R. de C. M. (2018). Pharmacological and biotechnological advances with *Rosmarinus officinalis* L. *Expert Opin. Ther. Pat.* 28, 399–413. doi:10.1080/13543776.2018.1459570
- Oliveira, J. R., Esteves, S., and Camargo, A. (2019). *Rosmarinus officinalis* L. (rosemary) as therapeutic and prophylactic agent. *J. Biomed. Sci.* 8, 5. doi:10.1186/s12929-019-0499-8
- Oliviero, F., Scanu, A., Zamudio-Cuevas, Y., Punzi, L., and Spinella, P. (2018). Anti-inflammatory effects of polyphenols in arthritis. *J. Sci. Food Agric.* 98, 1653–1659. doi:10.1002/jsfa.8664
- Paiva, A., Craveiro, R., Aroso, I., Martins, M., Reis, R. L., Duarte, A. R. C., et al. (2014). Natural deep eutectic solvents - solvents for the 21st century. *ACS Sustain. Chem. Eng.* 2, 1063–1071. doi:10.1021/sc500096j
- Radošević, K., Čurko, N., Gaurina Srček, V., Cvjetko Bubalo, M., Tomašević, M., Kovačević Ganić, K., et al. (2016). Natural deep eutectic solvents as beneficial extractants for enhancement of plant extracts bioactivity. *LWT - Food Sci. Technol.* 73, 45–51. doi:10.1016/j.lwt.2016.05.037
- Radziejewska, I., Supruniuk, K., Nazaruk, J., Karna, E., Popławska, B., Bielawska, A., et al. (2018). Rosmarinic acid influences collagen, MMPs, TIMPs, glycosylation and MUC1 in CRL-1739 gastric cancer cell line. *Biomed. Pharmacother.* 107, 397–407. doi:10.1016/j.biopha.2018.07.123
- Rahbardo, M. G., and Hosseinzadeh, H. (2020). Therapeutic effects of rosemary (*Rosmarinus officinalis* L.) and its active constituents on nervous system disorders. *Iran. J. Basic Med. Sci.* 23, 1100–1112. doi:10.22038/ijbms.2020.45269.10541
- Ramírez, J., Gilardoni, G., Ramón, E., Tosi, S., Picco, A. M., Bicchì, C., et al. (2018). Phytochemical study of the ecuadorian species lepechinia mutica (Benth.) epling and high antifungal activity of carnosol against pyricularia oryzae. *Pharmaceuticals* 11, 33. doi:10.3390/ph11020033
- Reichardt, C. (1994). Solvatochromic dyes as solvent polarity indicators. *Chem. Rev.* 94, 2319–2358. doi:10.1021/cr00032a005
- Ruesgas-Ramón, M., Figueroa-Espinoza, M. C., and Durand, E. (2017). Application of deep eutectic solvents (DES) for phenolic compounds extraction: Overview, challenges, and opportunities. *J. Agric. Food Chem.* 65, 3591–3601. doi:10.1021/acs.jafc.7b01054
- Samarghandian, S., Borji, A., and Farkhondeh, T. (2017). Evaluation of antidiabetic activity of carnosol (phenolic diterpene in rosemary) in streptozotocin-induced diabetic rats. *Cardiovasc. Hematol. Disord. Drug Targets* 17, 11–17. doi:10.2174/1871529X16666161229154910
- Song, H. M., Li, X., Liu, Y. Y., Lu, W. P., Cui, Z. H., Zhou, L., et al. (2018). Carnosic acid protects mice from high-fat diet-induced NAFLD by regulating MARCKS. *Int. J. Mol. Med.* 42, 193–207. doi:10.3892/ijmm.2018.3593
- Stanojević, L. P., Todorović, Z. B., Stanojević, K. S., Stanojević, J. S., Troter, D. Z., Nikolić, L. B., et al. (2021). The influence of natural deep eutectic solvent glycine on the yield, chemical composition and antioxidative activity of essential oil from rosemary (*Rosmarinus officinalis* L.) leaves. *J. Essent. Oil Res.* 33, 247–255. doi:10.1080/10412905.2021.1873867
- Tang, W., and Row, K. H. (2020). Design and evaluation of polarity controlled and recyclable deep eutectic solvent based biphasic system for the polarity driven extraction and separation of compounds. *J. Clean. Prod.* 268, 122306. doi:10.1016/j.jclepro.2020.122306
- Tsukamoto, Y., Ikeda, S., Uwai, K., Taguchi, R., Chayama, K., Sakaguchi, T., et al. (2018). Rosmarinic acid is a novel inhibitor for Hepatitis B virus replication targeting viral epsilon RNA-polymerase interaction. *PLoS One* 13, e0197664. doi:10.1371/journal.pone.0197664
- Van Osch, D. J. G. P., Zubeir, L. F., Van Den Bruinhorst, A., Rocha, M. A. A., and Kroon, M. C. (2015). Hydrophobic deep eutectic solvents as water-immiscible extractants. *Green Chem.* 17, 4518–4521. doi:10.1039/c5gc01451d
- Vladimir-Knežević, S., Perković, M., Zagajski Kučan, K., Mervi, M., and Rogošić, M. (2022). Green extraction of flavonoids and phenolic acids from elderberry (*Sambucus nigra* L.) and rosemary (*Rosmarinus officinalis* L.) using deep eutectic solvents. *Chem. Pap.* 76, 341–349. doi:10.1007/s11696-021-01862-x
- Wang, L. C., Wei, W. H., Zhang, X. W., Liu, D., Zeng, K. W., Tu, P. F., et al. (2018). An integrated proteomics and bioinformatics approach reveals the anti-inflammatory mechanism of carnosic acid. *Front. Pharmacol.* 9, 370. doi:10.3389/fphar.2018.00370
- Wang, T., Wang, Q., Guo, Q., Li, P., and Yang, H. (2021). A hydrophobic deep eutectic solvents-based integrated method for efficient and green extraction and recovery of natural products from *Rosmarinus officinalis* leaves, *Ginkgo biloba* leaves and *Salvia miltiorrhiza* roots. *Food Chem.* 363, 130282. doi:10.1016/j.foodchem.2021.130282
- Wojeiczkowski, J. P., Ferreira, A. M., Abranches, D. O., Mafra, M. R., and Coutinho, J. A. P. (2020). Using COSMO-RS in the design of deep eutectic solvents for the extraction of antioxidants from rosemary. *ACS Sustain. Chem. Eng.* 8, 12132–12141. doi:10.1021/acssuschemeng.0c03553
- Wojeiczkowski, J. P., Marques, C., Igarashi-Mafra, L., Coutinho, J. A. P., and Mafra, M. R. (2021). Extraction of phenolic compounds from rosemary using choline chloride - based Deep Eutectic Solvents. *Sep. Purif. Technol.* 258, 117975. doi:10.1016/j.seppur.2020.117975
- Yilmaz, F. M., Karaaslan, M., and Vardin, H. (2015). Optimization of extraction parameters on the isolation of phenolic compounds from sour cherry (*Prunus cerasus* L.) pomace. *J. Food Sci. Technol.* 52, 2851–2859. doi:10.1007/s13197-014-1345-3
- Zheng, Y., Zhang, Y., Zheng, Y., and Zhang, N. (2018). Carnosol protects against renal ischemia-reperfusion injury in rats. *Exp. Anim.* 67, 545–553. doi:10.1538/expanim.18-0067



## OPEN ACCESS

## EDITED BY

Manoj B. Gawande,  
Palacky University Olomouc, Czechia

## REVIEWED BY

Dibyendu Mondal,  
Institute of Plant Genetics (PAN), Poland  
Catarina Seica Neves,  
University of Aveiro, Portugal

## \*CORRESPONDENCE

Gao Fei,  
wanttofly407@qq.com  
Huan Weiwei,  
vivid96@aliyun.com

<sup>†</sup>These authors have contributed equally  
to this work and share first authorship

## SPECIALTY SECTION

This article was submitted to Green and  
Sustainable Chemistry,  
a section of the journal  
Frontiers in Chemistry

RECEIVED 04 April 2022

ACCEPTED 26 July 2022

PUBLISHED 06 September 2022

## CITATION

Bowen H, Durrani R, Delavault A,  
Durand E, Chenyu J, Yiyang L, Lili S,  
Jian S, Weiwei H and Fei G (2022),  
Application of deep eutectic solvents in  
protein extraction and purification.  
*Front. Chem.* 10:912411.  
doi: 10.3389/fchem.2022.912411

## COPYRIGHT

© 2022 Bowen, Durrani, Delavault,  
Durand, Chenyu, Yiyang, Lili, Jian,  
Weiwei and Fei. This is an open-access  
article distributed under the terms of the  
Creative Commons Attribution License  
(CC BY). The use, distribution or  
reproduction in other forums is  
permitted, provided the original  
author(s) and the copyright owner(s) are  
credited and that the original  
publication in this journal is cited, in  
accordance with accepted academic  
practice. No use, distribution or  
reproduction is permitted which does  
not comply with these terms.

# Application of deep eutectic solvents in protein extraction and purification

Hou Bowen<sup>1†</sup>, Rabia Durrani<sup>2†</sup>, André Delavault<sup>3</sup>,  
Erwann Durand<sup>4,5</sup>, Jiang Chenyu<sup>2</sup>, Long Yiyang<sup>1</sup>, Song Lili<sup>2</sup>,  
Song Jian<sup>6</sup>, Huan Weiwei<sup>6\*</sup> and Gao Fei<sup>1\*</sup>

<sup>1</sup>Zhejiang Provincial Key Laboratory of Resources Protection and Innovation of Traditional Chinese Medicine, Zhejiang A & F University, Hangzhou, China, <sup>2</sup>State Key Laboratory of Subtropical Silviculture, Zhejiang A & F University, Lin'an, Zhejiang, China, <sup>3</sup>Technical Biology, Institute of Process Engineering in Life Sciences II, Karlsruhe Institute of Technology, Karlsruhe, Germany, <sup>4</sup>CIRAD, UMR QUALISUD, Montpellier, France, <sup>5</sup>Qualisud, Univ Montpellier, Avignon Université, CIRAD, Institut Agro, Université de la Réunion, Montpellier, France, <sup>6</sup>Zhejiang Provincial Key Laboratory of Chemical Utilization of Forestry Biomass, College of Chemistry and Materials Engineering, Zhejiang A & F University, Hangzhou, Zhejiang, China

Deep eutectic solvents (DESs) are a mixture of hydrogen bond donor (HBD) and hydrogen bond acceptor (HBA) molecules that can consist, respectively, of natural plant metabolites such as sugars, carboxylic acids, amino acids, and ionic molecules, which are for the vast majority ammonium salts. Media such as DESs are modular tools of sustainability that can be pointed toward the extraction of bioactive molecules due to their excellent physicochemical properties, their relatively low price, and accessibility. The present review focuses on the application of DESs for protein extraction and purification. The in-depth effects and principles that apply to DES-mediated extraction using various renewable biomasses will be discussed as well. One of the most important observations being made is that DESs have a clear ability to maintain the biological and/or functional activity of the extracted proteins, as well as increase their stability compared to traditional solvents. They demonstrate true potential for a reproducible but more importantly, scalable protein extraction and purification compared to traditional methods while enabling waste valorization in some particular cases.

## KEYWORDS

deep eutectic solvent, protein, extraction, green solvent, biodegradability

## Introduction

In order to maintain the environmental balance, several sectors of industry, most notably the food industry, have started to use greener solvents as alternatives in their manufacturing processes rather than synthetic, petroleum-derived organic solvents (Ling and Hadinoto, 2022). Synthetic organic solvents are extensively used in foods, pharmaceuticals, and cosmetics for several purposes such as extraction and separation processes (Jesus and Filho, 2020). Depending on the polarity of the solvent selected, they have greater compatibility for hydrophilic or hydrophobic compounds. A number of these

TABLE 1 General formula for the classification of DESs.

Type	General formula	Terms
Type I	$\text{Cat}^+\text{X}^- z\text{MCl}_x$	$\text{M} = \text{Zn, Sn, Fe, Al, Ga, and In}$
Type II	$\text{Cat}^+\text{X}^- z\text{MCl}_x \cdot y\text{H}_2\text{O}$	$\text{M} = \text{Cr, Co, Cu, Ni, and Fe}$
Type III	$\text{Cat}^+\text{X}^- z\text{RZ}$	$\text{Z} = \text{CONH}_2, \text{COOH, and OH}$
Type IV	$\text{MCl}_x + \text{RZ} = \text{MCl}_{x-1}^+\text{RZ} + \text{MCl}_{x+1}^-$	$\text{M} = \text{Al and Zn and Z} = \text{CONH}_2 \text{ and OH}$

volatile solvents are obtained from fossil fuels and display several drawbacks to the environment like being toxic, non-degradable, and flammable (Fuad et al., 2021). Therefore, industrials are eager to shift to environmentally friendlier and greener solvent alternatives for the manufacturing of their products. Currently, some of these alternatives include supercritical fluids, ionic liquids (ILs), and deep eutectic solvents (DES). These solvents are less hazardous, environmentally less impactful, and consume less energy for their production and waste management (Anastas and Eghbali, 2009). Amongst these greener solvents, ILs and DESs are promising and well-known media of this new era of solvent engineering. ILs are non-flammable, have low vapor pressure, and are highly stable. In addition, they remain in the liquid state at a temperature below 100°C. However, due to their higher production cost, tedious recycling, and purification, their use is limited to the laboratory scale (Fuad et al., 2021). To cover such limitations, DESs are newly developed greener solvents that have much more significance with the aim of sustainability (Kudlak et al., 2015). They are, according to Kist et al., “cousins” of the ILs (Kist et al., 2020). DESs are eutectic mixtures of Lewis or Brønsted acids and bases, that is, hydrogen bond donors (HBDs) and hydrogen bond acceptors (HBAs). ILs and DESs have similar physical properties such as lower volatility, higher viscosity, and non-flammability and both have relatively good thermal stability. However, DESs are not completely like ILs as they can be partly or fully prepared from non-ionic compounds. This is in part the reason for their cost effectiveness, environmental friendliness, and degradability as they are made from naturally occurring metabolites. Given the superior possible number of combinations forming DESs, they are a versatile tool of sustainability that can be applied in various areas. Extraction and purification of proteins being topical and a currently investigated challenge as well for both academia and industry seemed logical that these two subjects merged into one. Being the greener solvent with greater interest, DESs represent a unique solution for a refinery in regard to a crucial need for sustainability. DESs are easy to prepare, and their supramolecular structures are often a good match for protein extraction, according to the three following conditions: affinity, solubility, and stability (Landa et al., 2020).

DESs are classified into four categories according to the general formula described in Table 1.

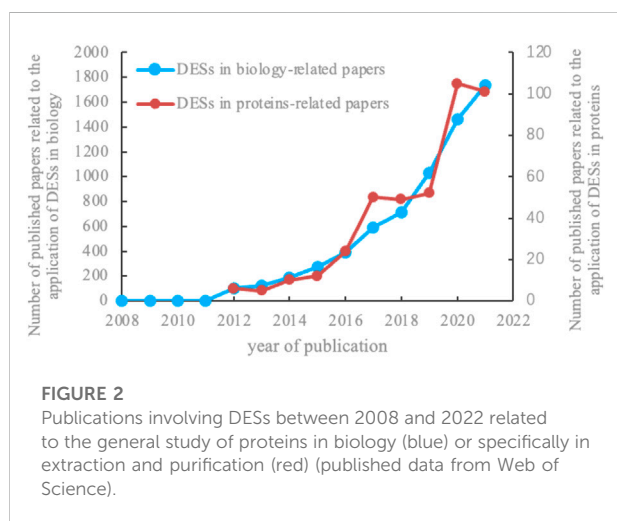
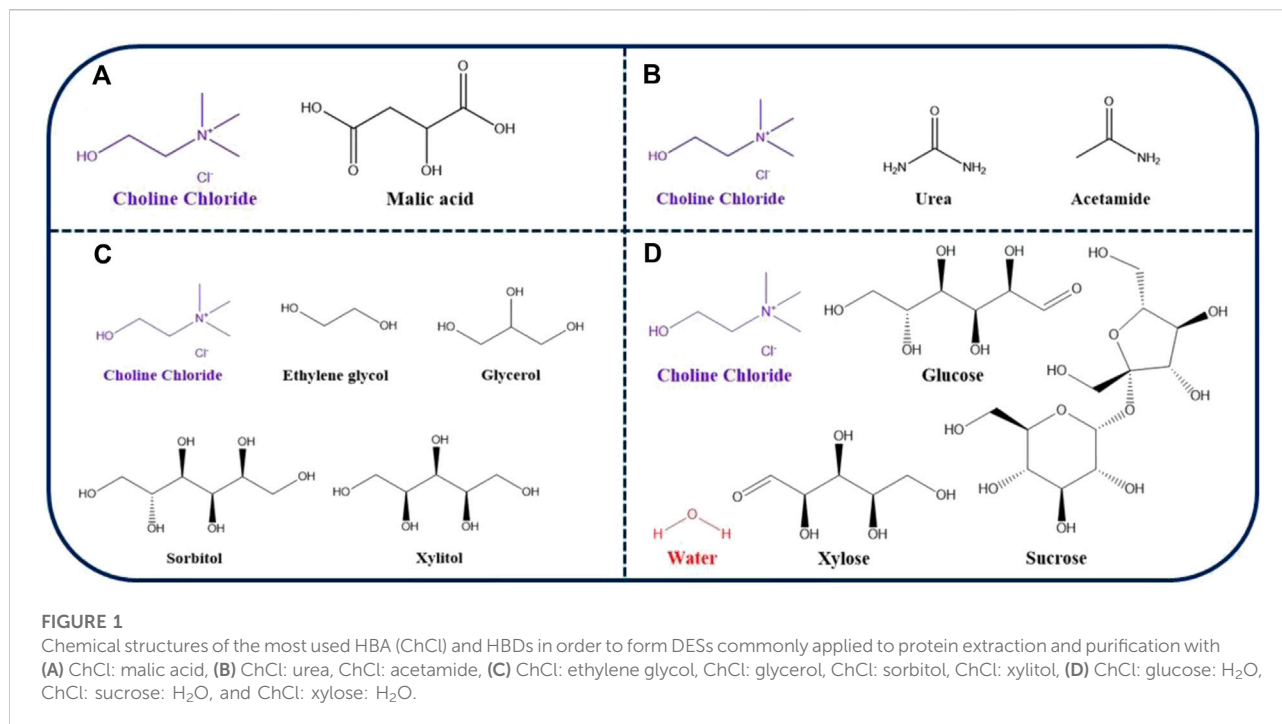
The most commonly used DES involved in protein studies belongs to type III and consists mostly of choline chloride (ChCl)

TABLE 2 Molar ratios used for the preparation of common ChCl-based DESs.

Deep eutectic solvents	ChCl: HBD
HBA: HBDs	(Molar ratio)
ChCl: urea	1:2
ChCl: acetamide	1:2
ChCl: ethylene glycol	1:2
ChCl: glycerol	1:2
ChCl: xylitol	1:1
ChCl: sorbitol	1:1
ChCl: glucose: H <sub>2</sub> O	5:2:5
ChCl: sucrose: H <sub>2</sub> O	5:2:5
ChCl: xylose: H <sub>2</sub> O	5:2:5
ChCl: malic acid	1:1

as HBA and amines, amide, carboxylic acids, sugars, and polyols as HBD (Zhang et al., 2012a). The molar ratio composing them is an essential factor, as depicted in Table 2 so that after mixing the HBD and HBA in the appropriate molar ratio, the ions are paired with available hydrogen ions to form a mixture that is stable at a temperature below their respective melting points (Ling and Hadinoto, 2022). DESs were first introduced by Abbott et al. (2003) in which ChCl (mp = 302°C) was mixed with urea (mp = 133°C) to form a resulting mixture with a melting point of 12°C. This drastic decrease in the melting point was explained by the delocalization of electrons that occurs from the hydrogen bonding between halide ions and HBDs (Abbott et al., 2003).

Type III is one of the simplest types of DES in its preparation, costing significantly less than other DESs and are highly biocompatible as they commonly use ChCl as HBA (Figure 1). ChCl is classified in the family of B vitamins and is a primary, ubiquitously occurring plant metabolite that is easily biodegradable, relatively cheap, and displays low toxicity. It is present in animal feed and food supplements (Kist et al., 2020). Due to their promising environmentally friendly nature, DESs are extensively used in the extraction and purification of proteins. Indeed, a number of researchers have worked on the extraction of proteins from biomass looking for superior extraction yields (Ling and Hadinoto, 2022).



Natural deep eutectic solvents (NADESs) are a concept first introduced by Choi et al. (2011), in which primary plant metabolites (sugars, acids, and amino acids) were used in order to form DESs that could be potentially identified in nature. They are also alternate solvents used for the extraction of proteins. They are far more environmental friendly due to their natural origin. It is thought that these natural solvents may be present in all organisms and involved in biosynthesis, solubility, and storage of hydrophobic metabolites in living organelles (Kist et al., 2020). These solvents are the most promising for the

extraction and purification of proteins and can open new gateways for industrialization.

## Deep eutectic solvents as media for protein extraction

Proteins are the fundamental unit of life that can be extracted from various sources like plants, animals, and microorganisms (Kumar et al., 2021). Investigations of efficient and sustainable protein extraction methods from various renewable biological sources are a growing area of interest in academia, as depicted in Figure 2 (Kaijia et al., 2015). Parallely, the incorporation of high-quality protein in diet and their formulation in nutraceuticals has led the industry to search for effective but greener methods for protein extraction as well (Justino et al., 2014). In the following subparts, DES-assisted protein extraction that includes solid-liquid extraction and liquid-liquid extraction will be detailed. Solid-liquid extraction involves mixing solid components into a liquid medium, and liquid-liquid extraction involves separation or partitioning of two compounds into an immiscible one (Ling and Hadinoto, 2022).

## Deep eutectic solvent-mediated solid-liquid extraction

A remarkable example of this concept has been made in the work of Yue et al. (2021), in which ChCl was mixed with diols of



TABLE 3 Effect of DESs made with iso-alcohol of different chain hydrocarbon lengths on oat protein extraction yield.

S. no	Types of DES	Protein content	Protein extraction yield
1	ChCl: 1,2-ethanediol (1: 3)	54.69 % $\pm$ 3.55%	25.41% $\pm$ 0.63%
2	ChCl: 1,3-propanediol (1: 3)	48.88% $\pm$ 1.58%	23.77% $\pm$ 0.90%
3	ChCl: 1,4-butanediol (1: 3)	45.25% $\pm$ 2.55%	25.17% $\pm$ 0.79%
4	ChCl: 1,2-ethanediol: H <sub>2</sub> O (1: 2: 1)	51.29% $\pm$ 2.58%	20.55% $\pm$ 1.32%
5	ChCl: 1,2-ethanediol: H <sub>2</sub> O (1: 3: 1)	56.38% $\pm$ 0.69%	25.01% $\pm$ 0.55%
6	ChCl: 1,3-propanediol: H <sub>2</sub> O (1: 2: 1)	54.58% $\pm$ 1.18%	31.46% $\pm$ 1.07%
7	ChCl: 1,3-propanediol: H <sub>2</sub> O (1: 3: 1)	50.71% $\pm$ 3.16%	32.29% $\pm$ 0.91%
8	ChCl: 1,4-butanediol: H <sub>2</sub> O (1: 2: 1)	62.50% $\pm$ 1.38%	35.76% $\pm$ 1.31%
9	ChCl: 1,4-butanediol: H <sub>2</sub> O (1: 3: 1)	57.17% $\pm$ 3.01%	37.15% $\pm$ 0.85%

various chain lengths for the extraction of oat protein (Table 3). Out of the nine different mixtures, they found that oat protein could be extracted with an extraction efficiency of up to 55.72% when using ChCl-1,4-butanediol/water. When reaching high solubility in the latter, better protein stability and foaming capacity were also enabled. Butanediol was shown to be the HBD responsible for facilitated extraction of oat protein. It was also observed that few DES mixtures could precipitate protein quickly, while binary mixtures took longer precipitation times. This mechanism may be due to the divergence and polarity of DESs which was advantageous for protein precipitation (Yue et al., 2021).

Convergently, Chen et al. (2021) mixed ChCl with glycerol for the extraction of soy protein and observed that DES-based extraction showed a yield higher by 10% than that of the acid-based precipitation method. Soy protein extracted by means of DESs also showed improved heat resistance and better hydrophobicity than native soy protein, indicating that DESs can enhance the physical properties of the proteins they solubilize, and thus, they can be further used as functional ingredients. Lin et al. (2021) extracted protein from bamboo shoots using an acidic DES based on ChCl and levulinic acid. They compared the extraction efficiency obtained with this mixture to a method using an aqueous solution of sodium hydroxide. The experiment resulted in an extraction yield enhanced by 60%, which ultimately provides another proof of DESs' suitability for the extraction of proteins from renewable raw biomasses (Chen et al., 2021).

Wahlstrom et al. (2017) used potassium and sodium salts of both formate and acetate for the production of DESs in combination with urea as HBD, in order to extract protein from brewer's spent grain originating from barley grain husk. They measured that NaOAc: urea (1:2) yielded a 79% protein extraction recovery while being composed of naturally occurring metabolites and could be assimilated to the NADES definition. In a need to develop formulations suitable for human consumption, NADESs are indeed a promising alternative that remain effective during the extraction process and could be applied widely in the

food industry (Wahlström et al., 2017). Still with an aim of waste valorization, Rodrigues et al. (2021) mixed betaine and propylene glycol in a 1:3 ratio for the extraction of proteins from sardine processing residues. When sardines enter the processing line in a factory, its head is mechanically removed, and entrails and other parts will be separated from the commercialized end-product, thus generating a significant amount of waste along the way. They found out that DES-based extraction yielded up to a concentration of 162.2 mg/g protein and compared their results to a simple water-based extraction method. Surprisingly, they found a great number of hydrophobic amino acids such as alanine, isoleucine, leucine, and valine to be suitable to form relatively less polar DESs that were in the end, a good match to extract proteins from sardine processing wastes. The resulting DES extracts also showed superior antioxidant and antimicrobial activities in comparison to water extracts. It was suspected that the presence of hydrophobic DES components facilitates the interaction between the antimicrobial peptides with the cell membrane of the tested microorganisms. This feature demonstrates the usefulness of low polarity DESs in comparison to a highly polar solvent such as water. This method, however, requires in-depth investigations to understand better the biological effects of protein-enriched DES extracts and ensure their safety for human consumption (Rodrigues et al., 2021).

Oppositely, Hernández-Corroto et al. (2020) used a highly polar and hydrophilic DES made of ChCl and acetic acid for the extraction of protein from pomegranate peels assisted by ultrasonication. This method resulted in a protein content of 19.2 mg/g and was compared to a simple liquid extraction method. The resulting high protein content showed high antihypertensive effects.

Finally, Liu et al. (2017) mixed various HBAs such as choline chloride (ChCl), glycine, betaine, alanine chloride, acetylcholine chloride, and nicotinic acid with PEG200 at a ratio of 1:4 for protein extraction from pumpkin seeds. They found that aqueous PEG200: ChCl and aqueous PEG200: glycine showed excellent extraction efficacies. They also explored isoelectric point-ethanol-DES ternary co-precipitation as a method for protein

TABLE 4 Methods used for protein precipitation in DESs using various protein sources.

Source of proteins	Protein precipitation method	Protein sedimentation yield	Reference
Pumpkin seed	Ternary co-precipitation	97% $\pm$ 0.8%	Liu et al. (2017)
	Four times the volume of ethanol precipitation	92% $\pm$ 1.08%	
	Isoelectric point precipitation	77% $\pm$ 2.8%	
	PEG 200-based DES self-precipitation	61% $\pm$ 1.3%	
Evening primrose cake	Water precipitation	19%	Grudniewska et al. (2018)
Rapeseed cake		34%	

recovery. They mixed PEG200-based DES with four-fold the volume of ethanol at pH 4.5 with the addition of 1 M HCl and separated the protein precipitate by centrifugation. The resulting precipitate was washed with water at pH 4.5 and centrifuged again. This straightforward approach combined isoelectric point-ethanol settlement, and DES self-settlement precipitation allowed to obtain a large amount of protein precipitate, thus reaching a remarkable settlement rate of 93.8% (Table 4).

Throughout these various studies, it was shown that DES-based extraction could be coupled with other techniques such as ultrasonication to improve the extraction efficiency of proteins and opens a promising horizon for development at the industrial scale, more notably for waste valorization in biorefineries. Nowadays, PEG-based DES extraction is getting more commonly used as it stabilizes the extracted proteins and is, in addition, approved by the FDA (Food and Drug Administration) (Morgenstern et al., 2017). This opens up many possibilities for more sustainable developments for sectors such as the pharmaceutical and agronomical industries. It can be argued that more research needs to be carried out to prove the scalability and practicability of PEG-based DES at the ton scale, albeit they demonstrate high affinity to proteins and are used as a precipitant to facilitate their crystallization (Kumar et al., 2009). A good hint is that in almost all methods depicting solid-liquid extraction covered in this study, water is used to reduce the viscosity of DESs and thus helps the extraction process in both efficiency and practicability. A higher viscosity in DES is actually related to a high number of hydrogen bonds, and it can hinder protein solubilization processes in some extreme cases. However, a proper amount of water should be used so that it may not disturb hydrogen bond interactions between the components of a DES as, oppositely, an excessive amount of water will end up wasting the useful properties of the DES (Ling et al., 2020).

## Deep eutectic solvent-mediated liquid-liquid extraction

Apart from solid-liquid extraction of proteins, liquid-liquid extraction of proteins has also been extensively studied and often

comes along aqueous two-phase systems (ATPS) as it ensures, in some cases, an efficient recovery of the targeted protein (Pei Xu, Zheng, Du, Zong, & Lou, 2015). This system is formed by mixing a water-soluble polymer with another polymer or inorganic salt above the critical concentration (Hatti-Kaul, 2000), for example, PEG-salt-water systems and ethylene oxide-propylene oxide or copolymer-polyoxyethylene detergent systems. Xu et al. (2015b) mixed ChCl and glycerol to form an ATPS with a salt solution for the extraction of BSA (bovine serum albumin). It was shown that 98.16% of BSA was actually extracted from the DES-phase, and further investigation also demonstrated that there was no change in the conformation of protein by UV-vis, FT-IR, and circular dichroism. They also showed that this protein separation process is not dependent on electrostatic interactions; indeed, it rather triggers the formation of protein aggregates as evidenced by transmission electron microscopy. Another study reported the formation of aggregates between DES and BSA for the uptake of protein by DES-based ATPS. This protein uptake by DES is facilitated by hydrogen bonding, salting out, and hydrophobic interactions, which are all inherent to DES's nature (Xu et al., 2015b).

Xu et al. (2019) extracted lysozyme using DES-based ATPS and found that 98% of the latter was contained in the DES-phase while maintaining 91.7% of its activity. Similarly, Meng et al. (2019) used a mixture of tetrabutylammonium chloride, polypropylene glycol 400 as an ATPS, and L-proline: xylitol as DES for the extraction of chymotrypsin based on the aforementioned principle. Superior extraction efficiencies of up to 97.3% could be reached, demonstrating the tremendous potential of DES-based ATPS.

## Limitations to deep eutectic solvent-assisted extraction of proteins

There are numerous chemicals that can fulfill the roles of HBD and HBA inside a DES, and thus, many combinations allowing a great number of DESs are possible. However, not every DES is suitable for protein extraction, and a universal method for their selection based on the desired application is lacking. Therefore, one needs to screen for suitable DESs that facilitate

protein extraction of a given biomass, thus demanding extensive time and resources (Smith et al., 2014). Inherently to DESs, temperature affects drastically the viscosity and conductivity of the latter. At room temperature, the viscosity of a DES is generally higher than that of water, but it will decrease with increasing temperature, and on the contrary, its conductivity will increase with the increasing temperature (Lores et al., 2016). Overall, these aspects can represent serious challenges of practicability and scalability that can repel applications in the industry.

Despite the reportedly high efficiencies of extraction that were previously compiled, the limitation to this system concerns the recovery and isolation of proteins extracted in the DES phase. This step is known as the back extraction and is crucial for both DES recycling and protein separation. Protein recovery from DES is very slow due to high interfacial mass transfer resistance (Kaijia et al., 2015). Xu et al. performed back extraction by changing the concentration of salt, practically speaking it consist of mixing DESs with a freshly prepared salt solution. In doing so, they recovered only 32.9% of the protein contained in DES and used ethanol combined with a saline solution for the recovery. Keeping in view this limitation, the protein back extraction methods and the recovery of DESs need to be further improved in order to make them attractive for industries (Li et al., 2016). Nonetheless, their uniqueness and innovative aspects among extraction media have drawn the attention of the scientific community, and they have been applied to the processing of many original renewable sources of proteins.

## Deep eutectic solvents as useful modular tools for extraction of valuable animal and plant proteins: Specific case studies

A wide range of raw biomasses have been identified in the previous literature as containing proteins and were compatible for a DES-mediated extraction (Table 4). Many of these proteins possess interesting properties and not only as an added value in nutrition but more importantly in their inherent functionality. Interesting cases have been made for rapeseed and *Oenothera biennis* oils that both reduce blood lipid and possess the anti-arteriosclerosis activity. However, the production of these oils generates a large amount of deoiled cake waste. Thus, extracting compounds from this process waste is economically viable for the industry due to its valorization. Grudniewska et al. (2018) extracted protein from rapeseed and *O. biennis* cakes with ChCl: glycerol (1:2) and obtained a protein-rich precipitate by adding water as an anti-solvent to the protein extraction solution.

More than simply extracting plant proteins, DESs are also involved in the extraction of protein from animal hair, that is, rabbit hair and wool fiber. As considerable amounts of wool waste are produced every year globally by the textile industry, a

tremendous environmental challenge arises. Herein, the concerned protein is keratin, a reactive, biocompatible, and biodegradable material that can be recovered when recycling wool. Wang et al. (2018) dissolved the latter in a DES composed of ChCl and oxalic acid. They extracted and separated keratin with molecular weights of 3.8–5.8 kDa and presented a high amount of serine, glutamic acid, cysteine, leucine, and arginine. Furthermore, using this same acidic DES, they dissolved rabbit hair with protein solubility greater than 70%, which was before unheard of. However, extraction from other protein-rich animal tissues possessing, that is, high nutritional or functional values using DESs has not been explored further but offers promising horizons (Wang and Tang, 2018).

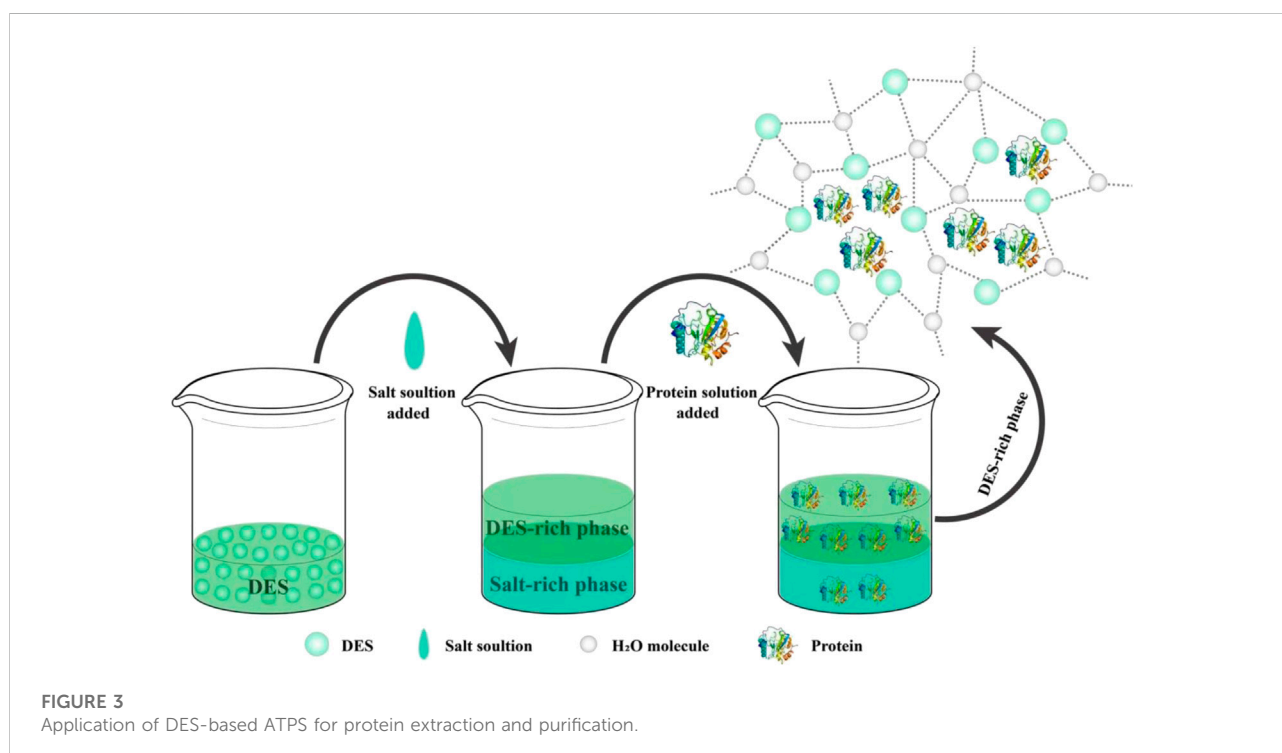
## Deep eutectic solvent-mediated protein purification

Preparation of pure protein is of prime importance for research, the pharmaceutical industry, and other sectors of industry in order to commercialize safe products for use or actual consumption. Conventional ways of protein purification include alkali, ammonium sulfate or acetone precipitation; salting-out, ion exchange (Unsal et al., 2006), electrophoresis (Hajduch et al., 2001), and affinity chromatography are also methods that are still used to this end (Wolschin et al., 2005; Raveendran et al., 2012). However, these traditional methods have disadvantages like deleterious effects on the protein activity induced by denaturation or complexation, higher costs, and setup complexity. DES-mediated liquid-liquid extraction has been shown previously to be a promising alternative method for protein purification in contrast to traditional methods resorting to the use of water or aqueous buffers in combination with organic solvents. Indeed, this last method is not desirable for protein purification because proteins can be easily denatured and lose partly or totally their activity as the essential water shell, for example, an enzyme can be disrupted by an excessively polar solvent. Keeping this in mind, an innovative protein purification method has been investigated that includes the use of ATPS. This system has been advantageously used to purify proteins because of its short purification time, capacity to ensure retention of the bioactivity, short phase separation time, high biocompatibility, and low toxicity (Gai et al., 2011; Oshima et al., 2010). DESs have been used as a part of ATPS to purify proteins as well (Table 5) (Saravanan et al., 2008; Zeng et al., 2016).

Bridges et al. (2007) were the first to report an IL-based ATPS system in 2003. The advantages of this system were shorter separation time of proteins, low viscosity, and better extraction efficiency, which was quite an efficient transition from traditional ATPS methods and was a great contribution to a potentially scalable protein separation technique.

TABLE 5 Application of DES-based ATPS for protein purification.

ATPS	ATPS	Target protein	Protein purification rate (%)	Reference
Associated with DES	Betaine: glycerol: H <sub>2</sub> O (1: 2: 1) -K <sub>2</sub> HPO <sub>4</sub>	BSA	99.82	Li et al. (2016a)
	ChCl: glycerol (1: 1)-K <sub>2</sub> HPO <sub>4</sub>	BSA	98.71	Xu et al. (2015b)
	ChCl: glycerol (1: 1)-K <sub>2</sub> HPO <sub>4</sub>	Try	94.36	Xu et al. (2020)
	ChCl: urea (1: 2)-K <sub>2</sub> HPO <sub>4</sub>	R-phycoerythrin	92.60	Xu et al. (2020)
Other examples of purified protein by MSPE	PEG4000-MgSO <sub>4</sub>	BSA	82.68	Saravanan et al. (2008)
	Betaine-K <sub>2</sub> HPO <sub>4</sub>	BSA	90	Zeng et al. (2016)



In this aim, Li et al. (2016b) prepared six different DESs by using betaine as the HBA and urea, methyl urea, glucose, sorbitol, glycerol, and ethylene glycol as HBD. These six DESs were used to extract and purify bovine serum albumin (BSA) using an ATPS, as depicted in Figure 3. They showed that DES in combination with ATPS can be used to extract and purify BSA from complex systems with efficiencies reaching 99.82% under optimized conditions. In that case, the betaine: urea combination was regarded as the most suitable DES.

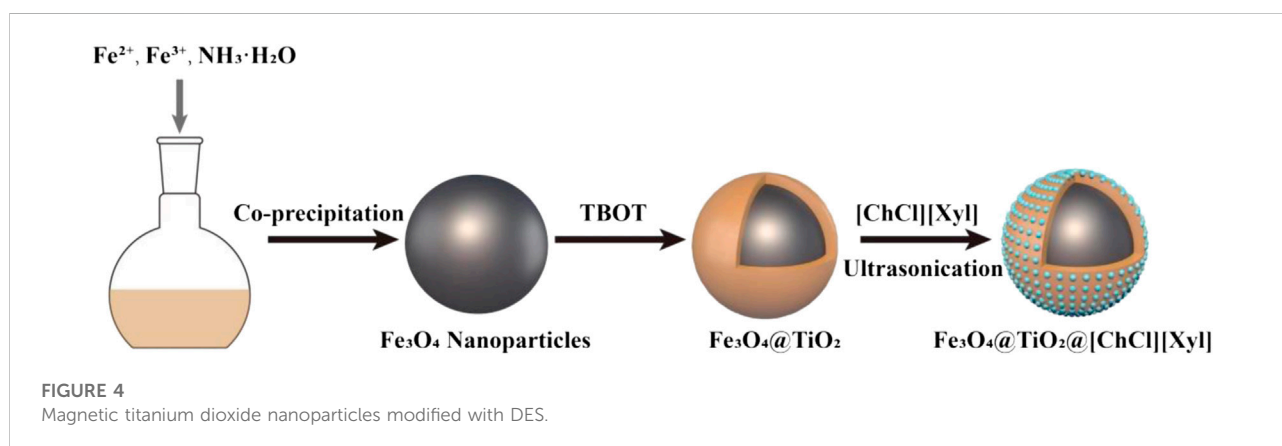
Similar studies have shown the effects of DES on the purification of proteins by ATPS. Indeed, Xu et al. (2015a) used ChCl as the HBA and ethylene glycol, glycerol, glucose, and sorbitol as HBD to prepare four DESs for extraction and purification of proteins presenting catalytic activities such as BSA

and trypsin in an ATPS. ChCl: glycerol in a 1:1 molar ratio was selected as the most suitable DES, and the conditions were optimized further by varying parameters such as pH, temperature, and time. Under the optimal extraction conditions, both BSA and trypsin were obtained with extraction rates of 98.71% and 94.36%, respectively.

Similarly, R-phycoerythrin, a red protein-pigment complex used for fluorescence-based detection with a broad absorption spectrum in the visible region was isolated from red algae. Xu et al. (2020) identified ChCl: urea (1:2) as the most suitable eutectic system for purification. Then, they established a ChCl: urea-K<sub>2</sub>HPO<sub>4</sub> aqueous two-phase system to purify R-phycoerythrin with a recovery efficiency reaching 92.60% (Zeng et al., 2014; Xu et al., 2020).

TABLE 6 Application of DES for protein purification using MSPE.

MSPE	MSPE	Target protein	Extraction capacity (mg g <sup>-1</sup> )	Reference
Associated with DES	Fe <sub>3</sub> O <sub>4</sub> @TiO <sub>2</sub> @ [ChCl][Xyl](1: 1)	Chy	347.8	Li et al. (2021)
	MB-NH <sub>2</sub> @CD@ [BeCh][Tri](1: 2)	Chy	549.87	Xu et al. (2020)
	Fe <sub>3</sub> O <sub>4</sub> -NH <sub>2</sub> @GO@ [ChCl] [glycerol] (1: 1)	BSA	44.59	Xu et al. (2015a)
	M-CNT@ N-[APTMAC][Xyl](1: 1)	BSA	225.15	Ni et al. (2019)
Other examples of purified proteins by MSPE	Fe@GO@Amino functional dicationic ionic liquid	BSA	89.7	Wen et al. (2016)
	Fe@GO	BSA	6.7	



## Promising innovation: Magnetic solid-phase extraction

Magnetic solid-phase extraction (MSPE) based on magnetic adsorbents can be seen as a complementary approach to ATPS in order to recover purely isolated proteins (Liu et al., 2012). In MSPE, magnetic adsorbents are dispersed into the sample solution, and these magnetic nanoparticles capture the analytes, that is, proteins, to be later separated directly from the sample matrix by means of an external magnetic field. Compared with standard solid-phase extraction methods, MSPE removes time-consuming steps such as centrifugation and filtration, ending up in a much-shortened processing time (Huang et al., 2015). In addition, analytes are easily eluted from the magnetic adsorbents to facilitate the recovery of both targeted molecules and adsorbents (Table 6) (Wen et al., 2016).

Li et al. (2021) used four DESs such as ChCl: xylitol (1:1), ChCl: glycerol (1:1), tetrabutylammonium bromide: lactic acid (1:2), and benzyltributylammonium bromide: lactic acid (1:2) for the preparation of magnetic titanium dioxide nanoparticles modified by DES and applied them to MSPE of chymotrypsin (Figure 4). They found that Fe<sub>3</sub>O<sub>4</sub>@TiO<sub>2</sub>@[ChCl][Xylitol] gave the best results among the four DES-modified particles, when using 10% sodium dodecyl sulfate-acetic acid as the eluent to

reach an extraction efficiency of 85.9%. In addition, Fe<sub>3</sub>O<sub>4</sub>@TiO<sub>2</sub>@[ChCl][xylitol] particles maintained excellent extraction efficiency toward chymotrypsin after six cycles of use (Li et al., 2021). MSPE in combination with DES is a novel approach for protein purification, allowing superior recovery of protein. This method permits to reach higher protein purity while using mild processing conditions that do not affect the functions of the targeted molecules. Therefore, it is a promising strategy that could play a considerable role in future protein purification processes (Huang et al., 2015).

## Conclusion

DES are a class of greener alternative solvents that have attracted considerable attention in biorefinery research due to their biodegradability, sustainability, low toxicity, and facile preparation. In addition to their numerous applications in biocatalysis, they are currently used as greener solvents but nonetheless efficient extraction and separation media for the recovery of animals and plants as protein-rich renewable biomass and thus provides new perspectives to biorefineries. Despite technical limitations intrinsic to DESs, such as viscosity, they have been shown to be a promising alternative solvent for



extraction of a wide variety of proteins and can be compatible with various raw biomasses. It is to foresee that their implementation in industrial refineries could solve technical and methodological issues that are currently encountered in the food industry such as the valorization of wastes or the volatility of currently used organic solvents. Selection of isomeric analogs of HDB, the presence of water during DES formation, and the structure–function relationship existing between extracted proteins and DESs need to be kept in mind. Therefore, optimization of DES preparation in order to be simple and environmentally friendly needs to be a priority when designing protein extraction processes when starting from either animal or plant sources. Further research should facilitate the use of DESs in the sustainable development of protein purification in the food industry by notably demonstrating proof of their scalability.

## Author contributions

CRedit roles: Conceptualization: RD and AD. Writing: HB, RD, and AD. Figures and Revision of manuscript: GF. Resources: SL. Supervision: GF, SL. Roles/Writing-original draft: HB, RD, AD. Writing-review & editing: RD, AD, ED.

## References

- Abbott, Andrew P., Capper, Glen, Davies, David L., Rasheed, Raymond K., and Tambyrajah, Vasuki. (2003). Novel solvent properties of choline chloride/urea mixtures. *Chem. Commun.* (1), 70–71. doi:10.1039/B210714G
- Anastas, P., and Eghbali, N. (2009). Green Chemistry: Principles and practice. *Chem. Soc. Rev.* 39, 301–312. doi:10.1039/B918763B
- Bridges, N. J., Gutowski, K. E., and Rogers, R. D. (2007). Investigation of aqueous biphasic systems formed from solutions of chaotropic salts with kosmotropic salts (salt–salt ABS). *Green Chem.* 9 (2), 177–183. doi:10.1039/B611628K
- Chen, Q., Chaihu, L., Yao, X., Cao, X., Li, S., Lin, J., et al. (2021). Molecular property-tailored soy protein extraction process using a deep eutectic solvent. *ACS Sustain. Chem. Eng.* 9, 10083–10092. doi:10.1021/acssuschemeng.1c01848
- Choi, Y. H., Van-Spronsen, J., Dai, Y., Verberne, M., Hollmann, F., Arends, I. W., et al. (2011). Are natural deep eutectic solvents the missing link in understanding cellular metabolism and physiology? *Plant Physiol.* 156, 1701–1705. doi:10.1104/pp.111.178426
- Fuad, F., Mohd Nadzir, M., and Kamaruddin, A. (2021). Hydrophilic natural deep eutectic solvent: A review on physicochemical properties and extractability of bioactive compounds. *J. Mol. Liq.* 339, 116923. doi:10.1016/j.molliq.2021.116923
- Gai, Q., Qu, F., Zhang, T., and Zhang, Y. (2011). Integration of carboxyl modified magnetic particles and aqueous two-phase extraction for selective separation of proteins. *Talanta* 85, 304–309.
- Grudniewska, A., Melo, E., Chan, A., Gnlika, R., Boratyński, F., and Matharu, A. (2018). Enhanced protein extraction from oilseed cakes using glycerol–choline chloride deep eutectic solvents: A biorefinery approach. *ACS Sustain. Chem. Eng.* 6, 15791–15800. doi:10.1021/acssuschemeng.8b04359
- Hajdich, M., Rakwal, R., Agrawal, G., Yonekura, M., and Pretova, A. (2001). High-resolution two-dimensional electrophoresis separation of proteins from metal-stressed rice (*Oryza sativa* L.) leaves: Drastic reductions/fragmentation of ribulose-1, 5-bisphosphate carboxylase/oxygenase and induction of stress-related proteins. *Electrophoresis* 22, 2824–2831. doi:10.1002/1522-2683(200108)22:13<2824::aid-elps2824>3.0.co;2-c
- Hatti-Kaul, R. (2000). Aqueous Two-Phase Systems 19, 269–277.
- Hatti-Kaul, R. (2001). Aqueous two-phase systems. A general overview. *Mol. Biotechnol.* 19 (3), 269–278. doi:10.1385/MB:19:3:269
- Hernández-Corroto, E., Plaza, M., Marina, M., and García, M. (2020). Sustainable extraction of proteins and bioactive substances from pomegranate peel (*Punica granatum* L.) using pressurized liquids and deep eutectic solvents. *Innovative Food Sci. Emerg. Technol.* 60, 102314. doi:10.1016/j.ifset.2020.102314
- Huang, Y., Wang, Y., Pan, Q., Wang, Y., Ding, X., Xu, K., et al. (2015). Magnetic graphene oxide modified with choline chloride-based deep eutectic solvent for the solid-phase extraction of protein. *Anal. Chim. Acta X* 877, 90–99. doi:10.1016/j.aca.2015.03.048
- Jesus, S., and Filho, R. (2020). Recent advances in lipid extraction using green solvents. *Renew. Sustain. Energy Rev.* 133, 110289. doi:10.1016/j.rser.2020.110289
- Justino, C. I. L., Duarte, K., FreTitas, A., Duarte, A., and Rocha-Santos. (2014). Classical methodologies for preparation of extracts and fractions. *Compr. Anal. Chem.* 65, 35–57. doi:10.1016/B978-0-444-63359-0.00003-3
- Kaijia, X., Wang, Y., Huang, Y., Li, N., and Wen, Q. (2015). A green deep eutectic solvent-based aqueous two-phase system for protein extracting. *Anal. Chim. Acta* 864, 9–20. doi:10.1016/j.aca.2015.01.026
- Kim, J., Shi, Y., Kwon, C., Cao, Y., and Mitragotri, S. (2021). A deep eutectic solvent-based approach to intravenous formulation. *Adv. Healthc. Mat.* 10, 2100585. doi:10.1002/adhm.202100585
- Kist, J., Zhao, H., Mitchell-Koch, K., and Baker, G. (2020). The study and application of biomolecules in deep eutectic solvents. *J. Mat. Chem. B* 9, 536–566. doi:10.1039/D0TB01656J
- Kudlak, B., Owczarek, K., and Namieśnik, J. (2015). Selected issues related to the toxicity of ionic liquids and deep eutectic solvents—A review. *Environ. Sci. Pollut. Res.* 22, 11975–11992. doi:10.1007/s11356-015-4794-y
- Kumar, M., Tomar, M., Potkule, J., Reetu, Dr. P., Mahapatra, A., Kennedy, J., et al. (2021). Advances in the plant protein extraction: Mechanism and recommendations. *Food Hydrocoll.* 115, 106595. doi:10.1016/j.foodhyd.2021.106595
- Kumar, V., Sharma, V. K., and Kalonia, D. S. (2009). Effect of polyols on polyethylene glycol (PEG)-induced precipitation of proteins: Impact on solubility, stability and conformation. *Int. J. Pharm.* 366 (1), 38–43. doi:10.1016/j.jipharm.2008.08.037

## Funding

This work was supported financially by the Zhejiang Provincial Academy Cooperative Forestry Science and Technology Project (2021SY01), Key R & D projects of Zhejiang Province in 2021 (2021C02001) and (2021C02013).

## Conflict of interest

The authors declare that the research was conducted in the absence of any commercial or financial relationships that could be construed as a potential conflict of interest.

## Publisher's note

All claims expressed in this article are solely those of the authors and do not necessarily represent those of their affiliated organizations, or those of the publisher, the editors, and the reviewers. Any product that may be evaluated in this article, or claim that may be made by its manufacturer, is not guaranteed or endorsed by the publisher.

- Landa, M., Sebastian Pascual, P., Giannotti, M., Serrà, A., and Gómez, E. (2020). Electrodeposition of nanostructured cobalt films from a deep eutectic solvent: Influence of the substrate and deposition potential range. *Electrochimica Acta* 359, 136928. doi:10.1016/j.electacta.2020.136928
- Li, H. Q., Wang, Y., He, X., Chen, J., Xu, F. T., Liu, Z. W., et al. (2021). A green deep eutectic solvent modified magnetic titanium dioxide nanoparticles for the solid-phase extraction of chymotrypsin. *Talanta* 230, 122341. doi:10.1016/j.talanta.2021.122341
- Li, N., Wang, Y., Kaijia, X., Huang, Y., Wen, Q., and Ding, X. (2016b). Development of green Betaine-based deep eutectic solvent aqueous two-phase system for the extraction of protein. *Talanta* 152, 23–32. doi:10.1016/j.talanta.2016.01.042
- Li, N., Wang, Y. Z., Xu, K. J., Huang, Y. H., Wen, Q., and Ding, X. Q. (2016a). Development of green Betaine-based deep eutectic solvent aqueous two-phase system for the extraction of protein. *Talanta* 152, 23–32. doi:10.1016/j.talanta.2016.01.042
- Lin, Z., Jiao, G., Zhang, J., Celli, G., and Brooks, M. S.-L. (2021). Optimization of protein extraction from bamboo shoots and processing wastes using deep eutectic solvents in a biorefinery approach. *Biomass Conv. Bioref.* 11, 2763–2774. doi:10.1007/s13399-020-00614-3
- Ling, J., Chan, Y. S. S., Nandong, J., Chin, S., and Ho, B. (2020). Formulation of choline chloride/ascorbic acid natural deep eutectic solvent: Characterization, solubilization capacity and antioxidant property. *LWT* 133, 110096. doi:10.1016/j.lwt.2020.110096
- Ling, J., and Hadinoto, K. (2022). Deep eutectic solvent as green solvent in extraction of biological macromolecules: A review. *Int. J. Mol. Sci.* 23, 3381. doi:10.3390/ijms23063381
- Liu, Q., Shi, J., Cheng, M., Li, G., Cao, D., and Jiang, G. (2012). Preparation of graphene-encapsulated magnetic microspheres for protein/peptide enrichment and MALDI-TOF MS analysis. *Chem. Commun.* 48, 1874–1876. doi:10.1039/c2cc16891j
- Liu, R. L., Yu, P., Ge, X. L., Bai, X. F., Li, X. Q., and Fu, Q. (2017). Establishment of an aqueous PEG 200-Based deep eutectic solvent extraction and enrichment method for pumpkin (*Cucurbita moschata*) Seed Protein. *Food Anal. Methods* 10, 1669–1680. doi:10.1007/s12161-016-0732-y
- Lores, H., Romero, V., Costas, I., Bendicho, C., and Lavilla, I. (2016). Natural deep eutectic solvents in combination with ultrasonic energy as a green approach for solubilisation of proteins: Application to gluten determination by immunoassay. *Talanta* 162, 453–459. doi:10.1016/j.talanta.2016.10.078
- Meng, J., Wang, Y., Zhou, Y., Chen, J., Wei, X., Ni, R., et al. (2019). Development of different deep eutectic solvent aqueous biphasic systems for the separation of proteins. *RSC Adv.* 9, 14116–14125. doi:10.1039/C9RA00519F
- Morgenstern, J., Baumann, P., Brunner, C., and Hubbuch, J. (2017). Effect of PEG molecular weight and PEGylation degree on the physical stability of PEGylated lysozyme. *Int. J. Pharm.* 519, 408–417. doi:10.1016/j.ijpharm.2017.01.040
- Ni, R., Wang, Y., Wei, X., Chen, J., Meng, J., Xu, F., et al. (2019). Magnetic carbon nanotube modified with polymeric deep eutectic solvent for the solid phase extraction of bovine serum albumin. *Talanta* 206, 120215.
- Oshima, T., Suetsugu, A., and Baba, Y. (2010). Extraction and separation of a lysine-rich protein by formation of supramolecule between crown ether and protein in aqueous two-phase system. *Anal. Chim. Acta* 674, 211–219.
- Raveendran, S., Parameswaran, B., Bullett, B., Usha, K., Bullett, J., Sukumaran, R., et al. (2012). Organosolvent pretreatment and enzymatic hydrolysis of rice straw for the production of bioethanol. *World J. Microbiol. Biotechnol.* 28, 473–483. doi:10.1007/s11274-011-0838-8
- Rodrigues, L., Leonardo, I., Gaspar, F., Roseiro, L., Duarte, A., Matias, A., et al. (2021). Unveiling the potential of betaine/polyol-based deep eutectic systems for the recovery of bioactive protein derivative-rich extracts from sardine processing residues. *Sep. Purif. Technol.* 276, 119267. doi:10.1016/j.seppur.2021.119267
- Saravanan, S., Rao, J. R., Nair, B. U., and Ramasami, T. (2008). Aqueous two-phase poly(ethylene glycol)–poly(acrylic acid) system for protein partitioning: Influence of molecular weight, pH and temperature. *Process Biochem.* 43, 905–911. doi:10.1016/j.procbio.2008.04.011
- Sim, S., Srv, A., Chiang, J. H., and Henry, J. (2021). Plant proteins for future foods: A roadmap. *Foods* 10, 11967. doi:10.3390/foods10081967
- Smith, E., Abbott, A. P., and Ryder, K. (2014). Deep eutectic solvents (DESs) and their applications. *Chem. Rev.* 114, 11060–11082. doi:10.1021/cr300162p
- Unsal, E., Irmak, T., Durusoy, E., Hayran, M., and Tuncel, A. (2006). Monodisperse porous polymer particles with polyionic ligands for ion exchange separation of proteins. *Anal. Chim. Acta* 570, 240–248. doi:10.1016/j.aca.2006.04.050
- Wahlström, R., Rommi, K. W.-K., Pia, E.-C., Dilek, H., Ulla, H., Kuutti, L., et al. (2017). High yield protein extraction from brewer's spent grain with novel carboxylate salt - urea aqueous deep eutectic solvents. *ChemistrySelect* 2, 9355–9363. doi:10.1002/slct.201701492
- Wang, D., and Tang, R. C. (2018). Dissolution of wool in the choline chloride/oxalic acid deep eutectic solvent. *Mat. Lett.* 23, 217–220. doi:10.1016/j.matlet.2018.08.056
- Wang, D., Yang, X. H., Tang, R. C., and Yao, F. (2018). Extraction of keratin from rabbit hair by a deep eutectic solvent and its characterization. *Polymers* 10, 993. doi:10.3390/polym10090993
- Wen, Q., Wang, Y., Xu, K., LiZhang, N. H., Yang, Q., Zhou, Y., et al. (2016). Magnetic solid-phase extraction of protein by ionic liquid-coated Fe@graphene oxide. *Talanta* 160, 481–488. doi:10.1016/j.talanta.2016.07.031
- Wolschin, F., Wienkoop, S., and Weckwerth, W. (2005). Enrichment of phosphorylated proteins and peptides from complex mixtures using metal oxide/hydroxide affinity chromatography (MOAC). *Proteomics* 5, 4389–4397. doi:10.1002/pmic.200402049
- Xu, K., Wang, Y., Huang, Y., Li, N., and Wen, Q. (2015a). A green deep eutectic solvent-based aqueous two-phase system for protein extracting. *Anal. Chim. Acta* 864, 9–20. doi:10.1016/j.aca.2015.01.026
- Xu, P., Wang, Y., Chen, J., Wei, X., Xu, W., Ni, R., et al. (2019). Development of deep eutectic solvent-based aqueous biphasic system for the extraction of lysozyme. *Talanta* 202, 10.1016/j.talanta.2019.04.053
- Xu, P., Zheng, Gao-Wei, Du, Peng-Xuan, Zong, Min-Hua, & Lou, Wen-Yong. (2015b). Whole-cell biocatalytic processes with ionic liquids. *ACS Sustain. Chem. Eng.* 4, 371–386. doi:10.1021/acssuschemeng.5b00965
- Xu, Y., Wang, Q., and Hou, Y. (2020). Efficient purification of R-phycoerythrin from marine algae (*Porphyra yezoensis*) based on a deep eutectic solvents aqueous two-phase system. *Mar. Drugs* 18, 618. doi:10.3390/md18120618
- Yue, J., Zhu, Z., Yi, J., Lan, Y., Chen, B., and Rao, J. (2021). Structure and functionality of oat protein extracted by choline chloride–dihydric alcohol deep eutectic solvent and its water binary mixtures. *Food Hydrocoll.* 112, 106330. doi:10.1016/j.foodhyd.2020.106330
- Zeng, C. X., Xin, R. P., Qi, S. J., Yang, B., and Wang, Y. H. (2016). Aqueous two-phase system based on natural quaternary ammonium compounds for the extraction of proteins. *J. Sep. Sci.* 39 (4), 648–654. doi:10.1002/jssc.201500660
- Zeng, Q., Wang, Y., Huang, Y., Ding, X., Chen, J., and Xu, K. (2014). Deep eutectic solvents as novel extraction media for protein partitioning. *Analyst* 139, 2565–2573. doi:10.1039/c3an02235h
- Zhang, M., Zhang, X., Liu, Y., Wu, K., Zhu, Y., Lu, H., et al. (2021). Insights into the relationships between physicochemical properties, solvent performance, and applications of deep eutectic solvents. *Environ. Sci. Pollut. Res.* 28 (27), 35537–35563. doi:10.1007/s11356-021-14485-2
- Zhang, Q., De Oliveira Vigier, K., Royer, S., and Jérôme, F. (2012b). Deep eutectic solvents: Syntheses, properties and applications. *Chem. Soc. Rev.* 41 (21), 7108–7146. doi:10.1039/c2cs35178a
- Zhang, Q., Vigier, K., Royer, S., and Jérôme, F. (2012a). Deep eutectic solvents: Syntheses, properties and applications. *Chem. Soc. Rev.* 41, 7108–7146. doi:10.1039/c2cs35178a



## OPEN ACCESS

## EDITED BY

Maria Luisa Di Gioia,  
University of Calabria, Italy

## REVIEWED BY

Guocai Tian,  
Kunming University of Science and  
Technology, China  
Johan Jacquemin,  
Mohammed VI Polytechnic University,  
Morocco

## \*CORRESPONDENCE

Xiaoyan Ji,  
xiaoyan.ji@ltu.se  
Aatto Laaksonen,  
aatto@mmk.su.se  
Francesca Mocci,  
fmocci@unica.it

## SPECIALTY SECTION

This article was submitted to Green and  
Sustainable Chemistry,  
a section of the journal  
Frontiers in Chemistry

RECEIVED 30 June 2022

ACCEPTED 28 October 2022

PUBLISHED 14 November 2022

## CITATION

Engelbrecht LV, Ji X, Carbonaro CM,  
Laaksonen A and Mocci F (2022), MD  
simulations explain the excess molar  
enthalpies in pseudo-binary mixtures of  
a choline chloride-based deep eutectic  
solvent with water or methanol.  
*Front. Chem.* 10:983281.  
doi: 10.3389/fchem.2022.983281

## COPYRIGHT

© 2022 Engelbrecht, Ji, Carbonaro,  
Laaksonen and Mocci. This is an open-  
access article distributed under the  
terms of the [Creative Commons  
Attribution License \(CC BY\)](#). The use,  
distribution or reproduction in other  
forums is permitted, provided the  
original author(s) and the copyright  
owner(s) are credited and that the  
original publication in this journal is  
cited, in accordance with accepted  
academic practice. No use, distribution  
or reproduction is permitted which does  
not comply with these terms.

# MD simulations explain the excess molar enthalpies in pseudo-binary mixtures of a choline chloride-based deep eutectic solvent with water or methanol

Leon de Villiers Engelbrecht<sup>1</sup>, Xiaoyan Ji<sup>2\*</sup>,  
Carlo Maria Carbonaro<sup>3</sup>, Aatto Laaksonen<sup>1,2,4,5,6\*</sup> and  
Francesca Mocci<sup>1\*</sup>

<sup>1</sup>Department of Chemical and Geological Sciences, University of Cagliari, Cagliari, Italy, <sup>2</sup>Division of Energy Science, Energy Engineering, Luleå University of Technology, Luleå, Sweden, <sup>3</sup>Department of Physics, University of Cagliari, Cagliari, Italy, <sup>4</sup>Division of Physical Chemistry, Arrhenius Laboratory, Department of Materials and Environmental Chemistry, Stockholm University, Stockholm, Sweden, <sup>5</sup>Center of Advanced Research in Bionanoconjugates and Biopolymers, "Petru Poni" Institute of Macromolecular Chemistry, Iasi, Romania, <sup>6</sup>State Key Laboratory of Materials-Oriented and Chemical Engineering, Nanjing Tech University, Nanjing, China

The addition of molecular liquid cosolvents to choline chloride (ChCl)-based deep eutectic solvents (DESs) is increasingly investigated for reducing the inherently high bulk viscosities of the latter, which represent a major obstacle for potential industrial applications. The molar enthalpy of mixing, often referred to as excess molar enthalpy  $H^E$ —a property reflecting changes in intermolecular interactions upon mixing—of the well-known ChCl/ethylene glycol (1:2 molar ratio) DES mixed with either water or methanol was recently found to be of opposite sign at 308.15 K: Mixing of the DES with water is strongly exothermic, while methanol mixtures are endothermic over the entire mixture composition range. Knowledge of molecular-level liquid structural changes in the DES following cosolvent addition is expected to be important when selecting such “pseudo-binary” mixtures for specific applications, e.g., solvents. With the aim of understanding the reason for the different behavior of selected DES/water or methanol mixtures, we performed classical MD computer simulations to study the changes in intermolecular interactions thought to be responsible for the observed  $H^E$  sign difference. Excess molar enthalpies computed from our simulations reproduce, for the first time, the experimental sign difference and composition dependence of the property. We performed a structural analysis of simulation configurations, revealing an intriguing difference in the interaction modes of the two cosolvents with the DES chloride anion: water molecules insert between neighboring chloride anions, forming ionic hydrogen-bonded bridges that draw the anions closer, whereas dilution of the DES with methanol results in increased interionic separation. Moreover, the simulated DES/water mixtures were found to contain extended hydrogen-bonded structures containing water-bridged

chloride pair arrangements, the presence of which may have important implications for solvent applications.

#### KEYWORDS

deep eutectic solvent, choline chloride, cosolvents, excess properties, pseudo-binary solvent mixture, MD simulations

## 1 Introduction

The deep eutectic solvents (DESs) are a diverse group of eutectic mixtures of two or more components, i.e., they have a lower melting point (mp) than expected for a corresponding ideal mixture of the components, and they exhibit a characteristic mp minimum, i.e., the eutectic point. In fact, the “DES” assignment implies that the mixture composition is close to, or at, this eutectic point (Smith et al., 2014). DESs are often composed of an ionic hydrogen bond acceptor (HBA), e.g., quaternary ammonium halide salt, and a metal salt or an electronically neutral hydrogen bond donor (HBD). The choline chloride (ChCl)-based DESs, involving a neutral HBD, typically urea or ethylene glycol, glycerol, or malonic acid, exhibit particularly favorable properties as alternative solvents, and are actively studied (Hansen et al., 2021); in fact, these so-called “type III” DESs have even been assigned unique names, e.g., the ChCl/urea 1:2 molar ratio mixture is widely referred to as “reline”, the corresponding mixture with ethylene glycol as “ethaline”, and so on. In these systems, the HBD is thought to strongly coordinate, or complex the chloride anion, reducing the strength of its electrostatic interactions with the organic cation, and thus the mp (Abbott et al., 2003; Ashworth et al., 2016).

DESs share many favourable solvent properties with the related ionic liquids (ILs), e.g., low vapor pressure, wide liquid temperature range, and low flammability, and they are often considered IL analogues (Ma et al., 2018). The ChCl-based DESs, in particular, exhibit a number of additionally advantageous properties compared to established ILs, which include facile synthesis from readily available, inexpensive, and environmentally benign starting materials under moderate conditions (Zhang et al., 2012). As for ILs, however, the typically high viscosities of these DESs under ambient conditions represent a major obstacle to their applications as solvents or lubricants (García et al., 2015; Ma et al., 2018). The addition of more highly mobile molecular cosolvents, including water or alcohols, to form a “pseudo-binary” (since the DES itself is a mixture) liquid mixture has been proposed as a possible solution to this problem (Xie et al., 2014; Yadav et al., 2014; Yadav and Pandey, 2014; Harifi-Mood and Buchner, 2017); moreover, many DESs (like ILs) are hygroscopic, readily absorbing atmospheric water. While the addition of cosolvents to DESs has been shown to effectively reduce their viscosity and modify other macroscopic liquid properties, e.g., density, and it is also expected to affect the characteristic intermolecular interactions and molecular arrangements within the DESs,

which may have important implications for their solvent characteristics.

Information regarding changes in intermolecular interactions and arrangements that occur when two liquids are mixed may be obtained through the measurement of excess thermodynamic properties, e.g., the excess molar enthalpy ( $H^E$ ), and/or excess molar volume ( $V^E$ ). DES/cosolvent mixtures have been found to exhibit significantly nonideal mixing behavior, often showing interesting, unexpected excess thermodynamic property variations as a function of cosolvent content (Ma et al., 2018). These include the sinusoidal (S-shaped)  $H^E$  trends of aqueous ChCl/urea DES mixtures as a function of water content, in which initially negative  $H^E$  (exothermic mixing, i.e., strong intermolecular interactions between DES components and water) changes to positive (endothermic) with increasing water content. Wang et al. (Wang Y. et al., 2020), in a recent thermodynamics study of mixtures of ethaline or the corresponding ChCl/glycerol 1:2 molar ratio DES (“glyceline”) with either water or methanol (at 308.15 and 318.15 K), found the  $H^E$  of aqueous mixtures to be strongly negative, while those of methanol mixtures were small positive values at all mixture compositions. While addition both water and methanol reduce the DES viscosity, the opposite sign of the resulting  $H^E$  point to different intermolecular interaction changes upon mixing.

The ChCl-based DESs themselves are characterized by considerable microstructural complexity (Spittle et al., 2022), in which different interaction modes among components are possible; in fact, these DESs have been described as an “alphabet soup” of hydrogen bonding (“H-bonding”) interactions (Ashworth et al., 2016). Computational techniques, and classical Molecular Dynamics (MD) simulations in particular, have been extensively employed to study the solvation of simple or complex solutes (Laaksonen et al., 2012; Engelbrecht et al., 2018), the structural organization in liquids and ILs (Wang Y.-L. et al., 2020; Engelbrecht et al., 2022), and to rationalize their experimentally observed properties (Mariani et al., 2017; Demurtas et al., 2021; Lengvinaitė et al., 2021). These computational methods are also increasingly used to study DESs and DES-containing systems (Velez and Acevedo, 2022), often in combination with experimental methods (Hansen et al., 2021; Spittle et al., 2022). Several MD simulation studies of DES/water pseudo-binary mixtures, which naturally are highly complex, have been reported in recent years (Gao et al., 2018; Kumari et al., 2018; Baz et al., 2019; Celebi et al., 2019; Kaur et al.,

TABLE 1 Details of simulated DES/cosolvent mixtures and respective pure solvents. The total number ( $N$ ) of units/molecules of each component (choline chloride ChCl, ethylene glycol EG, and water/methanol cosolvent) and the simulation average densities (308 K, 0.98 bar) are shown.

System	$x_{\text{cosolvent}}$	$N_{\text{ChCl}}$	$N_{\text{EG}}$	$N_{\text{cosolvent}}$	Density ( $\text{g}\cdot\text{cm}^{-3}$ )
Pure DES	—	300	600	—	1.1044
DES/water	0.125	300	600	129	1.1041
	0.250	300	600	300	1.1029
	0.500	300	600	900	1.0953
	0.750	300	600	2,700	1.0708
	0.875	150	300	3,150	1.0430
	1.000	—	—	3,000	0.9902
DES/methanol	0.125	300	600	129	1.0886
	0.250	300	600	300	1.0695
	0.500	300	600	900	1.0195
	0.750	150	300	1,350	0.9400
	0.875	75	150	1,575	0.8804
	1.000	—	—	1,000	0.7976

2020). The present work describes an MD simulation study of ethaline/water and ethaline/methanol mixtures, with an emphasis on first reproducing, and then rationalizing their striking experimental  $H^E$  sign difference (Wang Y. et al., 2020).

## 2 Methods

### 2.1 Force field

The General Amber Force Field (GAFF) was used to model the ChCl/ethylene glycol DES and its mixtures with methanol (Wang et al., 2004). The DES partial atomic charges of Perkins et al. (Perkins et al., 2014), developed specifically for use with GAFF parameters, were used (with ionic species charges scaled by a factor of 0.9). For methanol, an established set of partial atomic charges were obtained from the online R.E.D database, developed using the GAFF-consistent RESP (HF/6-31\*) fitting procedure (Dupradeau, 2005; Dupradeau et al., 2010); the SPC/E model was used for water (Berendsen et al., 1987).

### 2.2 Starting configurations

Starting configurations were prepared using the Packmol software (Martínez et al., 2009), randomly placing a total of 300 choline ( $\text{Ch}^+$ ) and chloride ( $\text{Cl}^-$ ) ions, and 600 ethylene glycol (EG) molecules in a periodic cubic simulation cell, with dimensions chosen such that the configuration is close to target density. For DES/cosolvent mixtures, appropriate numbers of

DES components and cosolvent molecules were placed in cubic cells of similarly chosen dimensions, detailed in Table 1. Here, the DES/cosolvent composition is expressed as a cosolvent mole fraction,  $x_{\text{cosolvent}}$ , which is computed as follows,

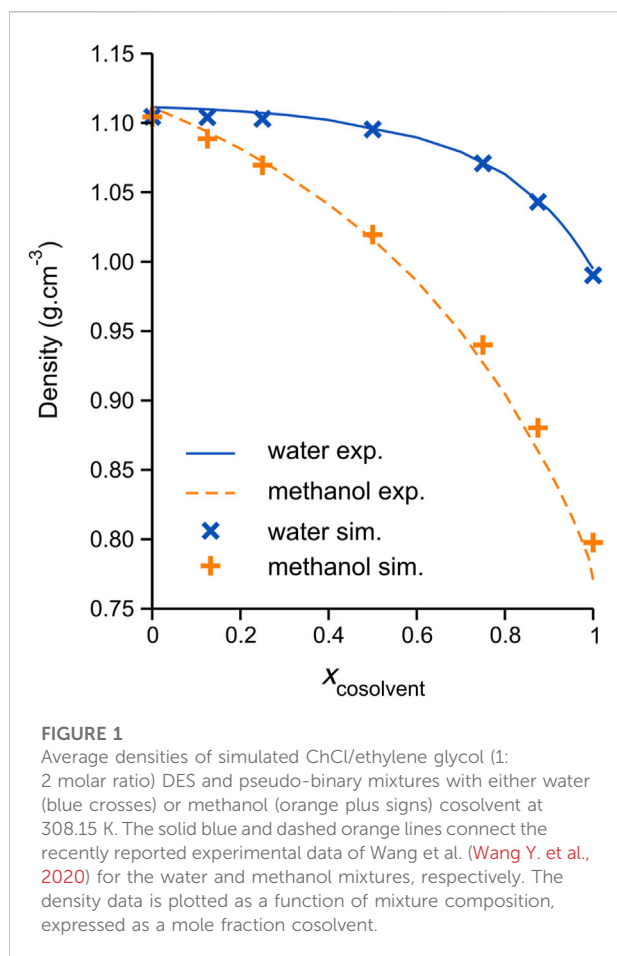
$$x_{\text{cosolvent}} = \frac{N_{\text{cosolvent}}}{N_{\text{ChCl}} + N_{\text{HBD}} + N_{\text{cosolvent}}} \quad (1)$$

where  $N_{\text{ChCl}}$  is the number of ChCl ion pairs,  $N_{\text{HBD}}$  is the number of HBD molecules, and  $N_{\text{cosolvent}}$  is the number of cosolvent molecules.

### 2.3 Simulation methods

All MD simulations were performed using the Amber 16 software package (Case et al., 2016). The simulation procedure was essentially similar to that described by Perkins et al. (Perkins et al., 2014): following system equilibration (see below), NPT simulations (308 K, 0.98 bar) were performed using Langevin dynamics (5 ps<sup>-1</sup> time constant), with weak (Berendsen et al., 1984) pressure coupling (1 ps time constant), and a 2 fs simulation time step; bonds involving hydrogen atoms were constrained using the SHAKE algorithm (Ryckaert et al., 1977). The nonbonded interaction cutoff was set at 15 Å, with long-range electrostatic interactions computed using the PME procedure (Darden et al., 1993), tolerance 10<sup>-5</sup>. The equilibration of the system was performed through a combination of steepest-descent energy minimization and NPT MD simulations; a detailed description of these steps is given in the Supplementary Material. After the equilibration phase, 20 ns





long NPT production simulation trajectories were generated for each system.

## 3 Results

### 3.1 Excess molar enthalpies

The accurate reproduction of experimental bulk liquid densities constitutes an important target in the validation of DES models (as for many other liquid systems); in fact, the current DES model ionic charges, originally developed by Perkins et al. (Perkins et al., 2014), were scaled by the authors (by a factor 0.9) to better reproduce experimental densities and transport properties compared to the corresponding model with full ionic charges ( $\pm 1$  e). Scaling of the ionic solute charges has been used in many previous investigations to account for the charge transfer phenomena; see Engelbrecht et al. (Engelbrecht et al., 2018) and references therein. The calculated average densities of all simulated DES/cosolvent systems are plotted in Figure 1, along with the recently reported experimental measurements of Wang et al. (Wang Y. et al., 2020); corresponding numerical data

are reported in Table 1. The simulation average values may be seen to be in generally good agreement with the experimental data, with the methanol mixtures showing increasing deviation at higher methanol content; in fact, the average density of the pure methanol model is noticeably higher than the experiment; 0.797 and 0.771 g/cm<sup>3</sup>, respectively. The discrepancies between simulated and experimental densities are of effectively comparable magnitude to those previously reported for classical MD simulations of these systems, specifically by Kaur et al. (Kaur et al., 2020) for the DES/water mixtures, using a refined CHARMM-based DES force field (Kaur et al., 2019) with SPC/E water (Berendsen et al., 1987), and, very recently, by Cea-Klapp et al. (Cea-Klapp et al., 2022) for the methanol mixtures, using the OPLS-AA-based (“OPLS-DES”) force field of Doherty and Acevedo (Doherty and Acevedo, 2018). Notably, the DES/methanol simulations of Cea-Klapp et al. more accurately reproduce the mixture density at high methanol content, which is not surprising considering the employed OPLS-AA methanol model was parameterized to reproduce bulk liquid properties (Jorgensen and Tirado-Rives, 1996).

The excess molar enthalpy,  $H^E$ , may be computed from computer simulations as follows (Dai et al., 2010),

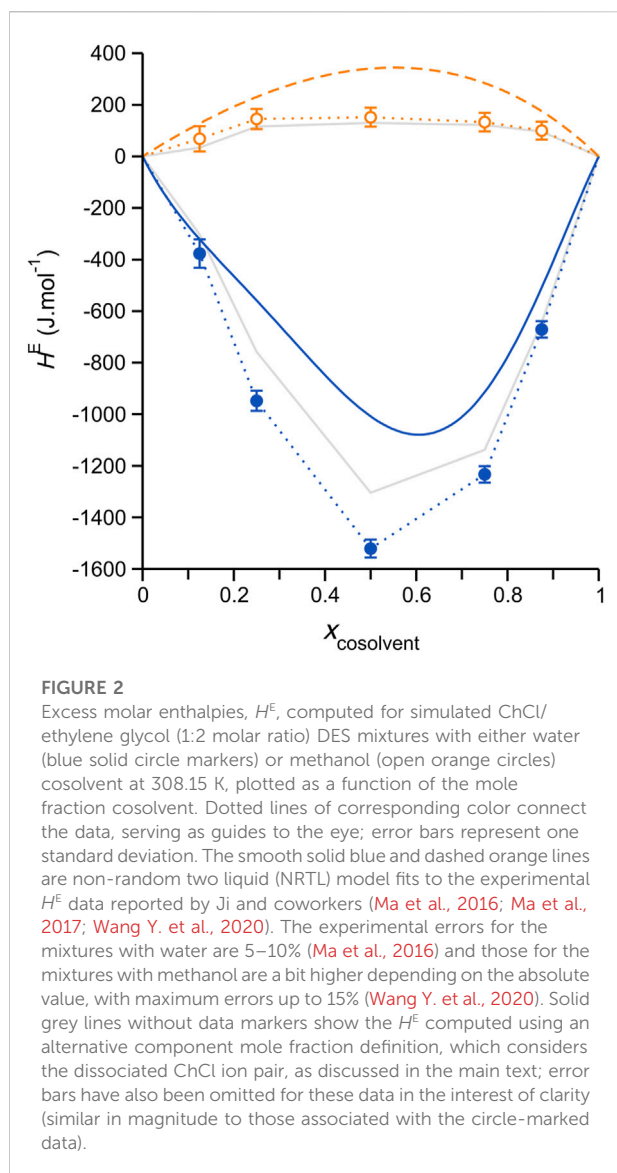
$$H^E = U_m - \sum x_i U_i + PV^E \quad (2)$$

where  $U_m$  is the average potential energy per molecule in the mixture,  $U_i$  is the corresponding values for the respective pure liquids, and  $x_i$  is their mole fractions in the mixture;  $p$  is the pressure, and  $V^E$  is the excess molar volume of the mixture. Since the  $V^E$  of liquid mixtures are small (Chitra and Smith, 2001), the  $PV^E$  term is often omitted from the calculation, in which case  $H^E$  is approximated as the excess molar potential energy,  $U^E$  (Walser et al., 2000; Wu et al., 2005):

$$H^E \approx U^E = U_m - \sum x_i U_i \quad (3)$$

The calculation of  $H^E$  from computer simulations of ChCl-based DES/cosolvent mixtures presents somewhat of a conceptual problem, since the DES component itself is a mixture containing a dissociable ionic component (ChCl); in fact, to the best of our knowledge, no computer simulation studies of the excess molar enthalpies of DES/cosolvent mixtures have been reported to date. Baz et al. (Baz et al., 2019), in their computational investigation of the thermophysical properties of glycine/water mixtures (including  $V^E$  and water activity coefficients), proposed an alternative mole fraction definition as appropriate for simulated DES/cosolvent systems, which considers the dissociated ChCl ion pair (as opposed to the more widely used definition in Eq. 1):

$$x_{\text{cosolvent}}^{\text{species}} = \frac{N_{\text{cosolvent}}}{N_{\text{Ch}^+} + N_{\text{Cl}^-} + N_{\text{HBD}} + N_{\text{cosolvent}}} \quad (4)$$



In the present work, the  $H^E$  results of the simulated systems were computed using Eq. 3, with average potential energies computed over the last 10 ns of each simulation. The statistical uncertainties in the computed data were evaluated by a block averaging procedure (Flyvbjerg and Petersen, 1989). In view of the established practice of computing  $H^E$  of simulated IL/cosolvent mixtures using mole fractions that consider IL ion pairs, e.g. (Wu et al., 2005), as well as considerations presented in a recent computational study of the vapor pressures of ChCl-based DESs (Salehi et al., 2021), including ethaline, the more common DES/cosolvent mole fraction definition in Eq. 1 was employed in the calculations. For comparison, we repeated the  $H^E$  calculations using the alternative mole fraction (species cosolvent) definition in Eq. 4, resulting in qualitatively similar trends (see below).

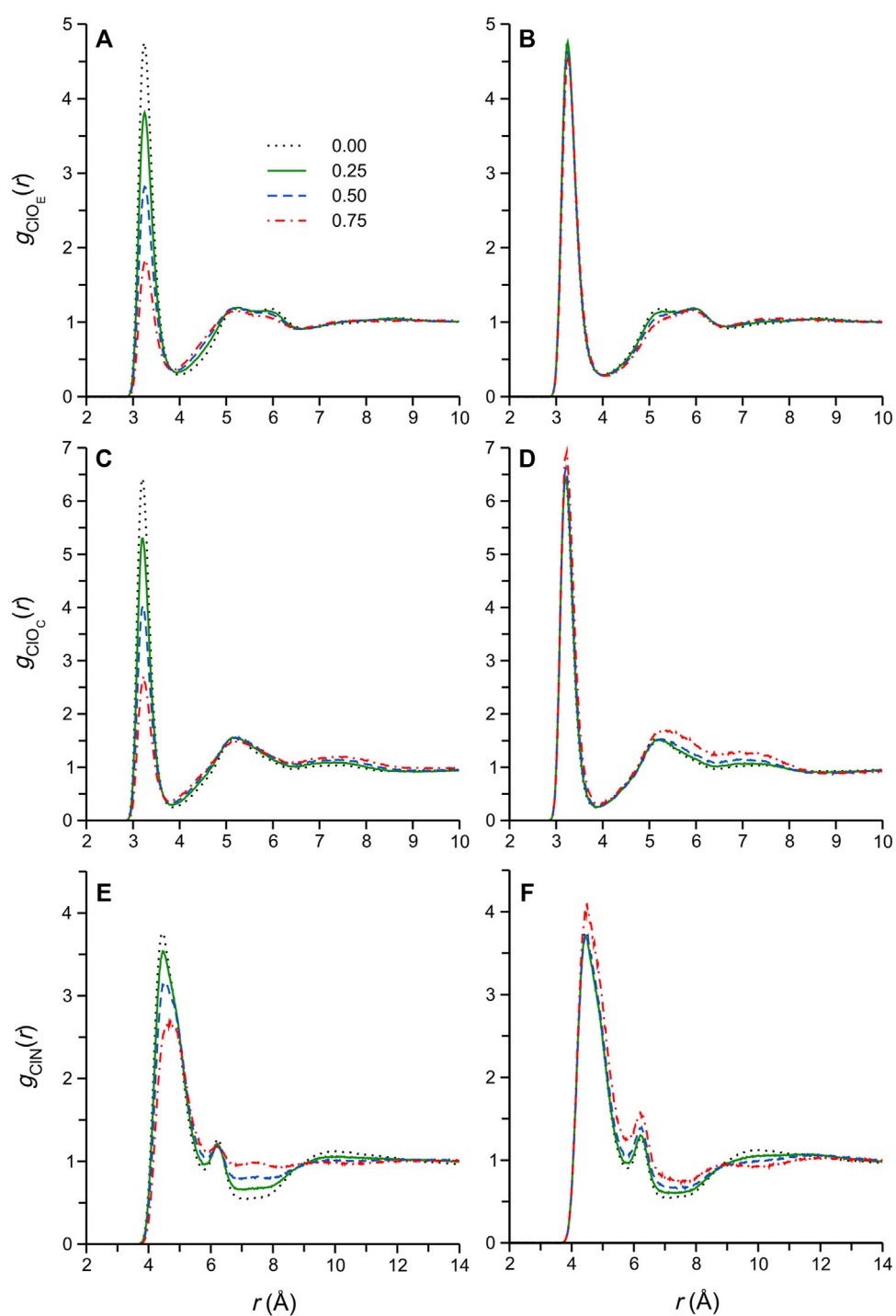
The  $H^E$  results obtained from our simulations are plotted in Figure 2, where they are compared with the experimental data of Wang et al. (Wang Y. et al., 2020). Despite substantial discrepancies, the simulations effectively reproduce the experimental sign difference (aqueous mixtures, strongly negative; methanol mixtures, low positive values) and essential trend shapes. Concerning the actual magnitude of the simulation/experimental deviations in Figure 2, it should be noted that these are generally consistent with those previously reported for liquid mixtures modeled using classical force fields, e.g. (Dai et al., 2010), including IL mixtures (Wu et al., 2005). The  $H^E$  values computed using the alternative mole fraction definition, Eq. 4, (solid grey lines with data markers omitted) are smaller in an absolute sense, substantially improving the agreement with the experiment for the aqueous mixtures. Finally, we note that the sign of deviations from the experiment are negative (i.e., smaller positive values for the DES/methanol systems, more negative values for the aqueous systems), which hints at an overestimation of the DES-cosolvent interaction strength in the simulations, likely electrostatic interactions (including H-bonding) (Engelbrecht et al., 2021). Nevertheless, despite uncertainty at this stage as to the more appropriate approach for computing  $H^E$  for these systems, the simulations clearly reproduce the key differences and general trends found experimentally.

## 3.2 Liquid structure

### 3.2.1 Radial distribution functions

The liquid structures of simulated DESs and their aqueous mixtures are routinely analyzed by radial distribution functions (RDFs), each describing the radially averaged correlation between a particle pair, and, together, representing the simulation average structure. These functions also have useful experimental counterparts, namely, neutron and X-ray scattering patterns, which have been reported for some ChCl-based DES systems (Hammond et al., 2016, 2017; Kumari et al., 2018; Kaur et al., 2019, 2020). While RDFs are widely used in the structural characterization of liquid systems (Engelbrecht et al., 2022), H-bonded liquids and mixtures in particular, the high structural complexity of DESs and their mixtures require the evaluation of a large number of such functions, and workers often resort to computing molecular “center-of-mass” (COM) RDFs in order to obtain more general information about structural rearrangements upon mixing (Kaur et al., 2017; Gao et al., 2018).

Strong ionic H-bonding interactions involving the DES  $\text{Cl}^-$  anion are widely accepted to play a central role not only in DES formation (Abbott et al., 2003), during which the anion is thought to be effectively coordinated by the HBD (thus disrupting strong electrostatic interactions between the ions, and decreasing the mp) (Ashworth et al., 2016), but also in determining the excess thermodynamic properties upon mixing

**FIGURE 3**

Radial distribution functions,  $g_{ClX}(r)$ , computed for  $Cl^-$ -X atom pairs for selected DES/water (A,C,E) and DES/methanol (B,D,F) systems, where  $X = O_E$  (EG oxygen atoms),  $O_C$  (cation oxygen atom), or N (cation N atom). The legend in (A) pertains to all other panels as well, and shows the mole fraction of the cosolvent in the corresponding simulated system.

of the DES with a cosolvent (Gao et al., 2018). In fact, a recent MD simulation study of aqueous DES mixtures, including ethaline, highlighted the critical role of  $\text{Cl}^-$  in determining the physical properties of these DES solutions (Celebi et al., 2019). In the present work, we start by considering Cl-X RDFs,  $g_{\text{ClX}}(r)$ , where the X are H-bond donor atoms of the DES and cosolvent. The RDFs for the pure DES and selected cosolvent mixtures are shown in Figure 3 (water mixtures data on the left, methanol mixtures on the right).

The RDFs for the pure DES and its aqueous mixtures (Figures 3A,C,E) have been reported under different, though similar, physical conditions, and analyzed in some detail (Perkins et al., 2014; Ferreira et al., 2016; Celebi et al., 2019; Kaur et al., 2019). In these previous reports, the sharp first (closest) maxima, or peak, of the  $g_{\text{ClO}}(r)$  functions, Figures 3A,C, is identified with H-bonding interactions ( $\text{Cl}^- \cdots \text{H}-\text{O}$ ) of  $\text{Cl}^-$  with EG and  $\text{Ch}^+$ , respectively. The intensity of these well-defined maxima, occurring at distances  $r_{\text{ClO}} = 3.3\text{--}3.2 \text{ \AA}$ , decreases with increasing water content, reflecting the entry of water molecules into the  $\text{Cl}^-$  coordination shell, where they displace DES components (Celebi et al., 2019). The  $g_{\text{ClN}}(r)$  results in Figure 3E, reporting spatial correlations between  $\text{Cl}^-$  and the  $\text{Ch}^+$  N atom, exhibit broad first maxima at greater distances,  $r_{\text{ClN}} > 4 \text{ \AA}$ , that result from electrostatic interactions between the anion and the bulky  $\text{Ch}^+$  ammonium group. At all aqueous mixture compositions, the second maximum of this function, occurring at  $r_{\text{ClN}} \approx 6 \text{ \AA}$ , arises from  $\text{Ch}^+$  cations interacting with  $\text{Cl}^-$  via so-called “doubly ionic” H-bonds, i.e.,  $\text{Ch}^+$  with relative orientations in which the  $-\text{OH}$  group is directed at  $\text{Cl}^-$ . In the pure DES, the  $g_{\text{ClN}}(r)$  first maximum has a noticeably asymmetric shape, suggesting the simultaneous presence of various (similarly favorable) interaction configurations, or modes, between  $\text{Cl}^-$  and the  $\text{Ch}^+$  ammonium group (Zahn et al., 2016; Stefanovic et al., 2017). Indeed, a number of different interaction modes were demonstrated by Ashworth et al. (Ashworth et al., 2016), and these are likely characterized by slightly different average Cl-N distances. The shape of the  $g_{\text{ClN}}(r)$  first maximum gradually changes with increasing water content, with the position of the actual maximum shifting from  $\sim 4.4$  to  $4.7 \text{ \AA}$ , suggesting a change in the predominant  $\text{Cl}^-$ - $\text{Ch}^+$  interaction mode upon dilution with water; this subtle change is also evident in the RDFs recently reported by Celebi et al. (Celebi et al., 2019) and Kaur et al. (Kaur et al., 2020).

Next, we consider the Cl-X RDFs of selected DES/methanol mixtures in Figures 3B,D,F, and note that these appear essentially invariant with respect to methanol content (compared to the corresponding functions for the aqueous mixtures), with first maximum intensities increasing slightly, and more noticeable changes only appearing at higher  $x_{\text{M}}$ , particularly at  $r_{\text{ClX}} > 4 \text{ \AA}$ . Interestingly, the asymmetric  $g_{\text{ClN}}(r)$  first peak profile of the pure DES largely persists in the methanol mixtures, even at high dilution, suggesting that the characteristic native DES  $\text{Cl}^-$ - $\text{Ch}^+$  interaction mode distribution does not change appreciably upon

the addition of methanol. These observations, which are in stark contrast to those described for the aqueous mixtures, are essentially consistent with the conclusions of Cea-Klapp et al. (Cea-Klapp et al., 2022), who very recently reported an MD simulation study of ethaline/methanol mixtures (to the best of our knowledge, the only other computational study of this system): “In DESs plus methanol mixtures, the basic characteristics of pure DESs are conserved. Despite this, adding methanol changes the structure of solvation shells, where the interaction of HBD with methanol takes centre stage”. The effectively constant RDF first maximum intensities with respect to methanol content in Figures 3B,D,E does not necessarily imply a more stable  $\text{Cl}^-$  coordination shell composition upon dilution with methanol as opposed to water, since the RDF intensities are normalized to the bulk particle density of the system, which changes with mixture composition; more complete information on the solvation shell composition may be obtained by appropriate RDF integration to yield coordination numbers (see below). Nevertheless, inspection of the RDFs in Figure 3 has provided interesting clues as to the different configurational changes in the  $\text{Cl}^-$  coordination shell region between the aqueous and methanolic DES mixtures.

In order to obtain direct information about DES-cosolvent interactions in these systems, the Cl-water oxygen ( $\text{O}_{\text{W}}$ ) and -methanol oxygen ( $\text{O}_{\text{M}}$ ) RDFs were computed; these functions relate to ionic H-bonding interactions between  $\text{Cl}^-$  and the respective cosolvents, and selected examples are shown in Figures 4A,B. As noted in Figure 3, the water mixtures show significant changes in the  $\text{Cl}^-$ - $\text{O}_{\text{W}}$  RDFs with increasing cosolvent content, while the  $\text{Cl}^-$ - $\text{O}_{\text{M}}$  RDFs remain more-or-less unchanged. The relative intensities of the first ( $r_{\text{ClO}} \approx 3.5 \text{ \AA}$ ) and broader second maxima ( $r_{\text{ClO}} \approx 4\text{--}6 \text{ \AA}$ ) in the RDFs of the aqueous systems show an interesting change with increasing water content, suggestive of changes in the mixture microstructure, specifically water self-association (Kaur et al., 2020). Such changes are not observed in the Cl- $\text{O}_{\text{M}}$  RDFs.

$\text{Cl}^-$ -cosolvent H-bonded coordination numbers,  $n_{\text{ClO}}$ , were obtained by integration of the corresponding  $\text{Cl}^-$ - $\text{O}_{\text{W/M}}$  RDF first maxima (i.e., taking the integral up to the first local minimum). The results of this procedure, plotted in Figure 4C, reveal that, despite the very noticeable differences in the RDF structural changes between the water and methanol systems (Figures 4A,B), the respective coordination numbers exhibit rather similar variations as a function of cosolvent content. Note that the  $\text{Cl}^-$ -cosolvent coordination numbers at effectively infinite dilution, i.e.,  $x_{\text{cosolvent}} = 1$ , were taken from literature (Impey et al., 1987; Powell et al., 1993); interestingly, experimental reports of the coordination numbers of  $\text{Cl}^-$  in methanol obtained by neutron and X-ray scattering methods vary considerably (Faralli et al., 2006), between ca. 3.5 (Yamagami et al., 1995) and 6.2 (Megyes et al., 2002), and thus it was decided to adopt an intermediate value (5) derived from the computer

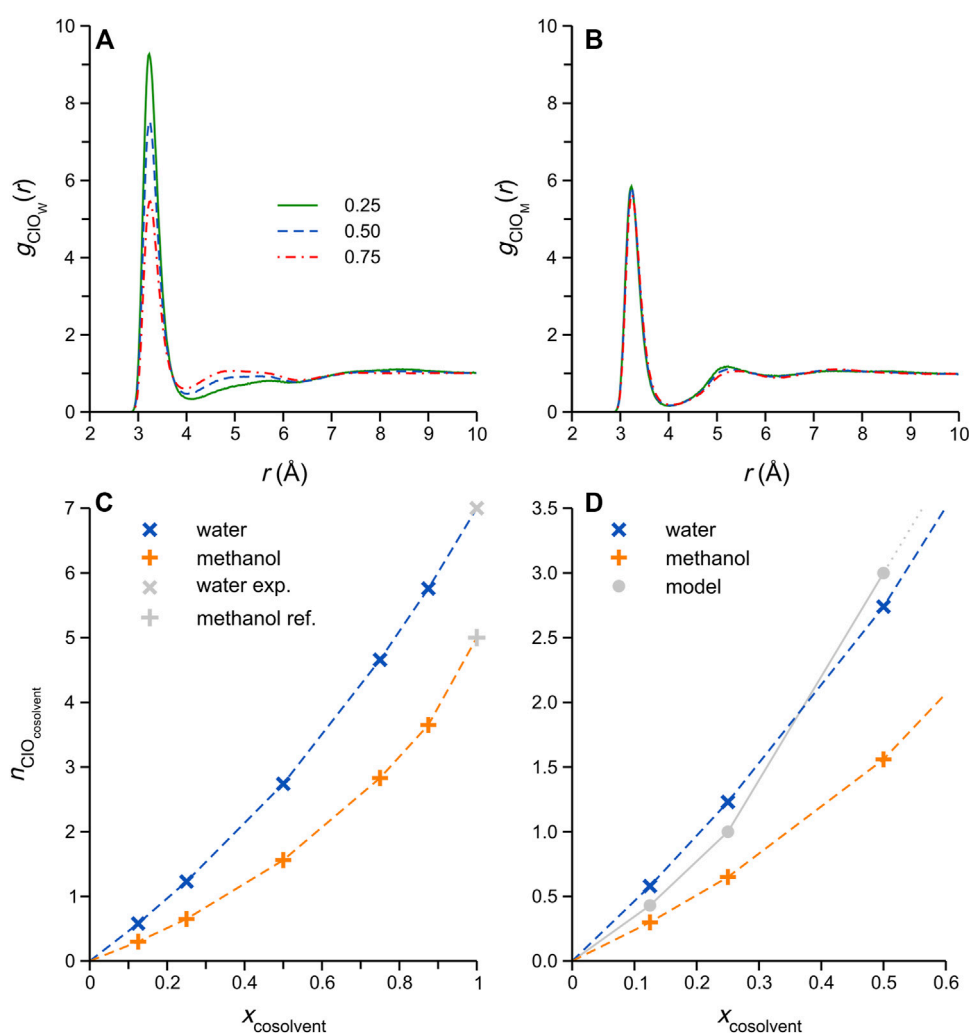


FIGURE 4

Cl<sup>-</sup>-O<sub>cosolvent</sub> RDFs for selected (A) DES/water, and (B) DES/methanol simulated mixtures; the legend in panel A refers to the cosolvent mole fraction, and applies to both (A,B). (C) Cl<sup>-</sup>-O<sub>cosolvent</sub> coordination numbers, computed by integration of corresponding  $g_{\text{ClO}}(r)$  first maxima, plotted as a function of cosolvent content. The Cl<sup>-</sup> coordination number in the respective cosolvents (i.e. effectively infinite dilution) was taken from literature sources: Powell et al. (Powell et al., 1993) for the coordination number in water, and Impey et al. (Impey et al., 1987) for methanol. (D) Expansion of the low  $x_{\text{cosolvent}}$  range in (C), showing the expected Cl<sup>-</sup>-cosolvent coordination number variation considering a simple strong Cl<sup>-</sup>-cosolvent attraction model (grey circles connected by solid grey line) described in the main text.

simulation (Impey et al., 1987). For both mixtures, the  $n_{\text{ClO}}$  data follow curved trends with increasing cosolvent content, with the water coordination numbers consistently higher. The latter observation is not surprising, considering the higher polarity (partial atomic charges) and smaller size of water. However, closer inspection of the  $n_{\text{ClO}}$  data at low cosolvent content ( $x_{\text{W}}/M < 0.5$ ) reveals that the Cl<sup>-</sup>-water coordination numbers are, indeed, unexpectedly high: consider a simple model in which the Cl<sup>-</sup>-cosolvent attraction is sufficiently strong (i.e., a sort of “strong-limit” scenario) that each cosolvent molecule added to the DES binds (via ionic H-bonding) to a single Cl<sup>-</sup> anion, displacing the required number of DES components in the Cl<sup>-</sup>

coordination shell; for both cosolvents, this scenario should result in the grey data points in Figure 4D, which is otherwise simply an expansion of the low cosolvent content-range in Figure 4C. At higher cosolvent content, the Cl<sup>-</sup> coordination shell would be saturated by cosolvent molecules within this hypothetical strong-attraction model, and this illustrative model becomes less useful. Interestingly, the average values of Cl<sup>-</sup>-water  $n_{\text{ClO}}$  obtained from our simulations are *higher* than the model predictions at  $x_{\text{W}} = 0.125$  and 0.25, which points to a significant tendency of water molecules to insert between two neighboring Cl<sup>-</sup> anions, i.e., acting as H-bonded bridges. This is not possible in the corresponding methanol mixtures, as



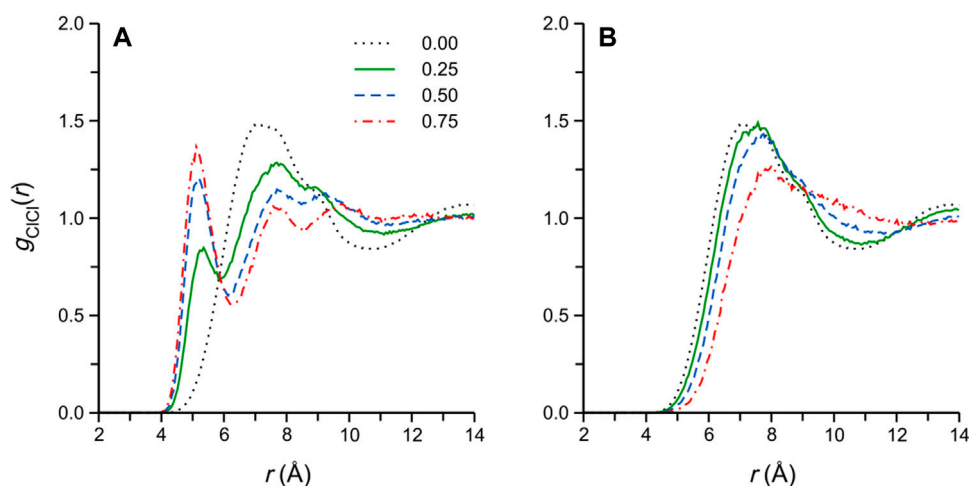


FIGURE 5

Cl<sup>−</sup>-Cl<sup>−</sup> RDFs of selected (A) DES/water and (B) DES/methanol simulated systems. The numbers in the legend in (A) refer to the cosolvent mole fraction, and applies to both panels.

methanol can donate a single H-bond only. The concept of such “bridging” arrangements has been explored in the pure ethaline DES (Kaur et al., 2020), in which Cl<sup>−</sup> anions have been described as bridges connecting Ch<sup>+</sup> and EG, rapidly dissolving upon the addition of water.

The Cl<sup>−</sup>-Cl<sup>−</sup> RDFs of selected simulated DES/water and methanol mixtures are reported in Figures 5A,B, respectively. These functions are frequently reported for the (simulated) pure DES and its aqueous mixtures (Perkins et al., 2014; Ferreira et al., 2016; Celebi et al., 2019; Kaur et al., 2019), though not for the DES/methanol mixtures (Cea-Klapp et al., 2022). In the pure ethaline DES, the function is characterized by a broad, apparently convoluted, first maximum at  $r_{\text{ClCl}} \approx 7\text{--}8\text{ Å}$  (we note that the corresponding RDF reported by Kaur et al. (Kaur et al., 2019) is somewhat different, displaying a clear shoulder at short distances at 303 K); this convoluted first-maximum structure likely arises from Cl<sup>−</sup> pairs located in the different characteristic “bridging” configurations in the DES (Kaur et al., 2020), i.e., either separated by an EG molecule or Ch<sup>+</sup>, both of which are conformationally flexible.

Turning to the DES/water and methanol mixtures, we note that the changes in, and differences among, the  $g_{\text{ClCl}}(r)$  in Figure 5 are intriguing, showing clear qualitative differences between the two cosolvents. In the DES/water systems (Figure 5A), a well-defined  $g_{\text{ClCl}}(r)$  local maximum appears upon the addition of water, first as a low- $r_{\text{ClCl}}$  shoulder around  $r_{\text{ClCl}} \approx 5.5\text{ Å}$  (at  $x_{\text{W}} = 0.125$ ), which then separates and sharpens, gradually shifting to  $r_{\text{ClCl}} = 5.0\text{ Å}$  (at  $x_{\text{W}} = 0.875$ ) with increasing water content. The appearance of this new  $g_{\text{ClCl}}(r)$  peak in ethaline/water mixtures was also reported in previous classical simulation studies (Celebi et al., 2019; Kaur

et al., 2020) and, interestingly, in a recent *ab initio* MD report by Kirchner and coworkers (Alizadeh et al., 2020), though it appears its significance has not yet received detailed consideration. Indeed, this short-range  $g_{\text{ClCl}}(r)$  feature is *completely absent* for the corresponding DES/methanol simulated systems (Figure 5B), where the broad first maximum of the pure DES simply loses definition and gradually shifts to larger  $r_{\text{ClCl}}$  with increasing methanol content, as may be expected from the dilution of the DES components.

The RDFs in Figures 3A–D may be similarly integrated to obtain H-bonded coordination numbers for other DES components to Cl<sup>−</sup>. The Cl<sup>−</sup>-Ch<sup>+</sup> and Cl<sup>−</sup>-EG coordination numbers reported in Supplementary Figure S6, for example, show that, on average, water molecules displace a larger fraction of H-bonded DES components from the Cl<sup>−</sup> coordination shell compared to methanol at all DES/cosolvent compositions. This finding further underscores the strength of Cl<sup>−</sup>-water ionic H-bonds in the DES/water mixtures.

### 3.2.2 Simulation configurations and cluster analysis

The short-range  $g_{\text{ClCl}}(r)$  maximum that appears in the DES/water mixtures implies the formation of geometrically well-defined structures in which Cl<sup>−</sup> pairs are drawn closer together compared to distances characteristic of the pure DES structure. This observation is also consistent with our conclusion of water H-bonded “bridges” connecting neighboring Cl<sup>−</sup> anions, inferred above from the consideration of Cl<sup>−</sup>-water coordination numbers (Figure 4D). Indeed, visual inspection of selected DES/water simulation configurations at low water content

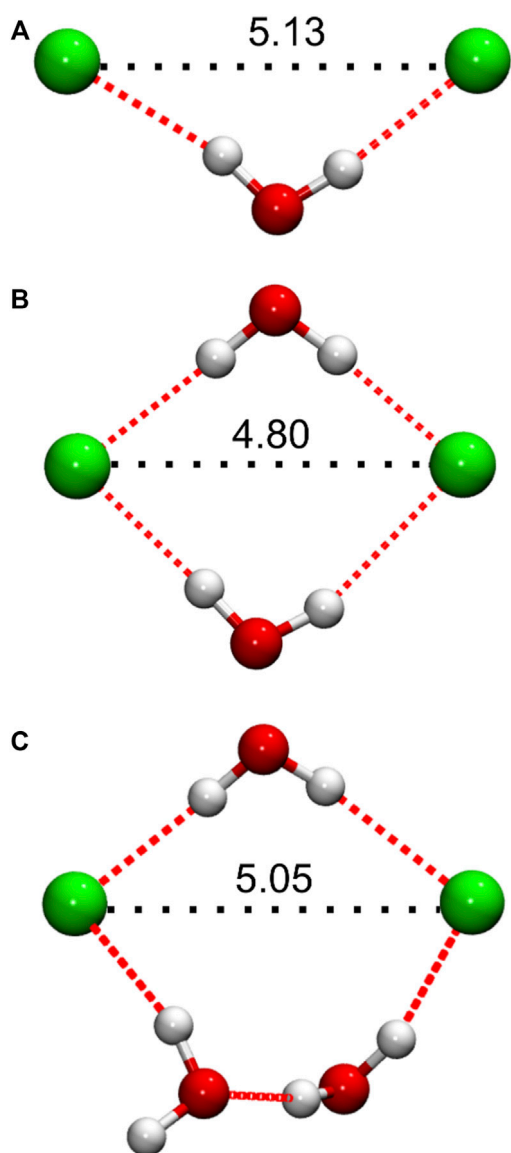


FIGURE 6

Representative  $\text{Cl}^-$  anion pair configurations from simulated DES/water systems, showing water molecules involved in the formation of H-bonded (dotted red lines) bridging structures, as discussed in the main text. Distances ( $\text{\AA}$ ) between the  $\text{Cl}^-$  anions are indicated in black, as relevant to the interpretation of the corresponding  $g_{\text{ClCl}}(r)$  functions. (A) Single, and (B,C) double H-bonded bridging arrangements. Configurations (A,B) were taken from the DES/water mixture with  $x_W = 0.125$ , while (C) was taken from  $x_W = 0.5$ .

reveals an abundance of such arrangements, in which  $\text{Cl}^-$  pairs are connected by one, or two, H-bonded water molecule “bridges”; representative configurations are shown in Figures 6A,B. A special case of two H-bonded water bridges connecting a  $\text{Cl}^-$  pair is also frequently observed, particularly at higher  $x_W$ , in which one of the bridges

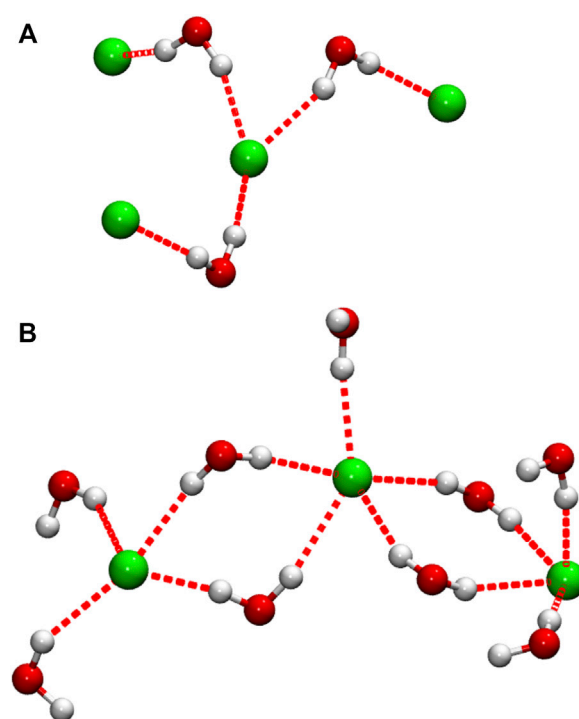


FIGURE 7

Selected configurations showing  $\text{Cl}^-$  anions connected by H-bonded water bridges. In the interest of clarity, only water molecules directly H-bonded (red dotted lines) to  $\text{Cl}^-$  are shown. Configuration (A) was taken from the DES/water mixture at the lowest water content studied ( $x_W = 0.125$ ), while (B) was taken from the highest water concentration ( $x_W = 0.875$ ); configuration (B) forms part of a more expansive H-bonded network.

consists of two H-bonded water molecules, as shown in Figure 6C. At low  $x_W$ , a cursory investigation of simulation configurations suggests that  $\text{Cl}^-$  pairs connected by a single H-bonded water molecule exhibit generally greater, and more variable, interionic separations (approximately,  $\sim 5 \text{ \AA} < r_{\text{ClCl}} \leq 5.8 \text{ \AA}$ ) compared to pairs connected by two water molecules, e.g., Figures 6B,C, for which often  $r_{\text{ClCl}} < 5 \text{ \AA}$ . With increasing water content,  $\text{Cl}^-$  pairs of the latter two types become more prominent, resulting in a decrease in the average  $r_{\text{ClCl}}$  associated with  $\text{Cl}^-$ -pair structures, consistent with the gradual shift of the  $g_{\text{ClCl}}(r)$  first maximum to  $r_{\text{ClCl}}$  with increasing  $x_W$  (Figure 5A).

In order to obtain information on the importance of the  $\text{Cl}^-$ -pair structures described above, a simple cluster analysis was performed, in which any two anions separated by  $r_{\text{ClCl}} \leq 5.1 \text{ \AA}$  are considered as the members of the same water-bridged  $\text{Cl}^-$  “cluster”; the chosen cutoff distance corresponds to the position of the closest  $g_{\text{ClCl}}(r)$  maximum observed in our simulations, at  $x_W = 0.875$ , and is also a distance at which the pure DES function has negligible intensity. The analysis shows that at the lowest water

content studied ( $x_W = 0.125$ ), on average, about 11% of anions occur in close  $\text{Cl}^-$  pairs. This number increases with increasing water content to ~30% in the equimolar DES/water mixture, indicating an increase in the occurrence of such pairs, after which it again decreases with further dilution to 16% at the highest DES dilution studied ( $x_W = 0.875$ ). Interestingly, the cluster analysis also reveals the presence of larger clusters of this type, containing up to ca. 5–7 anions, depending on the particular system, though these larger clusters account for only a very small anion fraction, < 1% for all systems studied. Examples of these intriguing cluster configurations are presented in Figure 7. Recently, Triolo et al. (Triolo et al., 2021) reported the formation of long H-bonded chains involving water-water and water- $\text{Cl}^-$  connections in their simulations of a ChCl/water natural DES, which suggests that water- $\text{Cl}^-$  H-bonded structures may be a more common feature of ChCl-based DES aqueous mixtures.

The  $\text{Cl}^-$  pair configuration in Figure 6C illustrates another important characteristic of the DES/water system, namely a tendency of water molecules to self-associate *via* H-bonding. In fact, in this particular configuration, each water molecule shown is engaged in at least one H-bond with a surrounding water molecule (not shown). The self-association of water molecules in the DES/water mixtures is further exemplified by the full  $\text{Cl}^-$ -pair coordination environment configuration shown in Supplementary Figure S7. Similarly, larger water-bridged  $\text{Cl}^-$  configurations, e.g., those shown in Figure 7, typically form part of more extended H-bonded water networks, which also frequently include more distant  $\text{Cl}^-$  anions (i.e., separated by two or more H-bonded water molecules from nearest  $\text{Cl}^-$  neighbors). The prominence of such extended H-bonded networks increases with increasing water content. Interestingly, the question of cosolvent self-association in DES/cosolvent mixtures has not yet received the same computational consideration as IL/water mixtures, for which the phenomenon has been extensively studied by computer simulation techniques (see, e.g. (Jiang et al., 2007), and the review articles (Bhargava et al., 2011; Ma et al., 2018), and references therein). In DESs, however, the situation is complicated considerably by the presence of the neutral HBD; in fact, EG has been reported to self-associate at higher water content in ethaline/water mixtures (Kaur et al., 2020). In their recent report on ethaline/methanol mixture simulations, Cea-Klapp et al. (Cea-Klapp et al., 2022) presented results on the self-association of mixture components, including methanol and EG; these alcohols, having similar H-bonding capabilities, are expected to be more freely miscible in the DES/methanol mixtures (compared to water, that can form H-bonded networks), though it may be interesting to perform an analysis of neutral aggregates containing either species. The extent of cosolvent (or, indeed, DES component) self-association was not studied in the present work, but presents an interesting topic for future detailed study. Moreover, knowledge of cosolvent self-association, or of other DES/cosolvent mixture components, may also contribute to understanding the excess thermodynamic properties of such mixtures, as outlined below.

### 3.3 Interpretation of excess molar enthalpies in context of structural results

The principal structural features of the simulated DES/water mixtures, namely, 1) water molecules interact strongly with DES  $\text{Cl}^-$  anions through ionic H-bonds, acting as H-bonded bridges connecting neighboring anions, and 2) water molecules tend to retain some of the pure water H-bonded network through self-association in the DES/water mixture, are consistent with their strongly exothermic mixing (Ma et al., 2017). Notably, these two structural features appear to be connected, in that  $\text{Cl}^-$  are incorporated into water H-bonded networks, as also recently reported for a ChCl/water natural DES (Triolo et al., 2021).

In the corresponding DES/methanol mixtures, the cosolvent also enters the  $\text{Cl}^-$  coordination shell, forming ionic H-bonds, partially displacing DES components  $\text{Ch}^+$  and EG. The latter, in particular, has been shown to engage in strong ionic H-bonding interactions with  $\text{Cl}^-$  in the pure ethaline DES (Kaur et al., 2019; Alizadeh et al., 2020), either by adopting a *gauche* conformation and coordinating the anion in a bidentate fashion, or by acting as an H-bonded bridge between neighboring anions (or between anions and cations). While methanol, like EG, can form ionic H-bonds with  $\text{Cl}^-$ , it cannot facilitate the H-bonded bridging structures that are present in the pure DES, and its displacement of EG from the  $\text{Cl}^-$  coordination shell leads to a reduction of the DES H-bonded network (Cea-Klapp et al., 2022). This structural change is evident in the loss of definition and gradual shift to longer distances of the  $g_{\text{ClCl}}(r)$  first maximum with increasing methanol content, and also explains the slightly positive  $H^E$  reported for these mixtures (Wang Y. et al., 2020).

The recent computational-theoretical study of Cea-Klapp et al. (Cea-Klapp et al., 2022) reports that methanol self-association does occur in ethaline/methanol mixtures; while the present study did not investigate this phenomenon, we find it unlikely that the favorable H-bonded ring or even chain structures that have been shown to characterize pure liquid methanol structure should persist in the DES mixtures (Allison et al., 2005), which would make a further positive contribution to  $H^E$ .

## 4 Conclusion

Computer simulation studies of ChCl-based DES/cosolvent mixtures (mainly aqueous mixtures) are increasingly reported, largely focusing on understanding their complex H-bonding interactions; to the best of our knowledge, none have attempted to compute or rationalize excess molar enthalpies. In view of the lack of an established protocol, we tested two related approaches for computing the equivalent excess molar enthalpies for classical MD simulations of mixtures of the DES ethaline (a 1:2 molar ratio mixture of ChCl and ethylene glycol) with either water or methanol. Both approaches reproduce the striking experimental sign difference and general composition

dependent variation of the property for the two mixture series (negative at all compositions for aqueous mixtures; positive for methanol mixtures) (Wang Y. et al., 2020).

Structural analyses were aimed at characterizing the DES  $\text{Cl}^-$  anion coordination environment, since strong ionic H-bonding interactions involving this anion are thought to play a central role in determining the excess thermodynamic properties of DES mixtures (Gao et al., 2018). For the aqueous DES mixtures, we showed the curious decrease in closest  $\text{Cl}^-$ - $\text{Cl}^-$  interionic distances with increasing water content—also previously reported in classical (Celebi et al., 2019; Kaur et al., 2020) and *ab initio* MD studies (Alizadeh et al., 2020) of this and related DESs—to be due to water molecules inserting between neighboring  $\text{Cl}^-$  anions, where they form ionic H-bonded bridges that draw the anions closer. The resulting structures are characterized by notably short ( $\leq 5$  Å) interionic separations. A cluster analysis aimed at identifying such “water-bridged”  $\text{Cl}^-$  pair and larger structures revealed that these account for a notable anion fraction, reaching a maximum of 30% in the equimolar DES/water system and decreasing with further dilution to 16% (water mole fraction  $x_{\text{W}} = 0.875$ ). Intriguing larger water-bridged  $\text{Cl}^-$  arrangements, both linear and branched, were also identified; this finding prompts future experimental studies to determine whether these are present in real samples, as their presence may have important implications for applications of the mixtures as solvents or reaction media.

While both water and methanol may be used as cosolvents for reducing the high bulk viscosities of DESs, different intermolecular interactions in the resulting DES/cosolvent - experimentally detectable by measurement of the excess molar enthalpy - may favor one the other for a particular application. We showed that classical MD simulations, that were never used before to calculate  $H^{\text{E}}$  for DES/cosolvent mixtures, can reproduce the sign and general trend of  $H^{\text{E}}$  for mixtures these highly complex “pseudo-binary” DES/cosolvent mixtures. Further studies on related systems, will be required to confirm the general applicability of the approach. In addition, considering the very recent development of polarizable force field for this DES (de Souza et al., 2021; Goloviznina et al., 2021), it would be interesting to compare their performance for the calculation of thermodynamical properties.

## Data availability statement

The raw data supporting the conclusion of this article will be made available by the authors, without undue reservation.

## Author contributions

LE performed the simulations; LE and FM analyzed the simulation trajectories. All the authors planned the research, discussed the data, and contributed to the writing of the manuscript.

## Acknowledgments

LE and AL gratefully acknowledge the computer resources and technical support provided by The PDC Center for High Performance Computing at the KTH Royal Institute of Technology, Sweden. Computational resources provided by the Swedish National Infrastructure for Computing (SNIC) at HPC2N. AL acknowledges Swedish Research Council for financial support, and partial support from a grant from Ministry of Research and Innovation of Romania (CNCS—UEFISCDI, project number PN-III-P4-ID-PCCF-2016-0050, within PNCDI III). XJ acknowledges Swedish Research Council for financial support. FM and LE acknowledge financial support from Progetto Fondazione di Sardegna (Grant CUP: F72F20000230007). FM, LE, and CC acknowledge MIUR, Project PRIN 2017 “CANDL2” (Grant 2017W75RAE). All the authors acknowledge the COSY COST ACTION CA21101.

## Conflict of interest

The authors declare that the research was conducted in the absence of any commercial or financial relationships that could be construed as a potential conflict of interest.

## Publisher's note

All claims expressed in this article are solely those of the authors and do not necessarily represent those of their affiliated organizations, or those of the publisher, the editors and the reviewers. Any product that may be evaluated in this article, or claim that may be made by its manufacturer, is not guaranteed or endorsed by the publisher.

## Supplementary material

The Supplementary Material for this article can be found online at: <https://www.frontiersin.org/articles/10.3389/fchem.2022.983281/full#supplementary-material>

## References

- Abbott, A. P., Capper, G., Davies, D. L., Rasheed, R. K., and Tambyrajah, V. (2003). Novel solvent properties of choline chloride/urea mixtures. *Chem. Commun.*, 70–71. doi:10.1039/B210714G
- Alizadeh, V., Malberg, F., Pádúa, A. A. H., and Kirchner, B. (2020). Are there magic compositions in deep eutectic solvents? Effects of composition and water content in choline chloride/ethylene glycol from ab initio molecular dynamics. *J. Phys. Chem. B* 124, 7433–7443. doi:10.1021/acs.jpcc.0c04844
- Allison, S. K., Fox, J. P., Hargreaves, R., and Bates, S. P. (2005). Clustering and microimmiscibility in alcohol-water mixtures: Evidence from molecular-dynamics simulations. *Phys. Rev. B* 71, 024201. doi:10.1103/PhysRevB.71.024201
- Ashworth, C. R., Matthews, R. P., Welton, T., and Hunt, P. A. (2016). Doubly ionic hydrogen bond interactions within the choline chloride-urea deep eutectic solvent. *Phys. Chem. Chem. Phys.* 18, 18145–18160. doi:10.1039/C6CP02815B
- Baz, J., Held, C., Pleiss, J., and Hansen, N. (2019). Thermophysical properties of glycine-water mixtures investigated by molecular modelling. *Phys. Chem. Chem. Phys.* 21, 6467–6476. doi:10.1039/C9CP00036D
- Berendsen, H. J. C., Grigera, J. R., and Straatsma, T. P. (1987). The missing term in effective pair potentials. *J. Phys. Chem.* 91, 6269–6271. doi:10.1021/j100308a038
- Berendsen, H. J. C., Postma, J. P. M., van Gunsteren, W. F., DiNola, A., and Haak, J. R. (1984). Molecular dynamics with coupling to an external bath. *J. Chem. Phys.* 81, 3684–3690. doi:10.1063/1.448118
- Bhargava, B. L., Yasaka, Y., and Klein, M. L. (2011). Computational studies of room temperature ionic liquid-water mixtures. *Chem. Commun.* 47, 6228–6241. doi:10.1039/C1CC10575B
- Case, D. A., Betz, R. M., Cerati, D. S., Cheatham III, T. E., Darden, T. A., Duke, R. E., et al. (2016). *Amber 2016*. San Francisco, CA: University of California.
- Cea-Klapp, E., Garrido, J. M., and Quinteros-Lama, H. (2022). Insights into the orientation and hydrogen bond influence on thermophysical and transport properties in choline-based deep eutectic solvents and methanol. *J. Mol. Liq.* 345, 117019. doi:10.1016/j.molliq.2021.117019
- Celebi, A. T., Vlught, T. J. H., and Moulton, O. A. (2019). Structural, thermodynamic, and transport properties of aqueous reline and ethaline solutions from molecular dynamics simulations. *J. Phys. Chem. B* 123, 11014–11025. doi:10.1021/acs.jpcc.9b09729
- Chitra, R., and Smith, P. E. (2001). Properties of 2, 2, 2-trifluoroethanol and water mixtures. *J. Chem. Phys.* 114, 426–435. doi:10.1063/1.1330577
- Dai, J., Li, X., Zhao, L., and Sun, H. (2010). Enthalpies of mixing predicted using molecular dynamics simulations and OPLS force field. *Fluid Phase Equilib.* 289, 156–165. doi:10.1016/j.fluid.2009.11.028
- Darden, T., York, D., and Pedersen, L. (1993). Particle mesh Ewald: An N-log(N) method for Ewald sums in large systems. *J. Chem. Phys.* 98, 10089–10092. doi:10.1063/1.464397
- de Souza, R. M., Karttunen, M., and Ribeiro, M. C. C. (2021). Fine-tuning the polarizable CL&amp;Pol force field for the deep eutectic solvent ethaline. *J. Chem. Inf. Model.* 61, 5938–5947. doi:10.1021/acs.jcim.1c01181
- Demurtas, M., Onnis, V., Zucca, P., Rescigno, A., Lachowicz, J. I., Engelbrecht, L. de V., et al. (2021). Cholinium-based ionic liquids from hydroxycinnamic acids as new promising bioactive agents: A combined experimental and theoretical investigation. *ACS Sustain. Chem. Eng.* 9, 2975–2986. doi:10.1021/acssuschemeng.1c00090
- Doherty, B., and Acevedo, O. (2018). OPLS force field for choline chloride-based deep eutectic solvents. *J. Phys. Chem. B* 122, 9982–9993. doi:10.1021/acs.jpcc.8b06647
- Dupradeau, F.-Y., Pigache, A., Zaffran, T., Savineau, C., Lelong, R., Grivel, N., et al. (2010). The R.E.D. Tools: Advances in RESP and ESP charge derivation and force field library building. *Phys. Chem. Chem. Phys.* 12, 7821–7839. doi:10.1039/C0CP00111B
- Dupradeau, F.-Y. (2005). R.E.D.D.B. project W-32. Available at: <https://upiv.q4md-forcefieldtools.org/REDDDB/projects/W-32/>.
- Engelbrecht, L. de V., Farris, R., Vasiliu, T., Demurtas, M., Piras, A., Cesare Maricola, F., et al. (2021). Theoretical and experimental study of the excess thermodynamic properties of highly nonideal liquid mixtures of butanol isomers + DBE. *J. Phys. Chem. B* 125, 587–600. doi:10.1021/acs.jpcc.0c10076
- Engelbrecht, L. de V., Mocci, F., Wang, Y., Perepelitsa, S., Vasiliu, T., and Laaksonen, A. (2022). “Molecular perspective on solutions and liquid mixtures from modelling and experiment,” in *Soft matter systems for biomedical applications*. Editors L. Bulavin and N. Lebovka (Cham: Springer), 53–84. doi:10.1007/978-3-030-80924-9\_3
- Engelbrecht, L., Mocci, F., Laaksonen, A., and Koch, K. R. (2018). 195Pt NMR and molecular dynamics simulation study of the solvation of [PtCl<sub>6</sub>]<sup>2-</sup> in water-methanol and water-dimethoxyethane binary mixtures. *Inorg. Chem.* 57, 12025–12037. doi:10.1021/acs.inorgchem.8b01554
- Faralli, C., Pagliai, M., Cardini, G., and Schettino, V. (2006). Structure and dynamics of Br<sup>-</sup> ion in liquid methanol. *J. Phys. Chem. B* 110, 14923–14928. doi:10.1021/jp061230o
- Ferreira, E. S. C., Voroshlyova, I. V., Pereira, C. M., and Cordeiro, M. N. D. S. (2016). Improved force field model for the deep eutectic solvent ethaline: Reliable physicochemical properties. *J. Phys. Chem. B* 120, 10124–10137. doi:10.1021/acs.jpcc.6b07233
- Flyvbjerg, H., and Petersen, H. G. (1989). Error estimates on averages of correlated data. *J. Chem. Phys.* 91, 461–466. doi:10.1063/1.457480
- Gao, Q., Zhu, Y., Ji, X., Zhu, W., Lu, L., and Lu, X. (2018). Effect of water concentration on the microstructures of choline chloride/urea (1:2)/water mixture. *Fluid Phase Equilib.* 470, 134–139. doi:10.1016/j.fluid.2018.01.031
- García, G., Aparicio, S., Ullah, R., and Atilhan, M. (2015). Deep eutectic solvents: Physicochemical properties and gas separation applications. *Energy Fuels* 29, 2616–2644. doi:10.1021/ef5028873
- Goloviznina, K., Gong, Z., Costa Gomez, M. F., and Pádúa, A. A. H. (2021). Extension of the CL&pol polarizable force field to electrolytes, protic ionic liquids, and deep eutectic solvents. *J. Chem. Theory Comput.* 17, 1606–1617. doi:10.1021/acs.jctc.0c01002
- Hammond, O. S., Bowron, D. T., and Edler, K. J. (2016). Liquid structure of the choline chloride-urea deep eutectic solvent (reline) from neutron diffraction and atomistic modelling. *Green Chem.* 18, 2736–2744. doi:10.1039/C5GC02914G
- Hammond, O. S., Bowron, D. T., and Edler, K. J. (2017). The effect of water upon deep eutectic solvent nanostructure: An unusual transition from ionic mixture to aqueous solution. *Angew. Chem. Int. Ed.* 56, 9782–9785. doi:10.1002/anie.201702486
- Hansen, B. B., Spittle, S., Chen, B., Poe, D., Zhang, Y., Klein, J. M., et al. (2021). Deep eutectic solvents: A review of fundamentals and applications. *Chem. Rev.* 121, 1232–1285. doi:10.1021/acs.chemrev.0c00385
- Harifi-Mood, A. R., and Buchner, R. (2017). Density, viscosity, and conductivity of choline chloride + ethylene glycol as a deep eutectic solvent and its binary mixtures with dimethyl sulfoxide. *J. Mol. Liq.* 225, 689–695. doi:10.1016/j.molliq.2016.10.115
- Impey, R. W., Sprik, M., and Klein, M. L. (1987). Ionic solvation in nonaqueous solvents: The structure of lithium ion and chloride in methanol, ammonia, and methylamine. *J. Am. Chem. Soc.* 109, 5900–5904. doi:10.1021/ja00254a002
- Jiang, W., Wang, Y., and Voth, G. A. (2007). Molecular dynamics simulation of nanostructural organization in ionic liquid/water mixtures. *J. Phys. Chem. B* 111, 4812–4818. doi:10.1021/jp067142l
- Jorgensen, W. L., and Tirado-Rives, J. (1996). Development and testing of the OPLS all-atom force field on conformational energetics and properties of organic liquids. *J. Am. Chem. Soc.* 118, 11225–11236. doi:10.1021/ja9621760
- Kaur, S., Gupta, A., and Kashyap, H. (2020). How hydration affects the microscopic structural morphology in a deep eutectic solvent. *J. Phys. Chem. B* 124, 2230–2237. doi:10.1021/acs.jpcc.9b11753
- Kaur, S., Malik, A., and Kashyap, H. K. (2019). Anatomy of microscopic structure of ethaline deep eutectic solvent decoded through molecular dynamics simulations. *J. Phys. Chem. B* 123, 8291–8299. doi:10.1021/acs.jpcc.9b06624
- Kaur, S., Sharma, S., and Kashyap, H. K. (2017). Bulk and interfacial structures of reline deep eutectic solvent: A molecular dynamics study. *J. Chem. Phys.* 147, 194507. doi:10.1063/1.4996644
- Kumari, P., ShobhnaKaur, S., and Kashyap, H. K. (2018). Influence of hydration on the structure of reline deep eutectic solvent: A molecular dynamics study. *ACS Omega* 3, 15246–15255. doi:10.1021/acsomega.8b02447
- Laaksonen, A., Lyubartsev, A., and Mocci, F. (2012). “M.DynaMix studies of solvation, solubility and permeability,” in *Molecular dynamics - studies of synthetic and biological macromolecules*. Editor L. Wang (London: IntechOpen), 85–106. doi:10.5772/35955
- Lengvinaitė, D., Kvedaravičiūtė, S., Bielskutė, S., Klimavičius, V., Balevicius, V., Mocci, F., et al. (2021). Structural features of the [C<sub>4</sub>mim][Cl] ionic liquid and its mixtures with water: Insight from a <sup>1</sup>H NMR experimental and QM/MD study. *J. Phys. Chem. B* 125, 13255–13266. doi:10.1021/acs.jpcc.1c08215
- Ma, C., Guo, Y., Li, D., Zong, J., Ji, X., Liu, C., et al. (2016). Molar enthalpy of mixing for choline chloride/urea deep eutectic solvent + water system. *J. Chem. Eng. Data* 61, 4172–4177. doi:10.1021/acs.jced.6b00569



- Ma, C., Guo, Y., Li, D., Zong, J., Ji, X., and Liu, C. (2017). Molar enthalpy of mixing and refractive indices of choline chloride-based deep eutectic solvents with water. *J. Chem. Thermodyn.* 105, 30–36. doi:10.1016/j.jct.2016.10.002
- Ma, C., Laaksonen, A., Liu, C., Lu, X., and Ji, X. (2018). The peculiar effect of water on ionic liquids and deep eutectic solvents. *Chem. Soc. Rev.* 47, 8685–8720. doi:10.1039/C8CS00325D
- Mariani, A., Caminiti, R., Ramondo, F., Salvitti, G., Mocci, F., and Gontrani, L. (2017). Inhomogeneity in ethylammonium nitrate-acetonitrile binary mixtures: The highest “low  $q$  excess” reported to date. *J. Phys. Chem. Lett.* 8, 3512–3522. doi:10.1021/acs.jpclett.7b01244
- Martínez, L., Andrade, R., Birgin, E. G., and Martínez, J. M. (2009). Packmol: A package for building initial configurations for molecular dynamics simulations. *J. Comput. Chem.* 30, 2157–2164. doi:10.1002/jcc.21224
- Megyes, T., Radnai, T., Grósz, T., and Pálkás, G. (2002). X-ray diffraction study of lithium halides in methanol. *J. Mol. Liq.* 101, 3–18. doi:10.1016/S0167-7322(02)00098-3
- Perkins, S. L., Painter, P., and Colina, C. M. (2014). Experimental and computational studies of choline chloride-based deep eutectic solvents. *J. Chem. Eng. Data* 59, 3652–3662. doi:10.1021/je500520h
- Powell, D. H., Neilson, G. W., and Enderby, J. E. (1993). The structure of Cl<sup>-</sup> in aqueous solution: An experimental determination of g<sub>ClH</sub>( $r$ ) and g<sub>ClO</sub>( $r$ ). *J. Phys. Condens. Matter* 5, 5723–5730. doi:10.1088/0953-8984/5/32/003
- Ryckaert, J.-P., Ciccotti, G., and Berendsen, H. J. C. (1977). Numerical integration of the cartesian equations of motion of a system with constraints: Molecular dynamics of n-alkanes. *J. Comput. Phys.* 23, 327–341. doi:10.1016/0021-9991(77)90098-5
- Salehi, H. S., Polat, H. M., de Meyer, F., Houriez, C., Coquelet, C., Vlucht, T. J. H., et al. (2021). Vapor pressures and vapor phase compositions of choline chloride urea and choline chloride ethylene glycol deep eutectic solvents from molecular simulation. *J. Chem. Phys.* 155, 114504. doi:10.1063/5.0062408
- Smith, E. L., Abbott, A. P., and Ryder, K. S. (2014). Deep eutectic solvents (DESs) and their applications. *Chem. Rev.* 114, 11060–11082. doi:10.1021/cr300162p
- Spittle, S., Poe, D., Doherty, B., Kolodziej, C., Heroux, L., Haque, M. A., et al. (2022). Evolution of microscopic heterogeneity and dynamics in choline chloride-based deep eutectic solvents. *Nat. Commun.* 13, 219. doi:10.1038/s41467-021-27842-z
- Stefanovic, R., Ludwig, M., Webber, G. B., Atkin, R., and Page, A. J. (2017). Nanostructure, hydrogen bonding and rheology in choline chloride deep eutectic solvents as a function of the hydrogen bond donor. *Phys. Chem. Chem. Phys.* 19, 3297–3306. doi:10.1039/C6CP07932F
- Triolo, A., Lo Celso, F., Brehm, M., Di Lisio, V., and Russina, O. (2021). Liquid structure of a choline chloride-water natural deep eutectic solvent: A molecular dynamics characterization. *J. Mol. Liq.* 133, 115750. doi:10.1016/j.molliq.2021.115750
- Velez, C., and Acevedo, O. (2022e1598). Simulation of deep eutectic solvents: Progress to promises. *WIREs Comput. Mol. Sci.* 12. doi:10.1002/wcms.1598
- Walser, R., Mark, A. E., van Gunsteren, W. F., Lauterbach, M., and Wipff, G. (2000). The effect of force-field parameters on properties of liquids: Parametrization of a simple three-site model for methanol. *J. Chem. Phys.* 112, 10450–10459. doi:10.1063/1.481680
- Wang, J., Wolf, R. M., Caldwell, J. W., Kollman, P. A., and Case, D. A. (2004). Development and testing of a general amber force field. *J. Comput. Chem.* 25, 1157–1174. doi:10.1002/jcc.20035
- Wang, Y.-L., Li, B., Sarman, S., Mocci, F., Lu, Z.-Y., Yuan, J., et al. (2020a). Microstructural and dynamical heterogeneities in ionic liquids. *Chem. Rev.* 120, 5798–5877. doi:10.1021/acs.chemrev.9b00693
- Wang, Y., Ma, C., Liu, C., Lu, X., Feng, X., and Ji, X. (2020b). Thermodynamic study of choline chloride-based deep eutectic solvents with water and methanol. *J. Chem. Eng. Data* 65, 2446–2457. doi:10.1021/acs.jced.9b01113
- Wu, X., Liu, Z., Huang, S., and Wang, W. (2005). Molecular dynamics simulation of room-temperature ionic liquid mixture of [bmim] [BF<sub>4</sub>] and acetonitrile by a refined force field. *Phys. Chem. Chem. Phys.* 7, 2771–2779. doi:10.1039/B504681P
- Xie, Y., Dong, H., Zhang, S., Lu, X., and Ji, X. (2014). Effect of water on the density, viscosity, and CO<sub>2</sub> solubility in choline chloride/urea. *J. Chem. Eng. Data* 59, 3344–3352. doi:10.1021/je500320c
- Yadav, A., and Pandey, S. (2014). Densities and viscosities of (choline chloride + urea) deep eutectic solvent and its aqueous mixtures in the temperature range 293.15 K to 363.15 K. *J. Chem. Eng. Data* 59, 2221–2229. doi:10.1021/je5001796
- Yadav, A., Trivedi, S., Rai, R., and Pandey, S. (2014). Densities and dynamic viscosities of (choline chloride + glycerol) deep eutectic solvent and its aqueous mixtures in the temperature range (283.15–363.15) K. *Fluid Phase Equilib.* 367, 135–142. doi:10.1016/j.fluid.2014.01.028
- Yamagami, M., Wakita, H., and Yamaguchi, T. (1995). Neutron diffraction study on chloride ion solvation in water, methanol, and N, N-dimethylformamide. *J. Chem. Phys.* 103, 8174–8178. doi:10.1063/1.470181
- Zahn, S., Kirchner, B., and Mollenhauer, D. (2016). Charge spreading in deep eutectic solvents. *ChemPhysChem* 17, 3354–3358. doi:10.1002/cphc.201600348
- Zhang, Q., De Oliveira Vigier, K., Royer, S., and Jérôme, F. (2012). Deep eutectic solvents: Syntheses, properties and applications. *Chem. Soc. Rev.* 41, 7108–7146. doi:10.1039/c2cs35178a

# Frontiers in Chemistry

Explores all fields of chemical science across the periodic table

Advances our understanding of how atoms, ions, and molecules come together and come apart.

It explores the role of chemistry in our everyday lives - from electronic devices to health and wellbeing.

## Discover the latest Research Topics

[See more →](#)

### Frontiers

Avenue du Tribunal-Fédéral 34  
1005 Lausanne, Switzerland  
[frontiersin.org](https://frontiersin.org)

### Contact us

+41 (0)21 510 17 00  
[frontiersin.org/about/contact](https://frontiersin.org/about/contact)



### Frontiers in Chemistry

